NASA-CR-202157

ANNUAL REPORT
NAG#5-2345

THE NATIONAL AERONAUTICS AND SPACE ADMINISTRATION

BY

THE UNIVERSITY OF THE DISTRICT OF COLUMBIA
4200 CONNECTICUT AVENUE N.W.
WASHINGTON D.C. 20008
TELEPHONE: (202) 274-5597
(202) 274-5263

A STUDY OF SURFACE TEMPERATURES, CLOUDS AND NET RADIATION

Submitted by Harbans Dhuria

Principal Investigator
Telephone# (202) 274-7456.
FAX# (202) 286-3706.
August 22, 1996.

ANNUAL REPORT

A Study of Surface Temperatures, Clouds and Net Radiation

The study focussed on examining seasonal relationships and interactions of climate parameters such as the surface temperatures, the net radiation, Long wave Flux, Shortwave Flux and clouds on a global basis for the period December 1984 to November 1989. The data for this period was obtained from the Earth Radiation Budget Experiment (ERBE) and International Satellite Cloud Climatology Program (ISCCP) products. The main emphasis is on obtaining the information about the interactions and relationships of Earth Radiation Budget parameters, cloud and temperature. The purpose is to gain additional qualitative and quantitative insight into the cloud climate relationship.

In addition to the proposed study we extended our study to include the analysis of the cloud forcing due to ERBE parameters, and the analysis of El-Nino's impact on ERBE parameters.

In our previous study we analyzed Nimbus-7 Earth Radiation Budget (ERB) and cloud data for the period June 1979 - May 1980. The previous study also consisted of an analysis of the combined Earth Radiation Budget Experiment (ERBE) and

International Satellite Cloud Climatology Program (ISCCP) Products for the period February 1985 to January 1987. Qualitatively the ERBE and ISCCP data have improved temporal sampling compared to the Nimbus-7 data. This study focussed on the analysis of ERBE and ISCCP Climate products for 5-year period extending from December 1985 to November 1989.

The data processing and analysis of the results were carried out according to our proposed plan. The global maps along with the contour plots of different parameters, cloud forcing, correlations, standard deviations, and changes in the climate parameters due to El-Nino (1986-87) year over the other years from December 1984 - November 1989 were addressed. The sophisticated technology of Computer System at Goddard Space Flight Center was instrumental in obtaining the plots for analysis purposes. Super Computer CRAY, UNITREE a mass storage system, and NCAR graphics system were used for data processing for conducting the research.

Based on our study A Manuscript, entitled "The Earth RADIATION Budget and its Annual and Inter-annual Cycle Correlations with Clouds and Surface Temperature" was completed. However, it may be revised further. A copy of the manuscript is enclosed with this report. This manuscript represents the status of our study. It describes our study effort and the data sets. It also includes the analyses and

interpretation of relationship of ERB parameter and ISCCP parameters. For study purposes all the necessary averaged annual and monthly global maps were considered. However, only 98 plots are included for interpretation and analysis of zonal means, regional variations, Annual means, correlations, cloud forcing, El-Nino event of climate parameters including net radiation, clouds and surface temperature and other parameters under study. Emphasis was placed on the variation of net radiation with cloud types geography and surface temperature.

Presentation of a paper

A paper entitled Cloud and Radiation Budget Perturbations in the Indian Ocean During the 1986/1987 ENSO was presented at the 1996 AGU Spring meeting at Baltimore was presented. A draft of the paper and a copy of the abstract is enclosed.

Status of the Study

The study continued according to the guidelines in the proposal, however the research also focussed on the meetings and discussions with the NASA technical monitor Dr. H. L. Kyle and colleagues who are involved in the related research work. The study also included the cloud forcing and El-Nino's effect on climate parameters.

The previous study was integrated with this study and conclusions and results that were obtained from the previous

study were also used in this study. Multi-variable correlations and regression analysis were also used to analyze the contribution of different parameters and surface temperatures to cloud forcing.

The study focussed on global and regional basis. Regions having specific characteristics based on significant climate conditions, differences in ERB and ISCCP parameters, land and ocean were also considered.

NASA
Reference
Publication
XXXX

1996

The Earth Radiation Budget and Its Annual and Interannual Cycle Correlations With Clouds and Surface Temperature

Harbans L. Dhuria, H. Lee Kyle, and Mitchell Weiss

NASA
Reference
Publication
XXXX

1996

The Earth Radiation Budget and Its Annual and Interannual Cycle Correlations With Clouds and Surface Temperature

Harbans L. Dhuria
University of the District of Columbia
Washington, D.C. 20008

H. Lee Kyle
Goddard Space Flight Center
Greenbelt, Maryland

Mitchell Weiss
Research and Data Systems Corporation
Greenbelt, Maryland

TABLE OF CONTENTS

1. INTRODUCTION

In the large-scale, the Earth can be considered as a heat engine that receives shortwave, high energy photons from the Sun. It uses this energy to drive the terrestrial climate and biosphere. The exhaust heat is emitted to space as longwave, low energy photons. The mean blackbody temperature of the incident solar radiation is about 5,570°K, while that of the exhaust radiation is only about 254°K. Over a year's time, the absorbed shortwave and the emitted longwave energy essentially balance out. In most studies, the net radiant energy exchange is assumed to be zero. However, on a monthly basis, the Earth receives more energy than it emits in December and January and suffers a net loss in June and July. The oceans act as large heat sinks that help make these seasonal imbalances less important to the average observer.

Global climate patterns and their seasonal and interannual variations are quite complex. Satellite observations provide a unifying perspective of the climate system and the Earth as a heat engine. Here we use 5 years (December 1984 to November 1989) of observations from the Earth Radiation Budget Experiment (ERBE; Barkstrom et al., 1989) to study both seasonal variations and interannual variations during this period. The basic radiation budget equation is:

$$NR = (1 - A)I_S - F_{LW}$$
$$= I_S - F_{SW} - F_{LW} \qquad (1)$$

where: NR is the net radiation

A is the scene albedo

I_S is the incident solar insolation

F_{LW} is the terrestrial emitted longwave radiation, measured 4 to >100 m

F_{SW} is the reflected solar shortwave radiation, measured 0.2 to 4 m

The measured quantities are I_S, F_{LW}, and F_{SW}, and they refer to the top of the atmosphere. The albedo is an important physical parameter and is determined by:

$$A = F_{SW} (I_S)^{-1} \qquad (2)$$

Seasonal variations are chiefly driven by the cyclic annual changes in the Earth/Sun geometry as the Earth revolves about the Sun in the ecliptic plane. As forcing factors of seasonal change, the eccentricity of the Earth's orbit and the obliquity of the plane of the Earth's orbit about the Sun (the ecliptic plane) are the most important parameters. Because of the eccentricity of the orbit, the Earth is about 3 percent closer to the Sun and receives 6.7 percent more energy on January 3 than it does on July 3. The Earth's equatorial plane makes an angle of about 23.5° with the ecliptic plane. This angle is termed the obliquity of the ecliptic plane and is the main driver of seasonal changes. In June and July, the Earth's North Pole is tilted towards the Sun and receives 24 hours of sunlight per day. In December and January, it is tilted away from the Sun and it is dark for 24 hours per day. At the Equator, the seasonal variations in the top of the atmosphere solar insolation are relatively small. When latitudinal zonal averages are considered, the tropics receive an excess of heat energy that oceanic and atmospheric currents carry to the energy-poor higher latitudes.

However, on a regional scale, local climate factors become quite important. These include surface type and the amount and type of cloud cover. The chief surface types are water and land, although snow is important at the higher latitudes. Compared to land, water has a lower and more uniform albedo and thus absorbs more solar energy. Its high heat capacity allows it to store large amounts of energy that water currents can move about. Water also cools by evaporation and produces the atmospheric water vapor. Air currents often carry the water vapor and its latent heat great distances before the vapor condenses to form clouds and eventually precipitation. On the other hand, land has a quite variable albedo, soil moisture content, and elevation. Arid land normally has a high albedo and low heat and energy storage capacities. However, the energy budget of tropical rain forests is similar to that over the ocean. Cloud amount and type can strongly affect both the emitted longwave and reflected shortwave radiation. But cloud amount and type are closely related to the regional climate. One of the basic purposes of this study is to explore the regional relationships between clouds and the radiation budget at the top of the atmosphere. The International Satellite Cloud Climatology Program (ISCCP) clouds (Rossow and Schiffer, 1991) are used for this purpose. These

data start in July 1983 and are still being received. We use the C2 dataset containing monthly diurnal averages.

The ISCCP algorithm uses measurements from geostationary satellites (GOES-E, GOES-W, Meteosat, and GMS) and from the NOAA polar orbiters (both morning and afternoon). The afternoon polar orbiters were used as a calibration standard to obtain a uniform ISCCP measurement set. During the 5 years we considered (December 1984 to November 1989), there were three afternoon polar orbiters that were used: NOAA-7 (July 1983 to January 1985), NOAA-9 (February 1985 to October 1988), and NOAA-11 (November 1988 past the end of our study period). Care was taken by the ISCCP team to normalize the calibration of these three satellites. The procedure used for the visible channel is described in Brest and Rossow (1992). At the two change-over points (February 1985 and November 1988), the normalization errors are estimated to be less than 7 percent in the visible channel and less than 3°K in the infrared channel. Time series analyses by Klein and Hartmann (1993) found discontinuities in the cloud-top temperature and pressure, and in the cloud albedo at the two cross over dates. A drop in the mean cloud top temperature of about 3°K occurred at the start of 1985, another decrease of about 1.5°K occurred at the end of 1988. These changes are within the estimated error bars. The mean cloud top temperature was found to be stable during the NOAA-9 period (February 1985 to October 1988).

The ERBE program consists of similar instruments on three satellites. The Earth Radiation Budget Satellite (ERBS) is in a circular orbit inclined at 57° to the Earth's Equator. The satellite precesses with respect to the local time. In 37 days, the satellite views each region below 57° latitude at least once during each hour of the day. Therefore, its measurements can be used to make reasonable estimates of the monthly mean diurnal shortwave and longwave radiation. The NOAA-9 and -10 weather satellites are in Sun-synchronous orbits with original local Sun time equator crossings of 2:20 a.m./p.m. and 7:30 a.m./p.m., respectively. The scanner measurements are used in this study. The ERBS scanner took data from November 5, 1984 to February 22, 1990; the NOAA-9 scanner operated from January 5, 1985 to January 20, 1987; and the NOAA-10 scanner from October 25, 1986 to May 22, 1989. Good diurnal means on a global basis were obtained by combining the

measurements from the three instruments. However, as Kyle et al. (1993) pointed out, the ERBS/NOAA-9 and ERBS/NOAA-10 combinations are not entirely consistent with one another. This chiefly arises from the different radiation budget characteristics at 7:30 a.m./p.m. and 2:20 a.m./p.m. Therefore, in this study we chose the combined measurements from February 1985 to January 1987 to study global seasonal variations. This contains 3 months of ERBS/NOAA-9/NOAA-10 data as well as 21 months of ERBS/NOAA-9 data; however, these two combinations are reasonably consistent. Interannual variations in the annual means and in the seasonal cycle are examined using the standalone ERBS data from December 1984 to November 1989 (5 years).

An overview of the Earth's radiation budget, surface temperature, and cloud cover are given in Section 2 in terms of zonal mean analysis and mean annual maps. Section 3 emphasizes the seasonal variations. Correlation and regression analysis is used to demonstrate the relationships between the radiation budget, clouds, and surface temperature. Interannual variations are considered in Section 4,

2. AN OVERVIEW OF THE EARTH'S MEAN RADIATION BUDGET

The seasonal cycle of the Earth's global mean Earth's radiation budget is given in Table 1 for the year (February 1985 through January 1986). Note that the outgoing longwave radiation (OLR) is largest in the June to August season when the Earth is farthest from the Sun and the global net radiation is negative. This is due to the warm northern continents whose mean cloud cover is lower than that over the oceans. Most of the Earth's land surface is in the northern hemisphere while the southern hemisphere is mostly ocean. On the other hand, the mean albedo is higher in the months November through February than during June through September. In the southern summer, the ice-covered Antarctic continent and its dense circle of surrounding clouds are brightly illuminated, but its albedo is so high that most of the incident solar energy is reflected back to space. Despite this, the tropical and mid latitude oceans absorb enough energy to create a positive global mean energy balance.

Due to some diurnal sampling and perhaps calibration deficiencies, the measured annual global mean net radiation is about 5.25 W/m^2 positive. This is a consistent feature of the measurements made during the 1980s and is not considered real. Such an imbalance, year after year, should cause a very noticeable climate change which in fact has not been observed. The second net radiation column is adjusted to have a zero annual net radiation as the common theory predicts. There is no generally agreed upon procedure for similarly adjusting the emitted longwave or reflected shortwave (or albedo) parameters.

Table 1. ERBS/NOAA-9 Scanner Global Monthly Mean
Earth Radiation Budget Parameters
February 1985 to January 1986

Month/Year	OLR (W/m^2)	Albedo (%)	Net Radiation (W/m^2)	
			Measured	Adjusted
January 1986	231.9	30.8	11.9	6.65
February 1985	229.4	30.1	15.0	9.75
March 1985	230.4	29.8	11.8	6.55
April 1985	234.5	29.7	3.9	-1.35
May 1985	234.9	30.1	-1.1	-6.35
June 1985	237.4	29.7	-4.6	-9.85
July 1985	237.5	29.2	-3.6	-8.85
August 1985	239.2	28.8	-2.4	-7.65
September 1985	237.2	28.7	3.4	-1.85
October 1985	234.1	29.8	7.0	1.75
November 1985	229.9	31.3	9.7	4.45
December 1985	231.0	31.0	12.0	6.75
Annual	234.0	29.9	5.25	0.0

The hemispherical seasonal cycles of the net radiation are shown in Figure 1. For comparison, the Nimbus-7 scanner data (June 1979 to May 1980; Kyle et al., 1991) is plotted together with the ERBS/NOAA-9 (February 1985 to January 1986). The minor differences that occur are attributed chiefly to algorithm and diurnal sampling differences. While the global means vary from +10 Wm^{-2} in February to -10 Wm^{-2} in June, the hemispherical variations are about 10 times as large. Note that the amplitude of the cycle is slightly larger in the southern hemisphere than in the north. This is chiefly due to the fact that the Earth is closest to the Sun in the southern summer and farthest away in the southern winter. The reverse occurs in the north.

2.1 Zonal Means

The Earth's mean radiation budget and its seasonal extremes are summarized in Figure 2 in terms of latitude band averages. Annual averages are shown in Figure 2a. The Earth's climate is dominated by the fact that the mean annual insolation is over twice as large in the tropics as in the polar regions. In addition, a higher percentage of the incident solar irradiance is absorbed at low latitudes. As a result, the regions between approximately ±36° of latitude show a positive annual net radiation, while the higher latitudes show a negative balance that must be made up by the transport of energy from the warmer regions by atmospheric and ocean currents. On a reduced scale, the net radiation (bottom curve) mimics the insolation (top curve) with only minor deviations. The diurnally averaged OLR is about 100 W/m^2 larger in the tropics than at the poles (less for north pole, more for south pole). The diurnally averaged reflected shortwave is nearly independent of latitude, but is slightly higher at the poles. This indicates that the regional albedo is much lower in the tropics than at the higher latitudes with the polar regions being the brightest. While the insolation shows a north/south symmetry, slight but significant asymmetries appear in the other quantities. The OLR is nearly 50 W/m^2 lower at the south pole than at the north pole in accordance with the lower Antarctic temperatures. The reflected radiation, however, is slightly larger at the south pole, due to the higher albedo of the southern ice cap. The OLR asymmetry is the larger so that the net radiation is algebraically lower by about 20 W/m^2 at the north pole than at the south pole. In the tropics, a slight peak in the reflected shortwave about 6° north of the equator indicates the mean position of the inter tropical convergence zone rain belt. A dip in the OLR at the same position is caused by the presence of many high clouds. Slight OLR maxima occur in the subtropical high pressure zones, at about ±20° latitude, indicating the cloud minima present.

The changes in the top-of-the-atmosphere insolation drive the seasonal changes in the ERB parameters. At the December solstice, the Sun is 23.5° south of the equator, while at the June solstice it is 23.5° north of the equator. Further, because of the eccentricity of the Earth's orbit, the solar irradiance at the Earth is about 6 percent larger in December and January than in June and July. These seasonal changes are illustrated in Figures 2b and 2c.

In December to February, the insolation is 450 W/m^2 or greater from 10°S latitude to the South Pole. However, north of the equator, the insolation drops steadily to zero just beyond the Arctic Circle. The reflected shortwave drops from over 300 W/m^2 at the bright South Pole to zero in the sunless Arctic. Note the steady decline in the reflected shortwave signal from the South Pole to 36°S latitude even though the insolation increases slightly. This is caused by the decrease in the regional albedos as the Antarctic ice and clouds give way to the relatively clear southern oceans. The high reflectivity in the south keeps the net radiation slightly negative in the Antarctic even when the insolation is large. In this season, the net radiation is positive from 14°N to 66°S latitude. At the North Pole, the net radiation drops to about -170 W/m^2. In June, July, and August, it is summer in the Arctic, but the Earth is farthest from the Sun so that the insolation is slightly smaller than in December to February. In the June to August season, the net radiation is positive from 70°N latitude to 10°S latitude.

2.2 Regional Variations

2.2.1 Mean Net Radiation Maps

The mean annual net radiation map for the year February 1985 to January 1986 is shown in Figure 3. The map depicts a non-El Niño/Southern Oscillation (ENSO) year. At a given latitude, the greatest longitudinal differences in the net radiation occur between 20° and 30°N latitude. Here the annual mean ranges from more than 40 W/m^2 over large stretches of the ocean to less than -40 W/m^2 over portions of the Sahara Desert in North Africa. Significant variations also occur along the equator. Values less than 40 W/m^2 along the west coast of South America and the east coast of Africa compare with values over 90 W/m^2 in the western Pacific and in the Indian Ocean. Significant, but less dramatic, differences also occur regionally between 20° and 30°S latitude. The maps show that more heat is lost at the North Pole than at the South. But the map does show large variations from -64 W/m^2 to -127 W/m^2 in various regions of the Antarctic continent. During the 6-month South polar night, atmospheric winds carry heat from the southern oceans to the cold, sunless continent. Thus, it is reasonable that the coastal regions both receive and lose more heat than the high south polar plateau.

The reasons for these observed regional differences depends both on regional surface physical differences and atmospheric and oceanic dynamics. In general, oceans are darker than land and will

therefore absorb more of the incident solar energy. The drier a land region is, the higher its albedo tends to be and the less the insolation is absorbed. The Sahara has a higher surface albedo than most deserts. Many regions of the Sahara with light cloud cover have albedos as high or higher than those of some other regions with heavy cloud cover. In addition, dry land has a low heat capacity. Thus, in sunshine the surface heats quickly and reradiates much of the absorbed energy. Both the surface temperature and the emitted longwave show a very strong diurnal signal over deserts. Oceans, on the other hand, have a high heat capacity and a much less variable diurnal and seasonal surface temperature than does land.

Variations in regional cloud amount are also important. In general, clouds are brighter and colder than the surface. Thus, they tend to increase the reflected shortwave and decrease the emitted longwave radiation. As discussed in Dhuria and Kyle (1990), cloud type is more important than cloud amount in modifying the regional net radiation. Low, thick clouds off the west coast of South America and South Africa are highly reflective, but also have relatively warm cloud tops. Thus, they sharply reduce the net radiation in these regions. However, in the equatorial Indian Ocean and Western Pacific, large fields of high, thin cirrus clouds often cause an increase in the net radiation.

2.2.2 Cloud Forcing

Ramanathan (1987) introduced the term cloud radiative forcing for the flux difference (clear sky minus mean sky). This is an observable quantity as the ERBE longwave and shortwave measurements are tagged as arising from clear, partly cloudy, or overcast scenes. The algorithm of Wielicki and Green (1989) is used to determine the amount of cloud cover. The ERBE monthly averages include both the mean sky and clear sky results. The relevant equations are:

$$CF = F(clear) - F(mean) \qquad (3)$$

Thus

$$CF_{SW} = F_{SW(clear)} - F_{SW(mean)} \qquad (4)$$

$$CF_{LW} = F_{LW(clear)} - F_{LW(mean)}$$

$$CF_{NR} = CF_{SW} + CF_{LW}$$

where: F = flux

CF = cloud forcing

SW = shortwave

LW = longwave

NR = net radiation

As a rule, the shortwave cloud forcing is negative and the longwave cloud forcing is positive. The net radiation cloud forcing can be either positive or negative, but it is usually negative.

The mean annual net cloud forcing (February 1985 through January 1986) is shown in Figure 4. Thick relatively low altitude cloud belts occur over the high latitude oceans in both the northern and southern hemispheres. The cloud belts increase the high latitude albedo and, thus, produce a strong negative net cloud forcing. Negative cloud forcing also predominates along the mid and low latitude west coasts of North and South America and Southern Africa where relatively cool surface water prevails. However, over Indonesia, the mixture of deep convective rain cells and surrounding high thin cirrus produce only a slightly negative net cloud forcing. Both to the east and to the west of Indonesia, predominately high thin clouds produce a slightly positive net cloud forcing. This type of cloud also produces the positive cloud forcing seen over the Sahara and other mid latitude deserts. Over the continents, the surface albedo is generally higher and the cloud cover less dense than over the oceans. Thus, the net cloud forcing tends to be negative but low over many large continental regions.

A major exception occurs over Southern China where persistent low clouds help make this a high energy deficit region as can be seen in Figure 3. The strong net cloud forcing in this region arises

from cold fronts from the north interacting with warm moist air from the South China Sea in a fairly mountainous area. As sometimes happens in the mid latitudes, the negative cloud forcing here is stronger in the winter months than in the summer. Latitude band averaged shortwave, longwave, and net cloud forcing are shown in Figure 5. The annual averages in Figure 5a show that the cloud belt around the Antarctic continent reduces the solar energy absorbed by the southern ocean by nearly 80 W/m^2. The clouds also reduce the OLR by about 40 W/m^2 so the net cloud forcing is about -40 W/m^2. Over the Antarctic continent, the shortwave, longwave, and net cloud forcing are all shown as small but positive in the figure. However, the ERBE algorithm does not accurately identify clouds over snow. Thus, the values over the Antarctic continent should not, at present, be given much weight. The very high albedo in the polar regions is, however, a dominant factor. Thus, whether it is caused by clouds or ice and snow, it still sharply reduces the absorbed solar energy. Thus, in Figure 2a no sharp break appears in the mean zonal curves at the Antarctic ocean/land boundary.

3. SEASONAL AND INTERANNUAL VARIATIONS

Seasonal variations are shown in terms of 5-year monthly means for the period December 1984 to November 1989, and by the correlation between the various parameters over the 12-month annual cycle. For reference, the 5-year (60-month) means are also given. Because the ERBS instrument could not view the polar latitudes, the maps are restricted to the belt 50°N to 50°S latitude. The major interannual climate perturbation in the 1985 to 1989 period was the 1986/87 ENSO event. Since it is described in detail in Section 4, only a brief discussion of the standard deviations of the 5-year means is given in this section. The parameters shown from the ERBS data set are the top of the atmosphere: net radiation, emitted longwave, and reflected shortwave radiation. From the ISCCP cloud data set are taken the near surface air temperature, mean diurnal cloud cover, and cloud top temperature. The annual cycle correlations in the variations of the parameters are discussed in Section 3.1; the mean annual maps appear in Section 3.2, and the mean monthly maps are reviewed in Section 3.3, while Section 3.4 covers the standard deviations.

3.1 Annual Cycle Correlations

As discussed in Section 1, the annual cycle in the latitude-dependent, top of the atmosphere, incident solar energy (insolation) drives the annual climate cycle (see Figures 2b and 2c). Therefore, regionally, a strong correlation usually exists between the seasonal variations in many climate parameters and the insolation cycle. Five years (December 1984 to November 1989) of monthly means were analyzed to derive most of the annual cycle correlations discussed here. Some variations occurred from year to year, but we will concentrate on the 5-year mean annual cycle.

The strongest annual cycle correlations exist between the net radiation and the solar insulation. As shown in Figure 6, the correlation is positive and over 95% everywhere except in an equatorial belt where the correlation decreases and several local minima occur. Values as small as 0.4 occur in

northeastern Brazil and near the west coast of Africa. The square of the correlation is called the explained variance. It is an estimate of the probability that if one of the variables changes, the other will show a related change. This estimate can be considered reliable only if sufficient data pairs are examined. We use the t-test to check the reliability of our correlations and explained variances (Devore, 1982). Even with correlations as low as 0.4 for the 60 months analyzed, the t-test indicates that there is over a 99.95 percent probability that there is a true connection between the annual cycle of the insolation and that of the regional net radiation. Over most of the Earth, the annual insolation cycle explains 90 percent or more of the net radiation cycle; but along the equator, the explained variance can drop to 20 percent or less. The insolation has only a weak annual cycle at the equator which, in fact, should be considered two 6-month cycles since the sub solar point crosses the equator going north in March and again going south in September. Because the changes in the insolation are small, local climate conditions, rather than the annual insolation cycle, tend to dominate the yearly equatorial net radiation cycle.

Both seasonally and regionally, the net radiation and its effect on the climate are strongly influenced by the local conditions. There is a feedback pattern with the absorbed net radiation affecting the surface temperature and cloud cover which, in turn, affect the absorbed shortwave (ASW) and the emitted longwave radiation. Figure 7 illustrates this relationship. An increase in the surface temperature increases the longwave radiation emitted by the surface. However, if the atmospheric water vapor and cloud amount also increase, the exhaust longwave radiation emitted to space from the top of the atmosphere may actually decrease. As the cloud cover increases, more of the solar radiation is reflected and less is absorbed. Depending on the conditions, these feedback mechanisms may increase, decrease, or leave the net radiation unchanged.

The effect of net radiation changes on the surface air temperature also depends on the local conditions. Arid land responds quickly when the net radiation changes. However, because of the high heat capacity of water, ocean regions respond slowly. This is illustrated in Figures 8a through 8d. In this analysis, the surface air temperature is lagged behind the net radiation by 0, 1, 2, and 3 months, respectively, in Figures 8a through 8d. For zero lag (Figure 8a), note the high correlations of 0.8 to

0.9 (explained variance of 64 percent to 81 percent) in western Australia, southern Africa, and southern Brazil in the southern hemisphere; and in southern China, the Sahara, and the North American Great Plains in the northern hemisphere. Other conditions besides the soil moisture can effect this relationship, but these are generally of lesser importance. Over most of the ocean and also in most of the equatorial land regions, the correlation is usually 0.5 (explained variance 25 percent) or less. For a lag of 2 months (Figure 8c), numerous mid- and high latitude ocean areas now show correlations of 0.9 or greater. Over the land, the correlation has generally decreased, and some negative correlations appear in tropical Africa and South America. A lag of 3 months (Figure 8d) shows that the correlation is starting to decrease over the oceans as well as over the land. In this analysis, 60 months of data were used for zero lag, but only 57 months for 3 months of lag. One month of correlation pairs was dropped for each month of lag.

Clouds are a prime modifying agent of the radiation budget. Figure 9a shows that while the regional annual cloud cycles are related to the insolation cycle, the local climate conditions dictate the sign of the correlation. There is zero lag in Figures 9a and 9b. In the monsoon regions, the clouds and the rain follow the Sun and correlations of 0.6 or higher are common. These regions include: India and northern Australia, Africa, central America and central South America, and the SPCZ. Many other regions are anti correlated with the insolation cycle and have more clouds in the winter than in the summer. Note, particularly, the regions in the tropical and southern Indian Ocean, the north Atlantic, the north tropical Atlantic, and the south Atlantic off Argentina, and the Pacific Ocean below Alaska in the northern hemisphere and west of Chile in the southern hemisphere.

The cloud cycle is generally considered to be more closely related to the surface air temperature (Figure 9b). Because of the variable lag time for net radiation versus surface air temperature, there are some noticeable differences between Figures 9a and 9b. The positions and the amplitudes of the maxima and minima show some shifts; however, there is a strong similarity in the overall global patterns.

The annual cycle correlation between the outgoing longwave radiation and the surface air temperature is shown in Figure 10. The surface emits longwave radiation essentially as a black body

$$LW = \varepsilon\sigma T^4$$

here LW = emitted radiation

ε = emissivity factor; it is normally = 1

σ = Stephen Boltzmann constant

T = temperature in degrees Kelvin

The surface temperature increases from the poles towards the equator and also varies seasonally with the smallest seasonal changes occurring in the tropics. However, in the mean, the top-of-the-atmosphere emitted longwave radiation is controlled more by the atmospheric conditions than by the surface temperature. The atmosphere forms an insulating blanket which slows the escape of the surface heat to outer space, and allows the surface to be warmer than it otherwise would be. This is called the atmospheric "greenhouse" effect, and water vapor is the most important of the heat trapping greenhouse gases. It is also the most variable of the important greenhouse gases. Over the ocean, the amount of water vapor in the atmosphere increases with the surface temperature. In the tropics, the amount of atmospheric water vapor is so large that variations in the water vapor amount generally control how much longwave radiation is emitted to space. Clouds, formed from condensed water vapor, reinforce the greenhouse effect. In the tropics, therefore, when the surface temperature decreases, so generally goes the atmospheric water vapor, and this causes an increase in the longwave radiation escaping to space. At higher latitudes, where the mean surface temperature is lower, there is less atmospheric water vapor and the annual cycle of the surface temperature controls that of the emitted longwave.

The reader should keep these various relationships in mind when examining the mean monthly maps shown in the following section.

3.2 Annual Means

Annual mean and 60-month standard deviation maps for the six parameters (net radiation, emitted longwave, reflected short wave radiation, surface temperature, total cloud fraction, cloud top temperature) are shown in Maps 1 to 12 for the region 50° N to 50° S latitude. There is a general positive correlation between the mean net radiation and the mean surface temperature over the ocean, but over land this is less true. The standard deviation maps are discussed in s
Section 3.4.

The annual mean maps represent an average picture of the Earth's climate. This has already been discussed in Section 2, and only a few additional comments will be made here. The actual climate is in a continual state of flux driven principally by the seasonal cycle. This is discussed below in Section 3.3. In the mean surface temperature map 7 note the great pool of warm water in the western Equatorial Pacific. Here the mean sea surface temperature is 302° K or a little higher.
The temperatures are several degrees cooler off the west coasts of Ecuador and Peru. The cloud top temperatures show the reverse pattern, low in the western tropical Pacific where deep convective activity is centered, and high in the eastern tropical Pacific where low cloud predominate.

3.3 Monthly Means

Monthly mean and standard deviation maps for the six parameters and their 5-year standard deviations are listed for the for mid season months: January, April, July and October. These are given in the following order for each month: net radiation, emitted longwave, reflected shortwave, near surface air temperature, mean diurnal cloud cover, and cloud top temperature. For convenient reference, the monthly 5-year means and standard deviations are grouped in pairs. The monthly means are discussed in this section while the standard deviations are discussed in Section 3.4. A brief discussion follows for each monthly set of maps.

3.3.1 January

In January (Maps 13-24) the Sun is high in the sky in the southern hemisphere,. The solar declination reaches its farthest south value of about -23.5° on December 22. In Antarctica (not shown), the Sun is above the horizon 24 hours per day for most of the month. In addition, the Earth has reached its closest approach to the Sun and receives about 6 percent more solar energy than it does in June and July. As a result, the net radiation is strongly positive in the southern hemisphere down to the map boundary at 50° latitude. Reference to the zonal averages in Figure 2b shows that because of the high albedo in the Antarctic, the net radiation there is slightly negative even in December and January.

Centered at about 30°S, patches of net radiation of over 140 Wm^{-2} occur over the southern oceans. The highest values tend to occur in the Atlantic Ocean off the coast of Patagonia at about 45°S latitude. Here the mean December high was 180 Wm^{-2}. These high net radiation regions are associated with a thin high cloud cover which keep down the outgoing longwave radiation, but allow most of the incident solar radiation to pass through. The persistent dry winds blowing off the Patagonia tableland during this season maintain the high net radiation area off the coast of Argentina. In contrast, low, fairly thick clouds off the west coast of South America at 20°S latitude sharply reduce the net radiation there. The net radiation generally decreases over the continents partially because of the higher surface albedo present. Note particularly the local minimum over Australia.

Except in the tropics, the net radiation is negative in the winter, northern hemisphere. Over the winter oceans, the net radiation contours are relatively smooth and tend to follow the parallels of latitude. However, over the continents variations in the surface albedo and seasonal cloud cover still present interesting patterns. Note that the high Tibetan Plateau and the region to its north has a higher net radiation than the neighboring regions. The combination of low surface temperature and low cloud cover contribute to this condition by decreasing the emitted longwave while increasing the absorbed shortwave radiation.

The emitted longwave, reflected shortwave, cloud cover, and cloud top temperature maps show related patterns which often show only a faint resemblance to the net radiation map. The major subsidence region just south of the equator, 90° to 150°W longitude is common to all four of the first-mentioned parameters. Here, a maximum occurs in the emitted longwave, while minima occur in the other three parameters. However, the region does not have a sharp demarcation on the net radiation map. This indicates that the longwave maximum and shortwave minimum tend to cancel each other. The net radiation extremes occur where the emitted longwave and absorbed shortwave radiation are out of balance.

Clouds reduce the emitted longwave and increase the reflected shortwave radiation, hence the relationship between these three parameters is expected. However, cloud altitude and cloud density effect the longwave and shortwave differently. Thus, variations in cloud type is a major factor in the distinctive appearance of the net radiation map. Over the ocean, the longwave radiation can be used as a proxy for the cloud top temperature and the albedo for the cloud optical thickness. At a fixed latitude, the mean top of the atmosphere solar irradiance does not vary with longitude, but only with the season of the year. Thus, for a given month and latitude, the reflected shortwave may be used in place of the albedo [see Eq.(2)]. Over land, these proxies are less accurate because of the greater variability in the surface albedo and temperature. Note that the cloud top temperature map and the emitted longwave radiation maps show fairly similar patterns, particularly over the oceans. When there is sparse cloud cover, these proxies often fail because the emitted longwave and reflected shortwave are then controlled by the clear-sky conditions particularly the surface albedo and temperature. Thus, over arid continental regions, the cloud top temperature and emitted longwave maps often show different patterns.

The near surface air temperature shows, over the oceans, a rough symmetry about the equator. Compared to the continents, the oceans show a relatively small seasonal variation in the surface temperature. This is due both to the high heat capacity of water and because oceanic and atmospheric currents help redistribute the stored energy. Warm water moves from the tropics to higher latitudes *principally along* the eastern continental coasts. Cool high latitude water returns to the tropics both by

surface currents and by deep ocean currents. Thus, the relatively cool temperatures off the west coast of central South America are caused by up welling of deep ocean water as well as by the cool, north flowing Peruvian current. Note the increase in temperature westward from Peru to the tropical warm water pool where the sea-surface temperature is generally at 302°K (29°C) or above.

The highest emitted longwave values are found over hot arid land regions. The highest value in January (300 Wm^{-2}) occurs over eastern Australia. However, over the oceans, the high values generally occur in subsidence regions in the winter tropics. Thus, high values of 291 to 294 Wm^{-2} occur at latitude 20°N, in the Atlantic north of South America, off the west coasts of India and Pakistan and near the Date Line in the Pacific. The high emitted longwave areas in the winter tropics occur because of low winter cloud cover over still warm oceans. In the summer tropics, the cloud cover usually increases thus decreasing the top of the atmosphere emitted longwave radiation, but note the subsidence area west of Peru with a high of 188 Wm^{-2}.

3.3.2 April

By April the Sun has moved just north of the equator, thus the highest net radiation is found in the northern tropics. Note the contrast between the maximum of +110 Watts per meter square off night temperatures are much lower than the afternoon ones. The the west coast of Mexico and the minima of -32 W/m^2 in the southern Sahara and +5.3 W/m^2 in southern China. The maximum below Baja California is in the ocean with low to moderate cloud cover and a warm but moderate sea surface temperature. Thus there is a maximum in the absorbed shortwave but not in the emitted longwave. The two land minima are basically caused by local minima in the absorbed shortwave (high albedo); the Sahara minimum is lower because of the higher surface temperature and emitted longwave radiation. The two minima are quite different in character. The Sahara has a moderate to low cloud cover but a high surface albedo. The absorbed solar radiation produces high surface temperatures during the day, but the emitted longwave energy is also high, hence the cooling is rapid and the south China minimum is caused by a dense low stratus cloud cover in the winter and spring which tends to

burn off in the summer and fall. Thus the south China net radiation minima is not prominent in the June net radiation map, but it has started to reappear by October.

3.3.3 July

In July (maps 37-48) the sub-solar point is about 20 degrees north of the equator and the net radiation maxima now occur in the northern mid latitude oceans. However note the local minimum of 35 Wm^{-2} just west of Baja California. This is due to dense low stratus clouds; compare the cloud amount and cloud top temperature maps with the net radiation map. On the other hand the minimum of -28 Wm-2 in the eastern Sahara is caused by the high surface reflectivity combined with the high surface temperature and accompaning high OLR value.

3.3.4 October

The sub-solar point is now just south of the equator. In the southern oceans notice the net radiation minima off the west coasts of South America and southern Africa compared to the high net radiation on the east coasts. This caused by differences in both cloud type and amount. Examination of the cloud and cloud top temperature maps indicates that the clouds are denser and lower off the west coasts. The sea surface temperatures are also a little cooler off the west coasts. In the northern hemisphere note that the net radiation is lower over cloud covered south China than over the high cooler Tibetan plateau. More solar radiation is absorbed over Tibet, but south China is warmed by winds from the China Sea. In addition, the denser cloud cover over south China acts as an insulating blanket and somewhat reduces the emitted longwave radiation.

3.4 Standard deviations

3.4.1 60-Month Standard deviations

The 60-month standard deviations are driven by the Seasonal migration of the sub solar point and hence of the insolation. At the higher latitudes this is most clearly seen in the net radiation, reflected shortwave, and surface temperature (maps 2, 6, 8). Map 8 shows the moderating effect of the oceans on the temperature variations. The great northern land masses show large seasonally driven standard deviations of 8^{o} K and larger. In the ocean dominated Southern Hemisphere the standard deviations are much lower, even over the land areas.

In the tropics, the monsoon seasons dominate the OLR and cloud standard deviations (maps 4 & 10). The Equatorial cloud belt is clumsy (map 9) with maxima over northern South America, Central Africa, the Indonesian island continent, plus a central Pacific belt. There is a seasonal motion following the Sun north and south across the Equator, and this creates many of the local tropical maxima in the standard deviation (map 10). The monsoon belt extends from about 5^{o} to 20^{o} latitude north and south of the Equator with centers near central America and Brazil, central and southern Africa, in Asia from India into western China, and northern Australia.

3.4.2 Calender Month Standard Deviations

These monthly standard deviations reflect the year to year changes in a given calendar month. The major perturbations in the net radiation tend to follow the Sun. Thus in January the standard deviations tend to be largest in the mid southern latitudes (25S to 50S) while in July they are largest in the mid northern latitudes. These perturbations are basically driven by shifts in the year to year cloud patterns. But note that the largest cloud and net radiation standard deviations are normally not co-located. The longwave and shortwave changes often nearly cancel when thick high cloud systems shift position. However this is not true in the case of low stratus clouds or high thin cirrus clouds. In

January and October there are large standard deviations off the West coasts of southern Africa and South America, the South Pacific convergence zone and the east and west coasts Australia. There are also significant year to year variations in southern China and off the west coast of North America. The latter occurs in all months, but the variations cover a larger area when the Sun is north of the Equator.

The surface air temperature standard deviations are largest over land and in certain months can exceed 10 degrees Celsius in Northern Chile and in Central Asia above India. Over the Ocean the deviations are generally less than 1 degree Celsius, but reach 2 degrees during several months in the South Pacific convergence zone and a few other areas. In general the largest interannual perturbations in all of the parameters were related to the 1986/87 event. This major climate perturbation is discussed in more detail in the following section.

4.0 THE 1986/87 ENSO EVENT

The El Niño/Southern Oscillation event of 1986/87 was the major perturbation in the Earth's climate and radiation budget field during the 5-year period from December 1984 to November 1989. ENSO events occur every few years, and the 1986/87 occurrence was considered moderate in size. Although the perturbations were largest in the central Pacific during the period from December 1986 to April 1987, important variations occurred on a worldwide basis and for a longer period. They were accompanied by major shifts in rain patterns and unwelcome draughts and floods.

4.1 Latitude Band Perturbations

A noticeable increase in the mean tropical near surface air temperature and top of the atmosphere OLR accompanied the event as shown in Figure 11. In this figure, the ERBS OLR has been adjusted and joined to the earlier Nimbus-7 measurements to extend the period back to 1979. To make a smooth fit, a bias adjustment was made in the mean ERBS OLR value. The temperature variations are taken from the Hansen and Lebedeff (1988) data. Twelve-month running means of both the OLR and the temperature differences were taken to remove seasonal variations. The in-phase variation of the mean tropical OLR and temperature is typical during the ENSO events. The smaller perturbation in the 1979/80 period coincided with a warming in the eastern tropical Pacific that was not large enough to be termed an ENSO event. The tropical cloud cover also increases during the ENSO event (Figure 12) but drops back sharply after a few months. On the other hand, the OLR and temperature peaks occur after the main phase of the ENSO event. This analysis is discussed in detail in Kyle et al. (1995).

Some important regional characteristics of the radiation budget perturbations are illustrated in Figure 13. Here the covariance of regional and the global mean OLR are plotted for the study period from December 1984 to November 1989. Twelve-month running means were analyzed to remove the

seasonal signal. The dashed lines indicate negative correlation where the regional OLR tended to decrease when the global mean increased. The solid contours indicate a positive correlation. In the central and eastern equatorial Pacific, the sea surface temperature increased during the ENSO and deep convective clouds formed. This resulted in a decrease in the emitted top of the atmosphere longwave radiation. Thus, here the temperature and the OLR are anti correlated. Smaller anti correlated regions occur around Florida and in the South Atlantic. Strong positively correlated OLR regions occur north, south, and west of the new high convective region in the central Pacific. In these regions, both the cloud cover and the mean cloud top height have decreased. A decrease in cloud cover also occurs around Madagascar, the Gulf of Arabia, and over northern Brazil. This figure indicates that the strongest OLR shifts occur over the ocean; however, there is considerable positive and negative cancellation over the oceans.

In fact, the strongest mean tropical OLR ENSO signal comes from the continents and not from the oceans. This can be seen in Figure 14 where 12-month running means of the northern tropical OLR and atmospheric precipitable waterare plotted separately for land and water regions. Coastal regions were omitted in order to emphasize the different land and ocean behavior. While the OLR perturbations are more dramatic over the ocean (map 62), there is also a strong tendency for the positive and negative regions to cancel when the average is taken. Map 64 shows that the surface air temperature increases during the ENSO are commen over land as well as over the oceans. Note particularly the band of higher temperatures stretching all across the Sahara, the Mid East, and up into Siberia. Part of the reason for the stronger OLR land signal is because over the ocean the atmospheric water vapor content increases with the surface temperature, but in the mean over the tropical land, it tends to decrease when the temperature increases. The OLR tends to show a negative correlation to the atmospheric water vapor over both land and ocean (Figure 14).

Note that there is normally less precipitable water over the land than over the ocean. The cloud cover is related to the precipitable water amount and both affect the OLR. For instance, in Figure 14 the ocean OLR minimum in the fall of 1986 is related to an increase in the high cloud amount over the

ocean. On the other hand, the small peak in the land OLR in 1989 is related to a minimum in the high cloud amount over land.

4.2 Annual Mean Regional Perturbations

The mean annual ENSO perturbations are shown in Maps 61 to 66. They are formed as the difference (4-year mean (for yrs 1,2,4,5) - ENSO (yr 3) mean). Thus regions where increases occur during the ENSO year show as negative regions (enclosed by a dotted line) on the maps.

The surface temperature perturbation map 64 shows a marked temperature increase in the eastern Pacific which extends to the coast of South America. In fact in the north it extends through Central America and into the Caribbean and Atlantic. Concurrent temperature decreases occur in the northern and southern eastern Pacific at mid latitudes. There is a temperature increase over north Africa and the Near East with a maximum of 5° C near the west coast of Africa. As normal the temperature swings over land can be larger than those over the ocean. Also note the temperature increase in the southwest Indian Ocean around Madagascar.

A major shift in the tropical cloud patterns accompanies the temperature changes (map 65). Cloud amount and height decrease over Indonesia and increase and increase in the central and eastern Pacific and over the Gulf of Mexico. At about 25° S. latitude, note the eastward shift of the South Pacific Convergence Zone. This causes a cloud decrease in the west and an increase in the east. Also note the decrease over Brazil. In this year draughts occurred over both Indonesia and Brazil while increased rain fall occurred in the eastern Pacific.

4.3. Time Development

The strongest ENSO perturbations are regional and tend to shift location from month to month.

For a given calendar month , the maps show the difference between the mean for the four non ENSO years and the ENSO month. The difference maps for the four mid season months (January, April, July and October) are given. To Show the month to month variation, all 12 OLR maps are shown. Figure 4.5a shows the OLR difference field (4 year December mean minus December 1986). First a mean December OLR map for the years 1984 to 1985 and 1987 to 1988 was formed; then the OLR

map for December 1986 was subtracted from it. This procedure emphasizes the ENSO-related perturbations as compared to the non-ENSO years. Negative values (dashed contours) indicate an increase in the OLR and generally a decrease in cloud amount and cloud-top altitude in December 1986 compared to the other 4 years. Positive values (solid contours) indicate a decrease in OLR in December 1986. Similar difference maps were constructed for the other parameters and the other 11 months. There is a considerable repetition of information in all these maps hence only a selected group are shown here. In December 1986 (Map 67) the ENSO event is well underway in the western Pacific but has not yet extended far in the eastern tropical Pacific. Note however that the SPCZ has started to shift to the east. The time development of the ENSO perturbations are detailed below seperatelyfor the Pacific, Indean Ocean and Atlantic regions.

4.3.1. The Pacific Region

The largest and the best studied ENSO perturbations occurred in the Pacific. Throughout out the period December 1986 - October 1987 the tropical sea surface temperature (SST) east of the Date Line are some what higher than normal while pockets of below normal temperatures occur at mid latitudes. In January the warm waters along the South American coast push west along the Equator to the Date line. Although considerable month to month variation occurs, this belt is essentially maintained through October. An important feature is the southward extension of the warm waters slightly to the east of the normal position of the South Pacific Convergence zone (SPCZ). This moves the SPCZ eastwards towards the South American coast. The ENSO related deep convective changes are best followed in the OLR anomaly maps. Along the Equator eastward of 160 E longitude there is an increase in deep convective activity associated with the increase in SST. The maximum OLR anomaly, 101 W/m^2, occurs in January at 165 W longitude. The mature ENSO pattern occurs in April. The deep convective clouds have reached the American coast from Peru north to Panama while an arm extended towards the south east moves the SPCZ eastward. The dashed contours indicate decreases in the normal cloud cover to the west, north and south of this eastern Pacific deep convective region. After April the anomalous cloud cover withdraws from the South American coast

and also decreases in magnitude. However a remnant of the pattern persists through October in the central Pacific and over Indonesia.. Related development patterns are shown in the Short Wave and the Cloud Top Temperature anomaly maps.

4.3.2 The Indian Ocean

From December 1986 through April 1987 high OLR anomalies, indicating fewer clouds and less rain, drift back and forth across southern Africa. In December the Anomaly is in the center. It drifts to the west coast in January and then to the east coast and includes Madagascar in February. By April it covers most of the east coast from Angola through Somalia, the Arabian Peninsula and much of the adjacent Indian Ocean. In June there is a brief return to normal, but in July the high OLR anomaly returns from Kenya around through the west coast of India, south India, and across the mouth of the Bay of Bengal. August is fairly normal, but by October anomalous high clouds occur in the west Indian Ocean and along the West coast of Indian.

Krishnamurti et al. (1989) state that the normal Indian Monsoon season starts in June and is completed by the end of September or early October. However in the summer of 1987 there was a severe drought over much of India during June and July. Although some area in the northeast and south of India received above normal rainfall in August and September, most parts of northwest India and Pakistan continued to have below normal rain fall. Li and Yanai (1996) point out that: "The onset of the Asian summer monsoon is concurrent with the reversal of the meridianal temperature gradient in the upper troposphere south of the Tibetan Plateau. The reversal is the result of large temperature increases in May to June over Eurasia centered on the Plateau with no appreciable temperature change over the Indian Ocean." In the spring the Tibetan Plateau becomes a major heat source for the regional atmosphere. The Indian summer monsoon is generally weak during ENSO years but just how weak depends on several factors besides the ENSO related changes in the sea surface temperatures. Li and Yanai (1996) state that: "The strong (weak) Asian summer monsoon years are associated with (a) positive (negative) tropospheric temperature anomalies over Eurasia, but negative (positive) temperature anomalies over the Indian Ocean and the eastern Pacific; (b) negative

(positive) SST anomalies in the equatorial eastern Pacific, Arabian Sea, Bay of Bengal, and South China Sea, but positive (negative) SST anomalies in the equatorial western Pacific; and (c) strong (weak) heating and cumulus convection over the Asian monsoon region and the western Pacific, but weaker (stronger) heating and convection in the equatorial Pacific." Although the 1986/87 ENSO was only of medium strength the Indian draught was particularly severe in the summer of 1987 due to additional perturbations in the tropical atmospheric circulation patterns caused by the above mentioned factors.. In contrast The summer monsoon of 1988 was unusually strong.

4.3.3 The Atlantic Ocean

In December 1986 the surface air temperature was above normal in large areas of Africa and South America while the sea surface temperature (SST) was below normal over most of the north tropical and extra-tropical Atlantic. In the south extra-tropics the SST was below average off the east coast of South America but above average off the coast of Namibia. As the seasons progressed the Atlantic north extra-tropics became warmer than normal in February and remained so throughout April, the southern extra-tropical temperature was also above average. Over the summer the tropical and extra-tropical Atlantic SST varied from normal to warmer than normal.

The OLR and cloud top temperature anomaly maps show that from December 1986 through June 1987 there were fewer and lower clouds than normal over the Gulf of Guinea. At the peak in April the low cloud, draught belt stretched south west from Nigeria, across the Atlantic and South America through Peru.

REFERENCES

Barkstrom, B. R., E. Harridan, G. Smith, R. Green, J. Killer, R. Cess, and the ERBE Science Team, 1989: Earth Radiation Budget Experiment (ERBE) Archival and April 1985 Results, *Bull. Amer. Meteor. Soc.*, **70**, 1254-1262.

Brest, C. L. and W. B. Rossow, 1992: Radiometric Calibration and Monitoring of NOAA AVHRR Data for ISCCP, *Int. J. Em. Sense.*, **13**, 235-273.

Devore, J. L., 1982: Probability and Statistics for Engineering and the Sciences, Brooks/Cole Publishing Co., Monterey, California, 640 pp.

Dhuria, H. L. and H. L. Kyle, 1990: Cloud Types and the Tropical Earth Radiation Budget, *J. Climate*, **3**, 1409-1434.

Fu, R., W. T. Liu, and R. E. Dickinson, 1996: Response of Tropical Clouds to the Interannual Variation of Sea Surface Temperature, *J. Climate*, **9**, 616-634.

Klein, S. A. and D. L. Hartmann, 1993: Spurious Changes in the ISCCP Data Set, *Geophys. Res. Lett.*, **20**, 455-458.

Krishnamurti, T. N., H. S. Bedi, and M. Subramaniam, 1989: The Summer Monsoon of 1987, *J. Climate*, **2**, 321-340.

Krishnamurti, T. N., H. S. Bedi, and M. Subramaniam, 1990: The Summer Monsoon of 1988, *Meteorol. Atmos. Phys.*, **42**, 19-37.

Kyle, H. L., R. R. Hucek, and B. J. Vallette, 1991: Atlas of the Earth's Radiation Budget as Measured by Nimbus-7: May 1979 to May 1980, NASA RP-1263, 133 pp.

Kyle, H. L., J. R. Hickey, P. E. Ardanuy, H. Jacobowitz, A. Arking, G. G. Campbell, F. B. House, R. Maschhoff, G. L. Smith, L.L. Stowe, and T. VonderHaar, 1993: The Nimbus Earth Radiation Budget (ERB) Experiment: 1975-1992, *Bull. Amer. Meteor. Soc.*, **74**, 815-830.

Kyle, H. L., M. Weiss, and P. Ardanuy, 1995: Cloud, Surface Temperature, and Outgoing Longwave Radiation for the period 1979-1990, *J. Climate*, **8**, 2644-2658.

Li, C., and M. Yanai, 1996: The onset and interannual variability of the Asian summer monsoon in relation to land-sea thermal contrast, *J. Climate*, **9**, 358-375.

Ramanathan V., 1987: The Role of Earth Radiation Budget Studies in Climate and General Circulation Research, *J. Geophys. Res.*, **92**, 4075-4095.

Rossow, B. R. and R. A. Schiffer, 1991: ISCCP Cloud Data Products, *Bull. Amer. Meteor. Soc.*, **72**, 2-20.

Wielicki, B. A. and R. N. Green, 1989: Cloud Identification for ERBE Radiative Flux Retrieval, *J. Appl. Meteor.*, **28**, 1131-1146.

ACRONYMS

ERBE	Earth Radiation Budget Experiment
ERBS	Earth Radiation Budget Satellite
ISCCP	International Satellite Cloud Climatology Project
ITCZ	inter tropical Convergence Zone
OLR	outgoing longwave radiation
LW	longwave
NOAA	National Oceanic and Atmospheric Administration (The acronym NOAA is also used as a suffix in the proper name of the polar orbiting weather satellites such as NOAA-9.)
NR	net radiation
SAT	surface air temperature
SPCZ	South Pacific Convergence Zone
SW	shortwave

Figure captions:

Figure 1. Monthly hemispherical averages of the net radiation are shown. The ERBE scanner measurements are for the year February 1985 to 1986. For comparison the Nimbus-7 ERB scanner measurements are shown for the period June 1979 to May 1980.
The small differences between the to curves are chiefly due to experimental errors rather than physical differences in the mean radiation budget during the two time periods.

Figure 2. Mean latitude band averages for the top of the atmosphere insolation (I), outgoing longwave radiation (LW), reflected shortwave (SW), and net radiation (NR) are graphed. The latitude is given in degrees with the South Pole on the left. The Earth Radiation Budget Experiment combined scanner data from the NOAA-9 and ERBS satellites is shown (Barkstrom et al., 1989) for: (a) the annual mean for February 1985-January 1986; (b) Northern Hemisphere winter, February & December 1985 plus January 1986; (c) Northern Hemisphere summer, June, July & August 1985.

Figure 3. ERBE scanner mean annual net radiation is mapped for February 1985 to January 1986. The units are W/m^2 and the contour interval is 20 W/m^2. The combined data from the NOAA-9 and ERBS satellites are shown.

Figure 4. ERBE annual net radiation cloud forcing is mapped for the year February 1985 to January 1986. the units are W/m^2 and the contour interval is 15 W/m^2. Solid contours indicate positive values and dashed contours show negative values. Dotted regions indicate data gaps (see 70^o S latitude).

Figure 5. ERBE latitude band averages of the longwave (LW), shortwave (SW), and net radiation (NR) cloud forcing for the: (a) annual mean, February 1985-January 1986; (b) Northern Hemisphere winter, February & December 1985 and January 1986; and (c) Northern Hemisphere summer, June - August 1985.

Figure 6. Annual cycle correlations between the net radiation and the solar insolation; a value of 1 would indicate a perfect positive correlation. Sixty monthly means (December 1984-November 1989) from the ERBS measurements were used. The contour step is 0.05 and contours are not printed for correlations less than 0.5.

Figure 7. Feedback relationships between the surface temperature, Ts, and the top-of-the-atmosphere net radiation (NR) are indicated.
The solar insolation (I), the absorbed shortwave radiation (ASW), the emitted longwave radiation (LW), the cloud amount (Cld), the cloud top temperature (Tc), and the temperature difference (T= Ts-Tc) are important quantities involved in the feedback loop as are the energy divergence terms (not shown). The contour interval is 0.2 from -0.9 to +0.9 and dashed contour indicate negative values.

Figure 8. Annual cycle correlations between the net radiation and the surface temperature are shown for the surface temperature lagged by: (a) 0 months, (b) 1 month, (c) 2 months, and (d) 3 months--see text. The contour interval is 0.2 from -0.9 to +0.9 and dashed lines indicate negative values.

Figure 9. The annual cycle correlations of cloud cover to (a) the insolation and (b) surface temperature. No lag time is included. The contour interval is 0.2 from -0.9 to +0.9 and dashed lines indicate negative values.

Figure 10. The annual cycle correlation between the outgoing longwave radiation and the surface air temperature is shown. The contour interval is 0.2 from -0.9 to +0.9 and dashed lines indicate negative values.

Figure 11. Topical (22.5°N-22.5°S) interannual surface air temprature and outgoing longwave radiation anomalies for the 1979-89. The data has been smoothed with a twelve month running mean
to remove seasonal variations.

Figure 12. Tropical (22.5oN-22.5oS) interannual surface air temperature and total cloud anomalies for the period 1979-1990.
The cloud data starts in april 1979 and the combining of the Nimbus-7 and ISCCP total cloud amounts is described in Kyle et al. (1995). The data has been smoothed with a twelve month running mean to remove seasonal variations.

Figure 13. The covariance of regional and the mean global OLR
are plotted for the peiod December 1984 to November 1989. The data has been smoothed with a 12 month running mean to remove seasonal variations.

Figure 14. Twelve month running means of the northern tropical OLR and atmospheric precipitable waterare plotted separately for land and water regions. Coastal regions were omitted in order to emphasize the different land and ocean behavior.

MAPS

Maps 1 - 12. Sixty month (5 year, December'84-November'89) means and standard deviations for net radiation, OLR, SW reflected, surface air temperature, cloud fraction, and cloud toip temperature.

Maps 13 - 60. Five year means and standard deviations for the four mid season calender months: January, April, July, and October. The means and standard deviations are for the five months in the period December'84-November'89.

Maps 61 - 66. Mean annual ENSO perpturbaions calculated as (four year annual mean (yrs 1,2,4,5) - ENSO year (3) annual mean).

Maps 67 - 98. Monthly mean ENSO perturbations calculated as (mean of month over 4 years (yrs. 1,2,4,5) - ENSO year (3) month). As usual the four mid season months are shown. In addition to show intra seasonal variations, the OLR perturbations are shown for all 12 months.

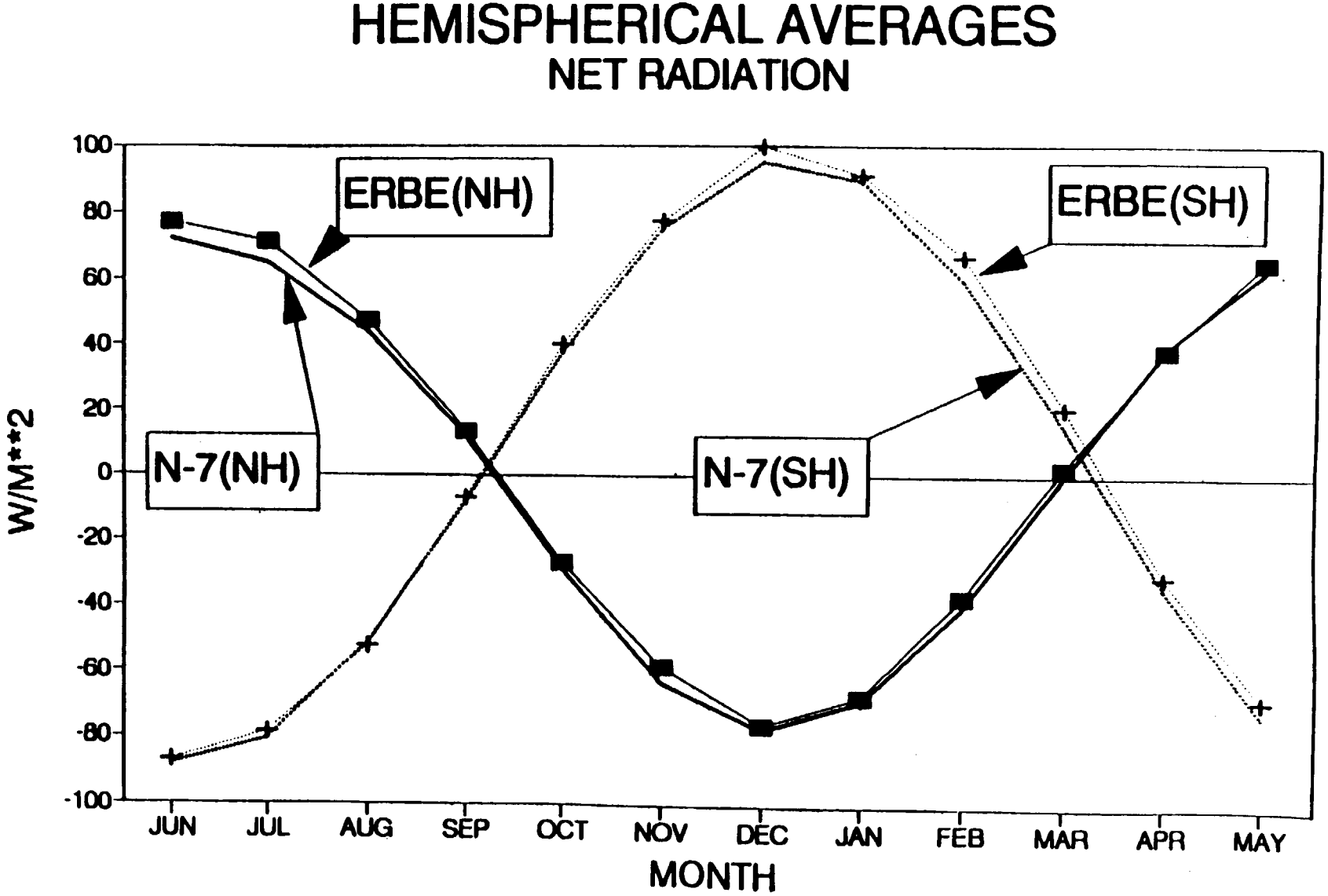
HEMISPHERICAL AVERAGES
NET RADIATION
ERBE(NH)
ERBE(SH)
N-7(NH)
N-7(SH)
W/M**2
100
80
60
40
20
0
-20
-40
-60
-80
-100
JUN
JUL
AUG
SEP
OCT
NOV
DEC
JAN
FEB
MAR
APR
MAY
MONTH

Fig. 1

ZONAL AVERAGES (ANNUAL)
N9ERBS SCANNER (ALL SKY)

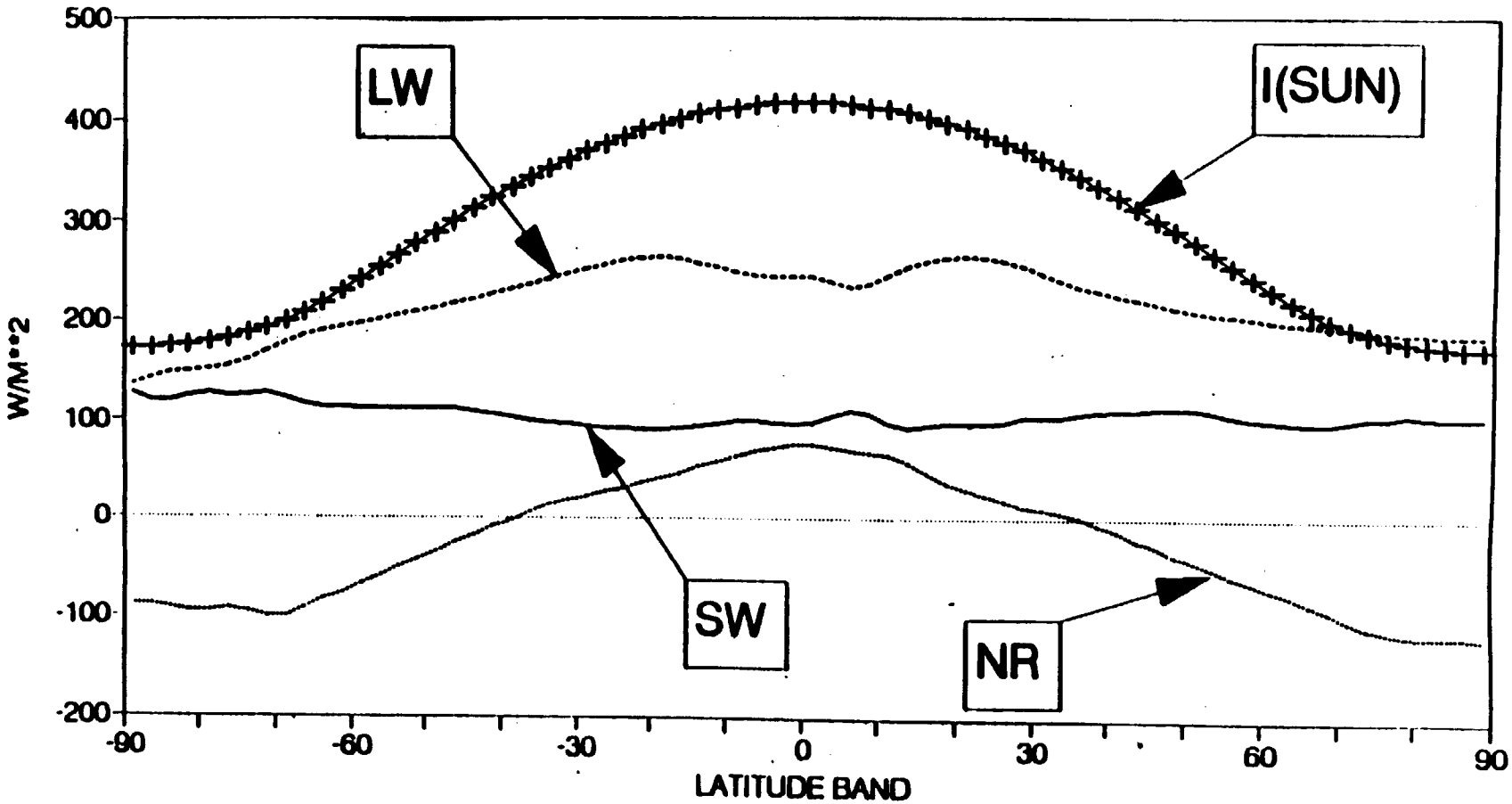

Fig. 2a

ZONAL AVERAGES (DJF)
N9ERBS SCANNER (ALL SKY)

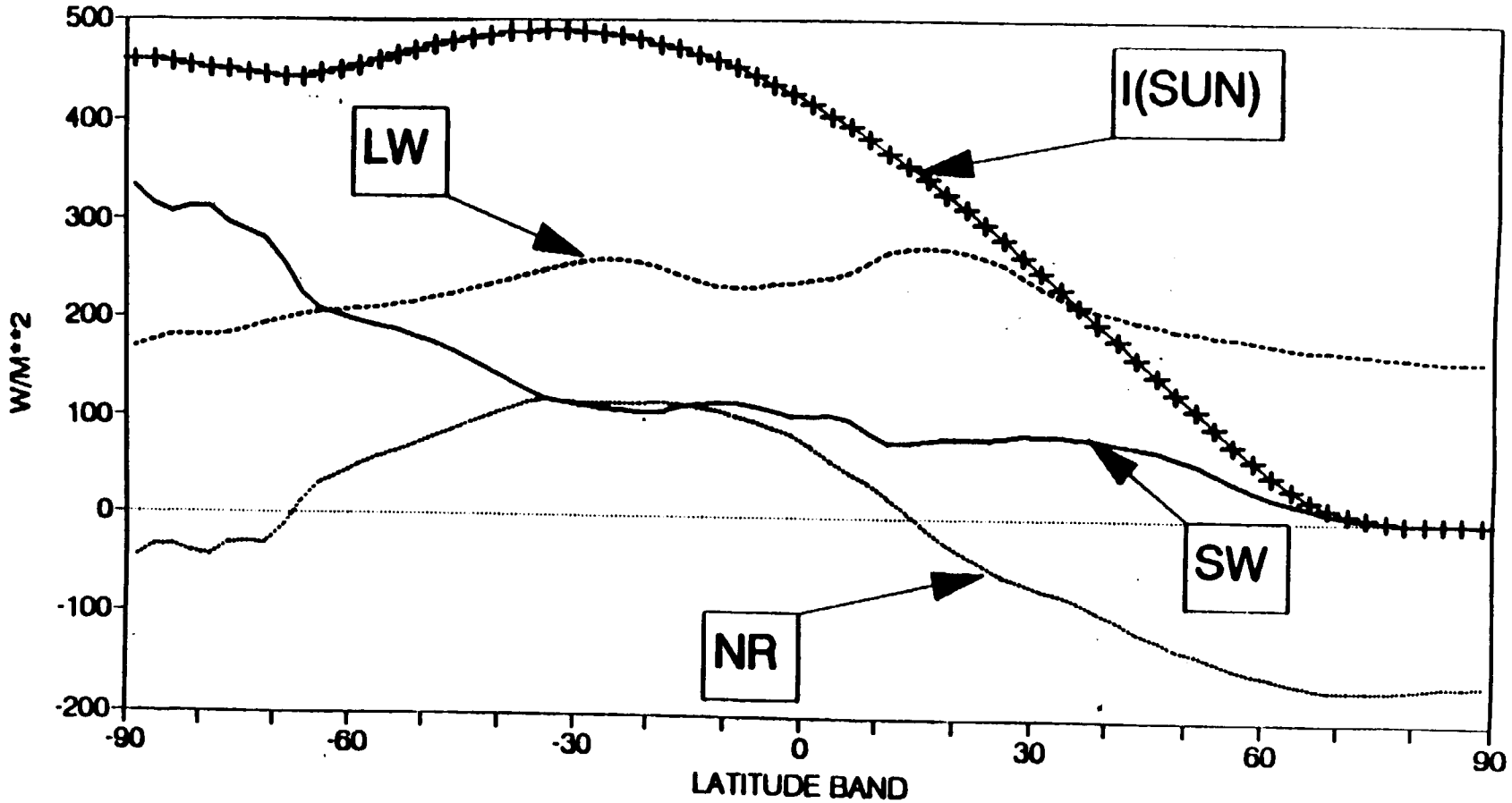

Fig. 2b

ZONAL AVERAGES (JJA)
N9ERBS SCANNER (ALL SKY)

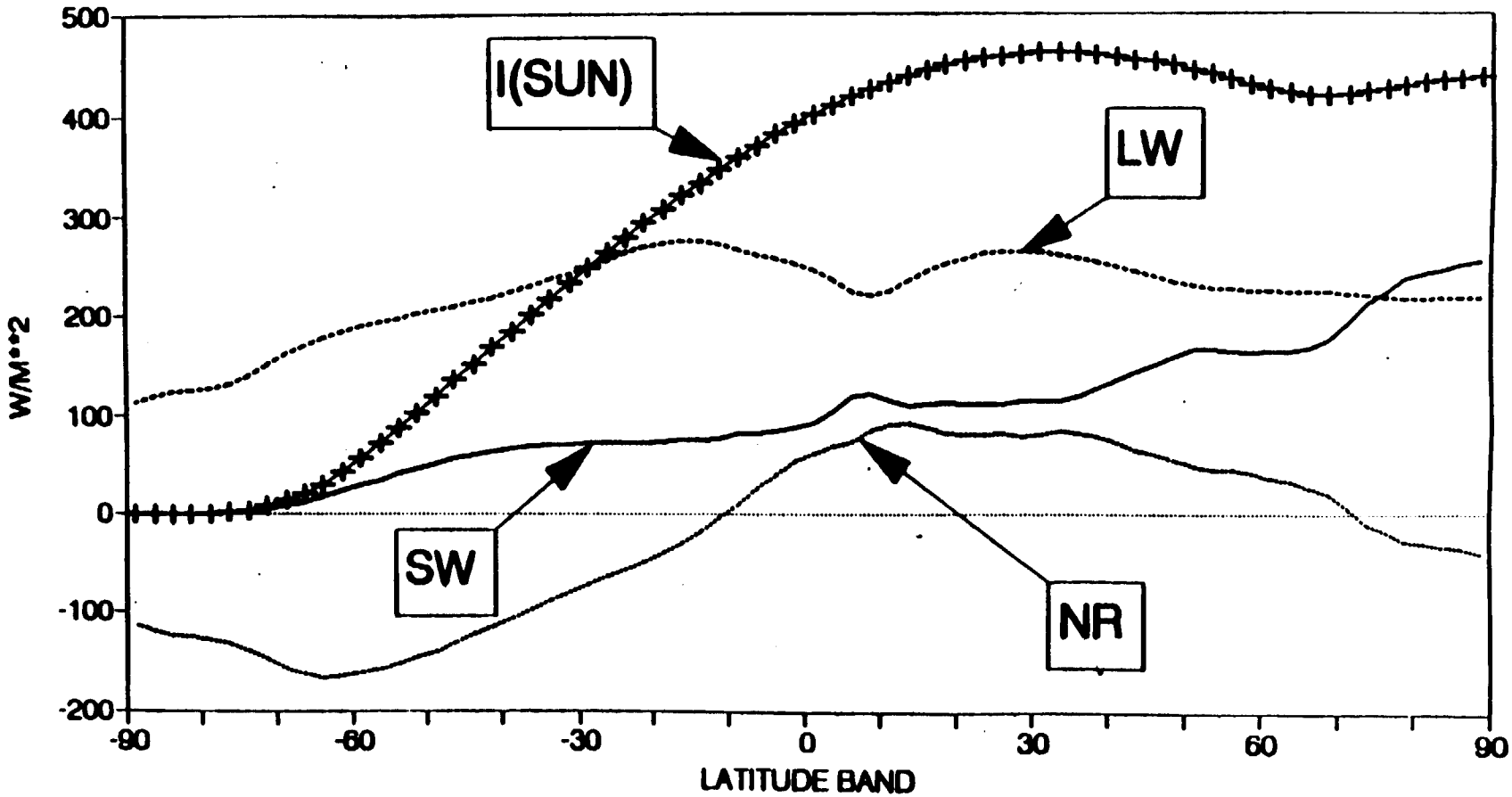

Fig 2c

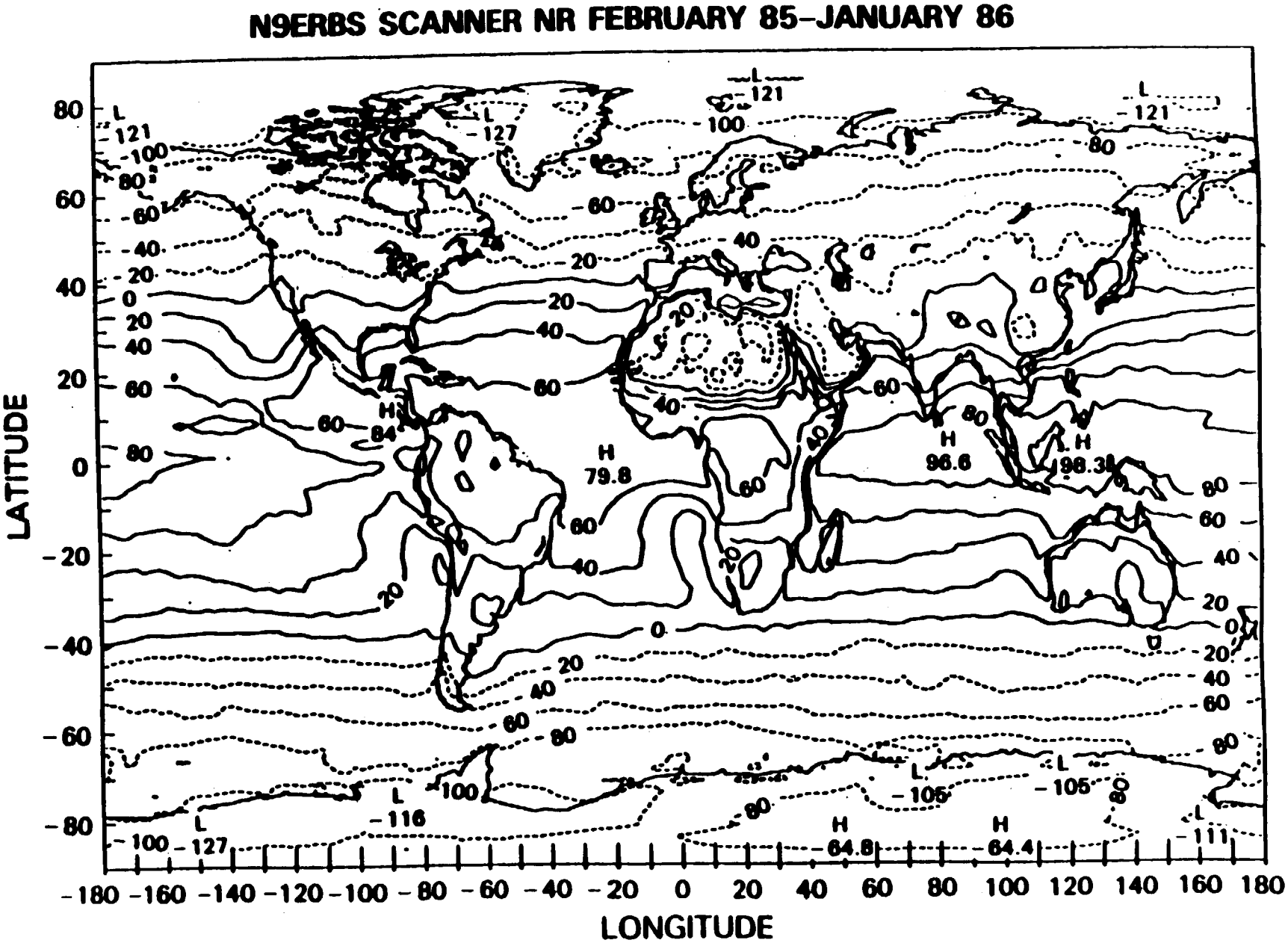
N9ERBS SCANNER NR FEBRUARY 85–JANUARY 86
LATITUDE
LONGITUDE
80
60
40
20
0
-20
-40
-60
-80
-180 -160 -140 -120 -100 -80 -60 -40 -20 0 20 40 60 80 100 120 140 160 180
L -121
L -127
L -116
L -105
L -111
H 79.8
H 96.6
H 98.3
H 64.8
H 64.4

Fig 3

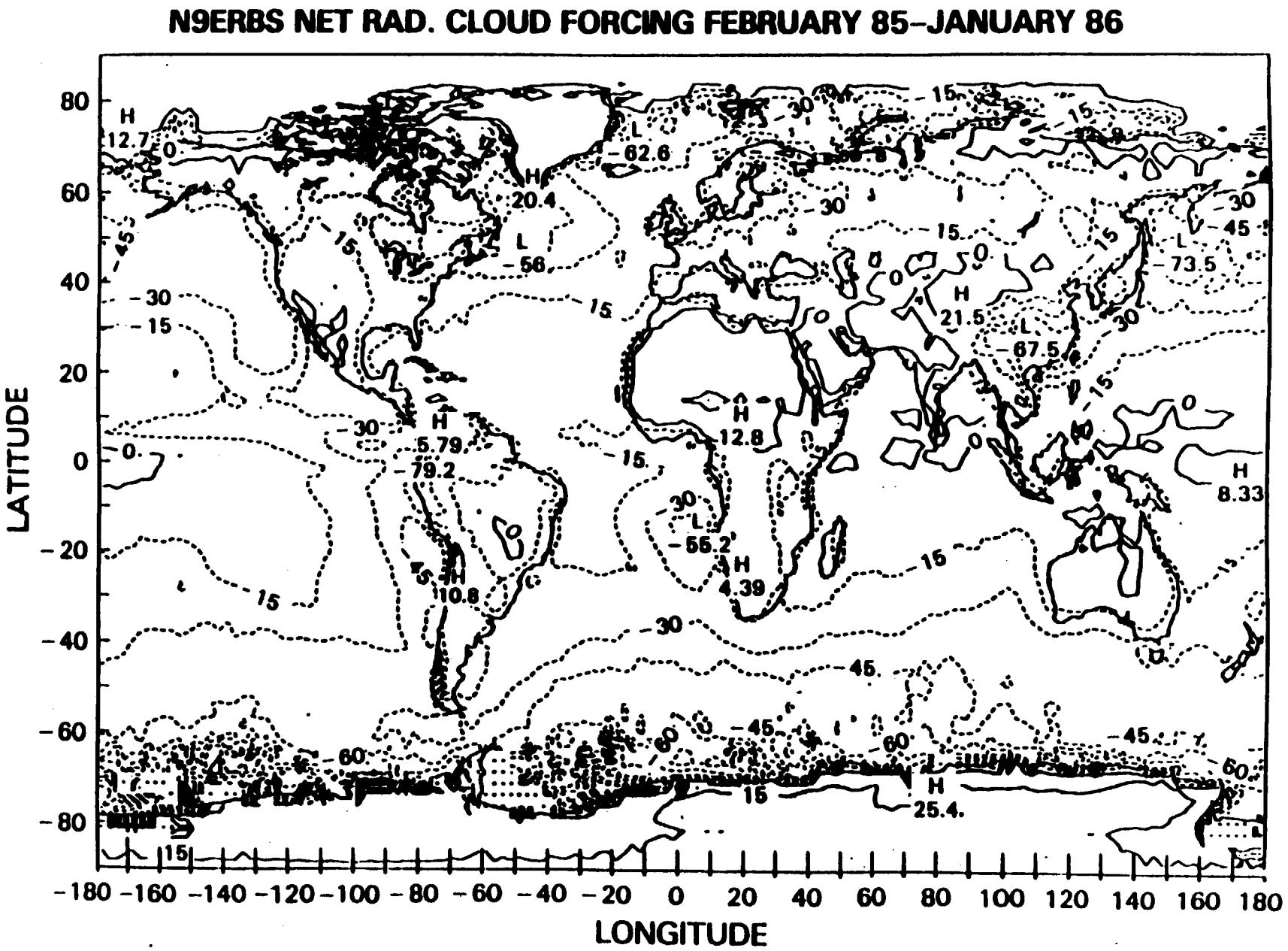
N9ERBS NET RAD. CLOUD FORCING FEBRUARY 85–JANUARY 86
LATITUDE
LONGITUDE
80
60
40
20
0
-20
-40
-60
-80
-180 -160 -140 -120 -100 -80 -60 -40 -20 0 20 40 60 80 100 120 140 160 180
H 12.7
L -62.6
H 20.4
L -56
H 21.5
L -67.5
L -73.5
H 5.79
-79.2
H 12.8
L -55.2
H 4.39
H 10.8
H 8.33
H 25.4.

Fig. 4

ZONAL AVERAGE CLOUD FORCING (ANNUAL)
N9ERBS SCANNER

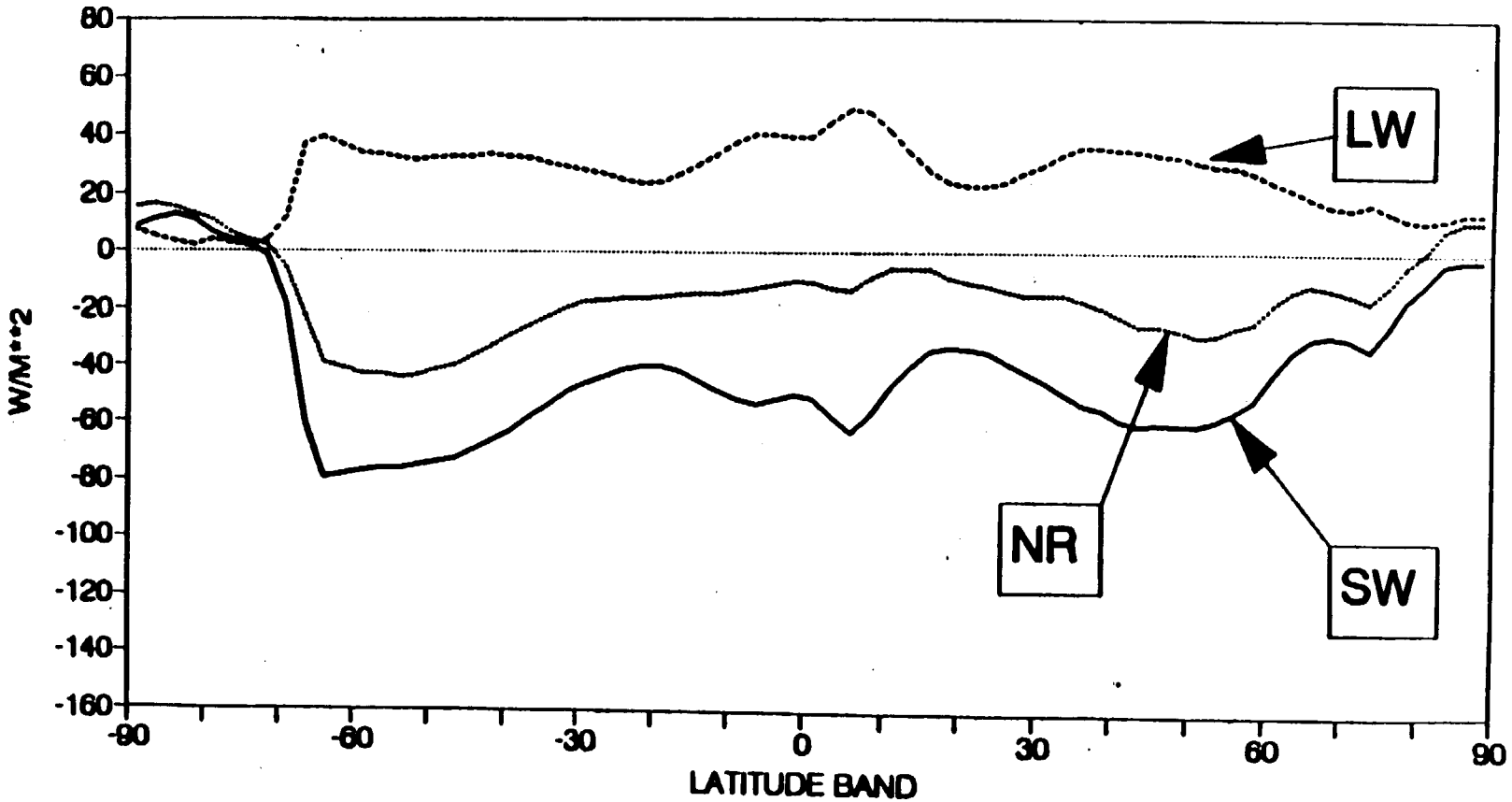

Fig. 5a

ZONAL AVERAGE CLOUD FORCING (DJF)
N9ERBS SCANNER

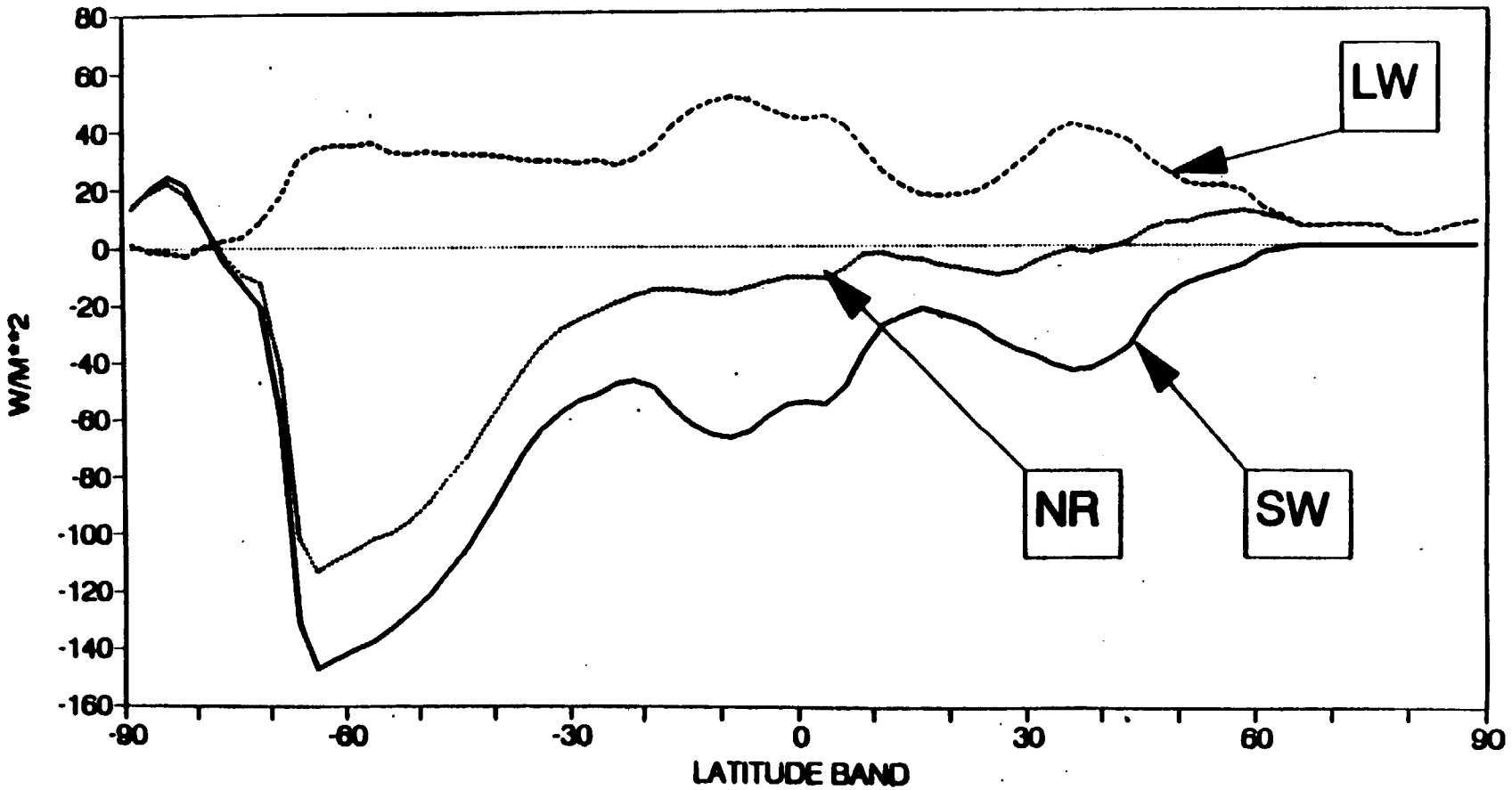

Fig. 5b

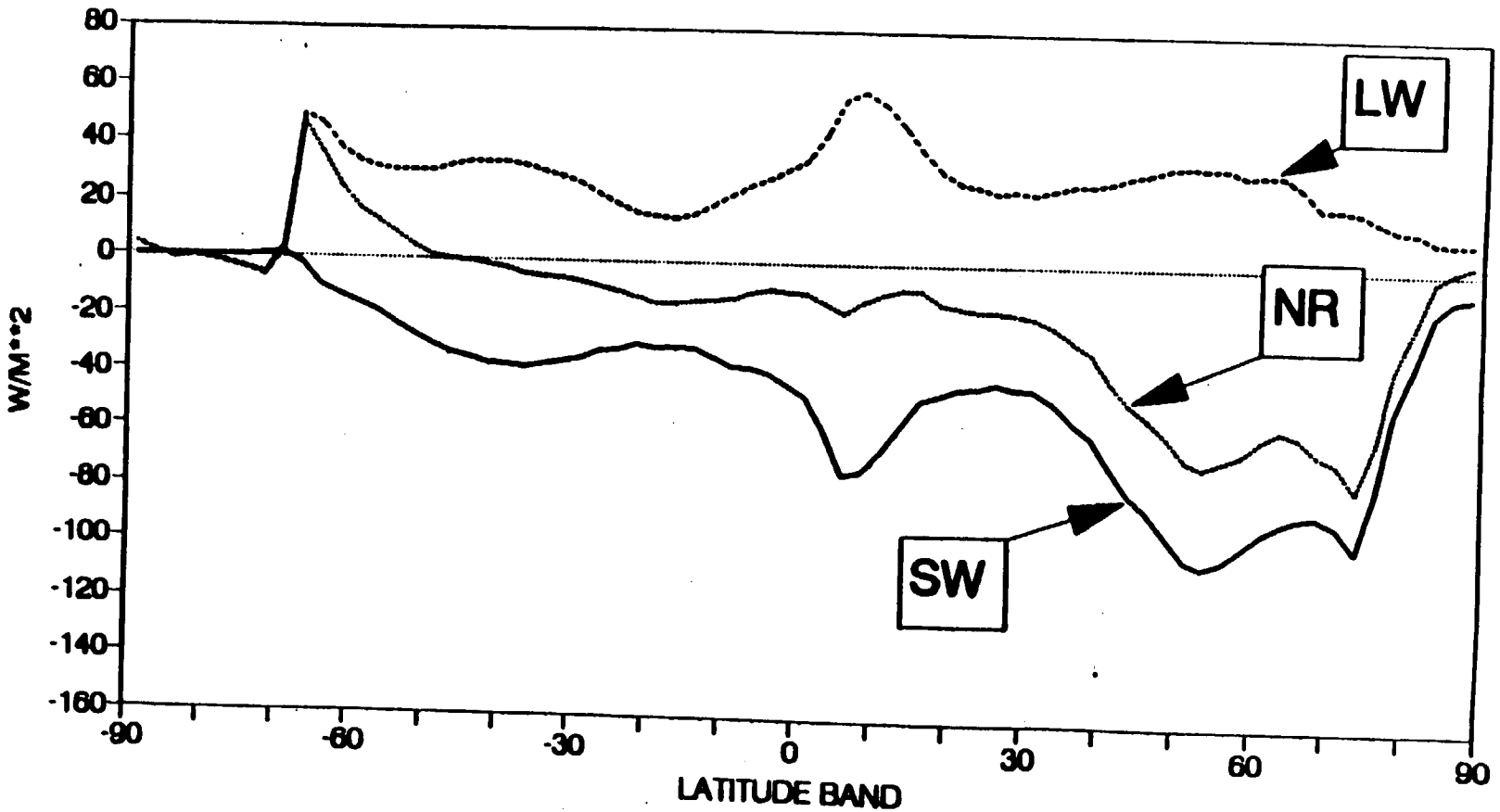
ZONAL AVERAGE CLOUD FORCING (JJA)
N9ERBS SCANNER
80
60
40
20
0
-20
-40
-60
-80
-100
-120
-140
-160
W/M**2
LW
NR
SW
-90
-60
-30
0
30
60
90
LATITUDE BAND

Fig. 5c

SOLR VS ASNT

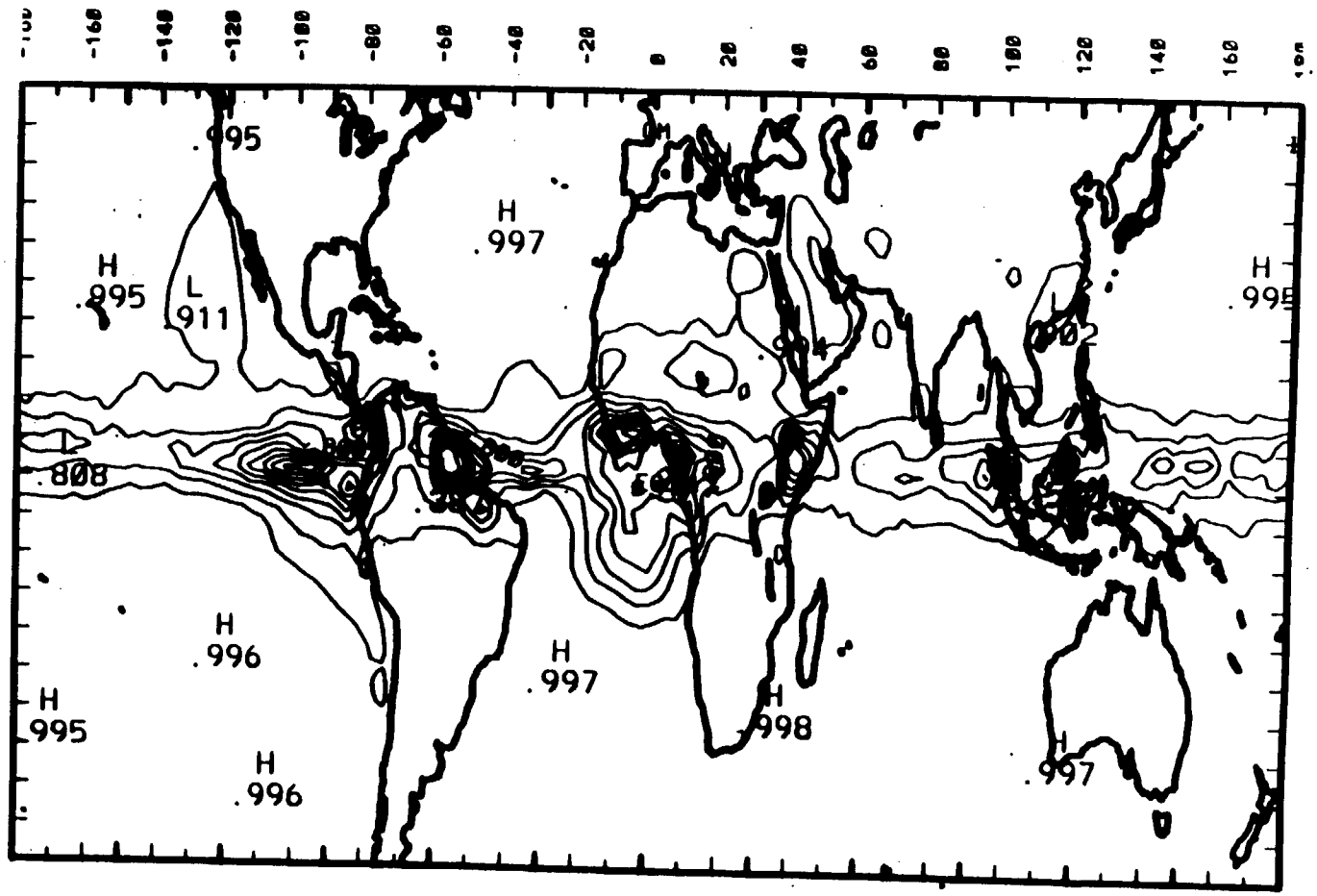

LONGITUDE

CONTOUR FROM 0.50000 TO 1.0000 CONTOUR INTERVAL OF 0.50000E-01 PT(3,3)= 0.99475

EXPECTED RELATIONSHIPS

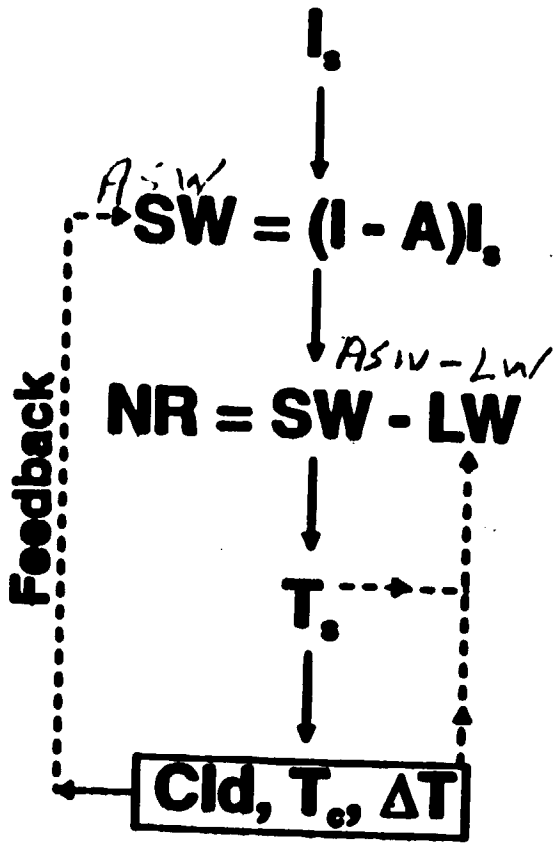

The response of T_s to variations in NR will depend upon the heat capacity of the surface, energy convection by oceanic and atmospheric currents plus other responses.

CORRELATIONS: LAG= Ø
NET RAD. VS SURF TEMP.

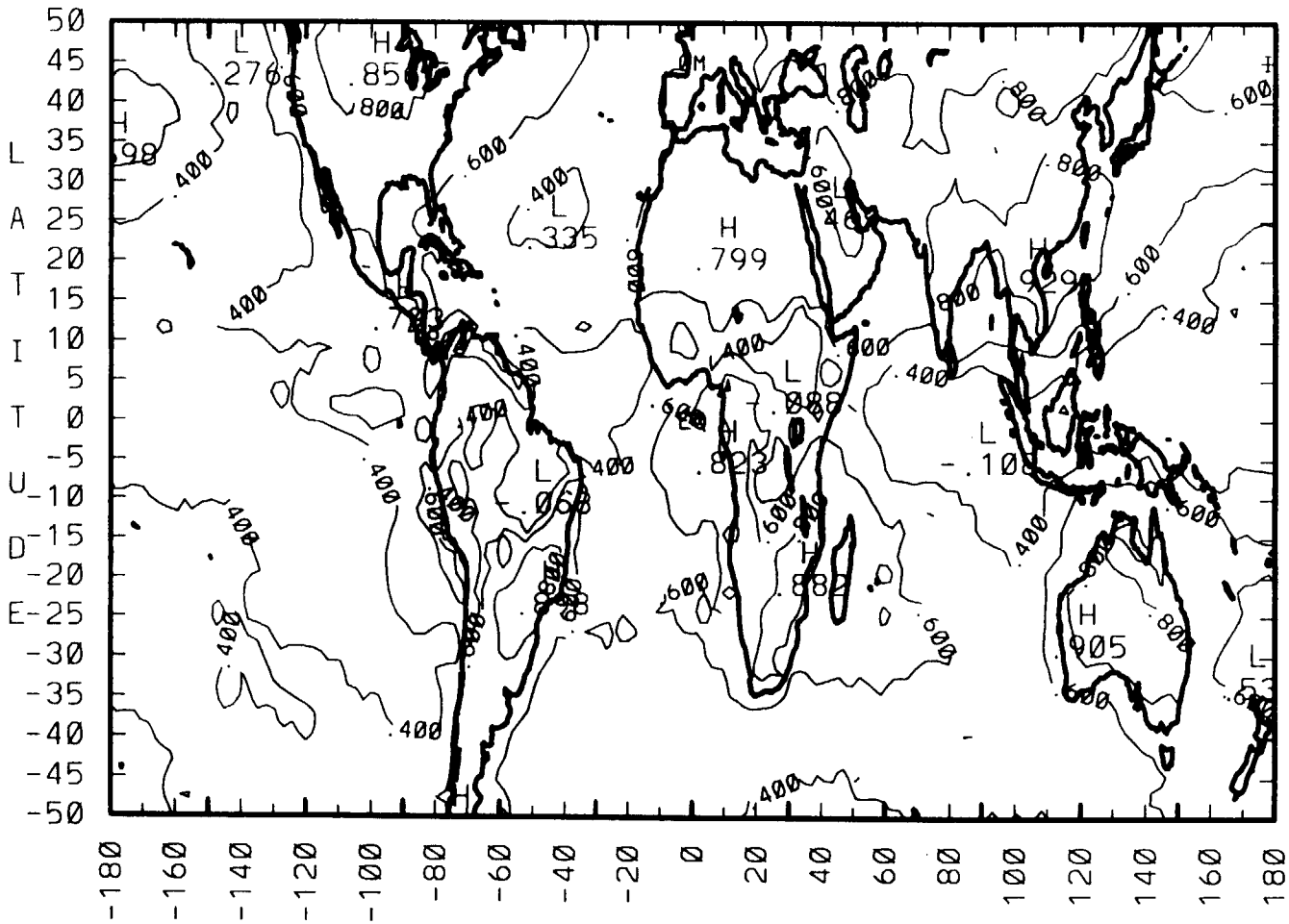

CONTOUR FROM 0140000 TO -0160000 CONTOUR INTERVAL OF 0.20000 PT(3,3)= 0.70405

Fig 8a

CORRELATIONS: LAG= 1
NET RAD. VS SURF TEMP.

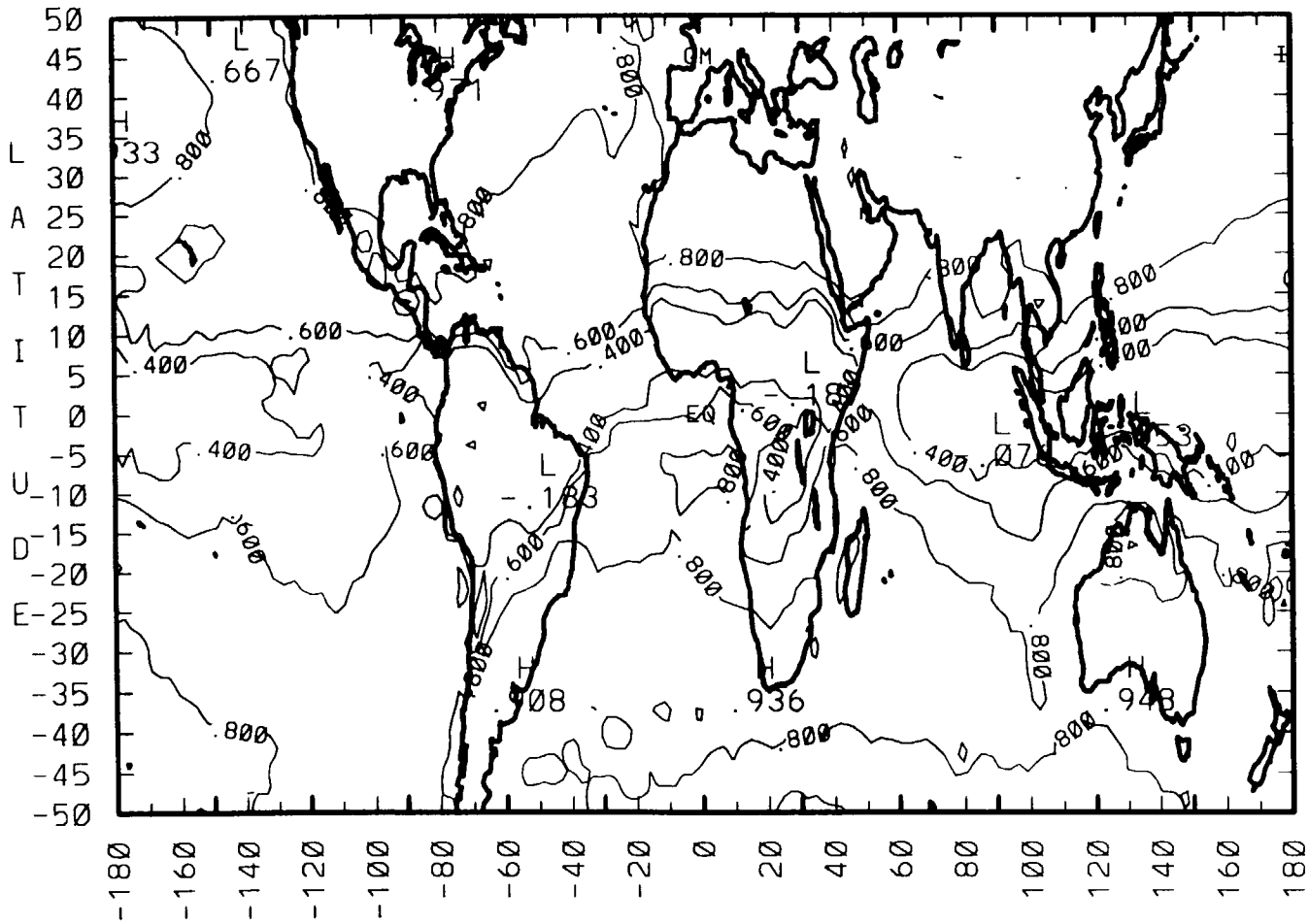

Fig 8b

CONTOUR FROM 0140000 TO -0160000 CONTOUR INTERVAL OF 0.20000 PI(3,3)= 0.90323

CORRELATIONS: LAG= 2
NET RAD. VS SURF TEMP.

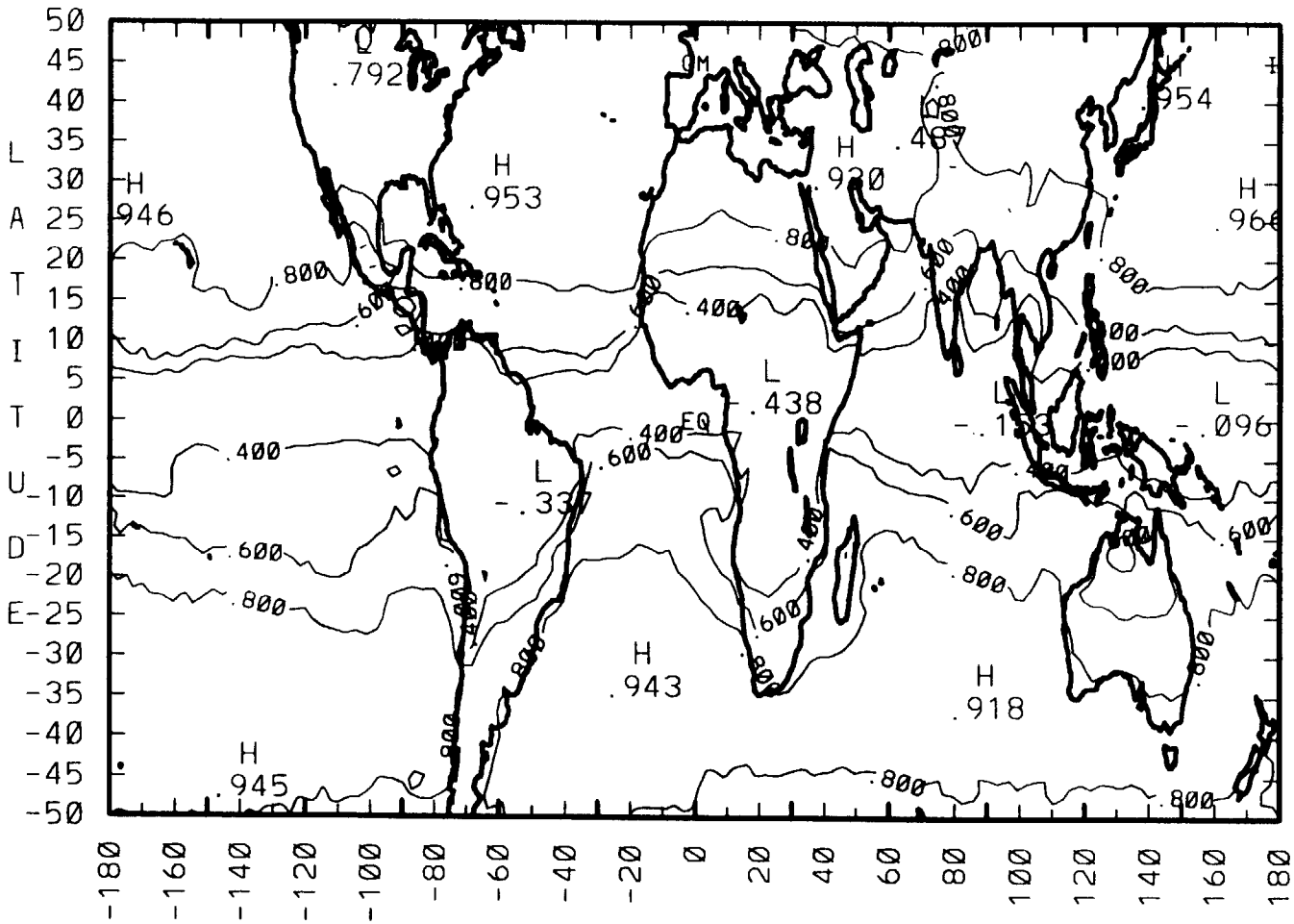

Fig 8c

CONTOUR FROM 0140000 TO -0160000 CONTOUR INTERVAL OF 0.20000 PT(3,3)= 0.86700

CORRELATIONS: LAG= 3
NET RAD. VS SURF TEMP.

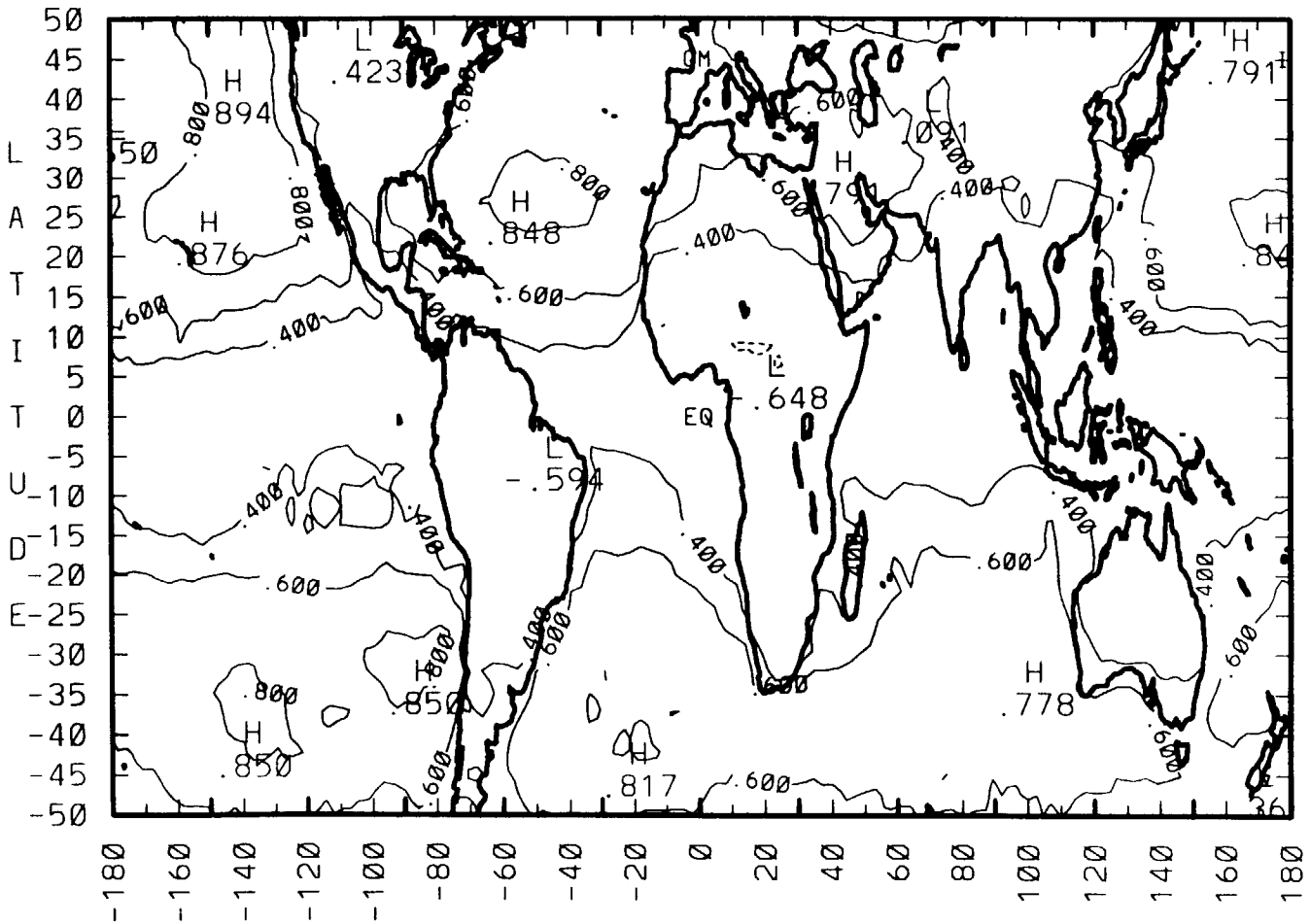

F,4 8a

CONTOUR FROM 0140000 TO -0160000 CONTOUR INTERVAL OF 0.20000 PT(3,3)= 0.58302

CORRELATIONS: LAG= Ø
SOLAR INS. VS CLD FRACT.

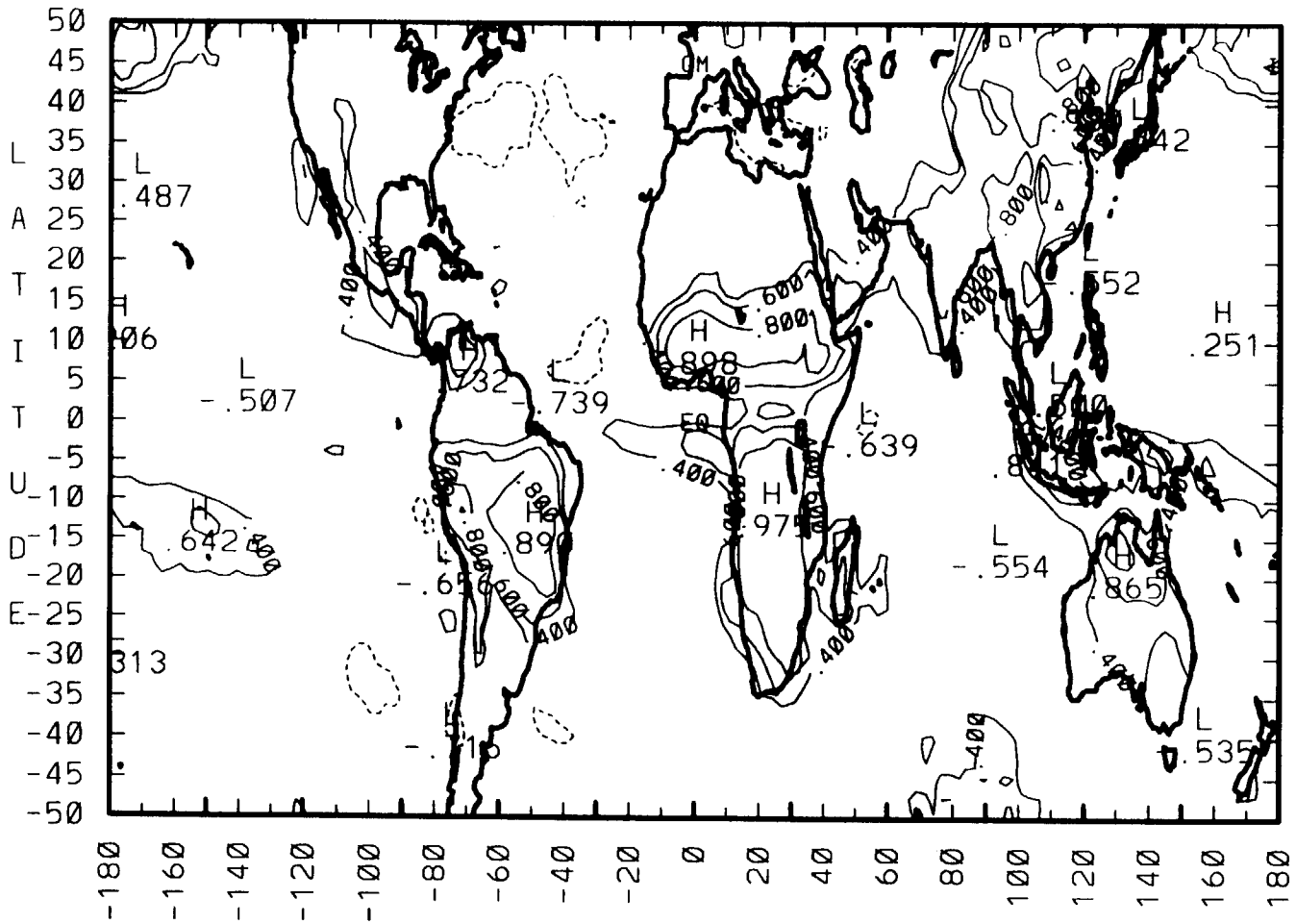

Fig 9a

CLPX VS NSFT - LAG=Ø

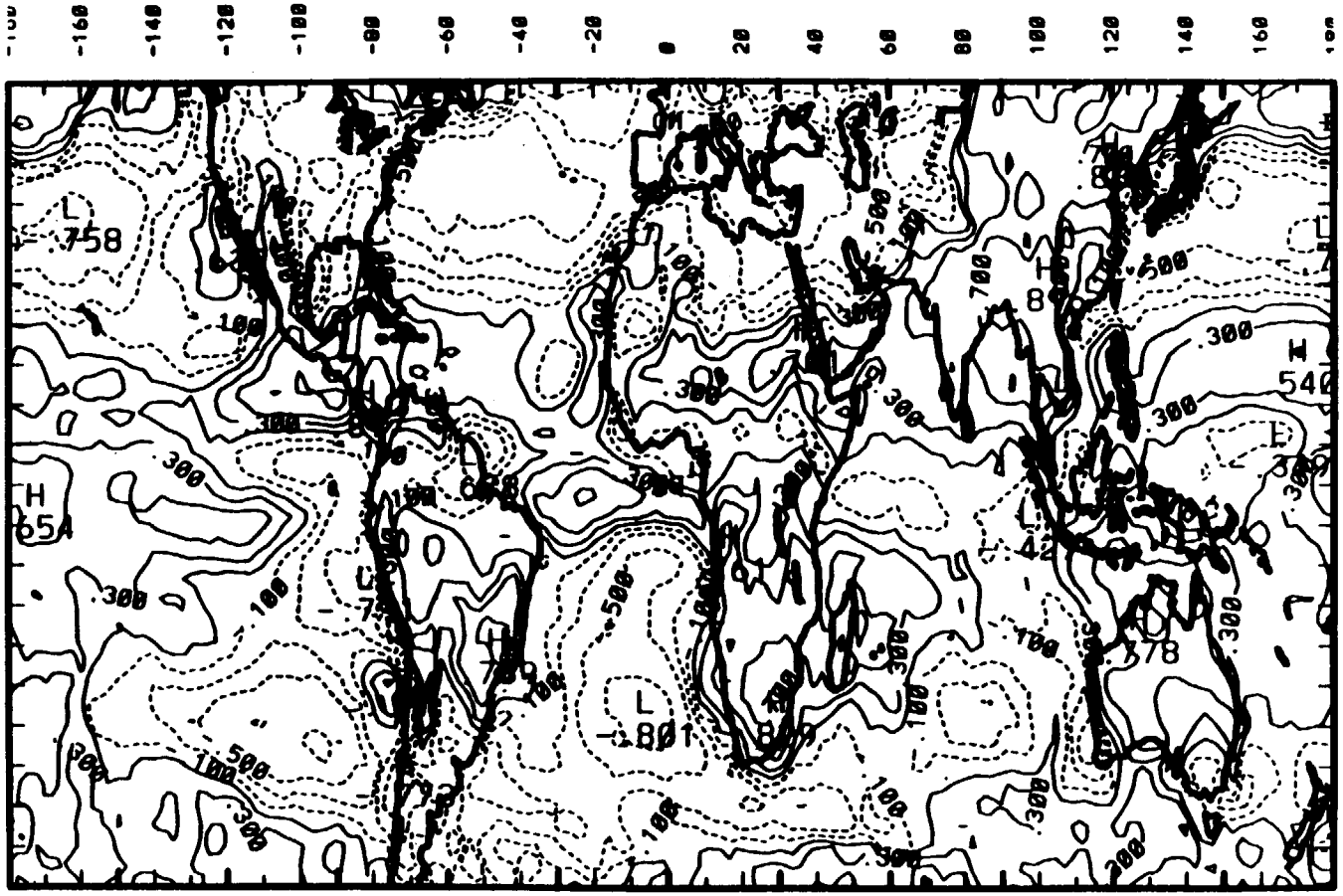

LONGITUDE

CONTOUR FROM -0.90000 TO 0.90000 CONTOUR INTERVAL OF 0.20000 PT(3,3)= -0.31891E-02

CORRELATIONS: LAG= Ø
OLR VS SURF TEMP.

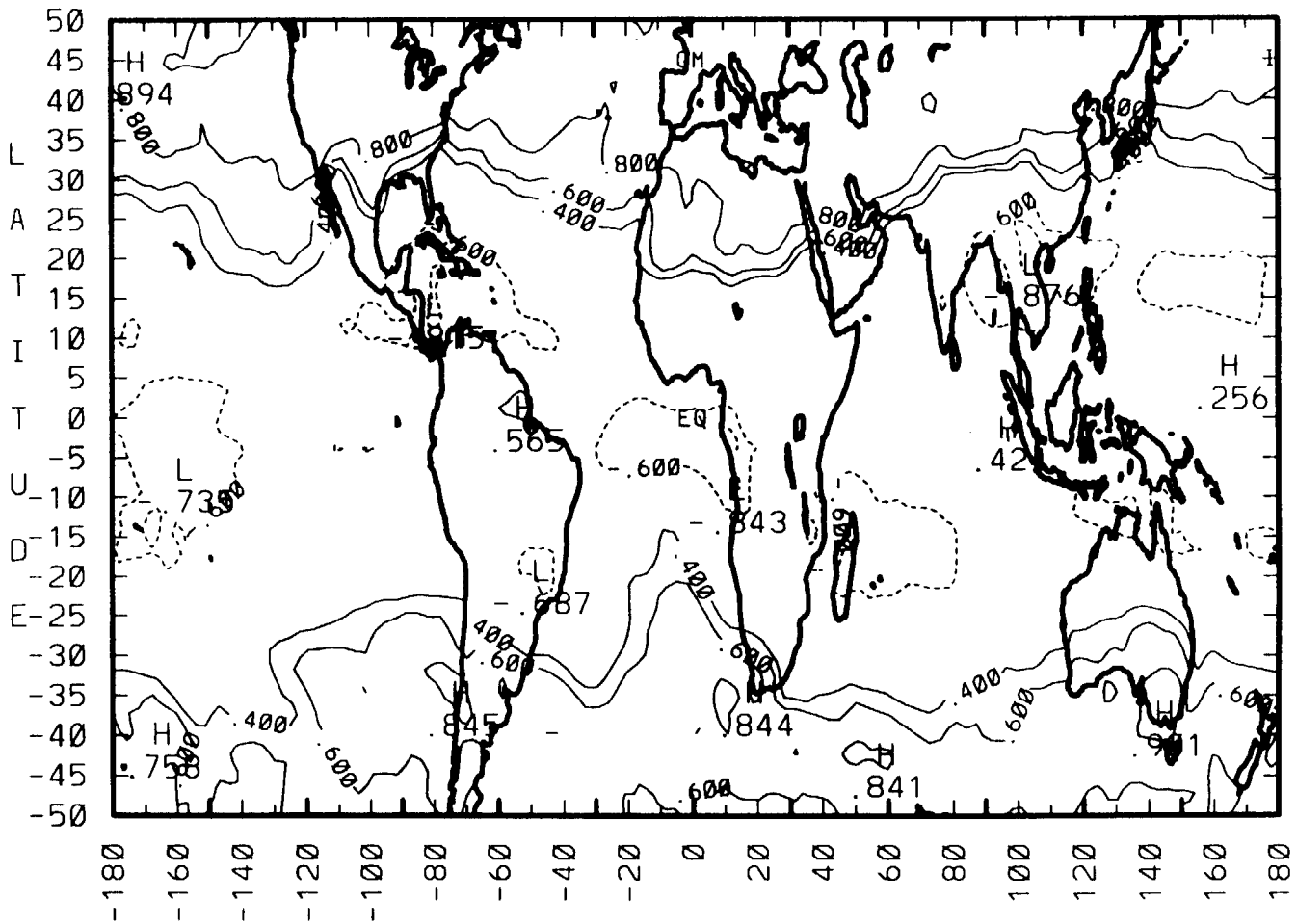

CONTOUR FROM Ø140000 TO -Ø160000 CONTOUR INTERVAL OF Ø.20000 PT(3,3)= Ø.70755

Fig 10

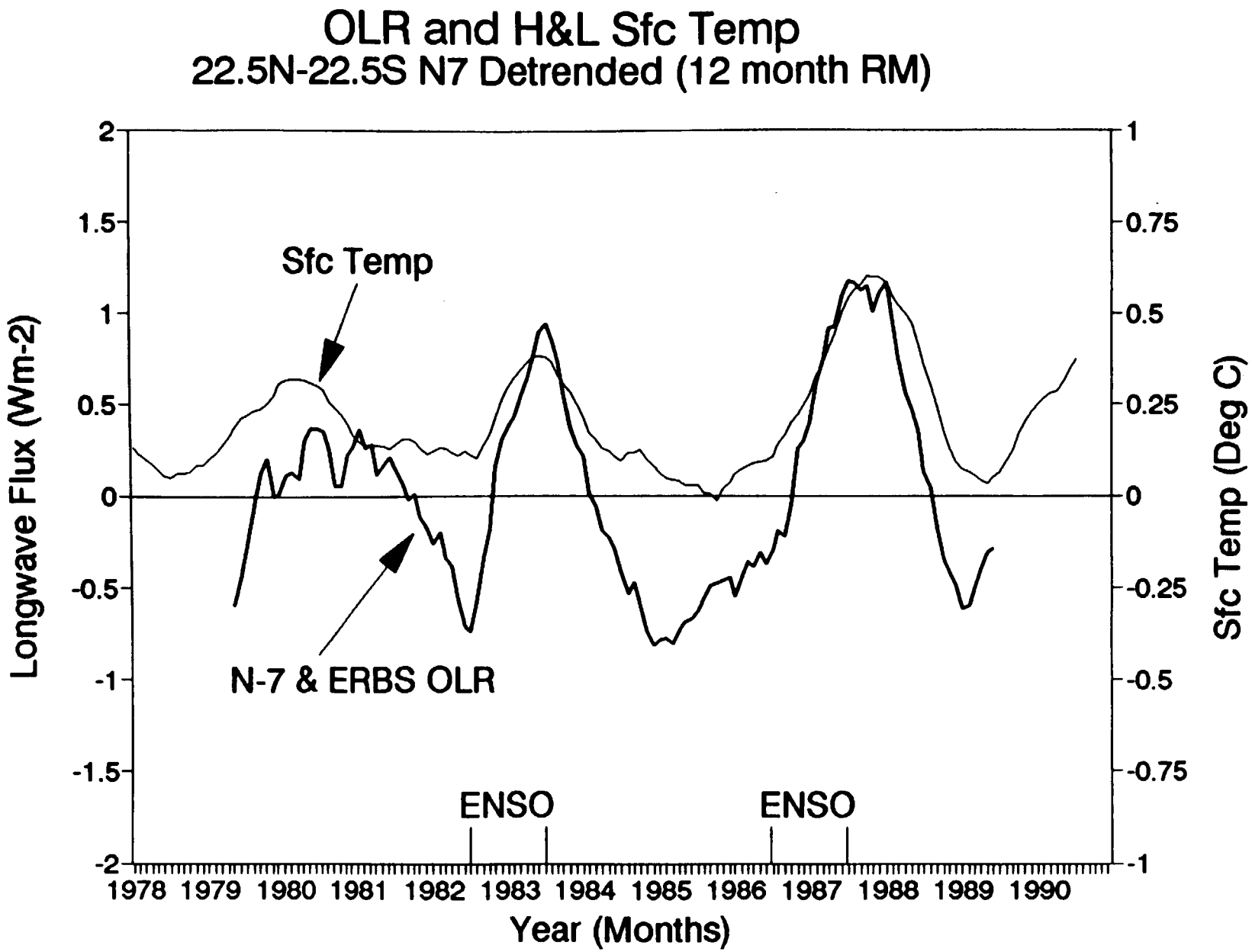

Fig. 1b. Tropical (22.5°N–22.5°S) interannual SAT and OLR anomalies for the period 1979–89. OLR anomalies are departures from the mean of the combined OLR dataset.

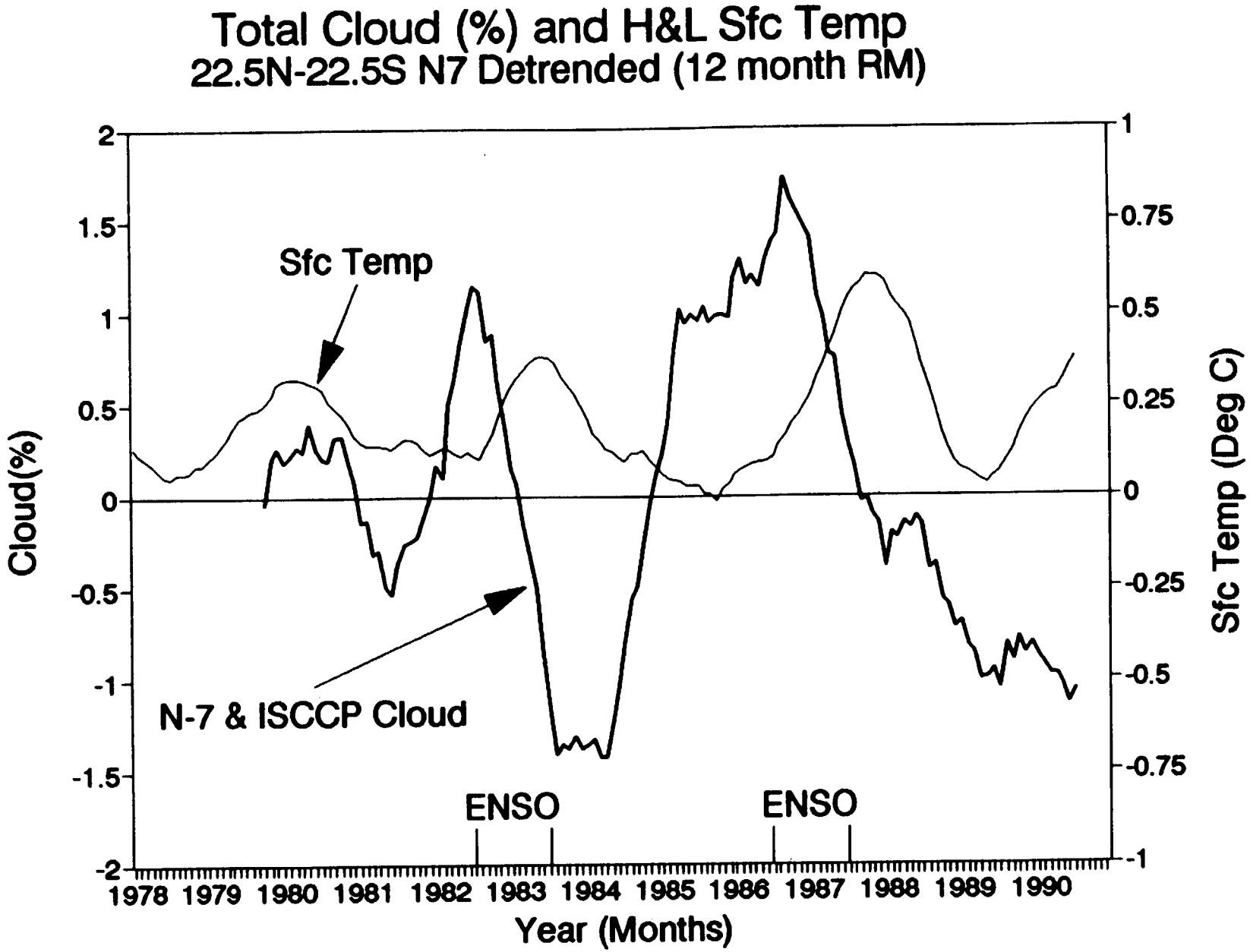
Total Cloud (%) and H&L Sfc Temp
22.5N-22.5S N7 Detrended (12 month RM)
Sfc Temp
N-7 & ISCCP Cloud
ENSO
ENSO
Cloud(%)
Sfc Temp (Deg C)
2
1.5
1
0.5
0
-0.5
-1
-1.5
-2
1
0.75
0.5
0.25
0
-0.25
-0.5
-0.75
-1
1978 1979 1980 1981 1982 1983 1984 1985 1986 1987 1988 1989 1990
Year (Months)

Fig 12

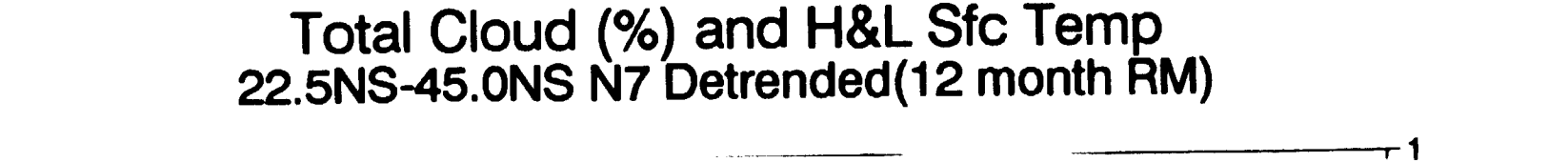
Total Cloud (%) and H&L Sfc Temp
22.5NS-45.0NS N7 Detrended(12 month RM)
1

REG VS GLO OLR COVAR (GLO TRND)

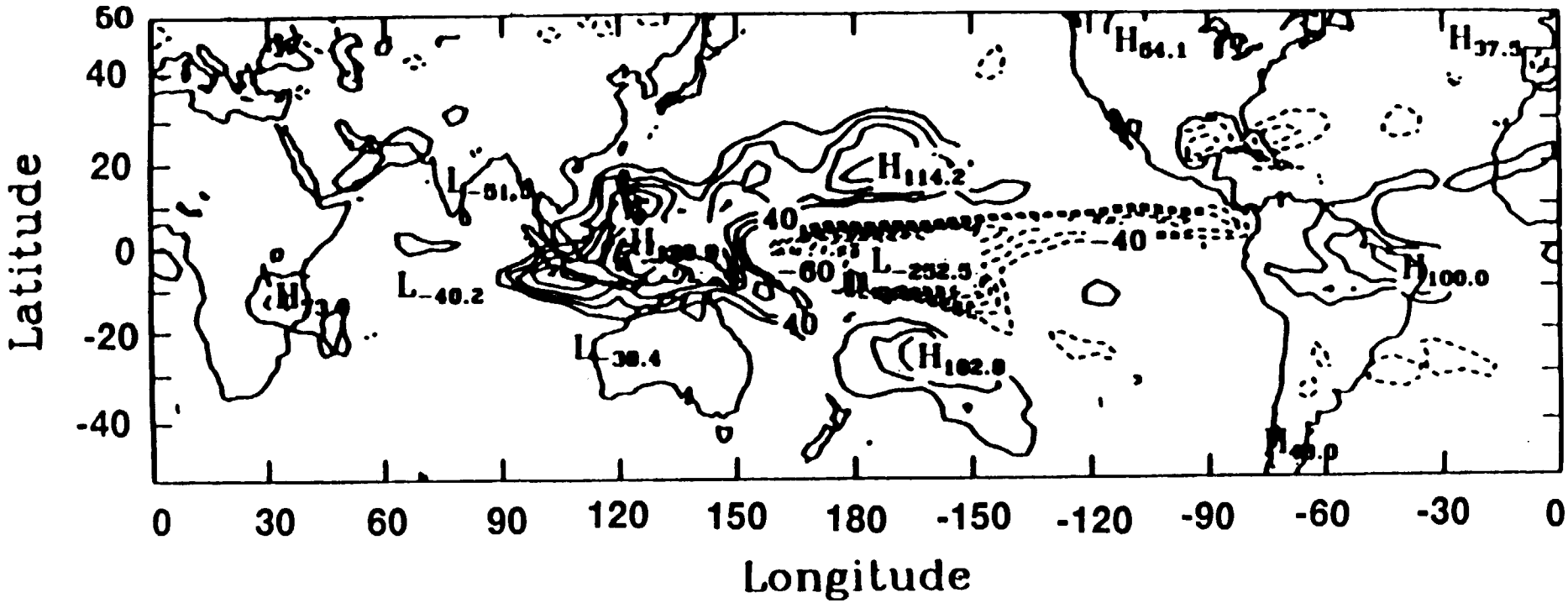

Fig 13

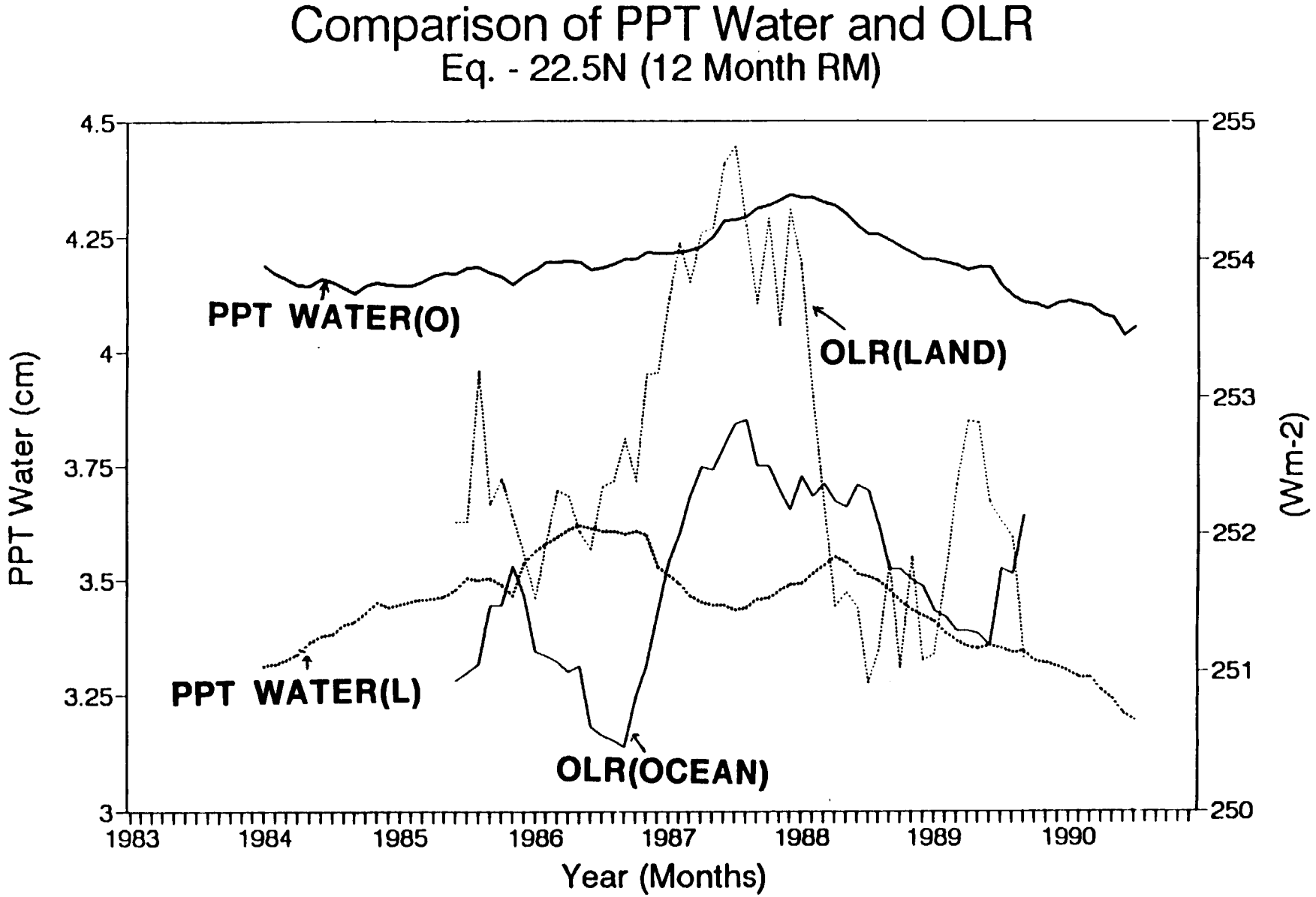
Comparison of PPT Water and OLR
Eq. - 22.5N (12 Month RM)
PPT Water (cm)
(Wm-2)
Year (Months)
PPT WATER(O)
PPT WATER(L)
OLR(LAND)
OLR(OCEAN)
4.5
4.25
4
3.75
3.5
3.25
3
255
254
253
252
251
250
1983
1984
1985
1986
1987
1988
1989
1990

Fig 4

5-YEAR MEANS (12/84 - 11/89)
NET RADIATION (Wm**2)

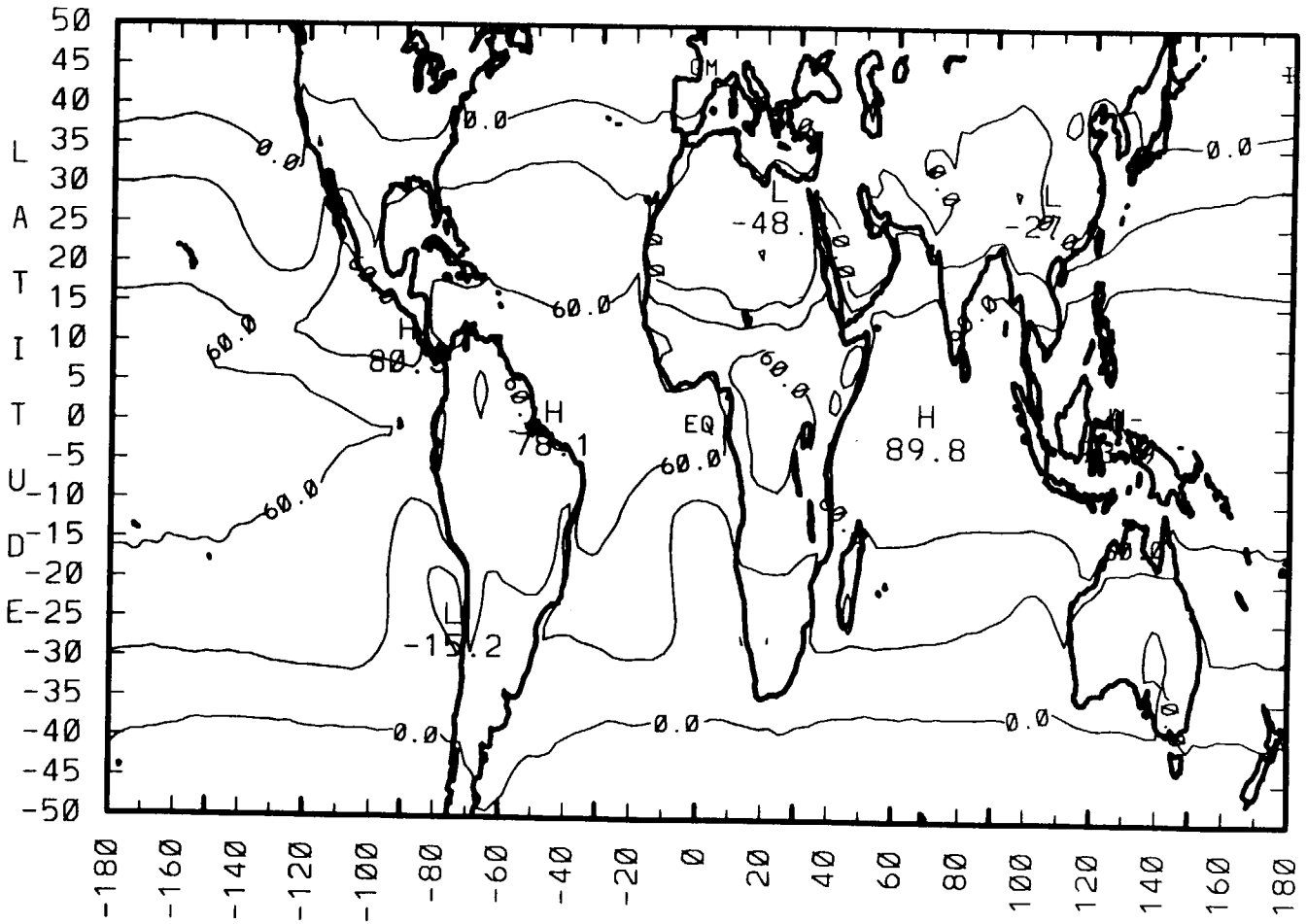

CONTOUR FROM 0.00000E+00 TO 240.00 CONTOUR INTERVAL OF 30.000 PT(3,3)= -18.932

M11

5-YR STANDARD DEVIATIONS
(1984 - 1989)
NET RADIATION (Wm**2)

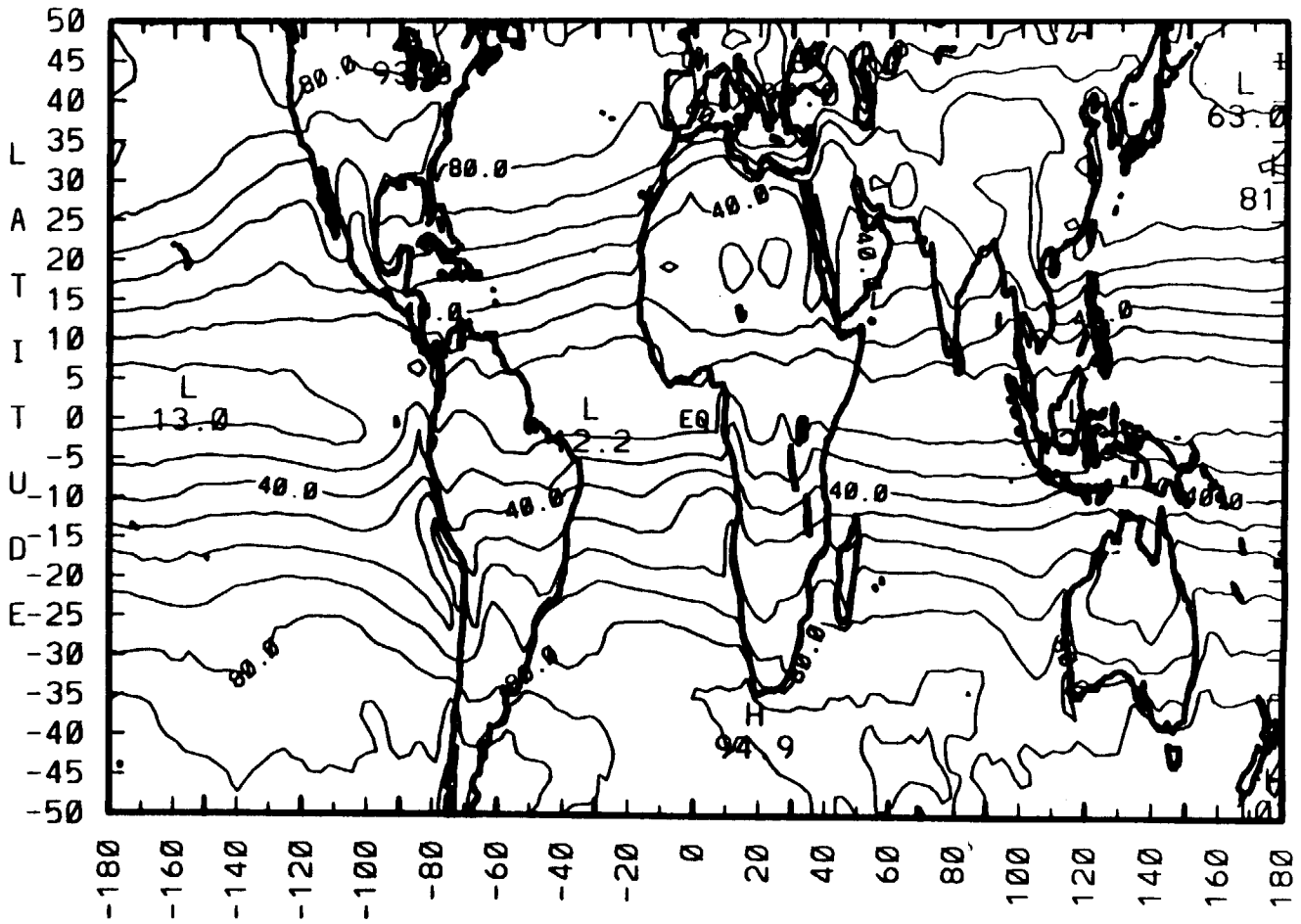

LONGITUDE

CONTOUR FROM 0.000000E+00 TO 100.00 CONTOUR INTERVAL OF 10.000 PT(3,3)= 94.480

M2

5-YEAR MEANS (12/84 - 11/89)
OLR (W/m**2)

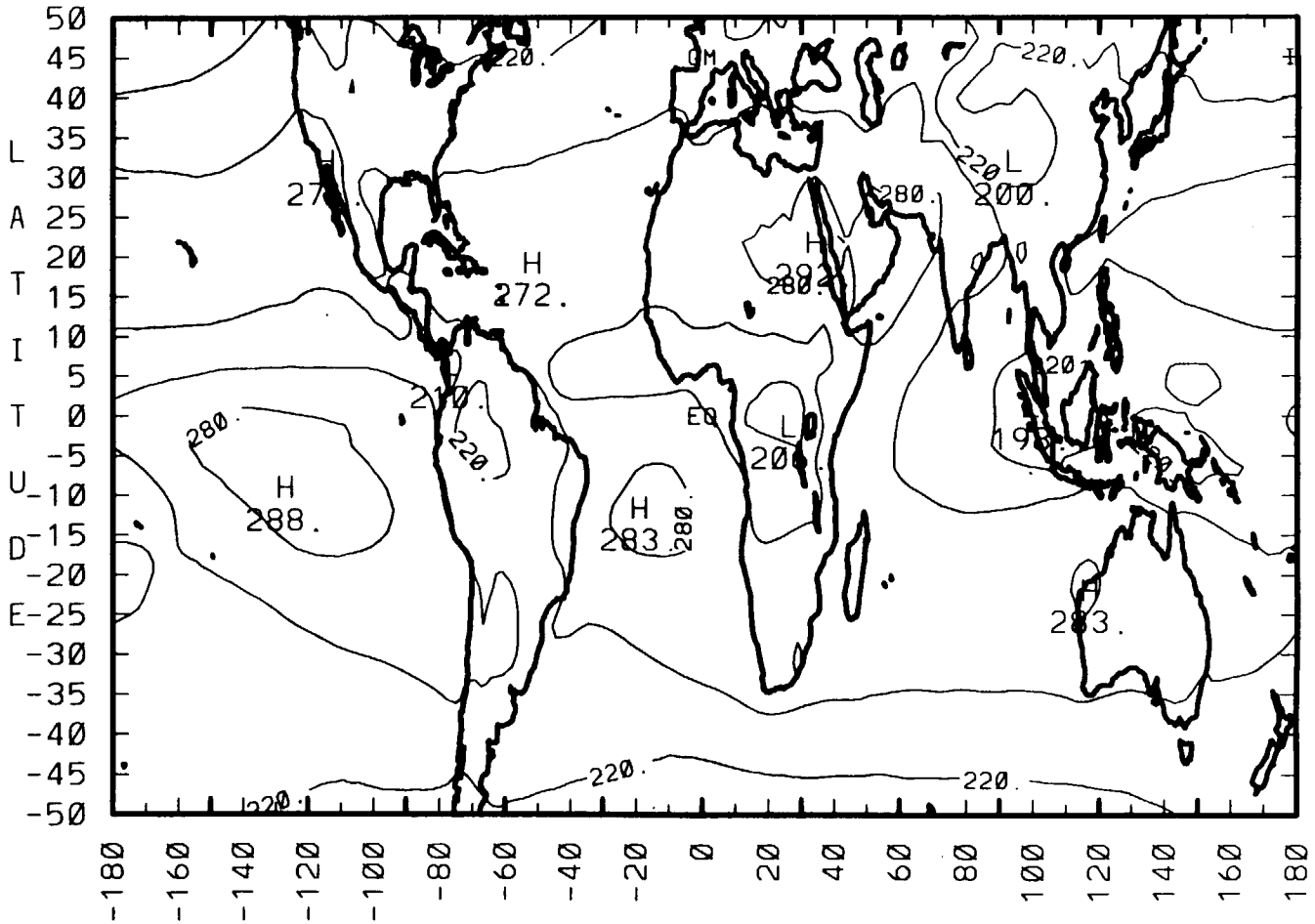

CONTOUR FROM 160.00 TO 280.00 CONTOUR INTERVAL OF 30.000 PT(3,3)= 229.53

5-YR STANDARD DEVIATIONS

(1984 - 1989)

OLR (W/m**2)

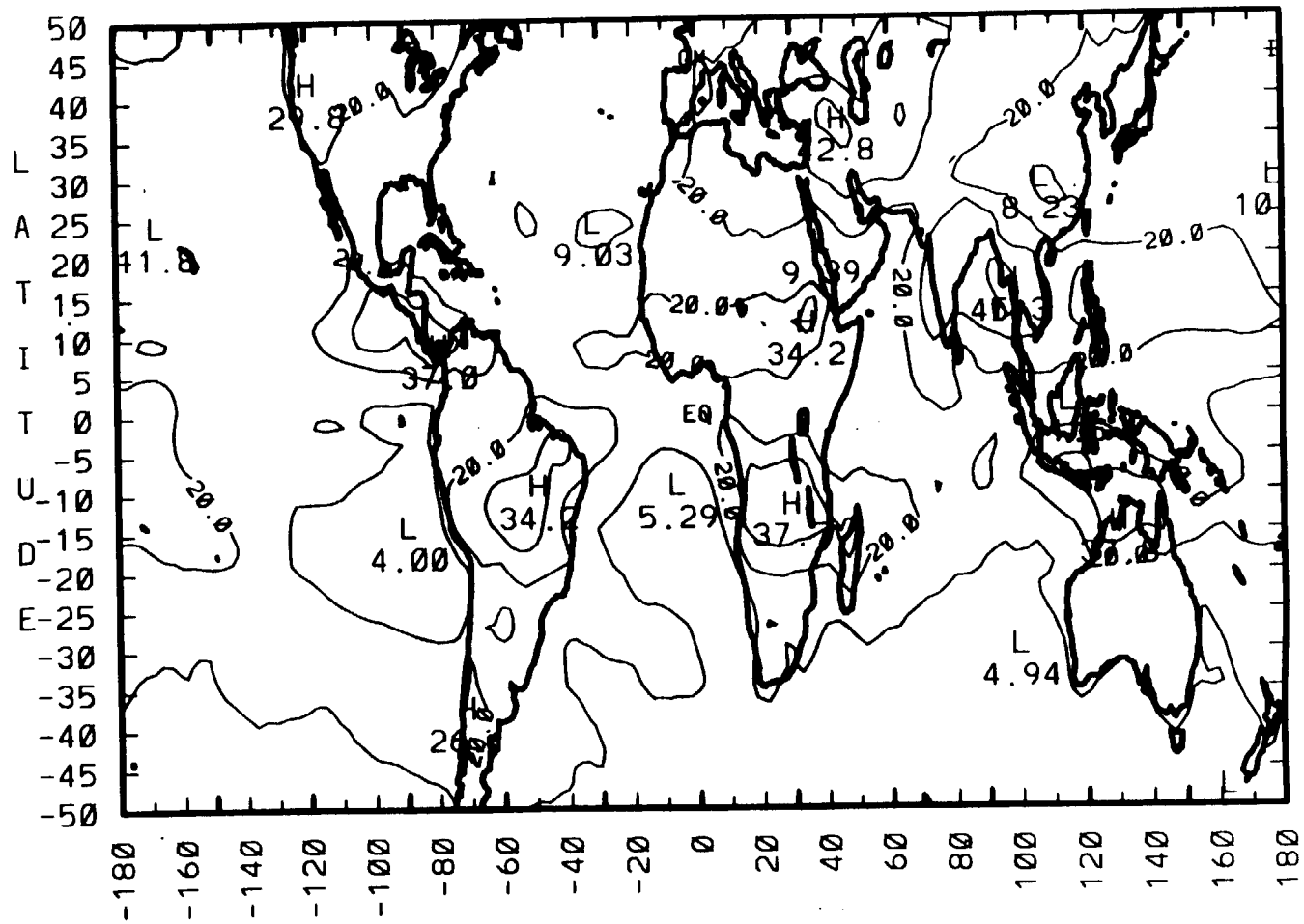

CONTOUR FROM 0.000000E+00 TO 50.000 CONTOUR INTERVAL OF 10.000 PT(3,3)= 0.8368

5-YEAR MEANS (12/84 - 11/89)
SW REFLECTED (WM**2)

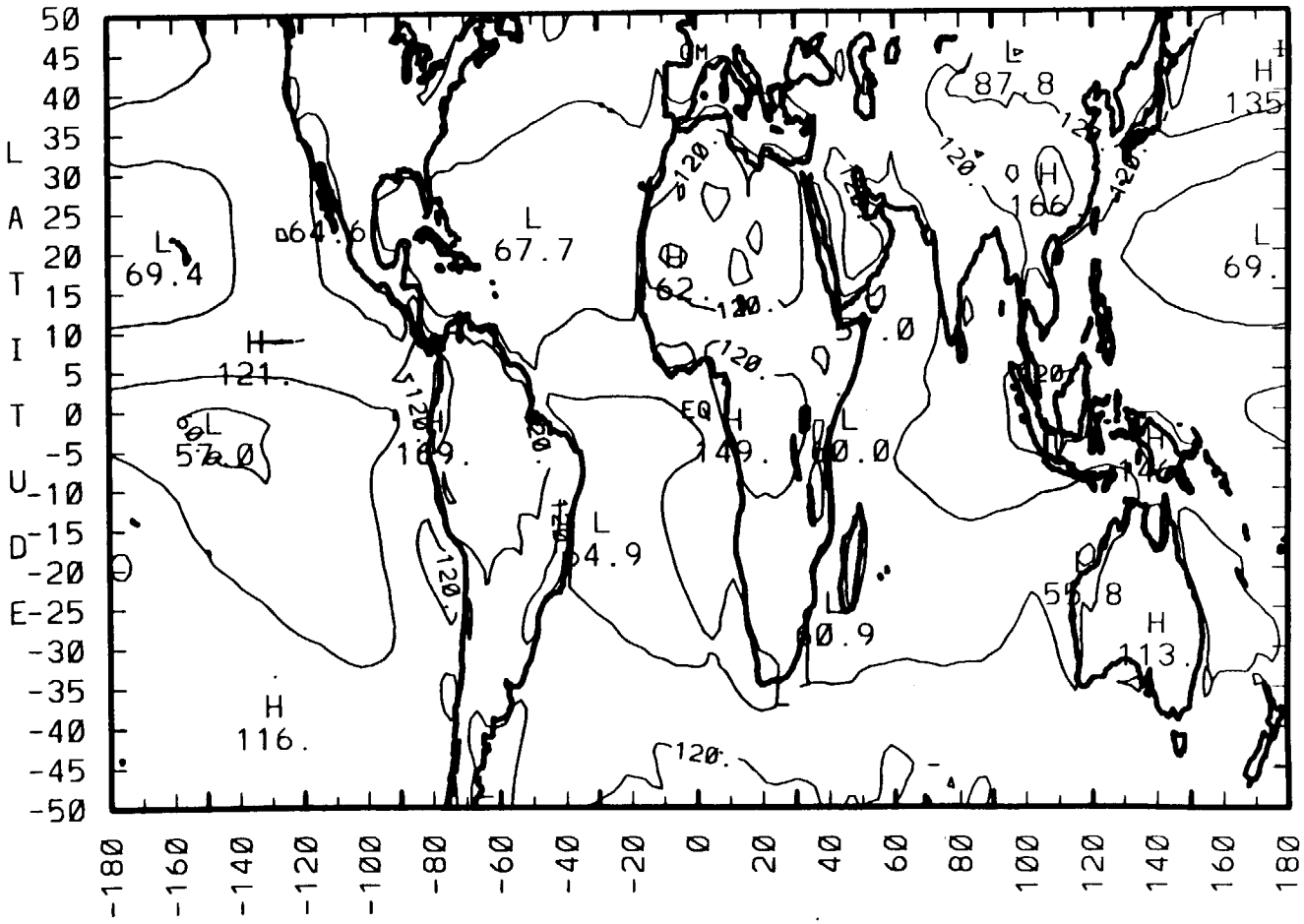

CONTOUR FROM 0.00000E+00 TO 240.00 CONTOUR INTERVAL OF 30.000 PT(3,3)= 103.26

5-YR STANDARD DEVIATIONS

(1984 - 1989)

SW REFLECTED (WM**2)

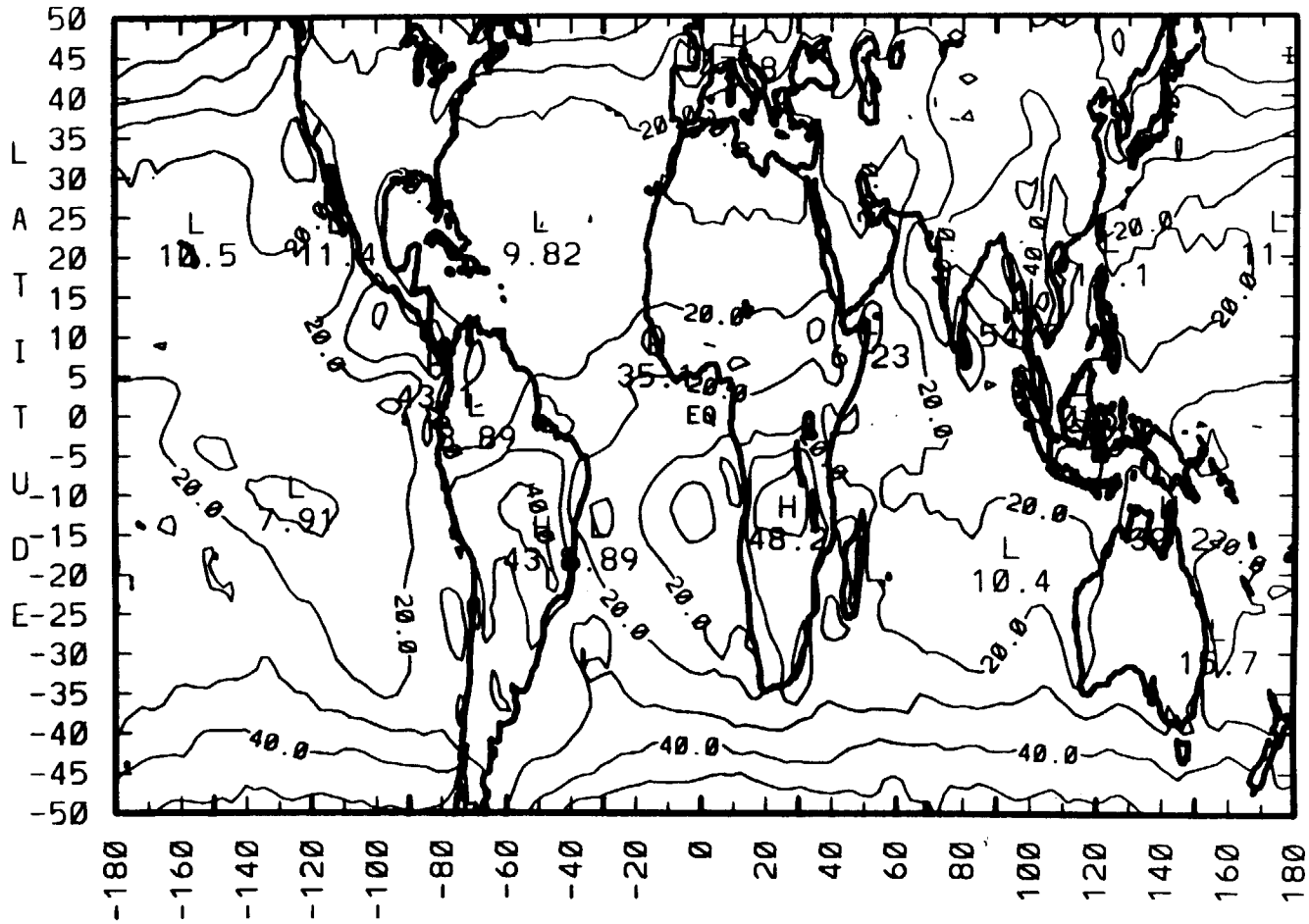

CONTOUR FROM 0.000000E+00 TO 50.000 CONTOUR INTERVAL OF 10.000 PT(3,3)= 40.898

5-YEAR MEANS (12/84 - 11/89)
SURFACE TEMP (DEG. K)

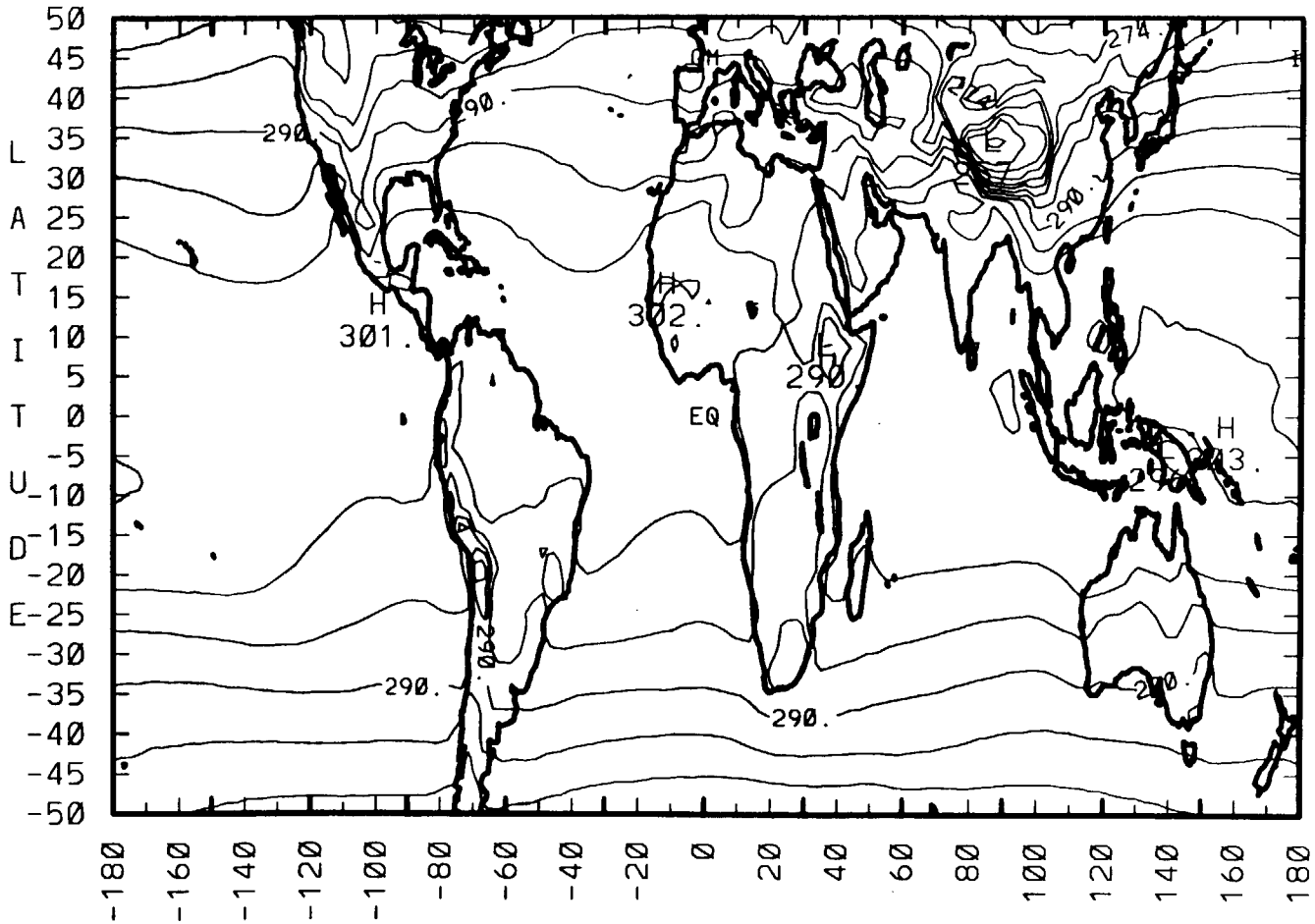

CONTOUR FROM 246.00 TO 310.00 CONTOUR INTERVAL OF 4.0000 PT(3,3)= 285.14

5-YR STANDARD DEVIATIONS
(1984 - 1989)
SURFACE TEMP (DEG. K)

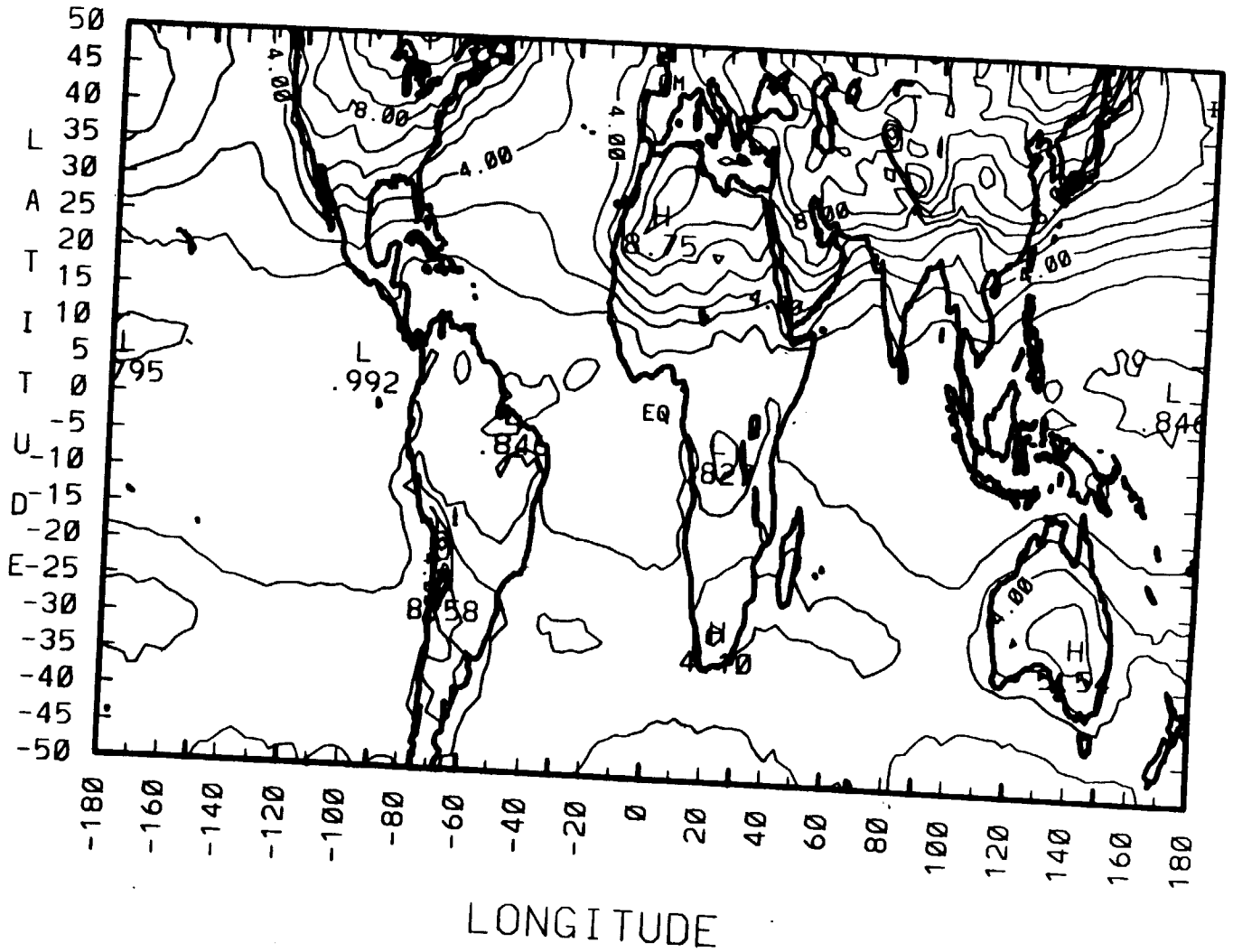

CONTOUR FROM 0.000000E+00 TO 39.000 CONTOUR INTERVAL OF 1.0000 PT(3,3)= 2.5475

5-YEAR MEANS (12/84 - 11/89)
CLOUD FRACTION (%)

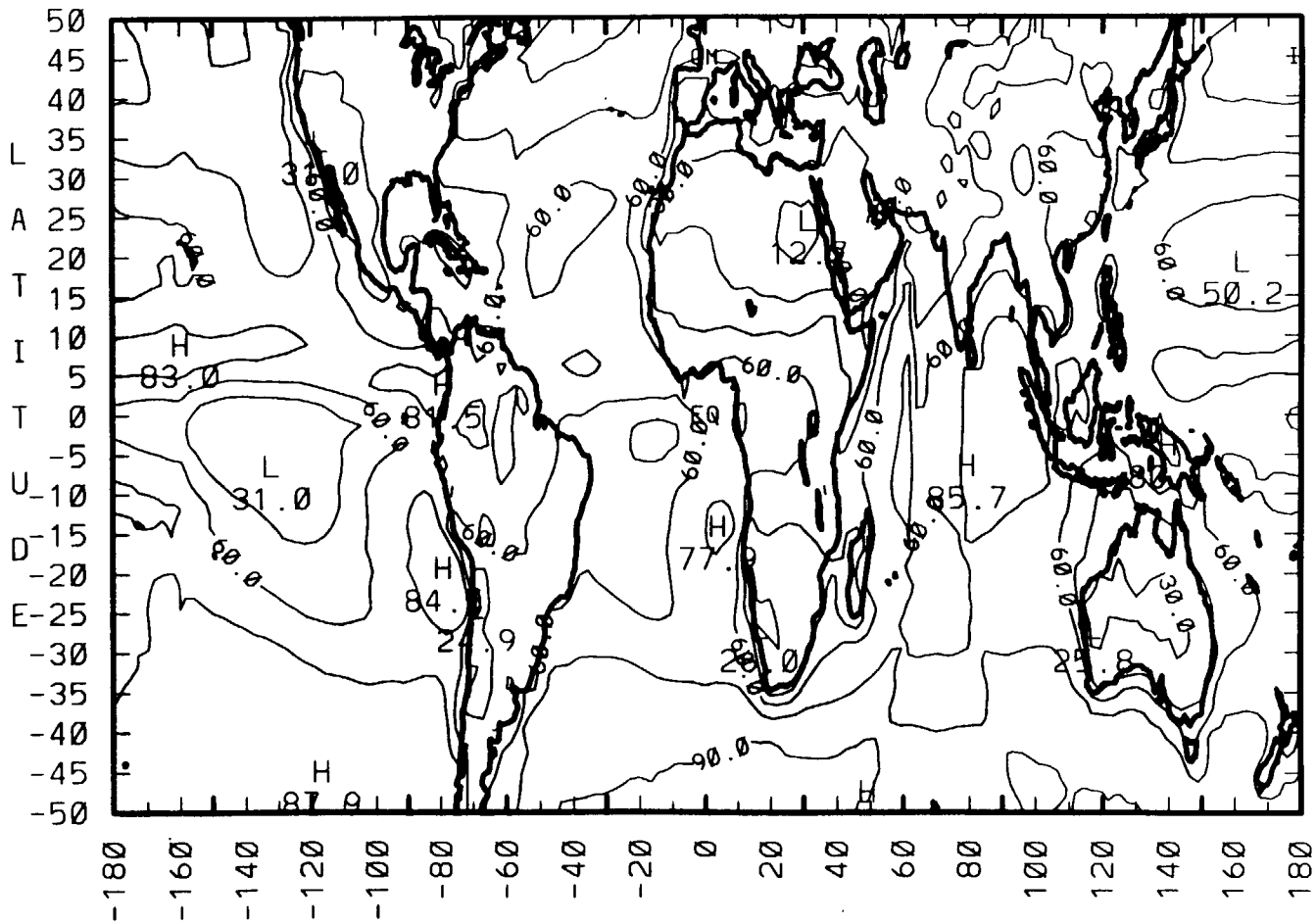

CONTOUR FROM 0.00000E+00 TO 90.000 CONTOUR INTERVAL OF 15.000 PT(3,3)= 87.225

5-YR STANDARD DEVIATIONS
(1984 - 1989)
CLOUD FRACTION (%)

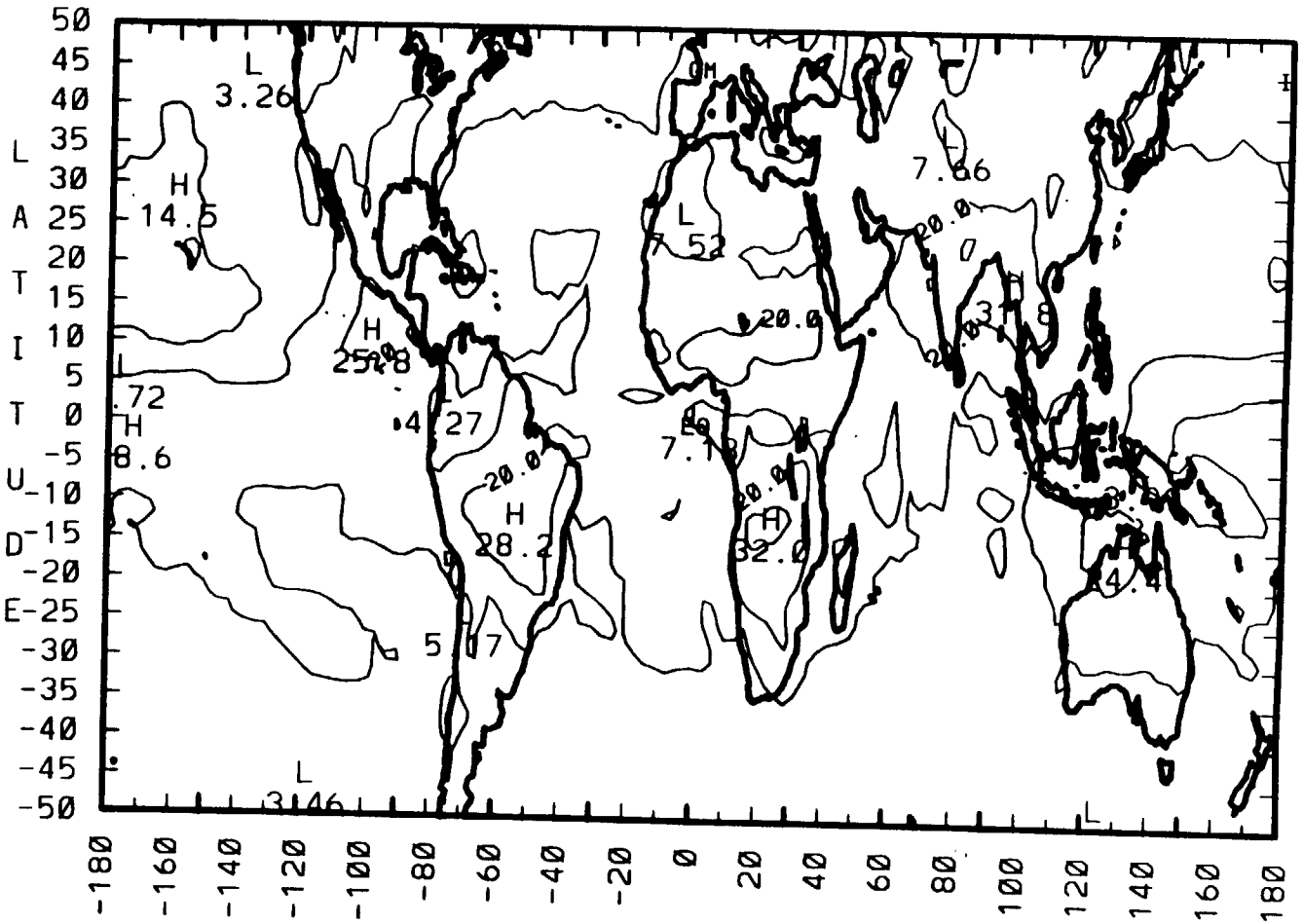

LONGITUDE

CONTOUR FROM 0.000000E+00 TO 50.000 CONTOUR INTERVAL OF 10.000 PT(3,3)= 4.8415

5-YEAR MEANS (12/84 - 11/89)
CLD TOP TEMP (DEG. K)

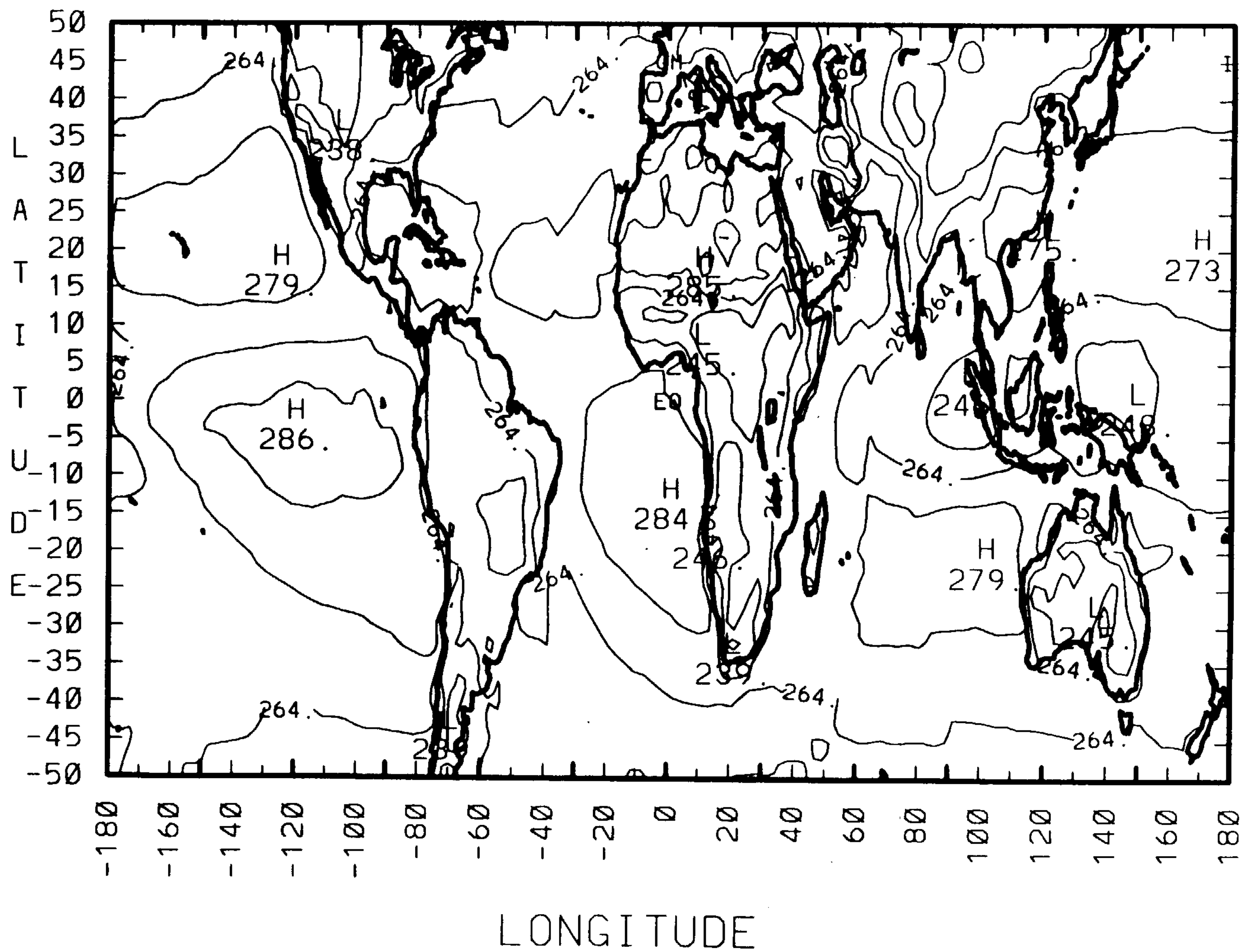

CONTOUR FROM 24.000 TO 284.00 CONTOUR INTERVAL OF 10.000 PT(3,3)= 263.74

5-YR STANDARD DEVIATIONS
(1984 - 1989)
CLD TOP TEMP (DEG. K)

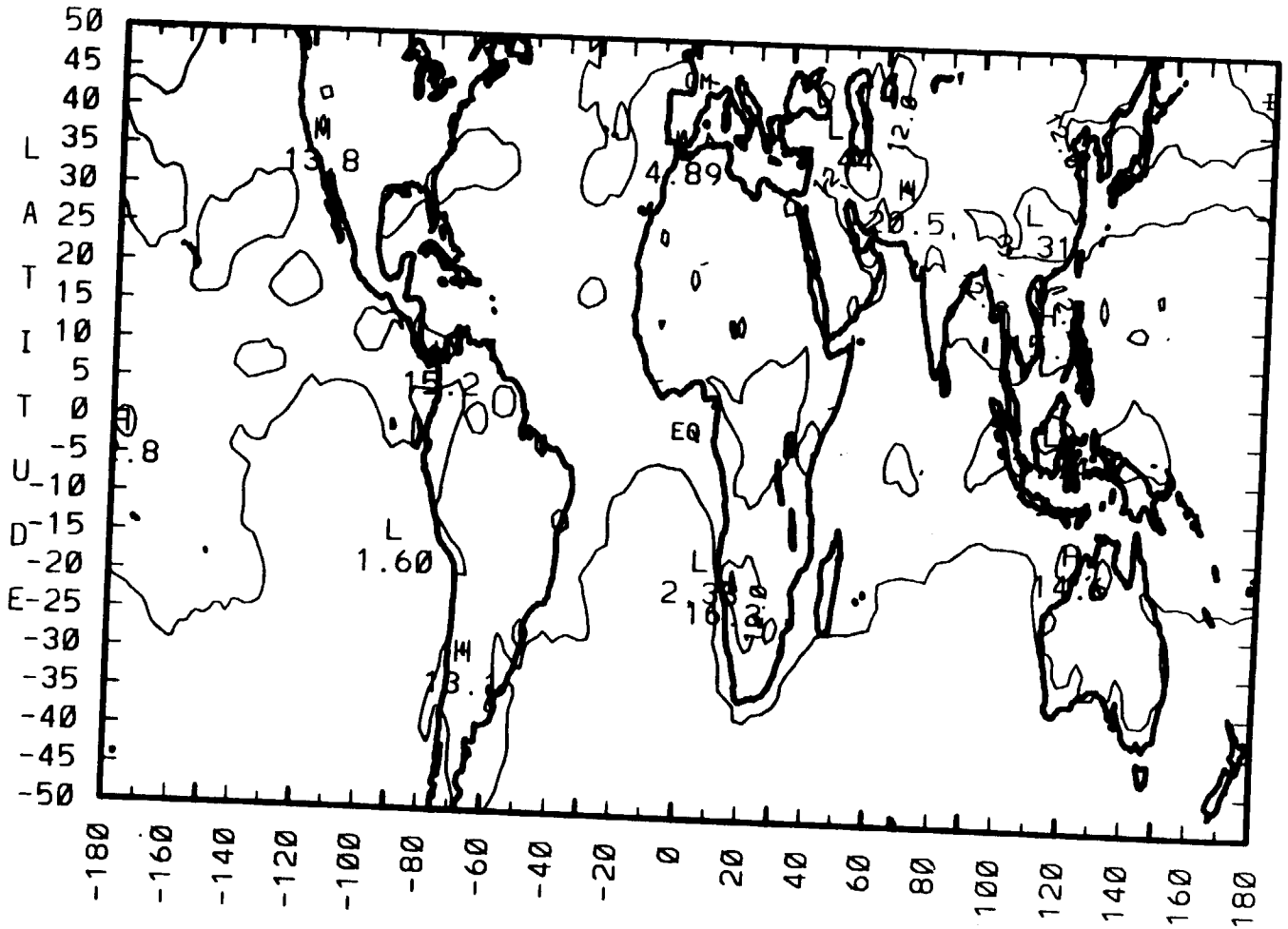

CONTOUR FROM 0.000000E+00 TO 48.000 CONTOUR INTERVAL OF 6.0000 PT(3,3)= 3.5331

M12

5-YEAR MONTHLY MEANS (12/84 - 11/89)
JAN NET RADIATION (Wm**2)

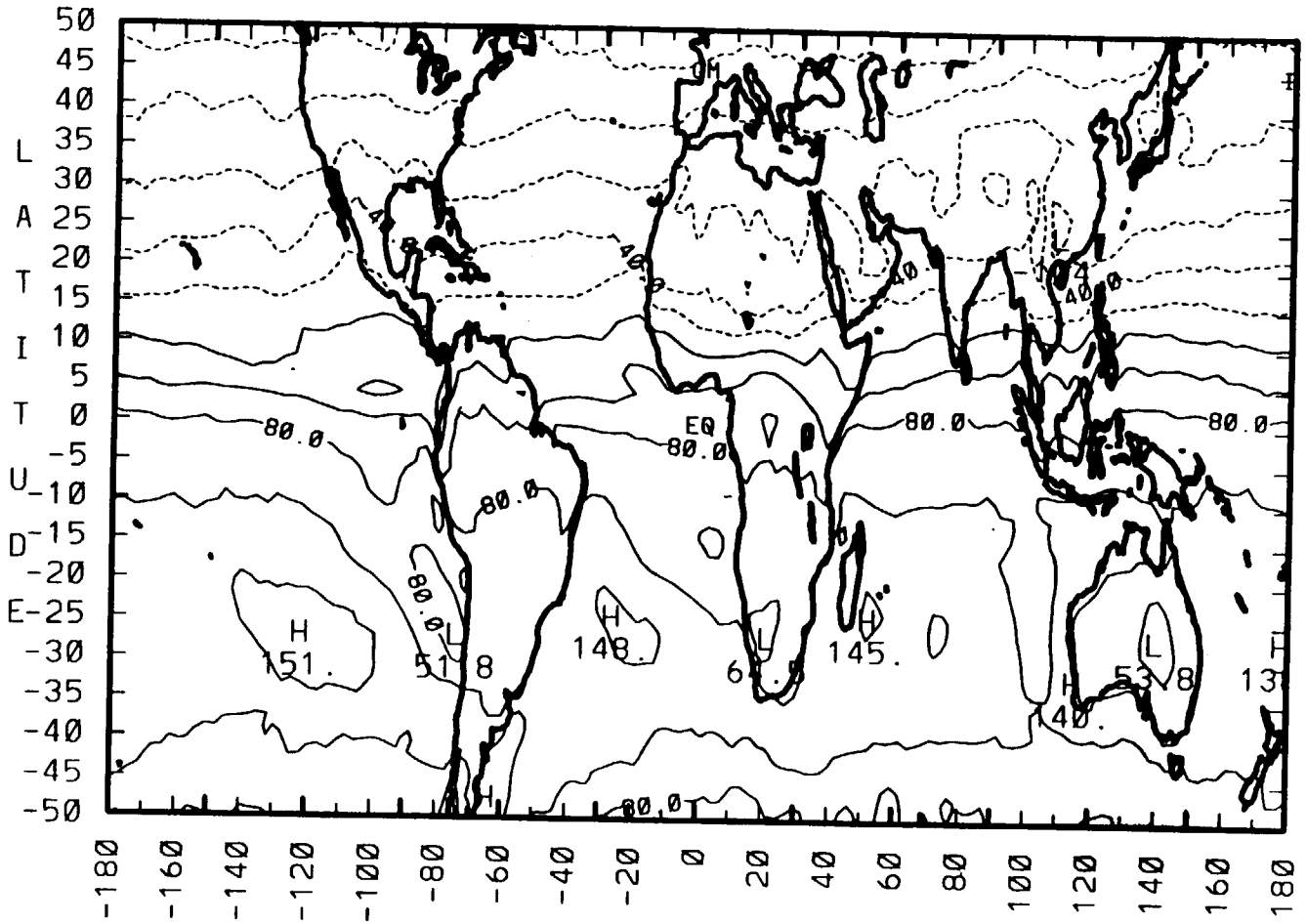

CONTOUR FROM -160.00 TO 140.00 CONTOUR INTERVAL OF 30.000 PT(3,3)= 106.82

M13

5-YR MONTHLY STANDARD DEVIATIONS

(1984 - 1989)

JAN NET RADIATION (Wm**2)

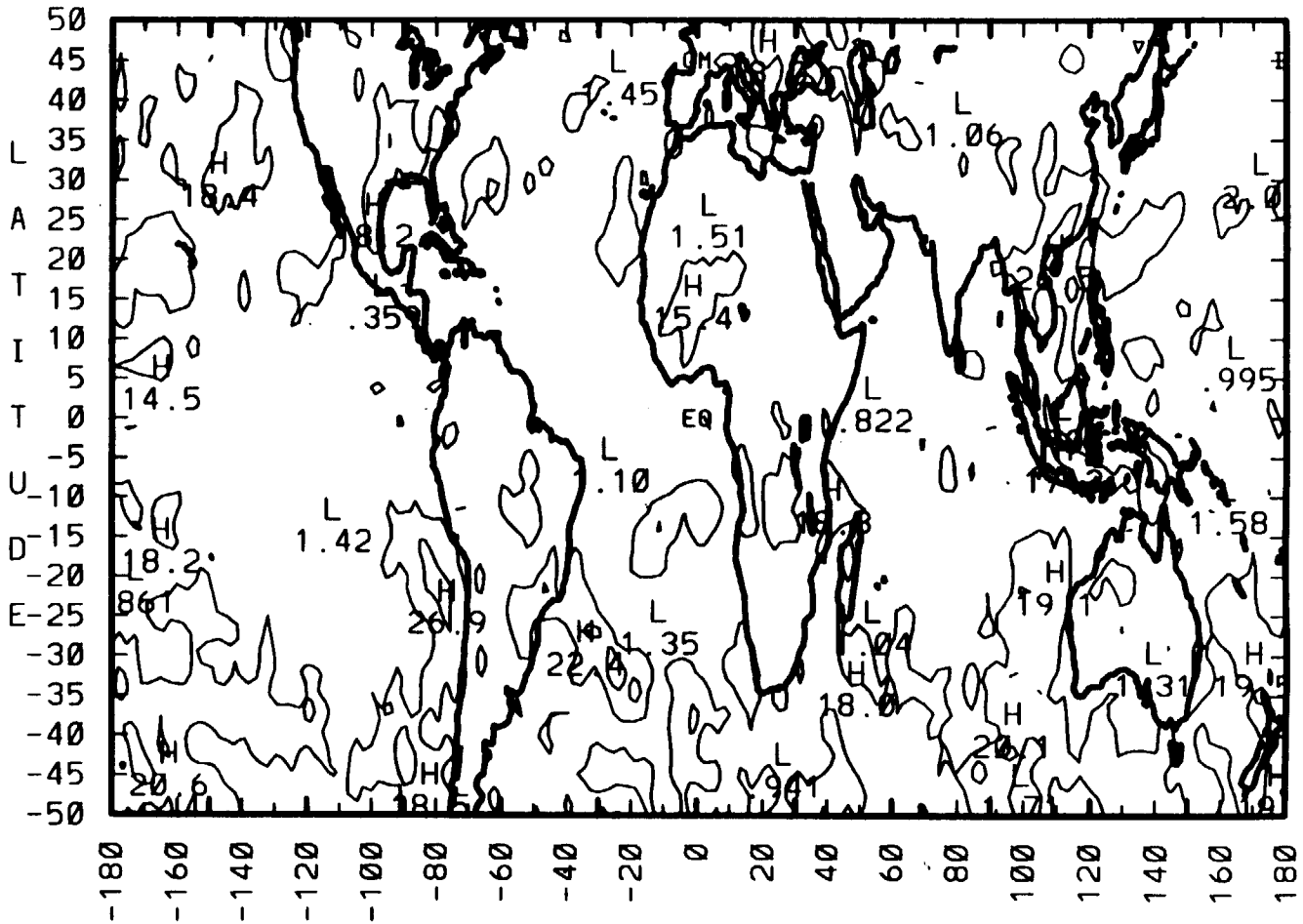

CONTOUR FROM 0.000000E+00 TO 50.000 CONTOUR INTERVAL OF 10.000 PT(3,3)= 12.363

5-YEAR MONTHLY MEANS (12/84 - 11/89)
JAN OLR (W/m**2)

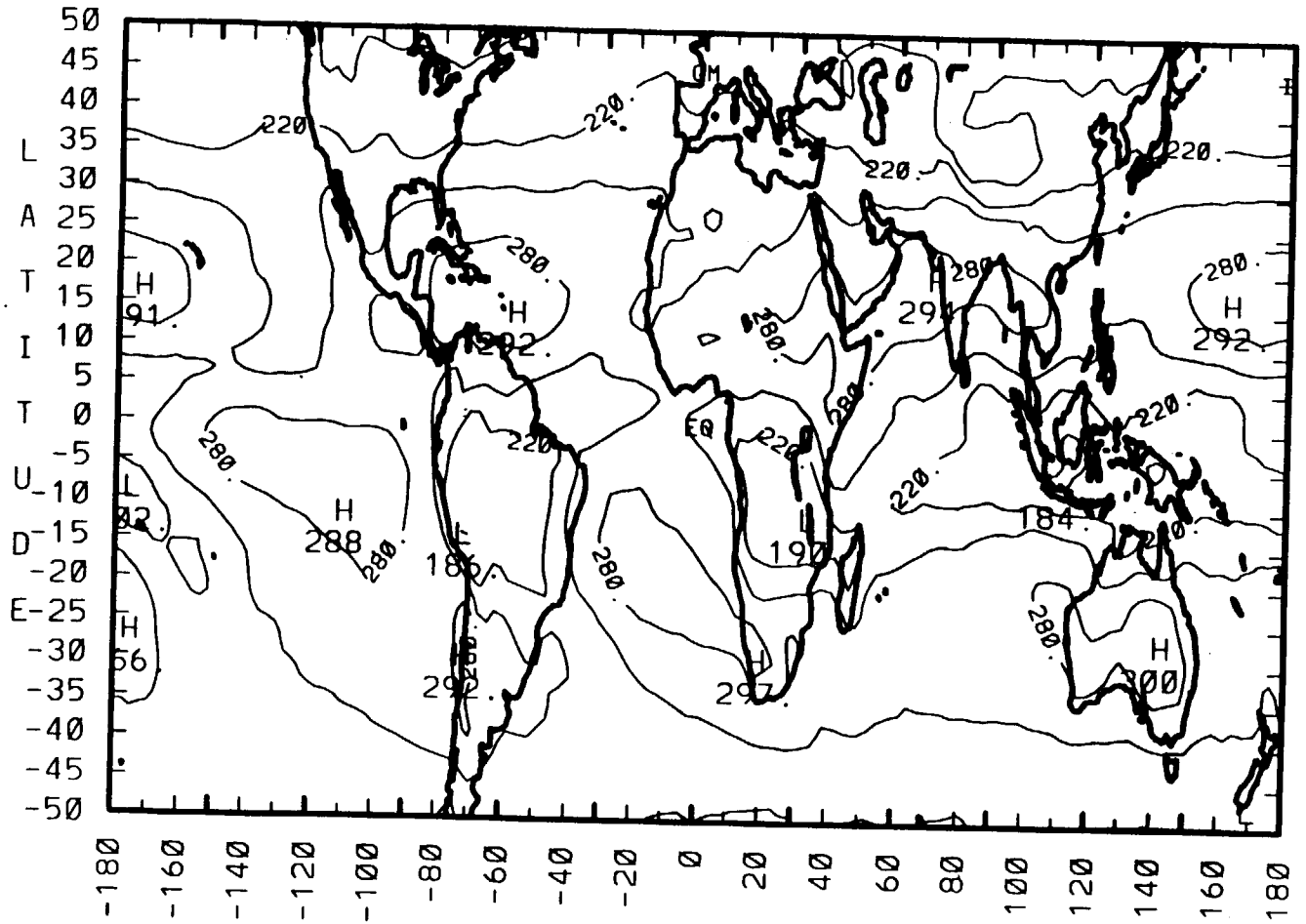

5-YR MONTHLY STANDARD DEVIATIONS

(1984 - 1989)

JAN OLR (W/m**2)

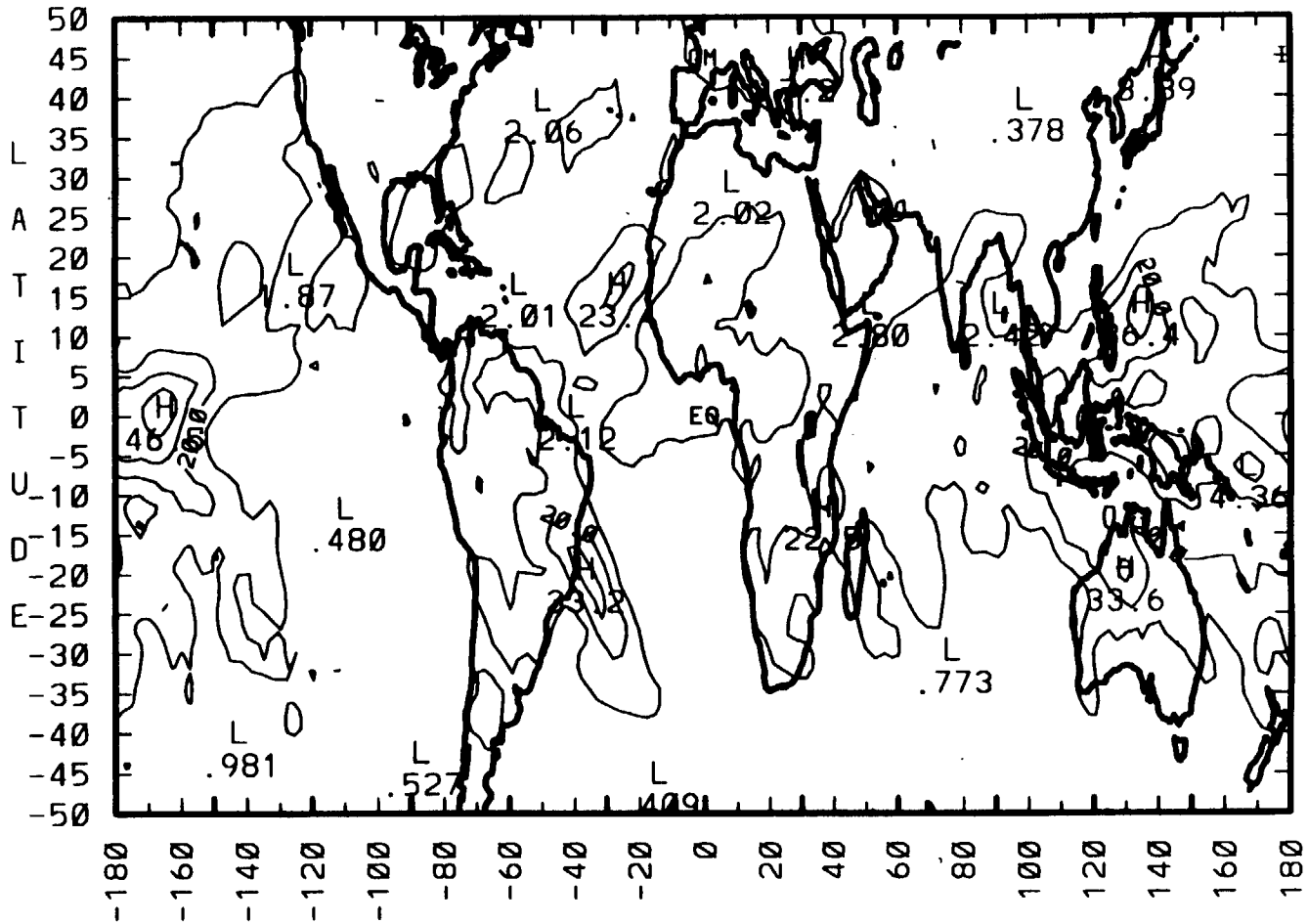

LONGITUDE

CONTOUR FROM 0.000000E+00 TO 50.000 CONTOUR INTERVAL OF 10.000 PT(3,3)= 4.5912

5-YEAR MONTHLY MEANS (12/84 - 11/89)
JAN SW REFLECTED (WM**2)

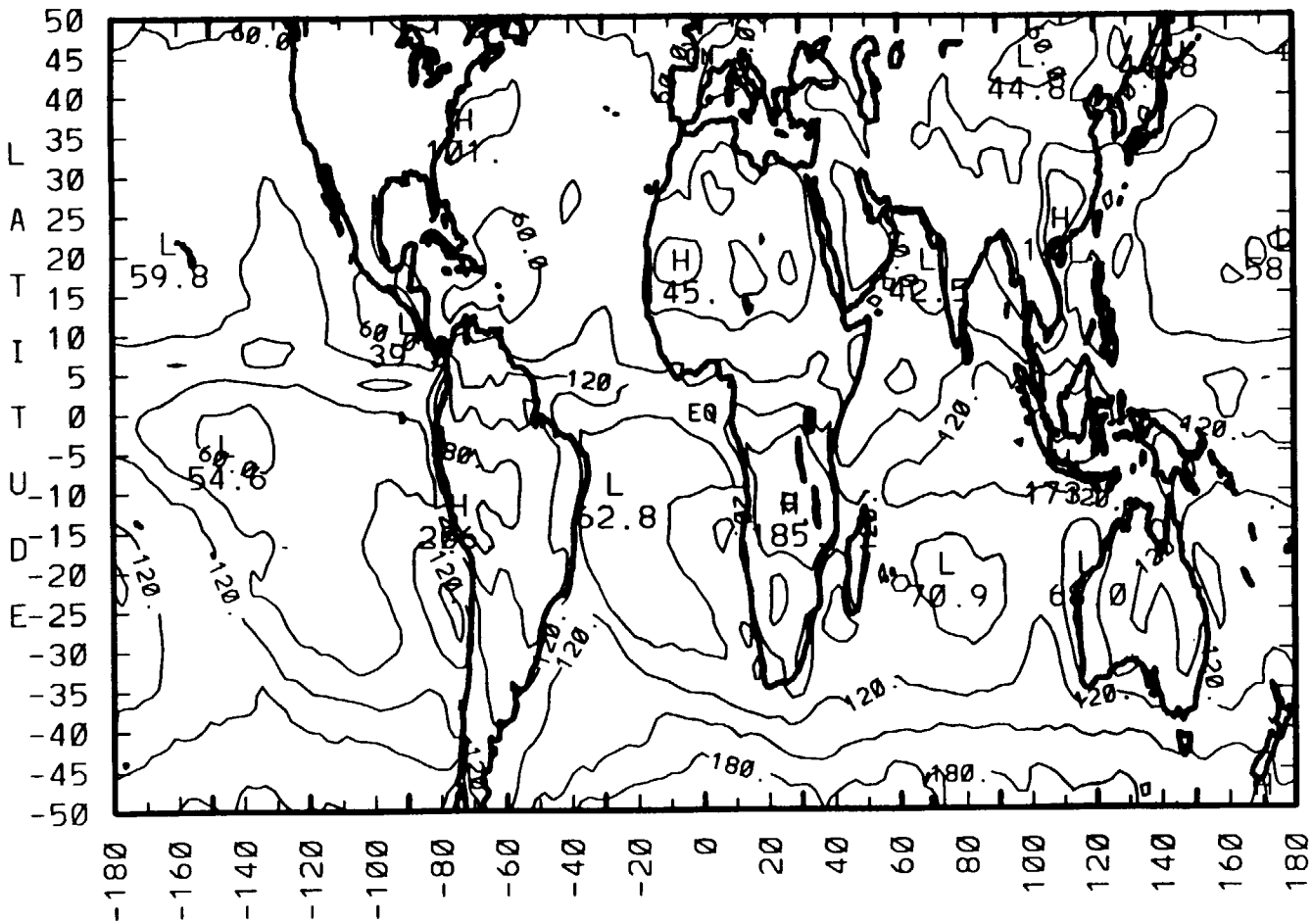

CONTOUR FROM 0.000000E+00 TO 240.00 CONTOUR INTERVAL OF 30.000 PT(3,3)= 151.60

5-YR MONTHLY STANDARD DEVIATIONS
(1984 - 1989)
JAN SW REFLECTED (WM**2)

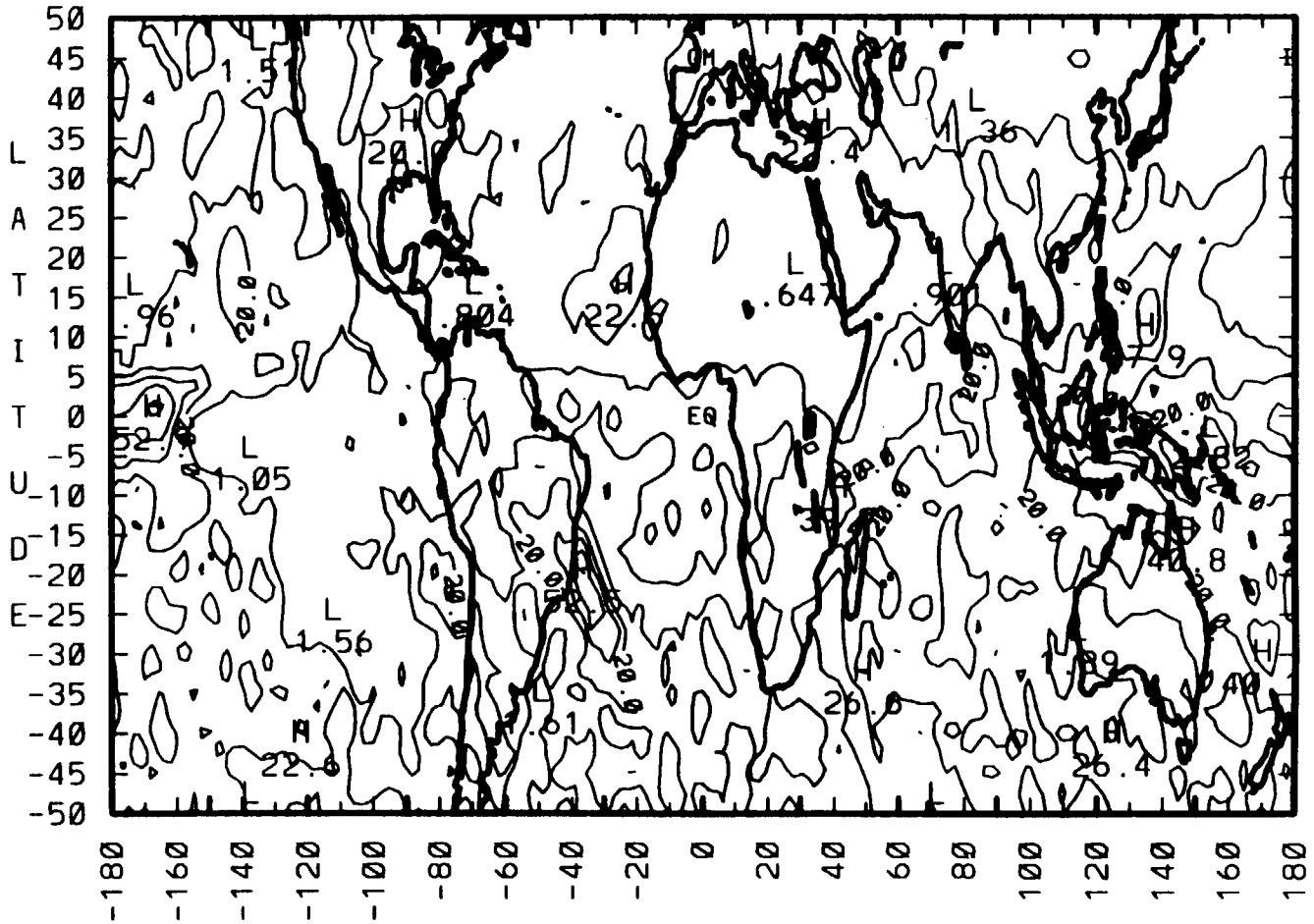

CONTOUR FROM 0.000000E+00 TO 50.000 CONTOUR INTERVAL OF 10.000 PT(3,3)= 16.174

5-YEAR MONTHLY MEANS (12/84 - 11/89)
JAN SURFACE TEMP (DEG. K)

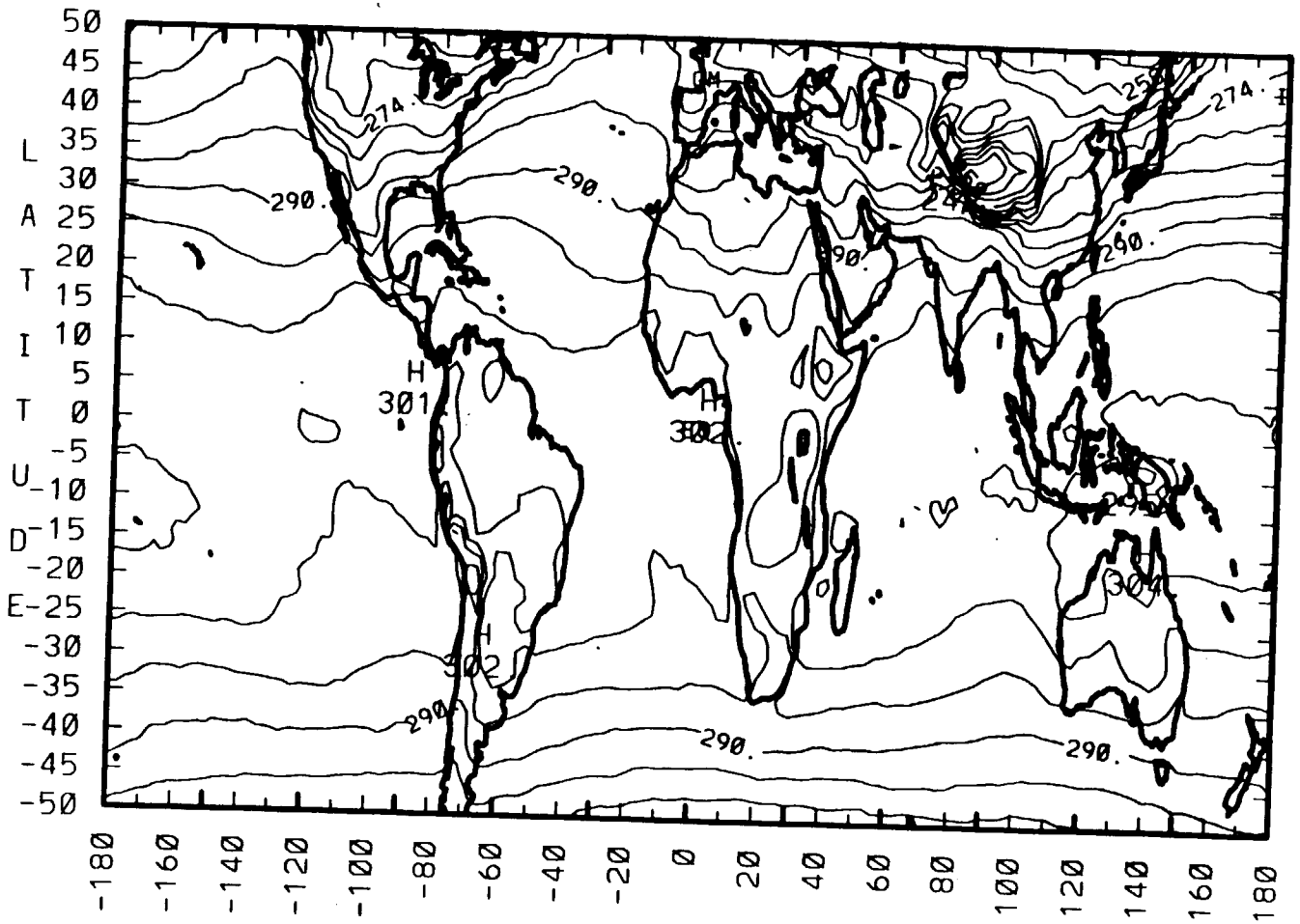

CONTOUR FROM 246.00 TO 310.00 CONTOUR INTERVAL OF 4.0000 PT(3,3)= 288.60

5-YR MONTHLY STANDARD DEVIATIONS
(1984 - 1989)
JAN SURFACE TEMP (DEG. K)

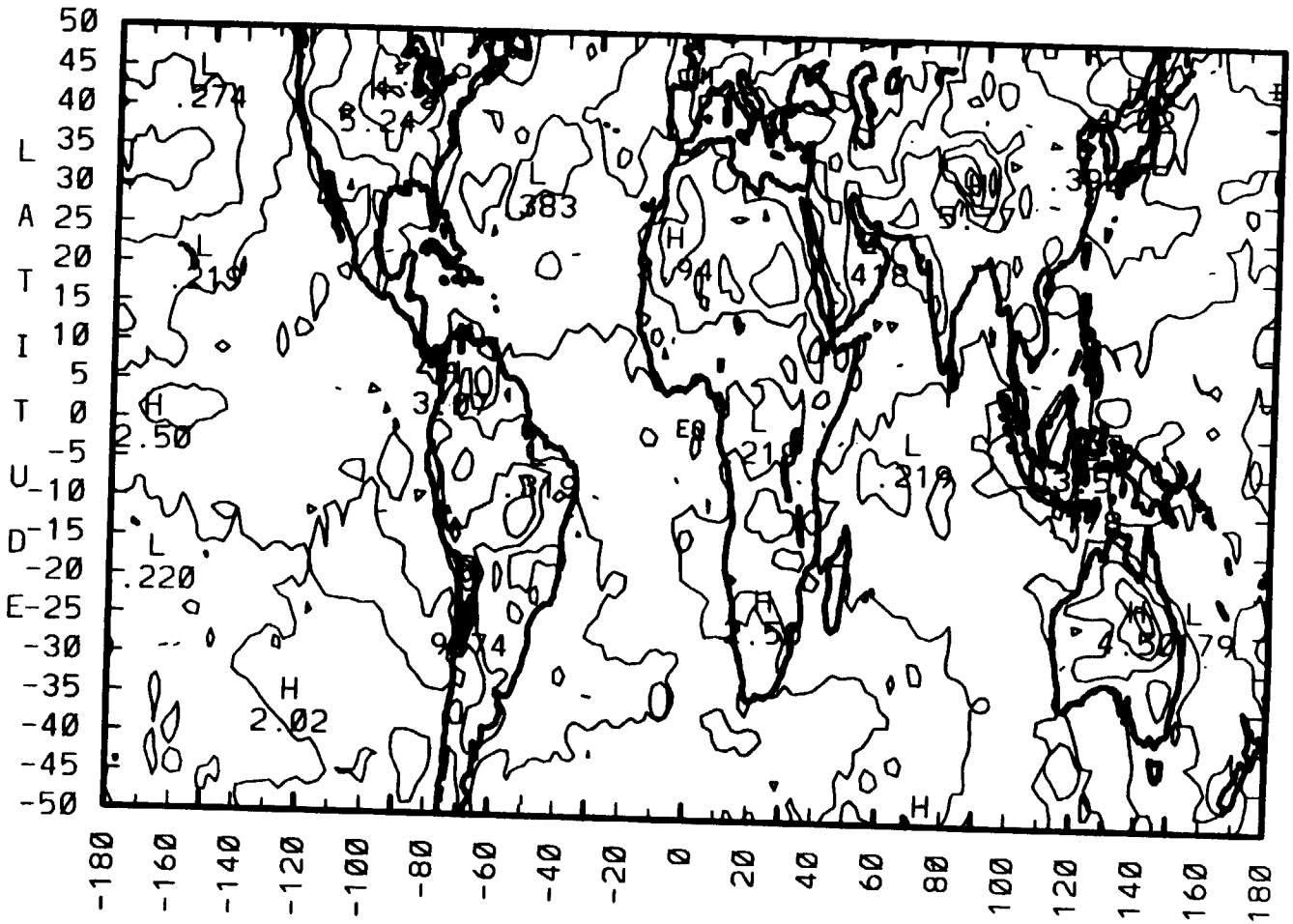

5-YEAR MONTHLY MEANS (12/84 - 11/89)
JAN CLOUD FRACTION (%)

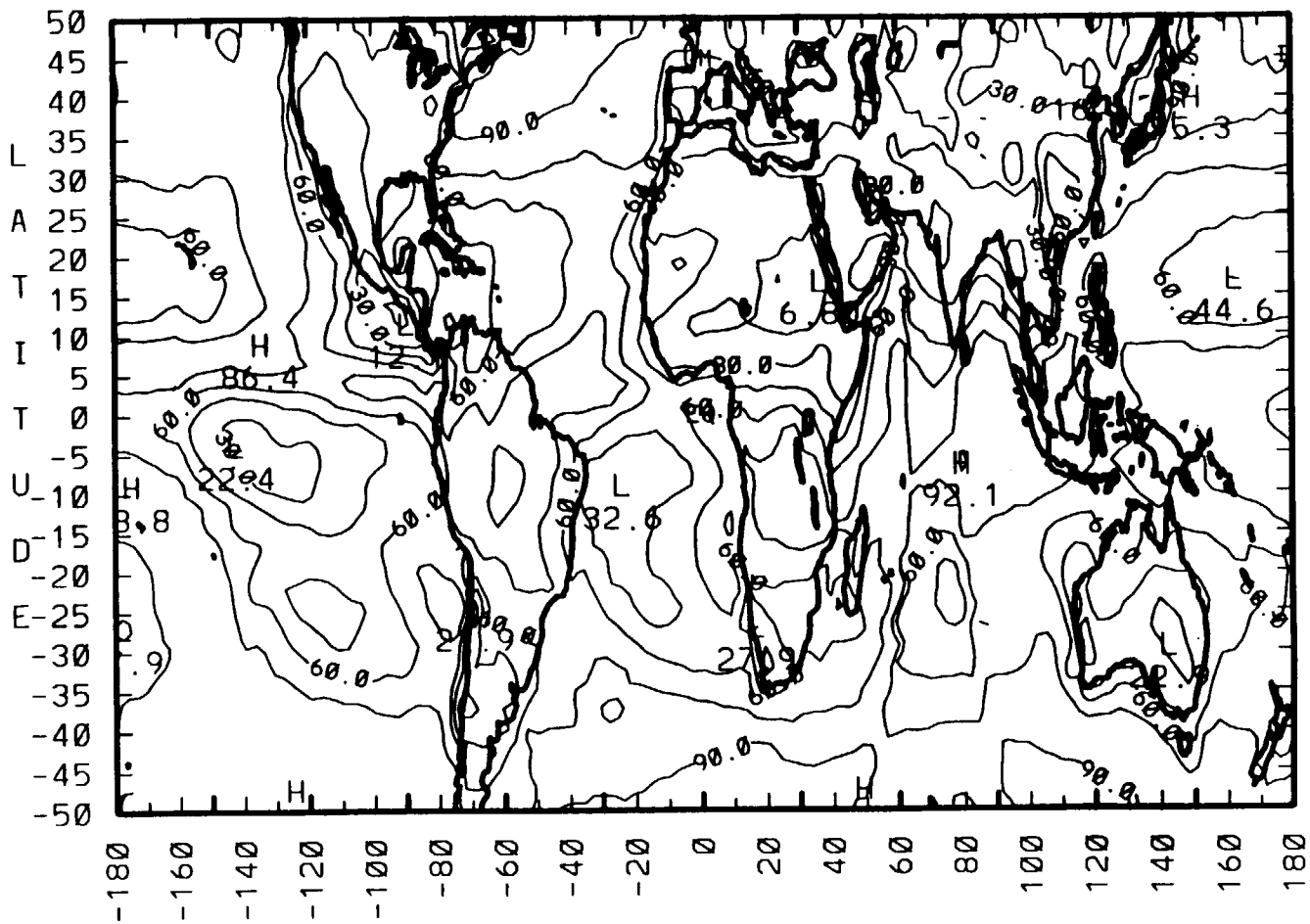

CONTOUR FROM 0.000000E+00 TO 90.000 CONTOUR INTERVAL OF 15.000 PT(3,3)= 85.000

5-YR MONTHLY STANDARD DEVIATIONS

(1984 - 1989)

JAN CLOUD FRACTION (%)

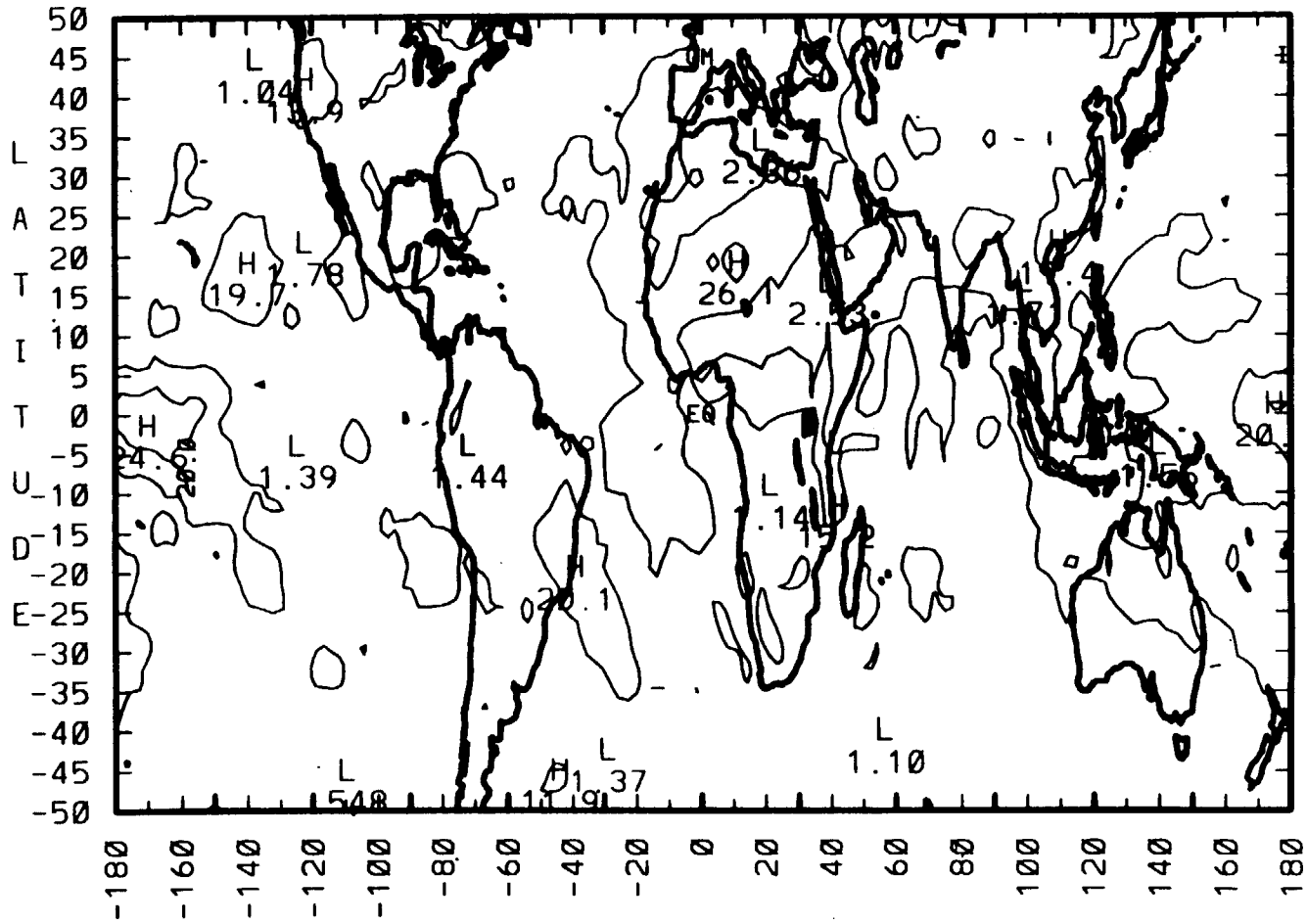

CONTOUR FROM 0.000000E+00 TO 50.000 CONTOUR INTERVAL OF 10.000 PT(3,3)= 4.6449

5-YEAR MONTHLY MEANS (12/84 - 11/89)
JAN CLD TOP TEMP (DEG. K)

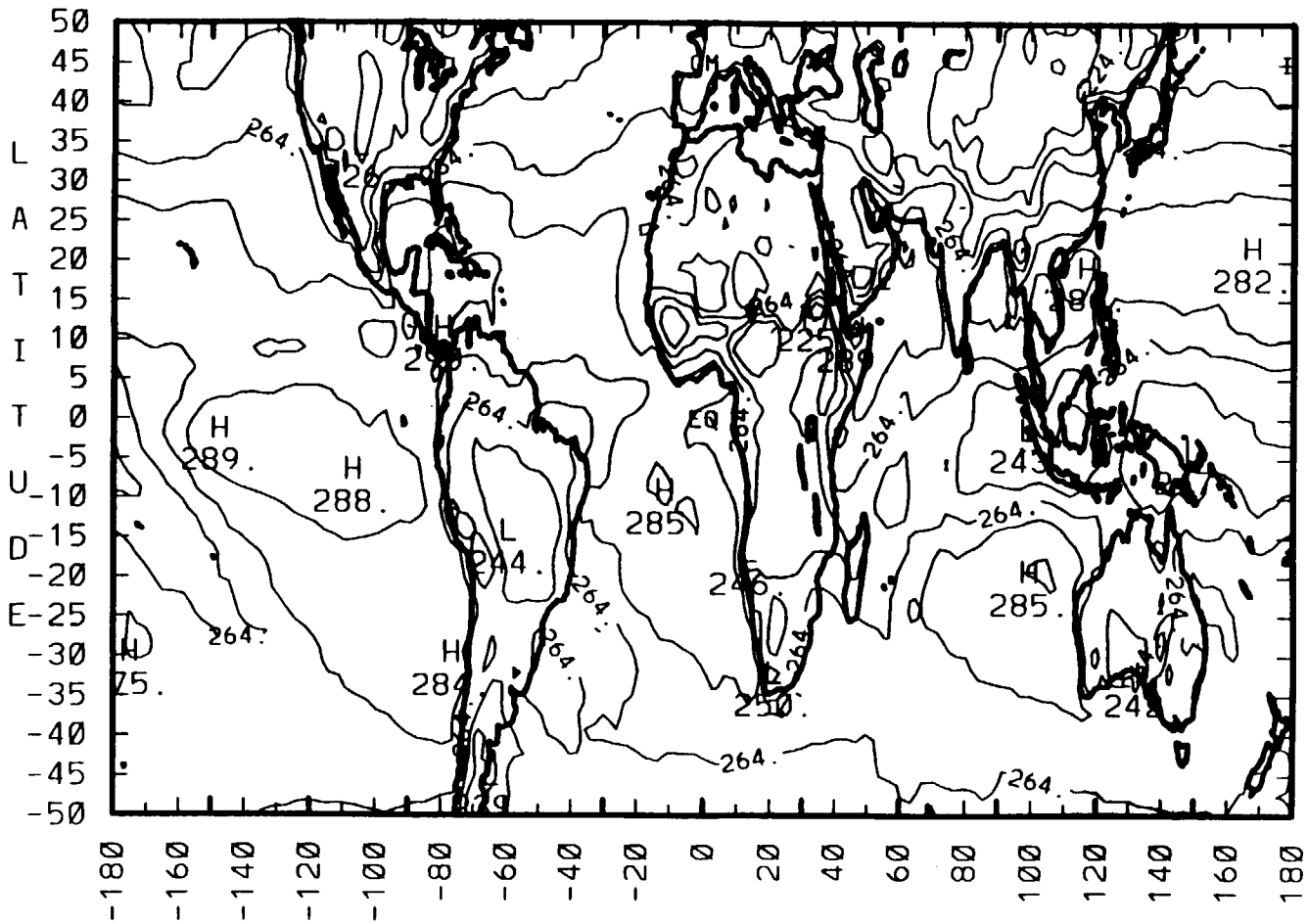

5-YR MONTHLY STANDARD DEVIATIONS
(1984 - 1989)
JAN CLD TOP TEMP (DEG. K)

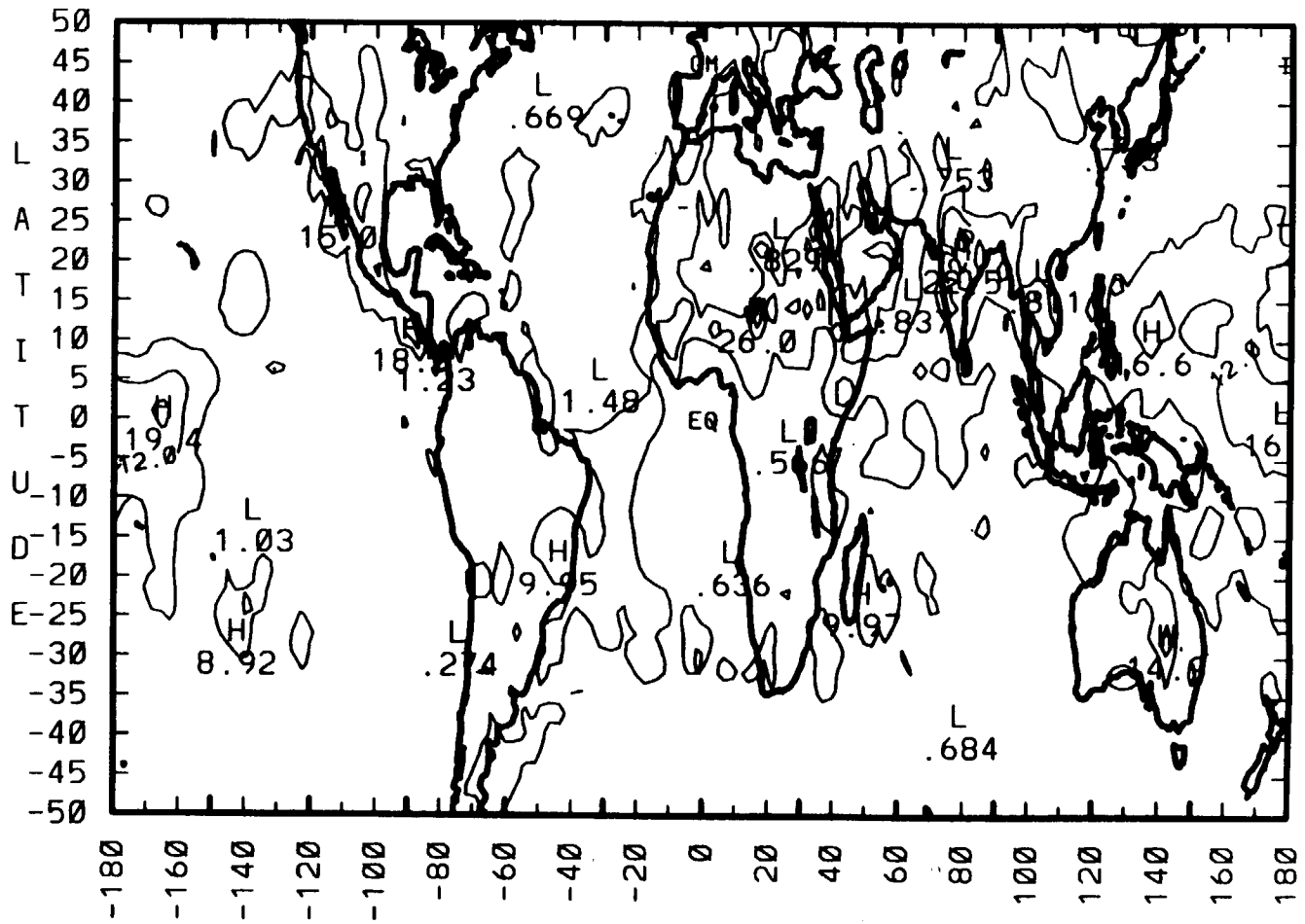

LONGITUDE

CONTOUR FROM 0.000000E+00 TO 48.000 CONTOUR INTERVAL OF 6.0000 PT(3,3)= 1.1262

M24

5-YEAR MONTHLY MEANS (12/84 - 11/89)
APR NET RADIATION (Wm**2)

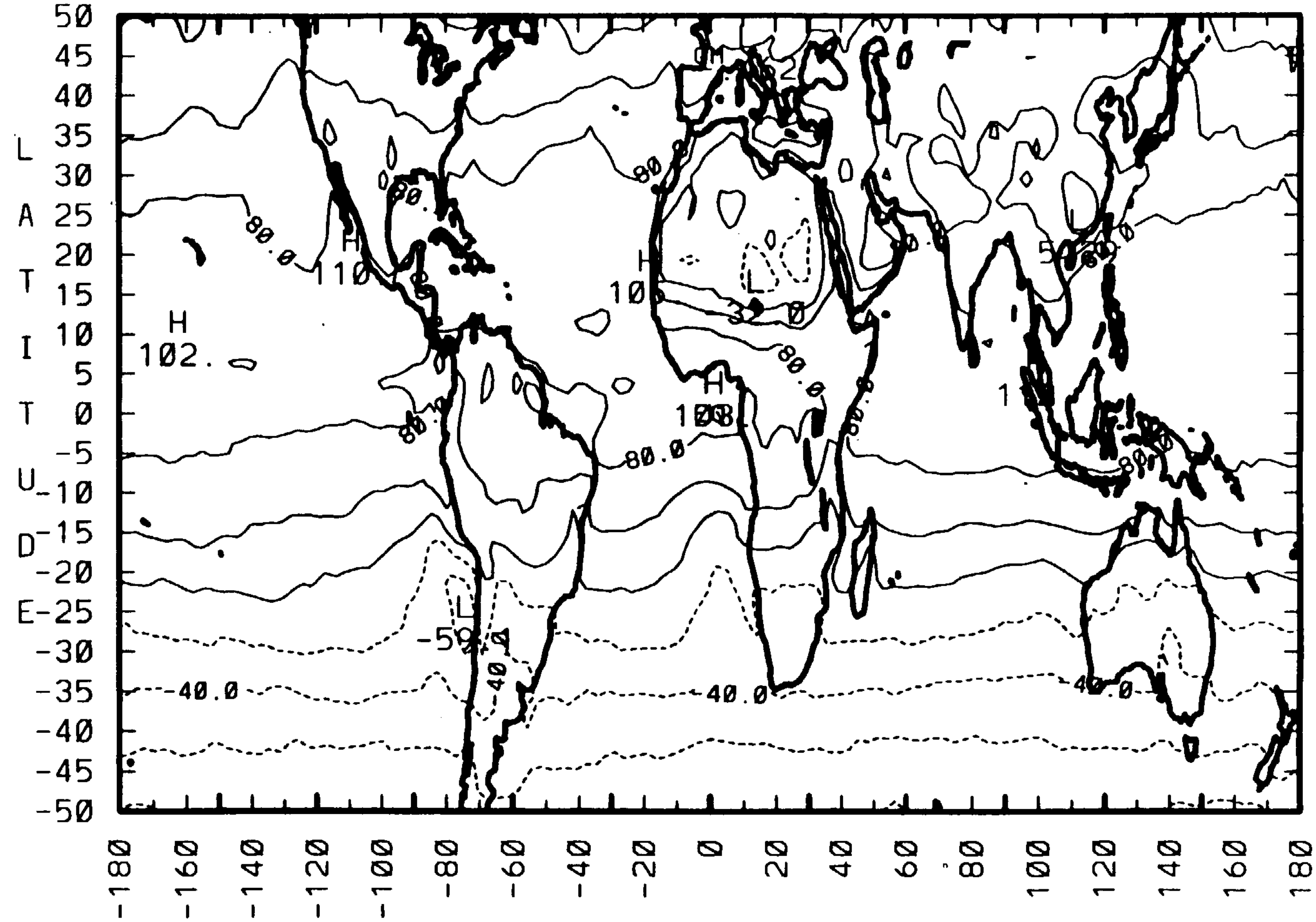

CONTOUR FROM -160.00 TO 140.00 CONTOUR INTERVAL OF 30.000 PT(3,3)= -79.549

M25

5-YR MONTHLY STANDARD DEVIATIONS

(1984 - 1989)

APR NET RADIATION (Wm**2)

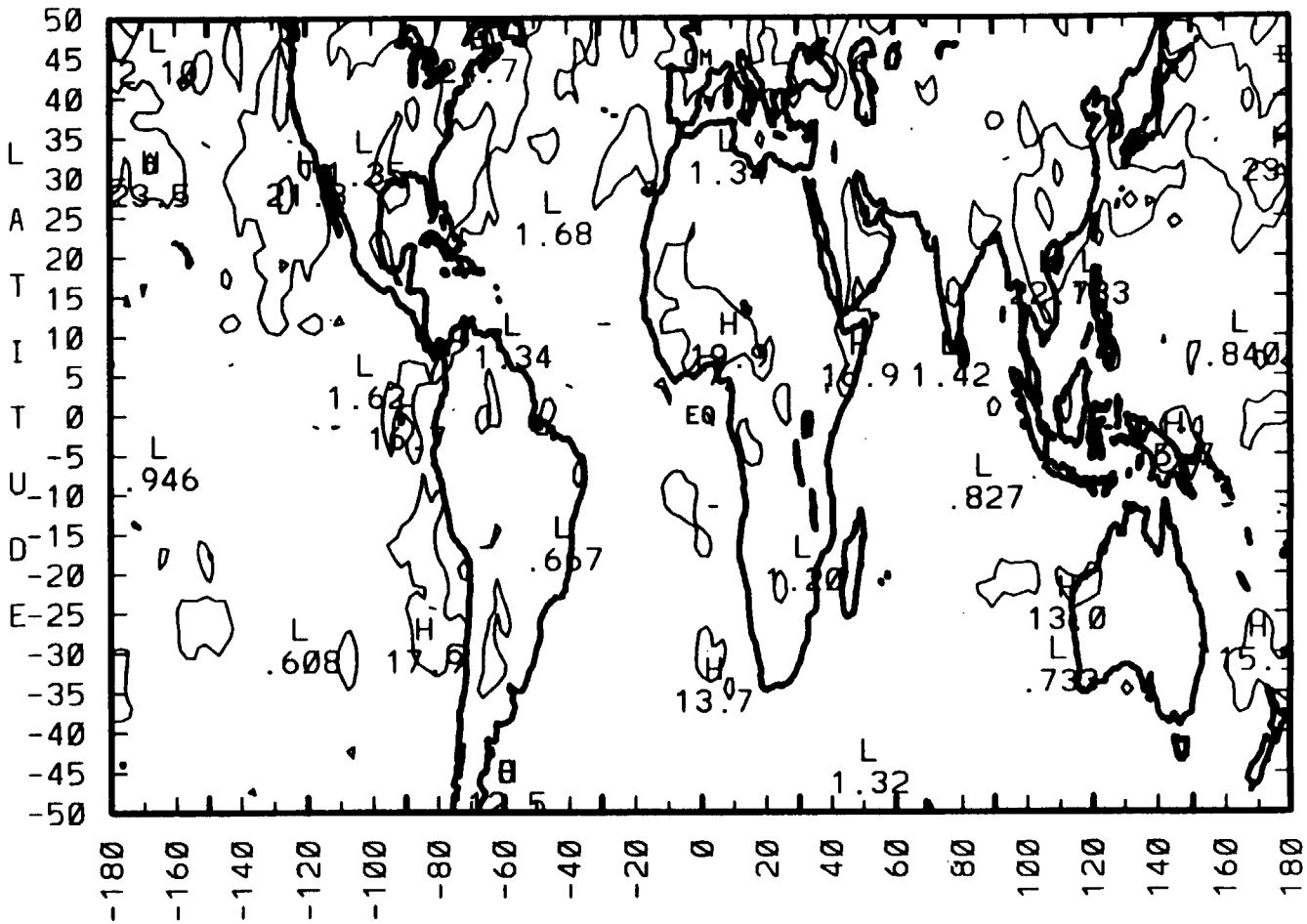

LONGITUDE

CONTOUR FROM 0.000000E+00 TO 50.000 CONTOUR INTERVAL OF 10.000 PT(3,3)= 3.5858

5-YEAR MONTHLY MEANS (12/84 - 11/89)
APR OLR (W/m**2)

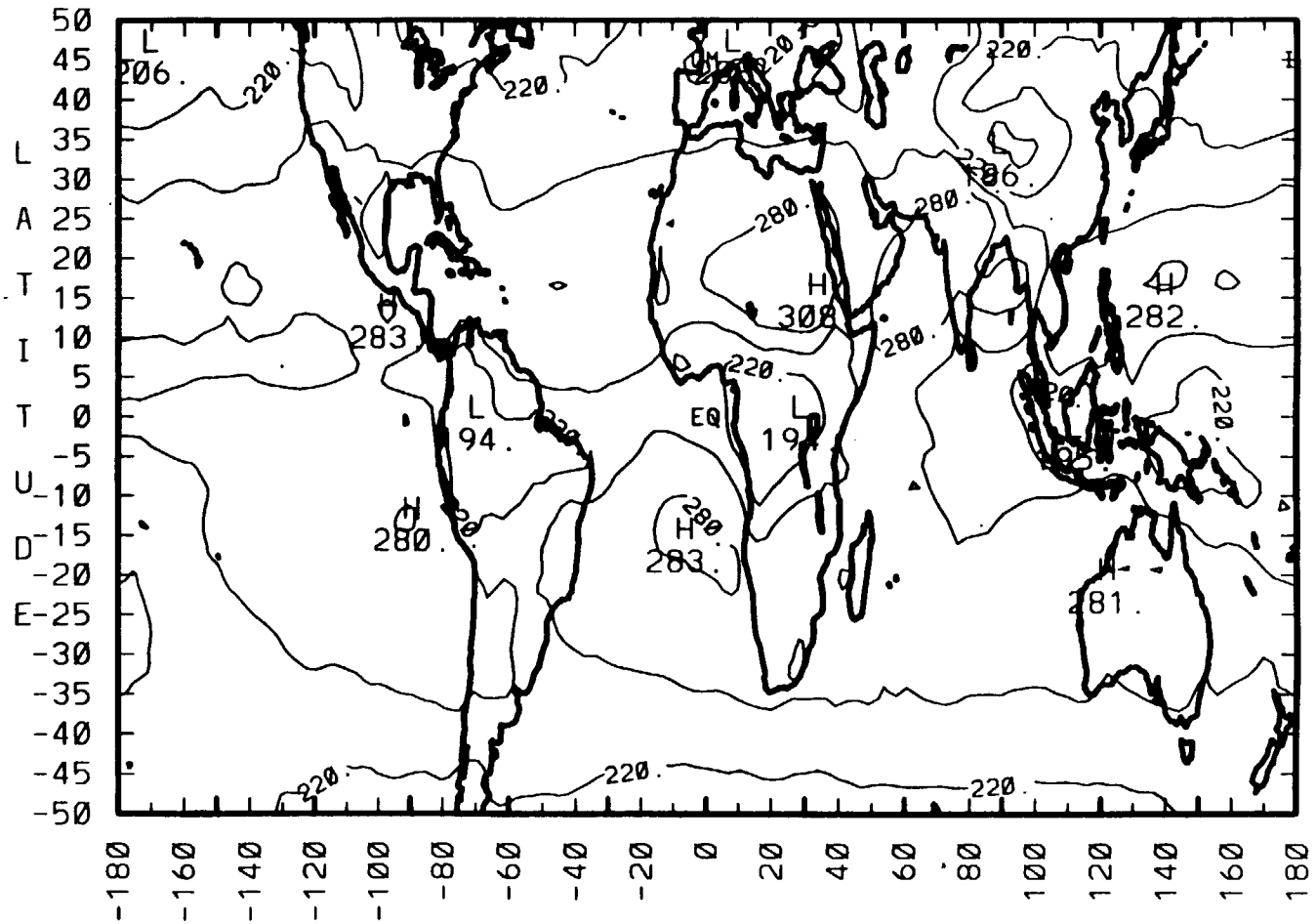

CONTOUR FROM 160.00 TO 280.00 CONTOUR INTERVAL OF 30.000 PT(3,3)= 234.16

5-YR MONTHLY STANDARD DEVIATIONS

(1984 - 1989)

APR OLR (W/m**2)

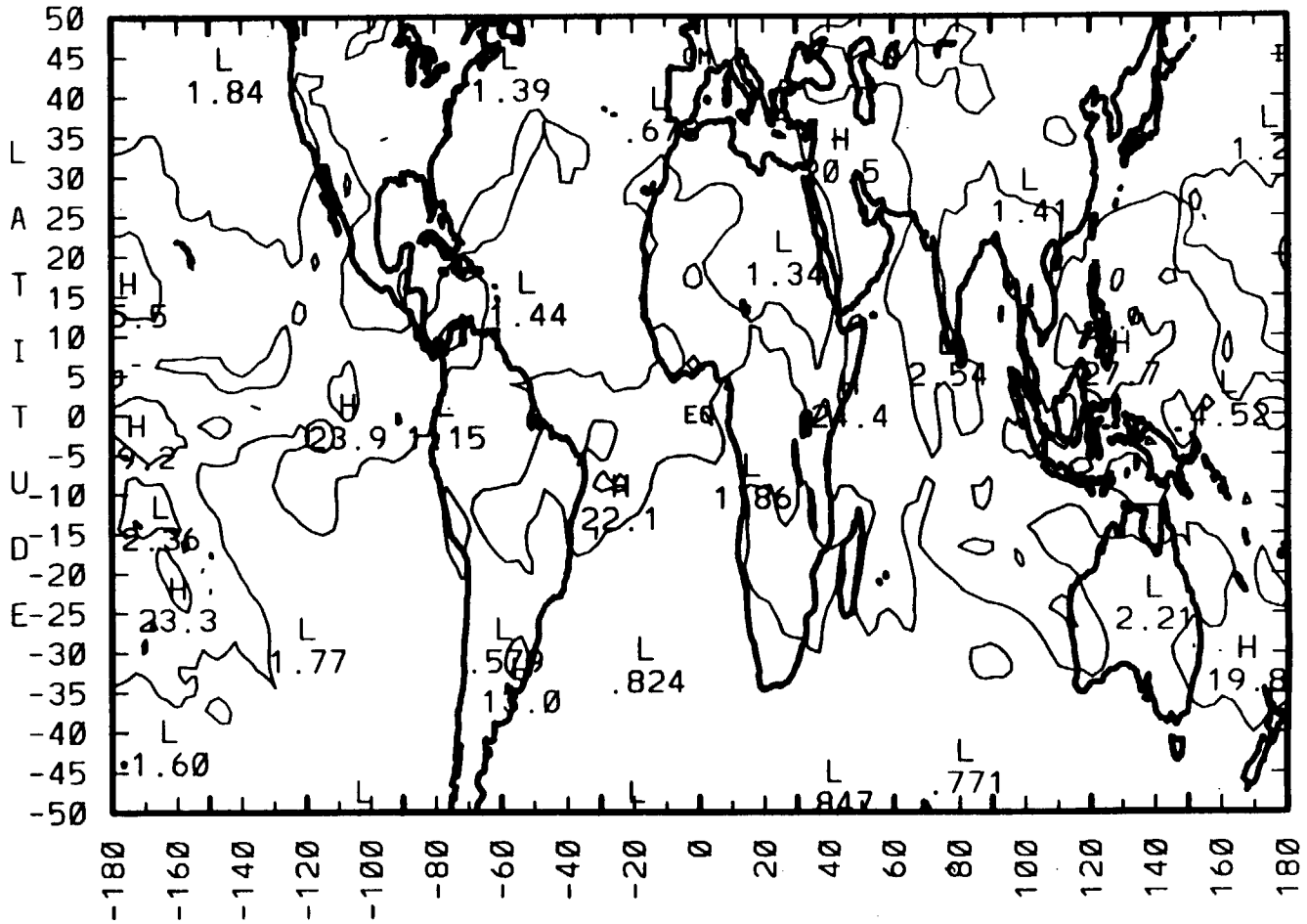

LONGITUDE

CONTOUR FROM 0.000000E+00 TO 50.000 CONTOUR INTERVAL OF 10.000 PT(3,3)= 5.0234

5-YEAR MONTHLY MEANS (12/84 - 11/89)
APR SW REFLECTED (WM**2)

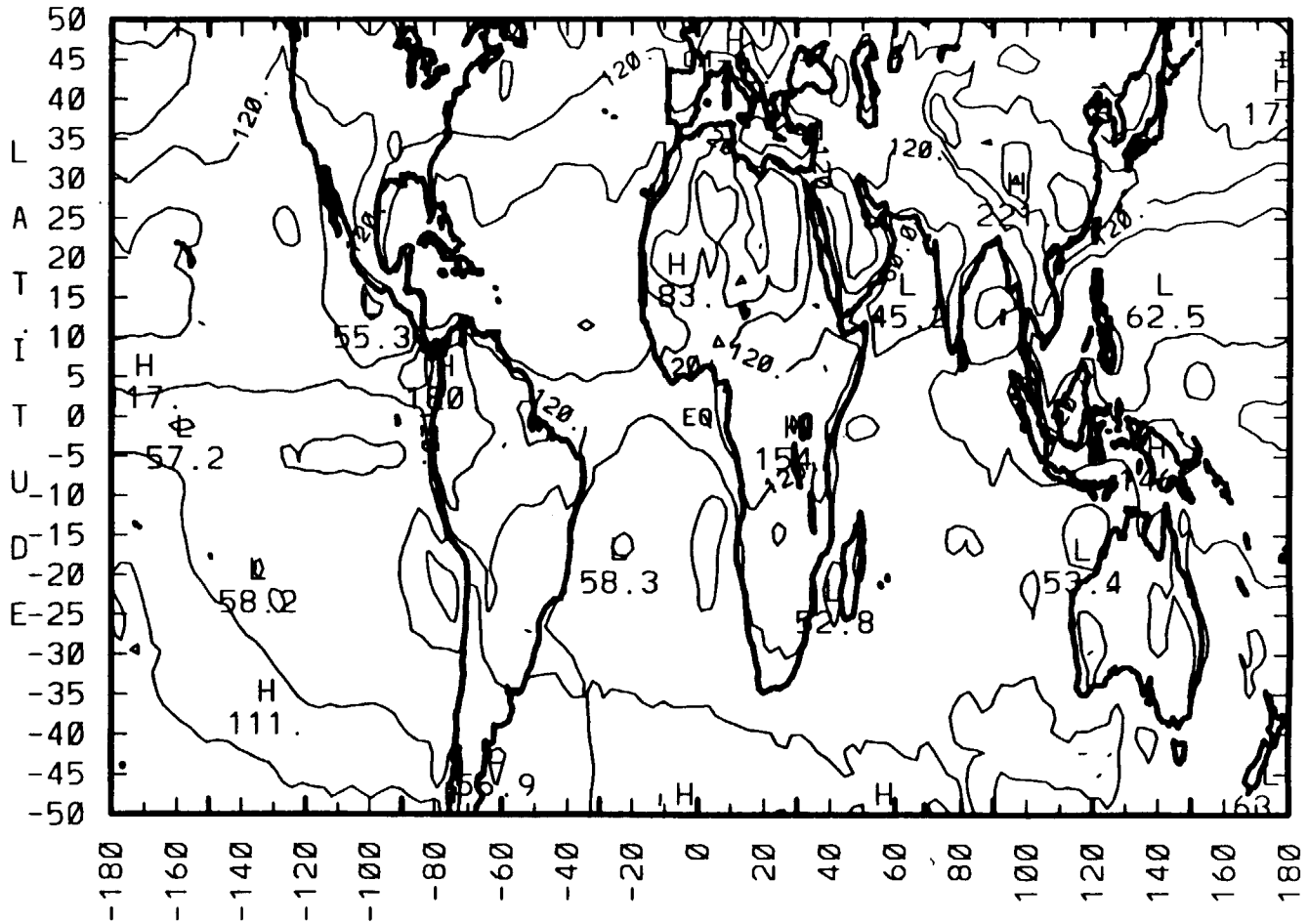

CONTOUR FROM 0.000000E+00 TO 240.00 CONTOUR INTERVAL OF 30.000 PT(3,3)= 79.439

5-YR MONTHLY STANDARD DEVIATIONS

(1984 - 1989)

APR SW REFLECTED (WM**2)

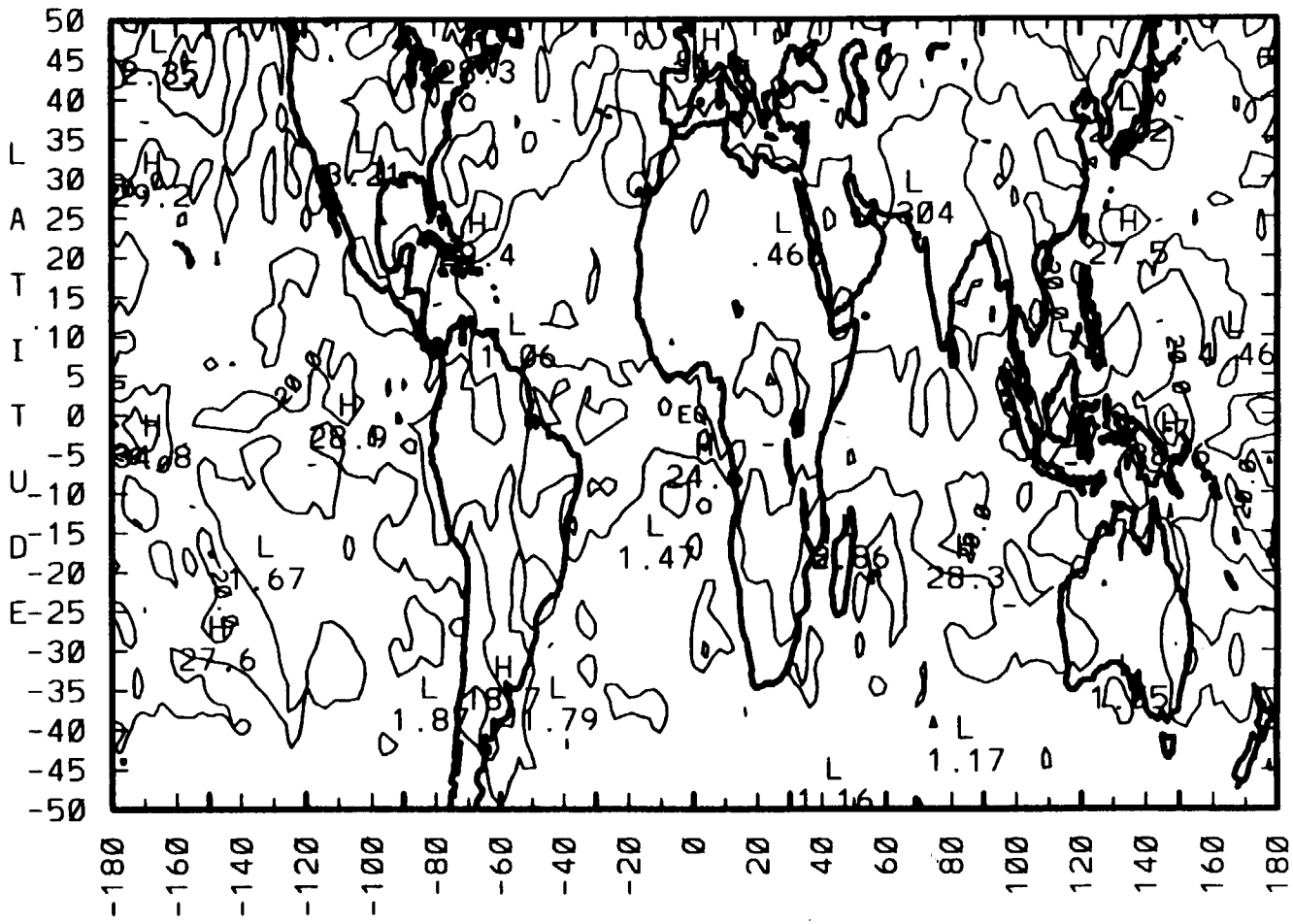

CONTOUR FROM 0.000000E+00 TO 50.000 CONTOUR INTERVAL OF 10.000 PT(3,3)= 7.2885

5-YEAR MONTHLY MEANS (12/84 - 11/89)
APR SURFACE TEMP (DEG. K)

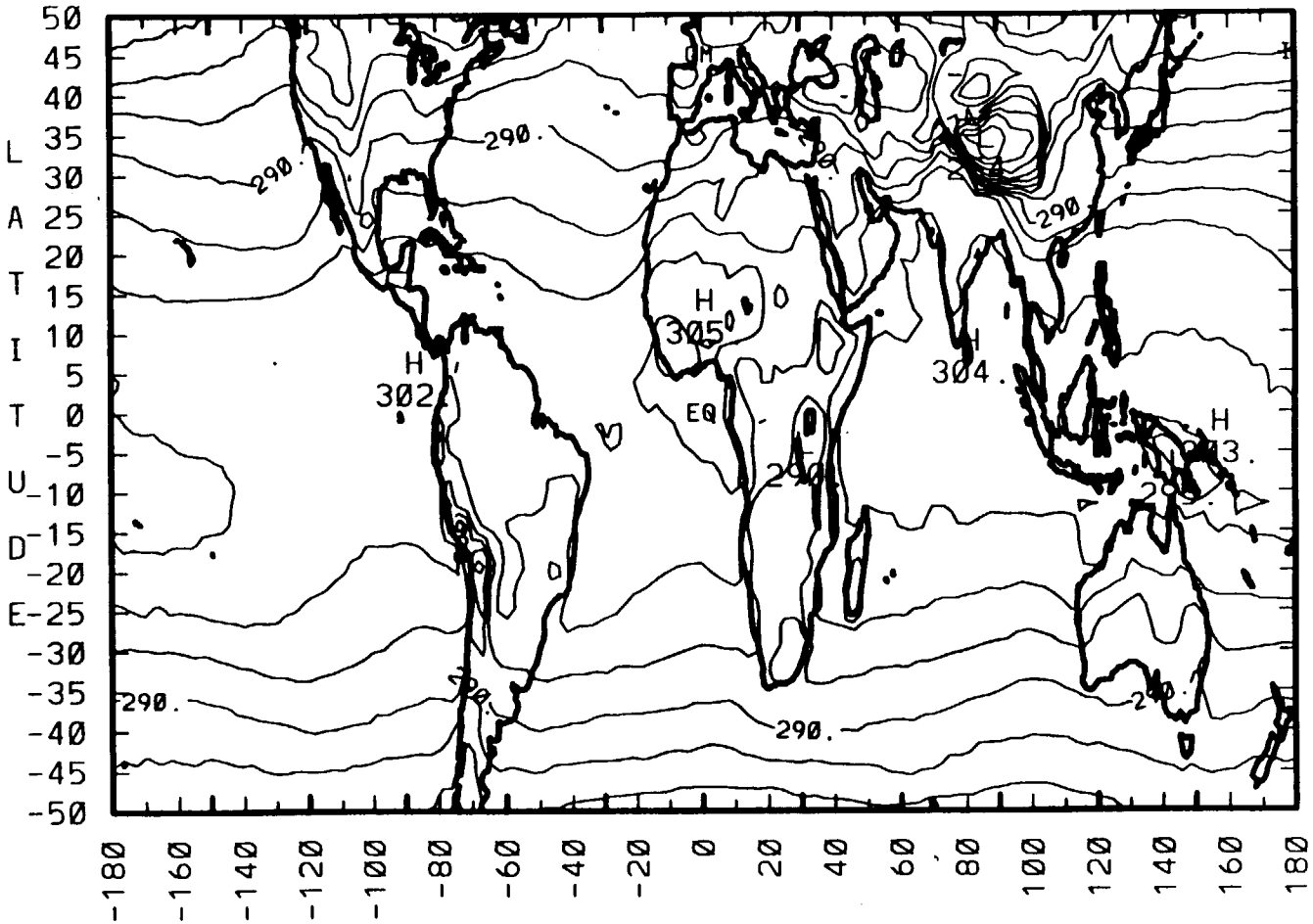

CONTOUR FROM 246.00 TO 310.00 CONTOUR INTERVAL OF 4.0000 PT(3,3)= 285.44

5-YR MONTHLY STANDARD DEVIATIONS

(1984 - 1989)

APR SURFACE TEMP (DEG. K)

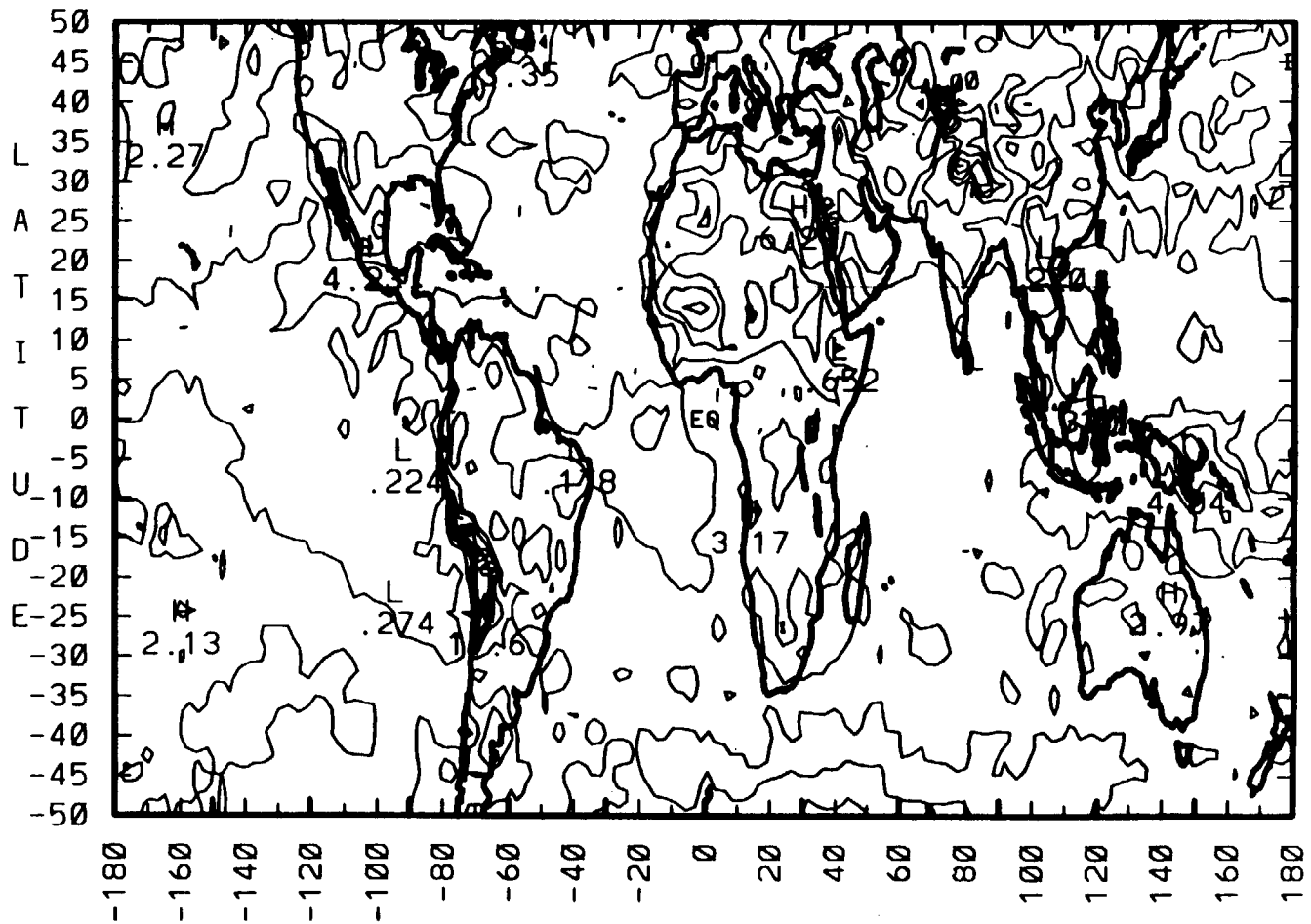

CONTOUR FROM 0.000000E+00 TO 39.000 CONTOUR INTERVAL OF 1.0000 PT(3,3)= 0.88536

5-YEAR MONTHLY MEANS (12/84 - 11/89)
APR CLOUD FRACTION (%)

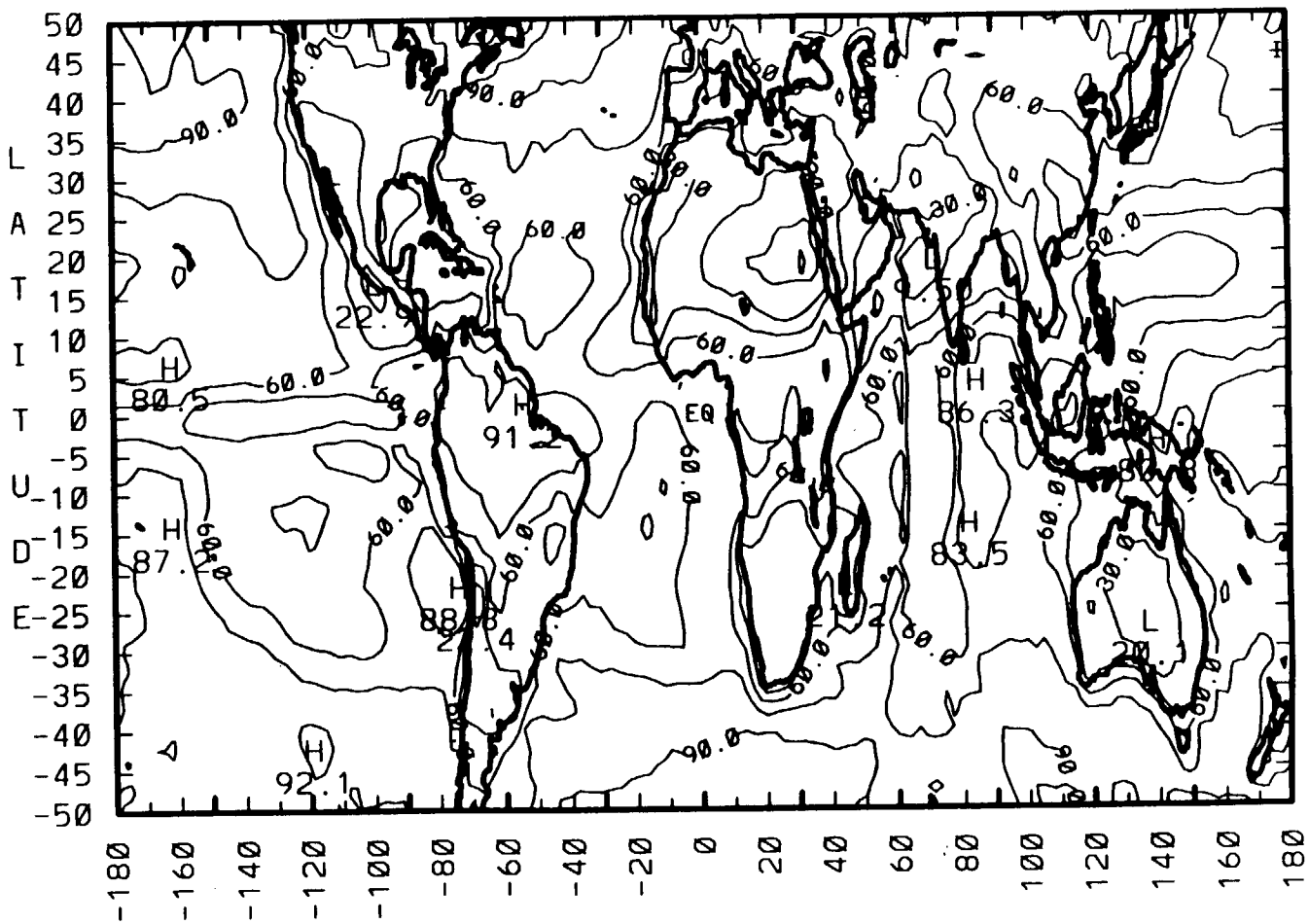

CONTOUR FROM 0.000000E+00 TO 90.000 CONTOUR INTERVAL OF 15.000 PT(3,3)= 86.500

5-YR MONTHLY STANDARD DEVIATIONS
(1984 - 1989)
APR CLOUD FRACTION (%)

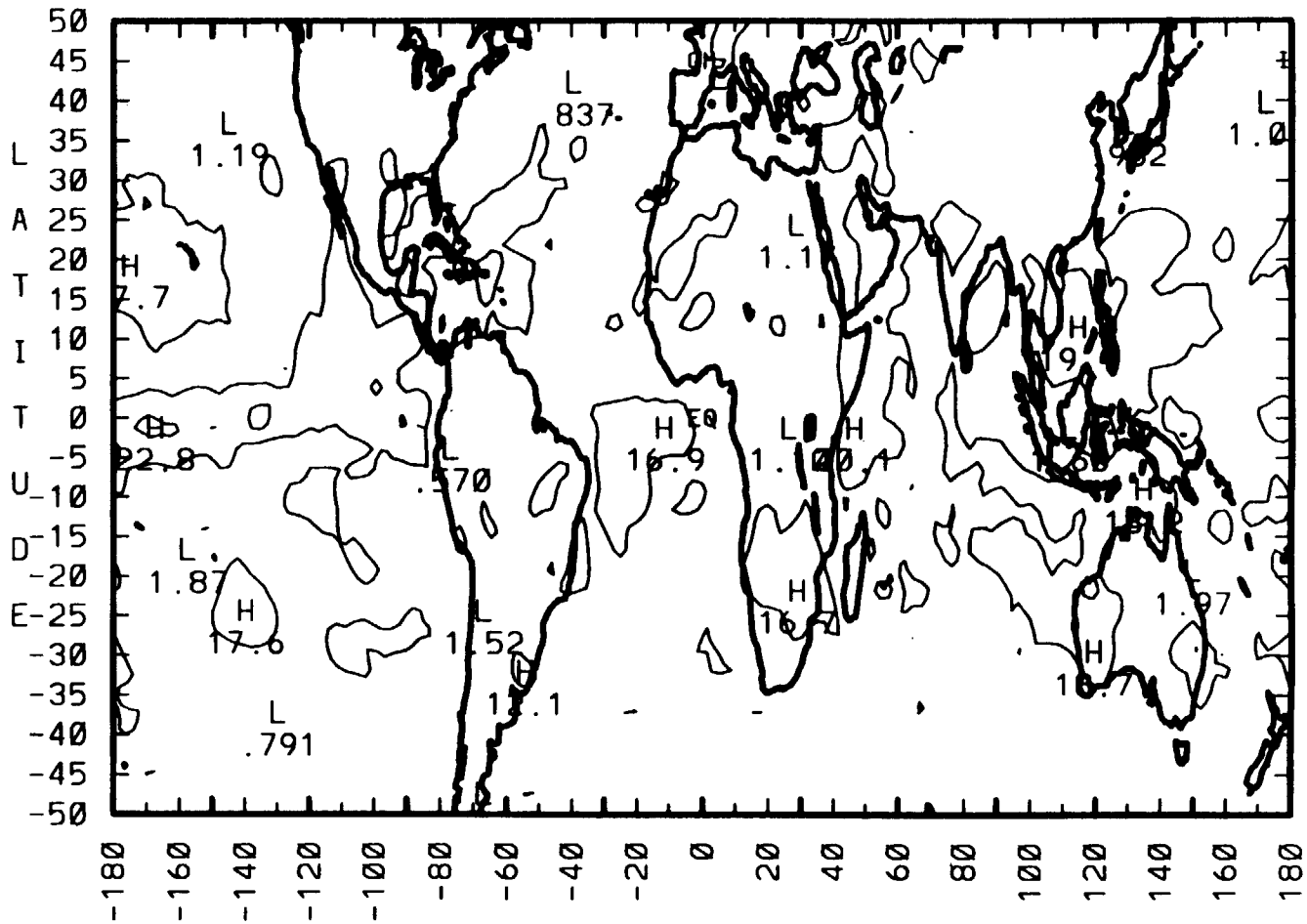

LONGITUDE

5-YEAR MONTHLY MEANS (12/84 - 11/89)
APR CLD TOP TEMP (DEG. K)

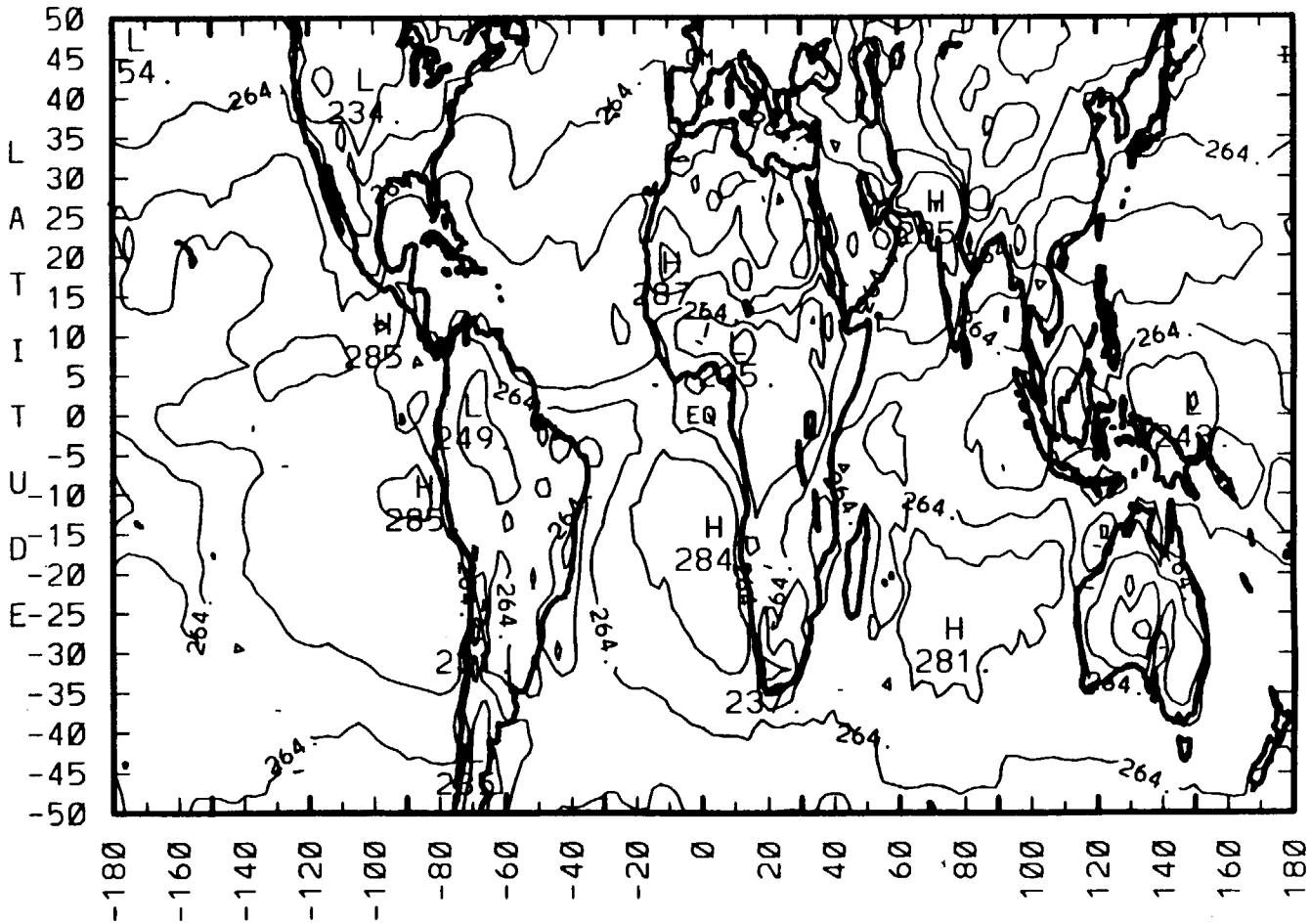

CONTOUR FROM 24.000 TO 284.00 CONTOUR INTERVAL OF 10.000 PT(3,3)= 265.28

5-YR MONTHLY STANDARD DEVIATIONS
(1984 - 1989)
APR CLD TOP TEMP (DEG. K)

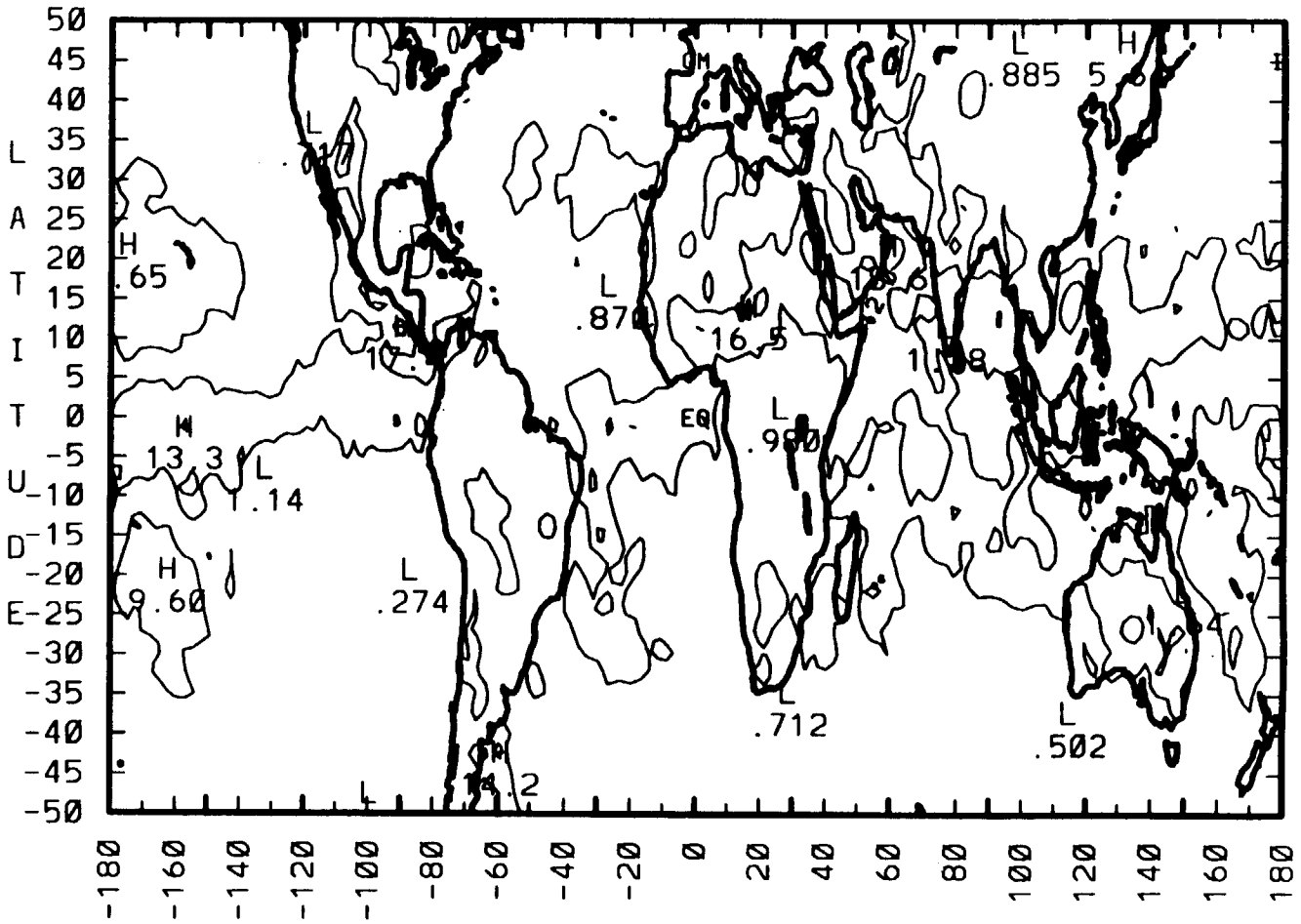

M36

5-YEAR MONTHLY MEANS (12/84 - 11/89)
JUL NET RADIATION (Wm**2)

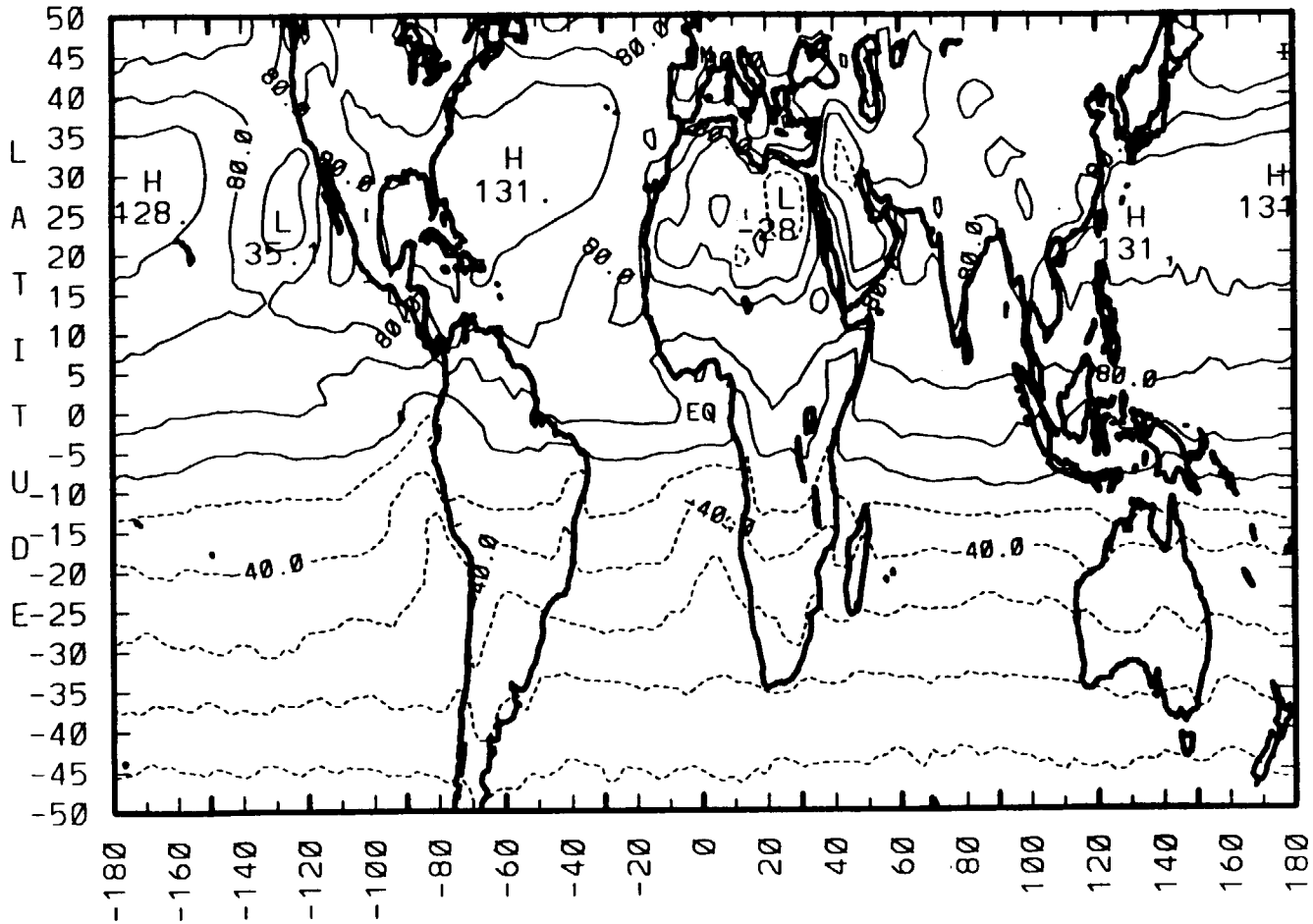

CONTOUR FROM -160.00 TO 140.00 CONTOUR INTERVAL OF 30.000 PT(3,31)= -127.89

M37

5-YR MONTHLY STANDARD DEVIATIONS
(1984 - 1989)
JULY NET RADIATION (Wm**2)

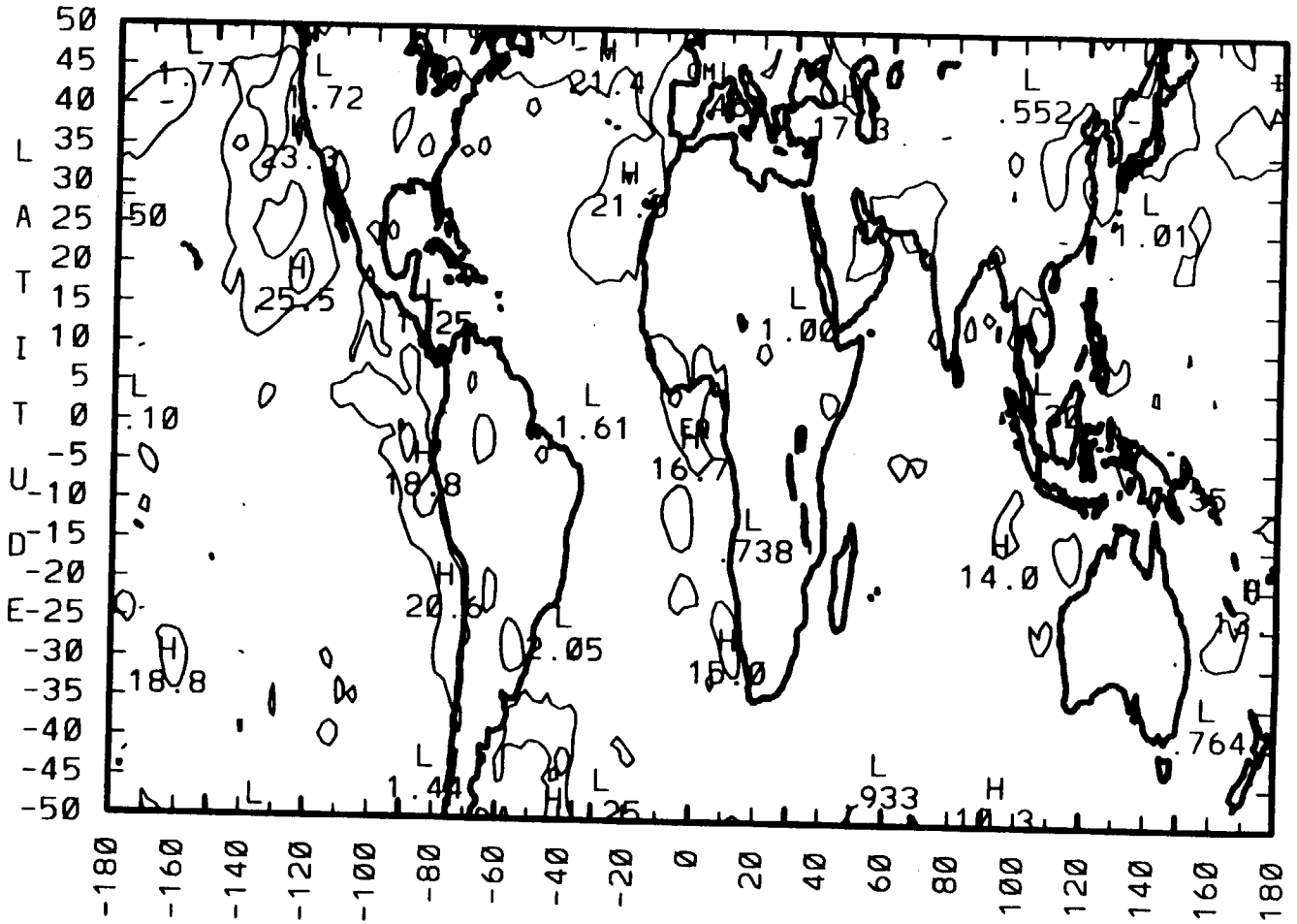

CONTOUR FROM 0.000000E+00 TO 50.000 CONTOUR INTERVAL OF 10.000 PT(3,3)= 5.7763

5-YEAR MONTHLY MEANS (12/84 - 11/89)
JUL OLR (W/m**2)

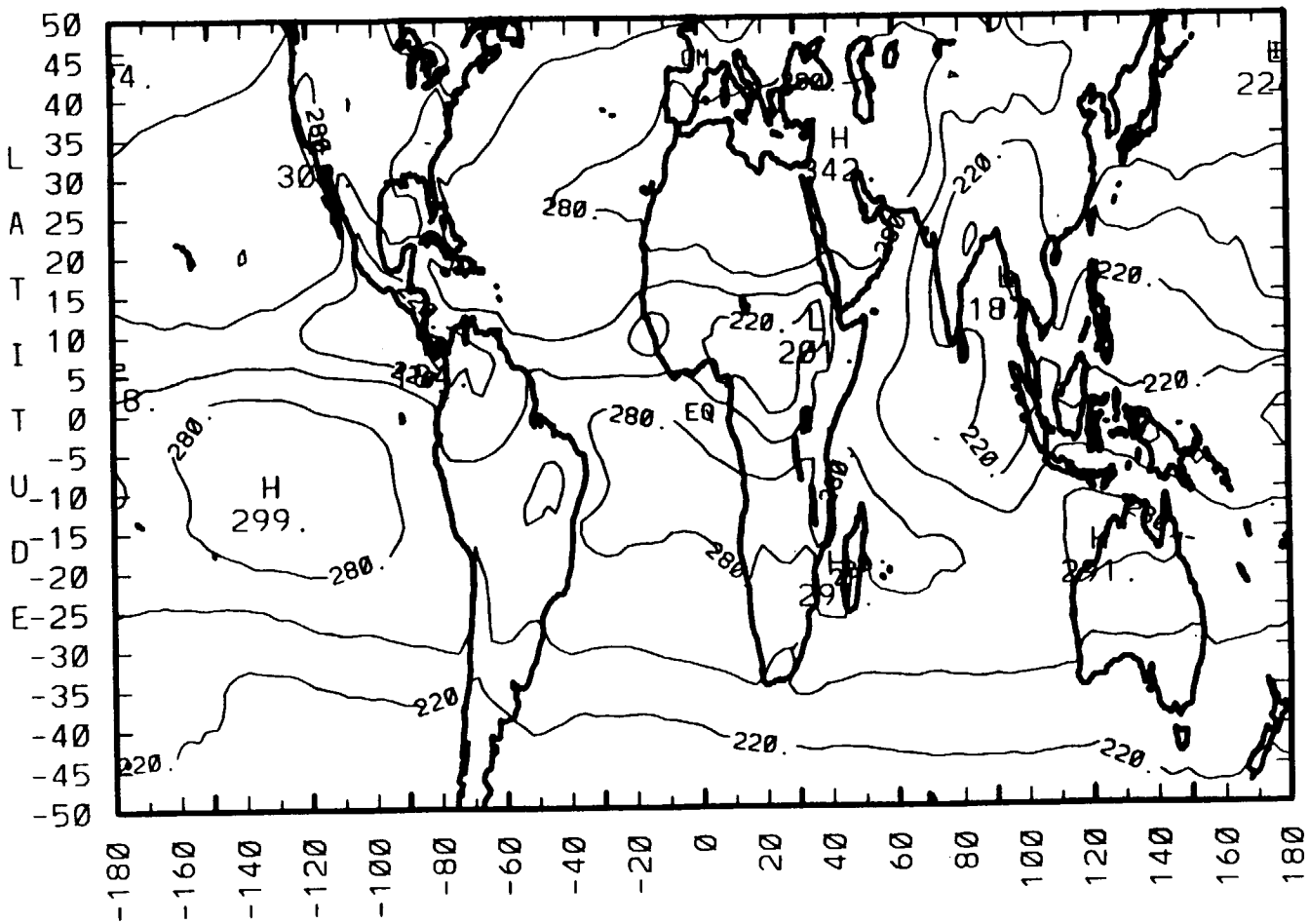

CONTOUR FROM 160.00 TO 280.00 CONTOUR INTERVAL OF 30.000 PT(3,3)= 218.28

5-YR MONTHLY STANDARD DEVIATIONS

(1984 - 1989)

JULY OLR (W/m**2)

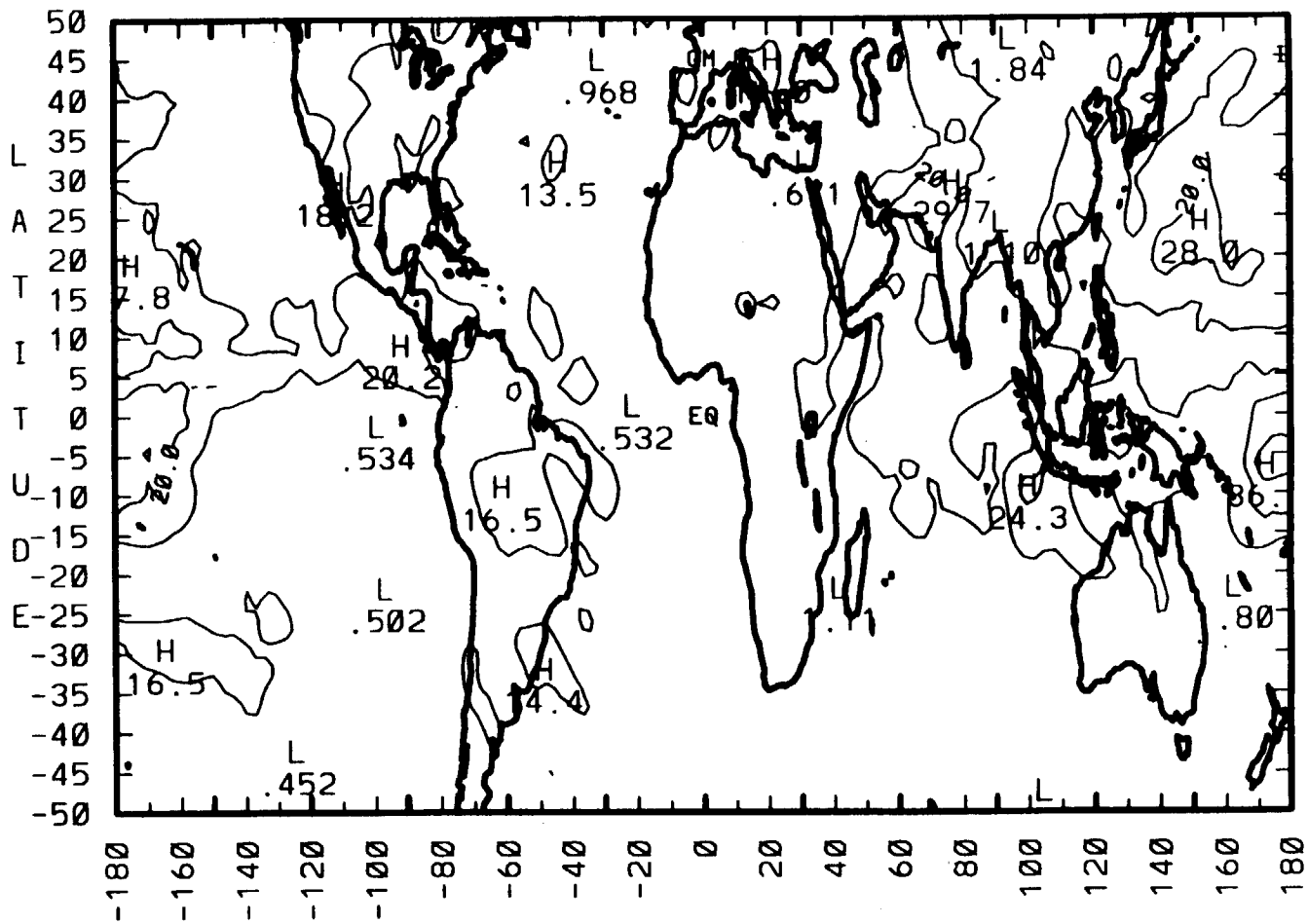

CONTOUR FROM 0.000000E+00 TO 50.000 CONTOUR INTERVAL OF 10.000 PT(3,3)= 4.2830

5-YEAR MONTHLY MEANS (12/84 - 11/89)
JUL SW REFLECTED (WM**2)

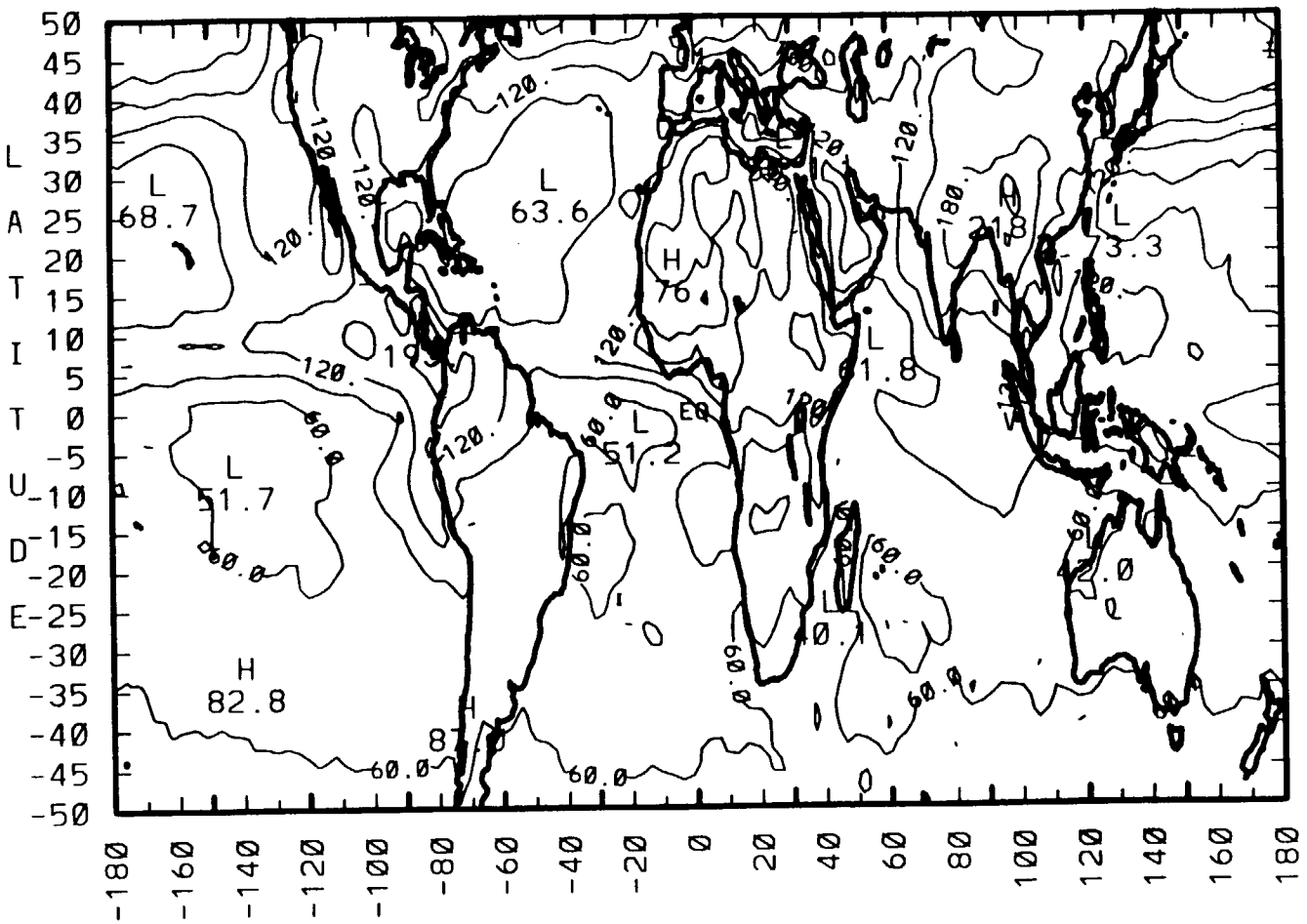

LONGITUDE

CONTOUR FROM 0.000000E+00 TO 240.00 CONTOUR INTERVAL OF 30.000 PT(3,3)= 47.179

5-YR MONTHLY STANDARD DEVIATIONS

(1984 - 1989)

JULY SW REFLECTED (WM**2)

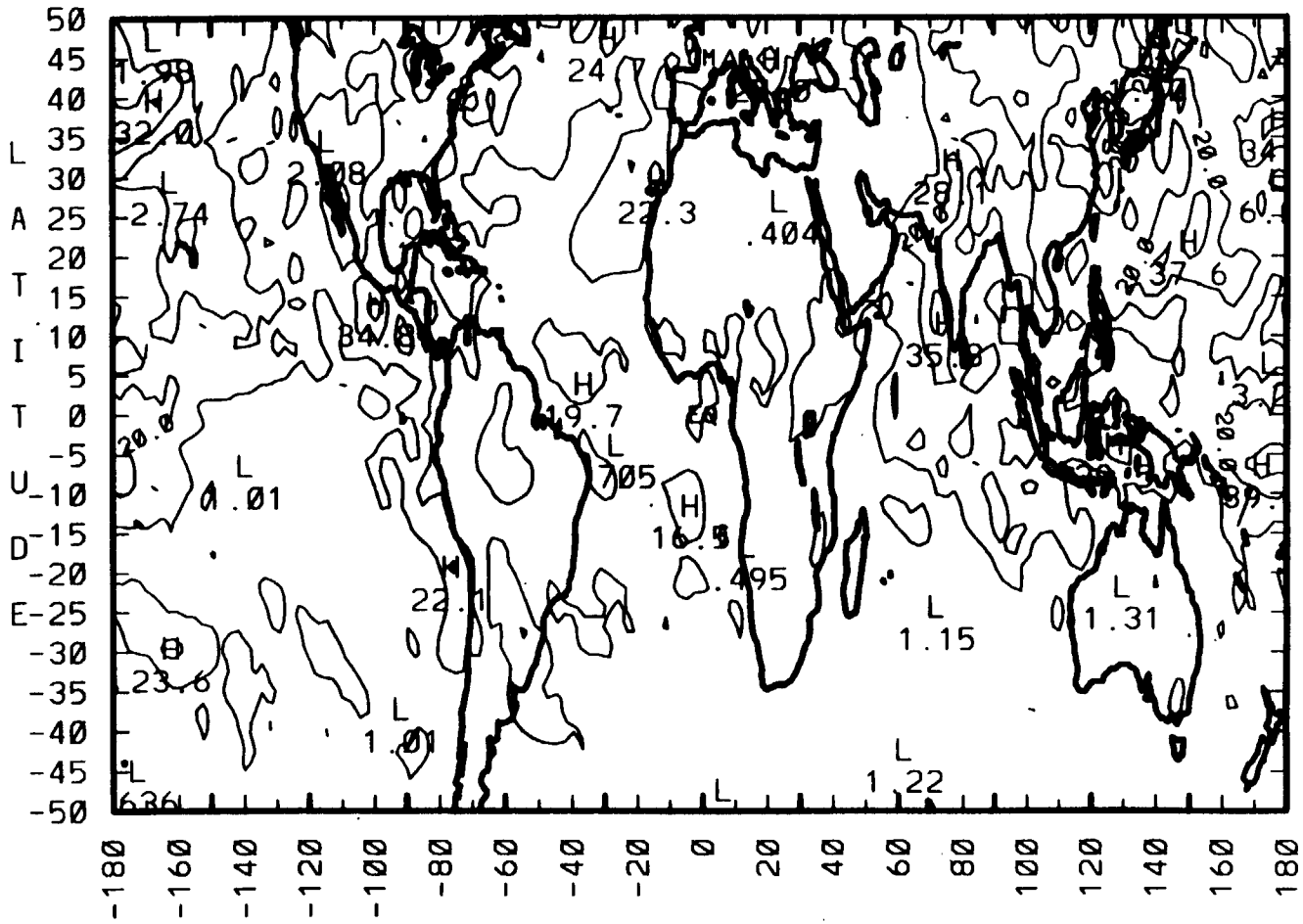

CONTOUR FROM 0.000000E+00 TO 50.000 CONTOUR INTERVAL OF 10.000 PT(3,3)= 3.5040

5-YEAR MONTHLY MEANS (12/84 - 11/89)
JUL SURFACE TEMP (DEG. K)

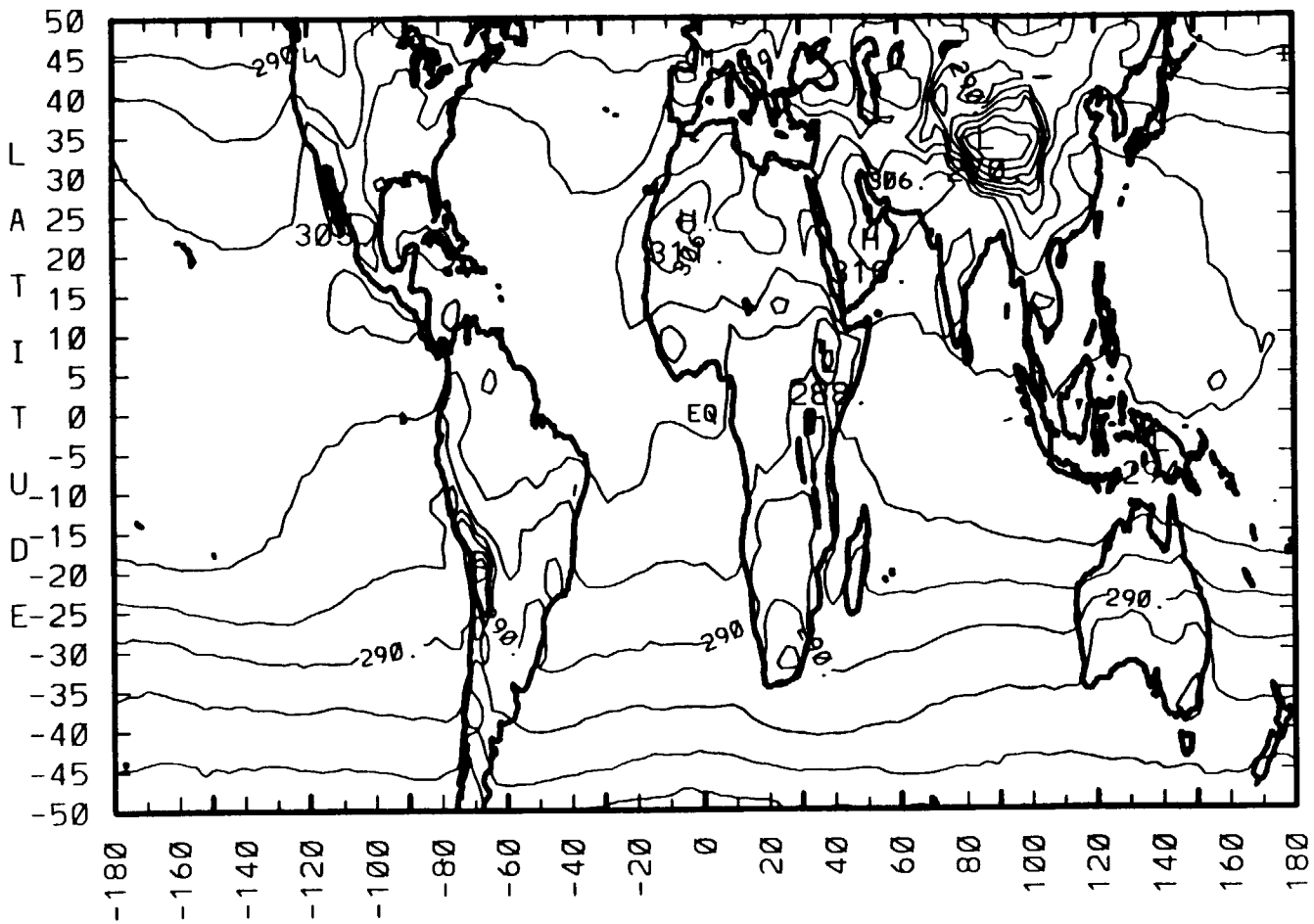

5-YR MONTHLY STANDARD DEVIATIONS

(1984 - 1989)

JULY SURFACE TEMP (DEG. K)

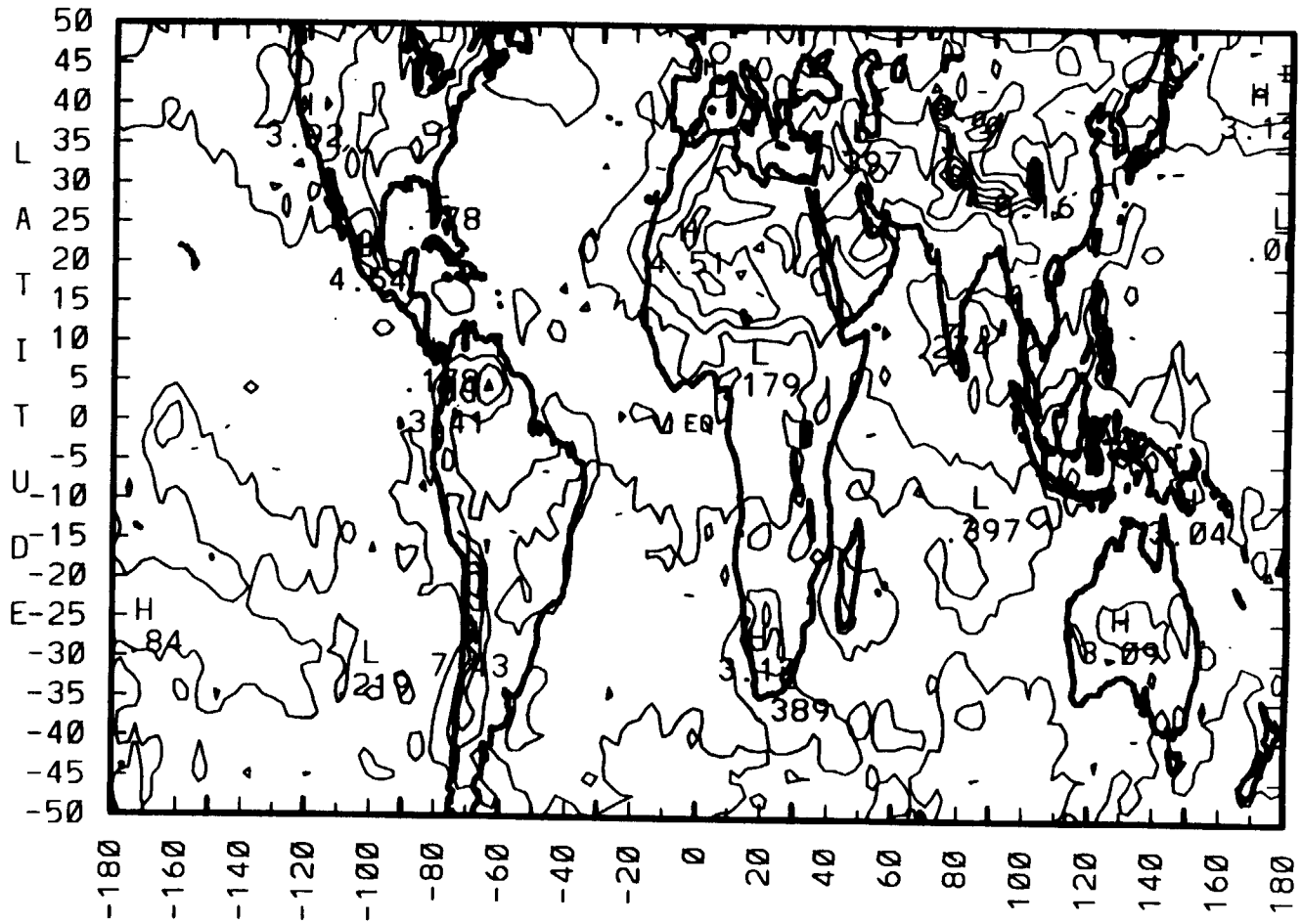

LONGITUDE

CONTOUR FROM 0.000000E+00 TO 39.000 CONTOUR INTERVAL OF 1.0000 PT(3,3)= 0.98849

5-YEAR MONTHLY MEANS (12/84 - 11/89)
JUL CLOUD FRACTION (%)

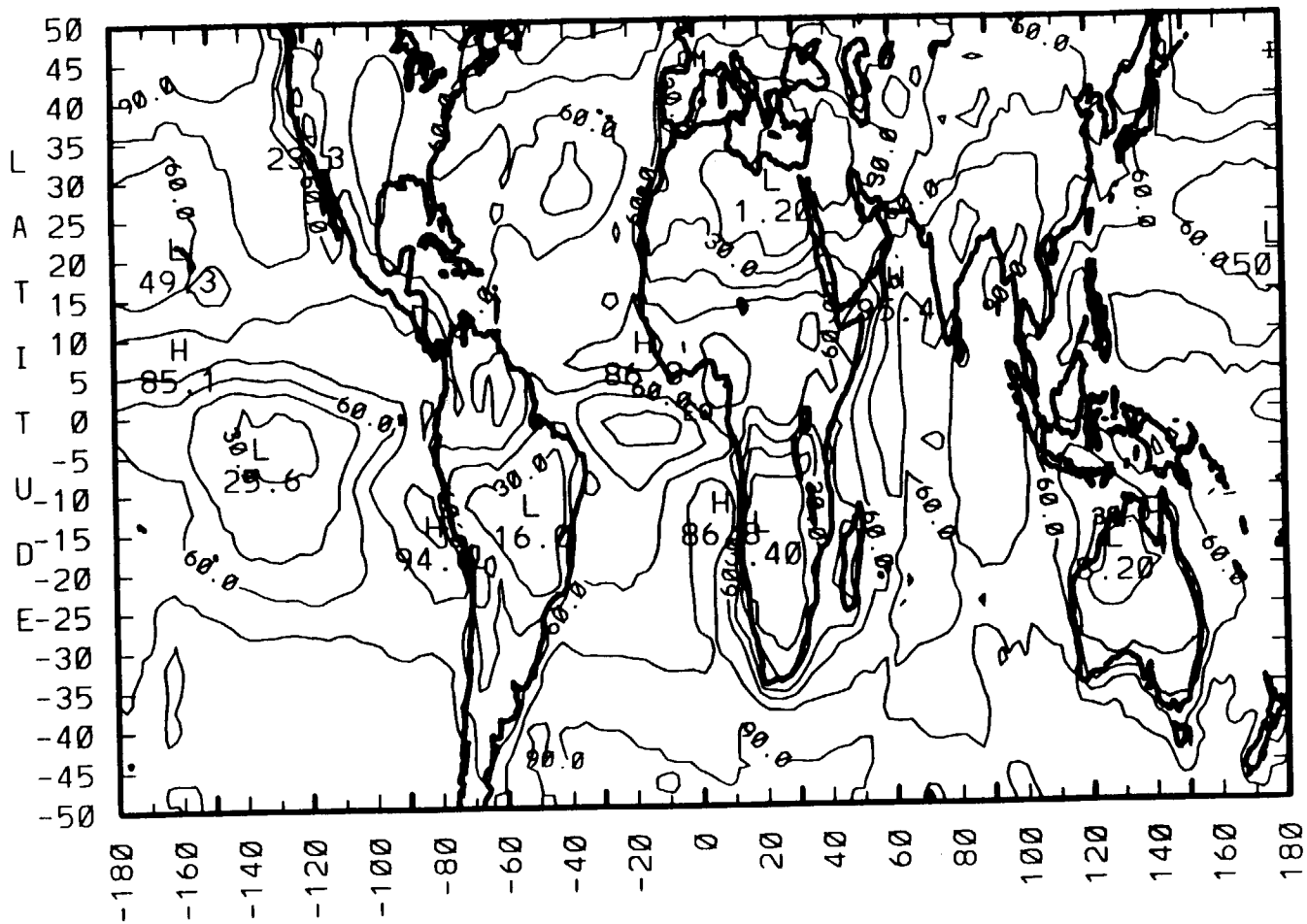

5-YR MONTHLY STANDARD DEVIATIONS
(1984 - 1989)
JULY CLOUD FRACTION (%)

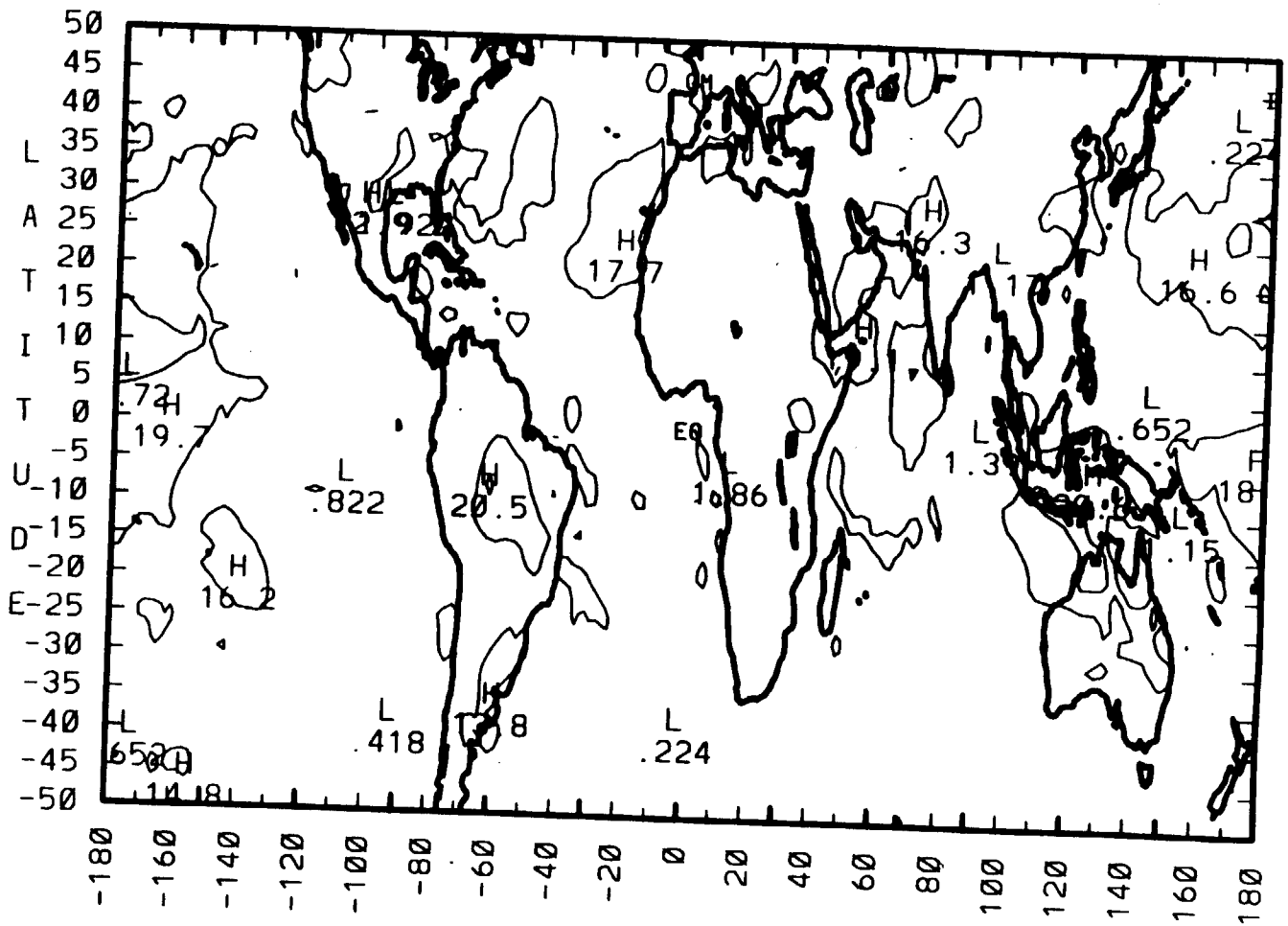

CONTOUR FROM 0.000000E+00 TO 50.000 CONTOUR INTERVAL OF 10.000 PT(3,3)= 3.8943

5-YEAR MONTHLY MEANS (12/84 - 11/89)
JUL CLD TOP TEMP (DEG. K)

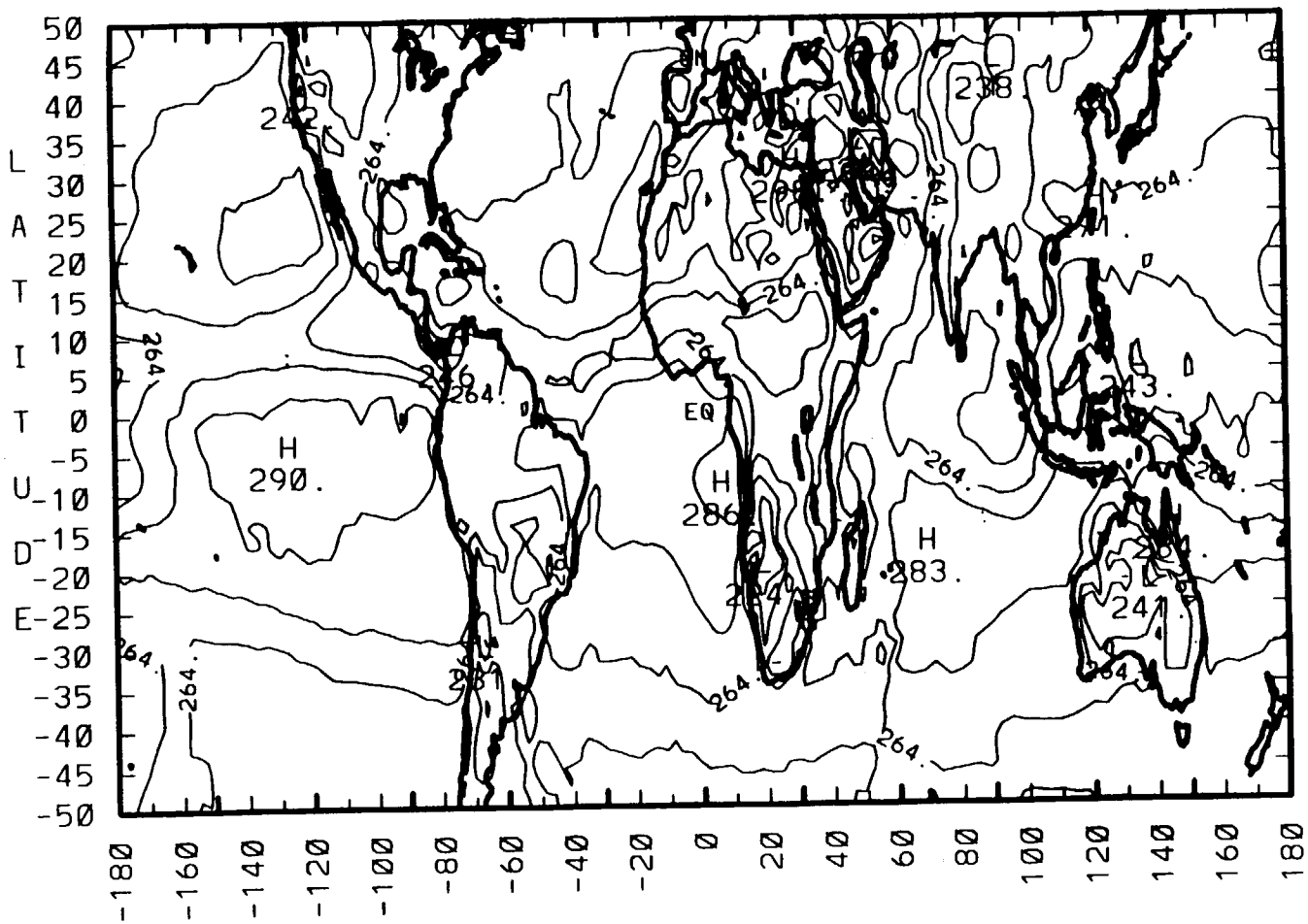

CONTOUR FROM 24.000 TO 284.00 CONTOUR INTERVAL OF 10.000 PT(3,3)= 259.98

5-YR MONTHLY STANDARD DEVIATIONS
(1984 - 1989)
JULY CLD TOP TEMP .(DEG. K)

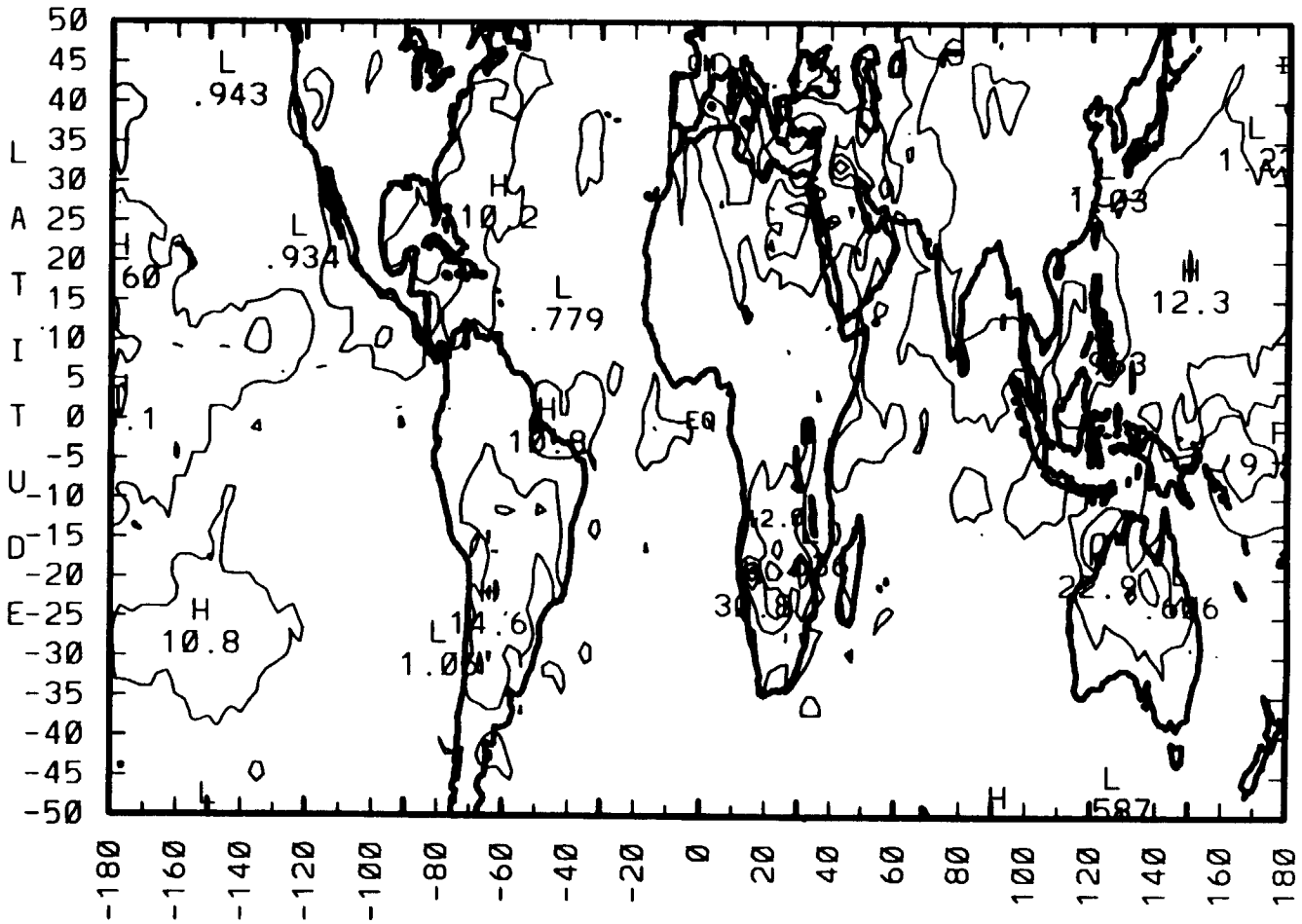

LONGITUDE

CONTOUR FROM 0.000000E+00 TO 48.000 CONTOUR INTERVAL OF 6.0000 PT(3,3)= 2.7523

M48

5-YEAR MONTHLY MEANS (12/84 - 11/89)
OCT NET RADIATION (Wm**2)

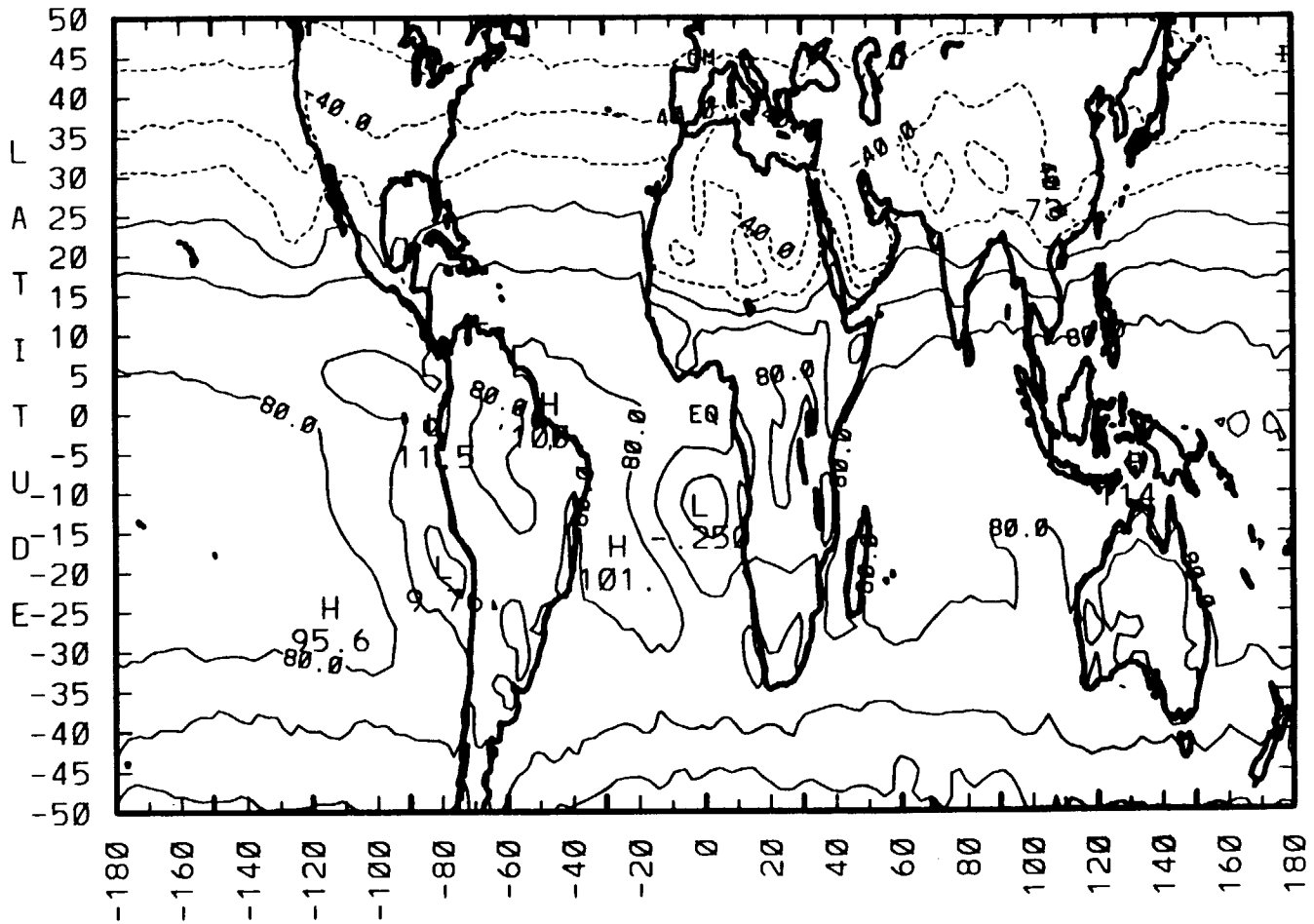

M49

5-YR MONTHLY STANDARD DEVIATIONS

(1984 - 1989)

OCT NET RADIATION (Wm**2)

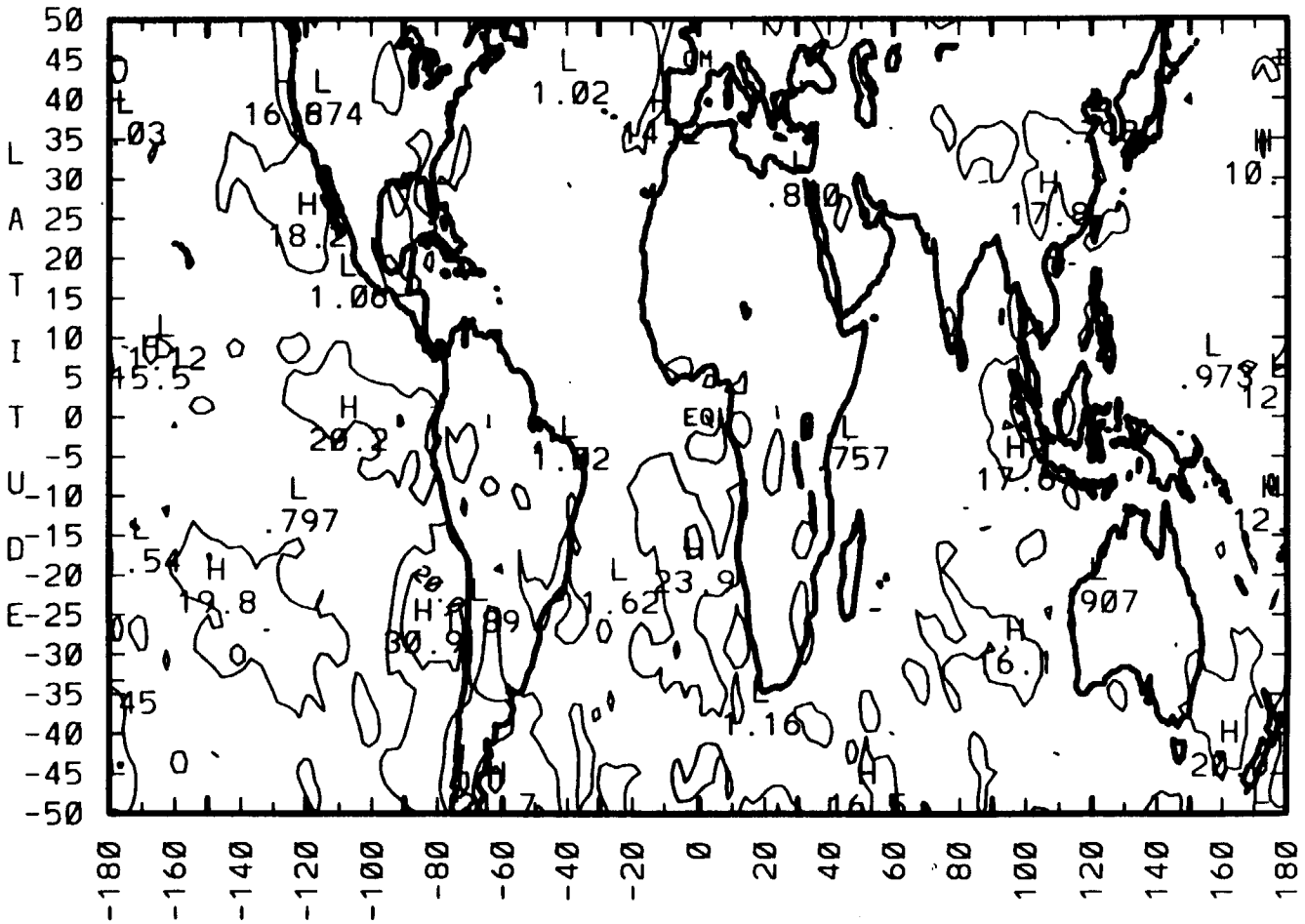

CONTOUR FROM 0.000000E+00 TO 50.000 CONTOUR INTERVAL OF 10.000 PT(3,3)= 18.591

5-YEAR MONTHLY MEANS (12/84 - 11/89)
OCT OLR (W/m**2)

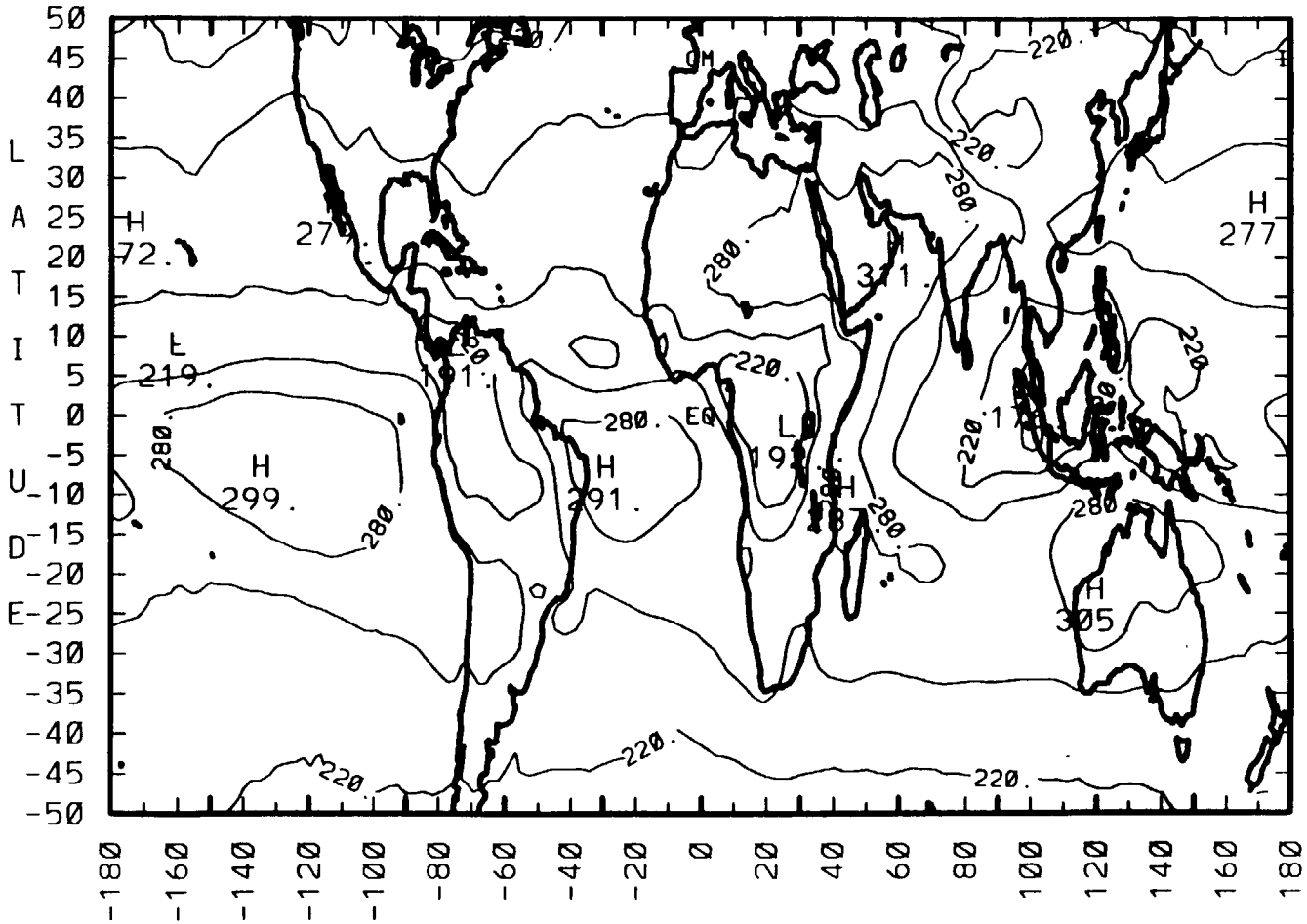

CONTOUR FROM 160.00 TO 280.00 CONTOUR INTERVAL OF 30.000 PT(3,3)= 225.80

5-YR MONTHLY STANDARD DEVIATIONS

(1984 - 1989)

OCT QLR (W/m**2)

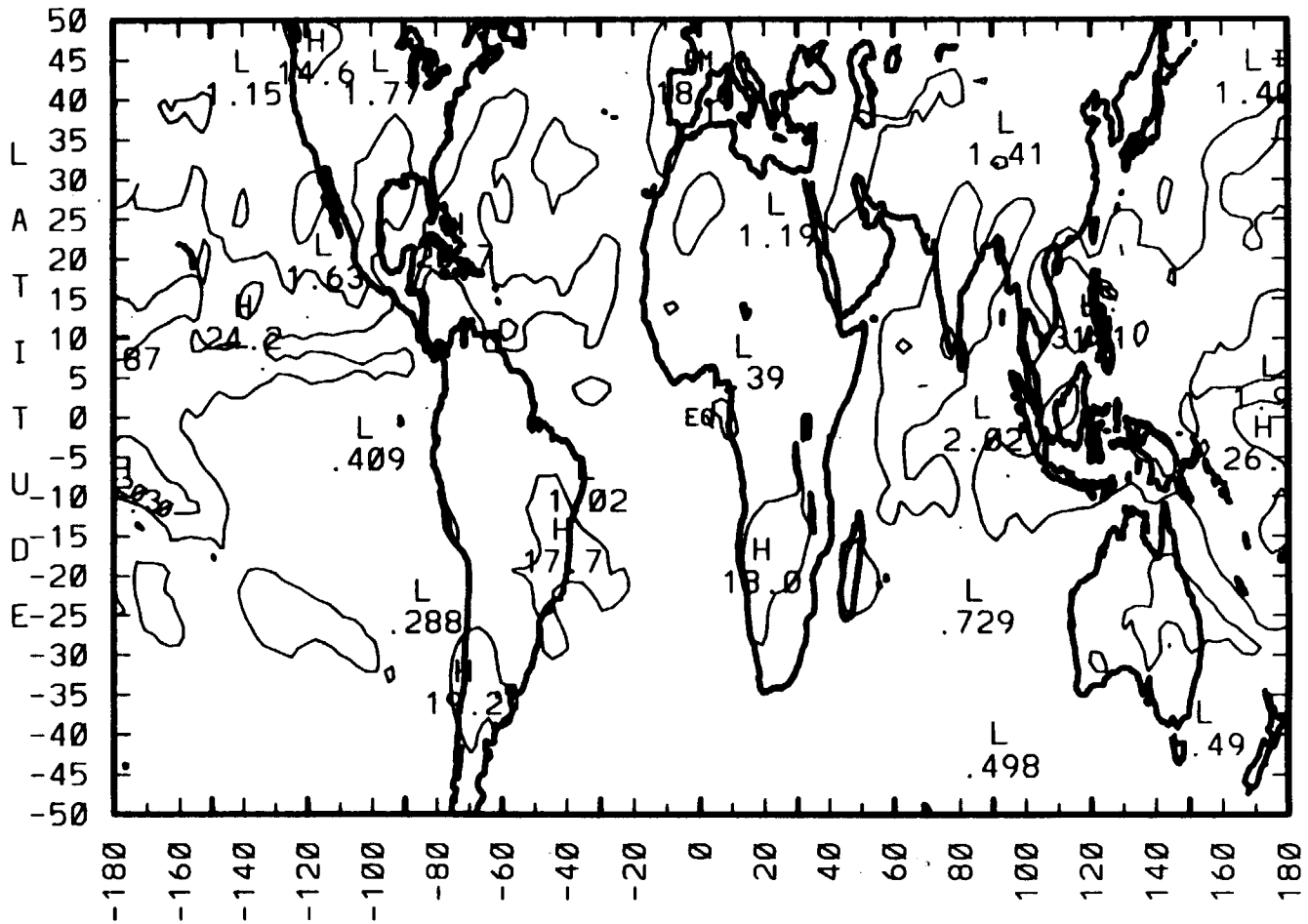

CONTOUR FROM 0.000000E+00 TO 50.000 CONTOUR INTERVAL OF 10.000 PT(3,3)= 5.0686

5-YEAR MONTHLY MEANS (12/84 - 11/89)
OCT SW REFLECTED (WM**2)

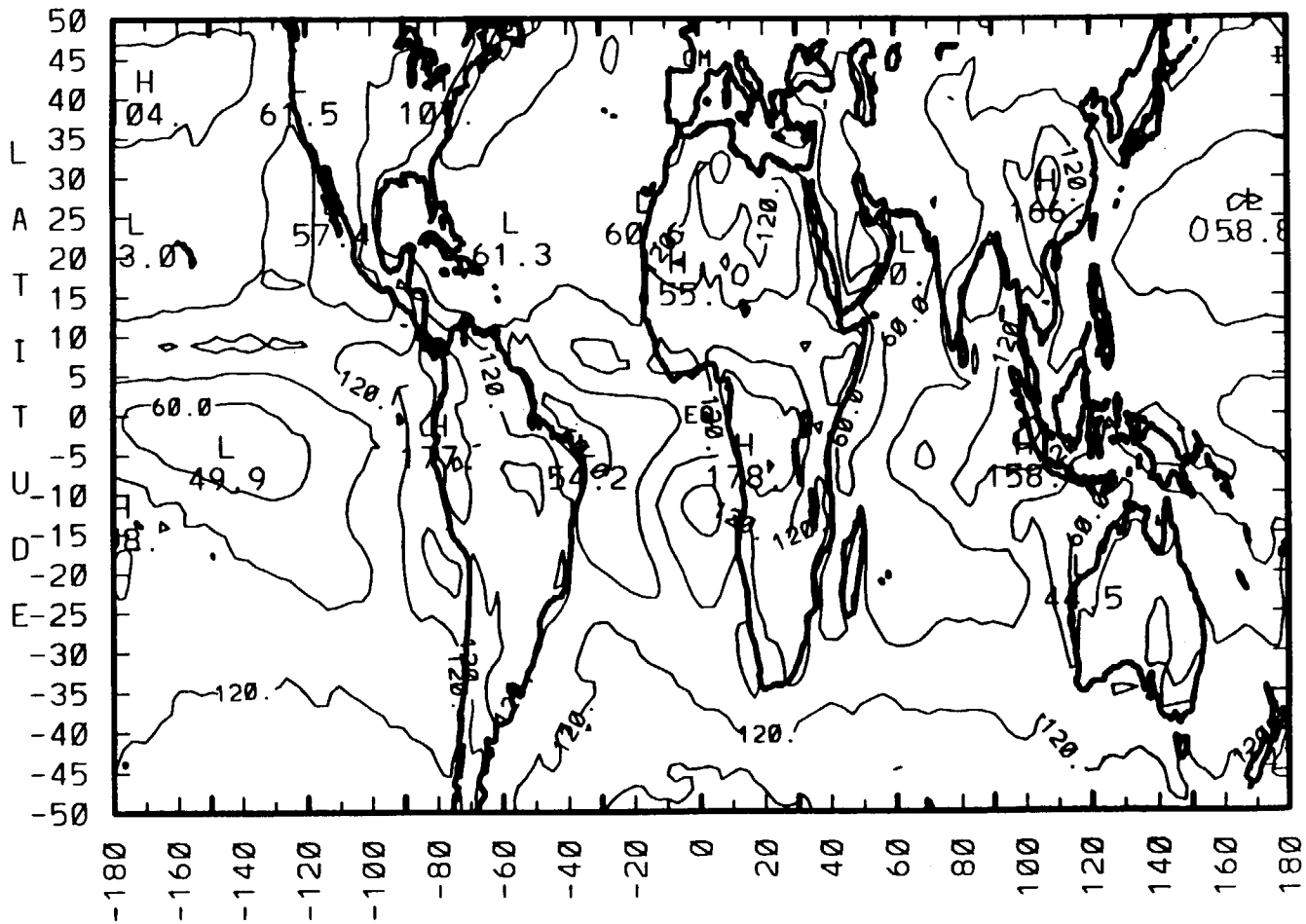

CONTOUR FROM 0.000000E+00 TO 240.00 CONTOUR INTERVAL OF 30.000 PT(3,3)= 131.56

5-YR MONTHLY STANDARD DEVIATIONS
(1984 - 1989)
OCT SW REFLECTED (WM**2)

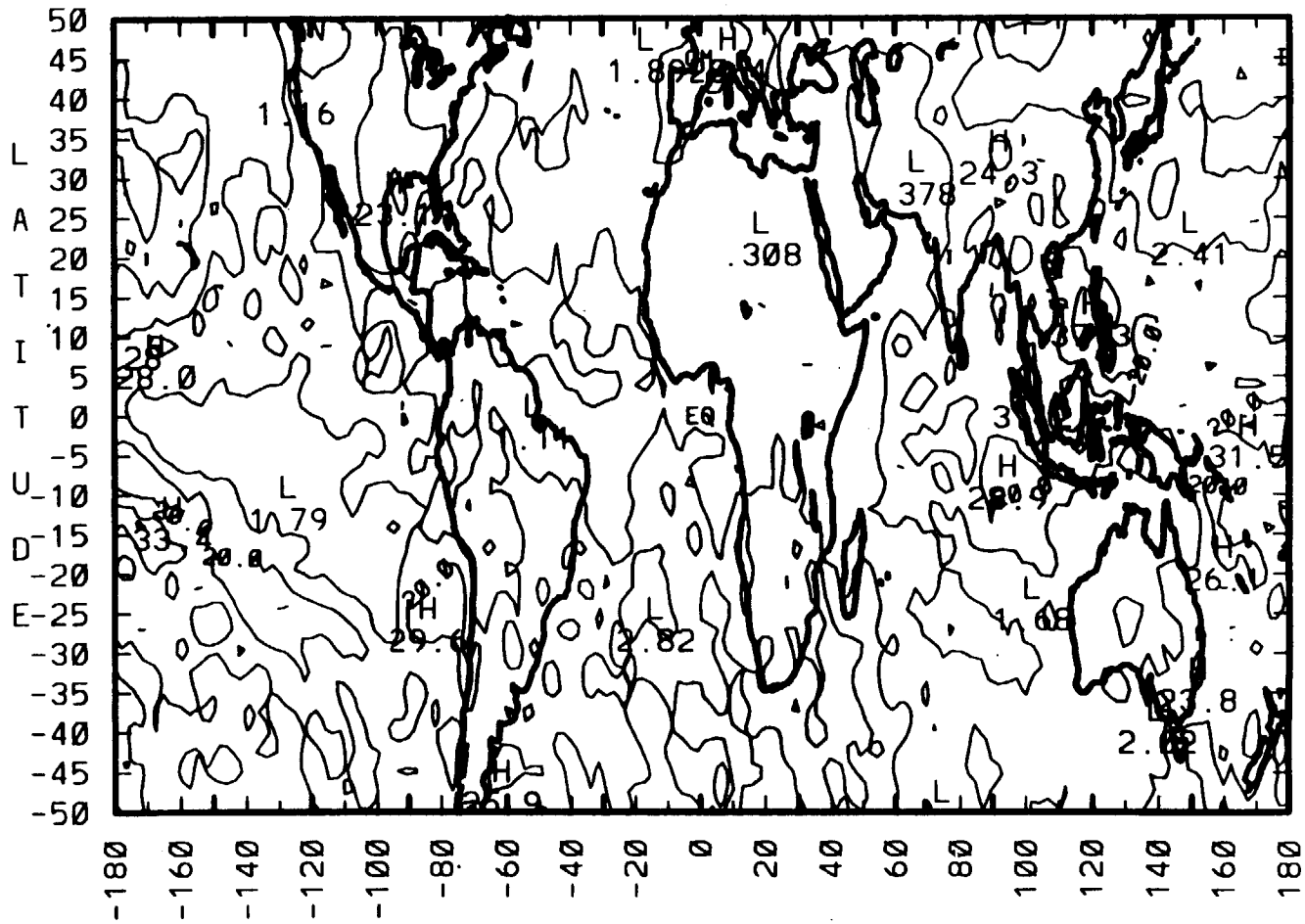

5-YEAR MONTHLY MEANS (12/84 - 11/89)
OCT SURFACE TEMP (DEG. K)

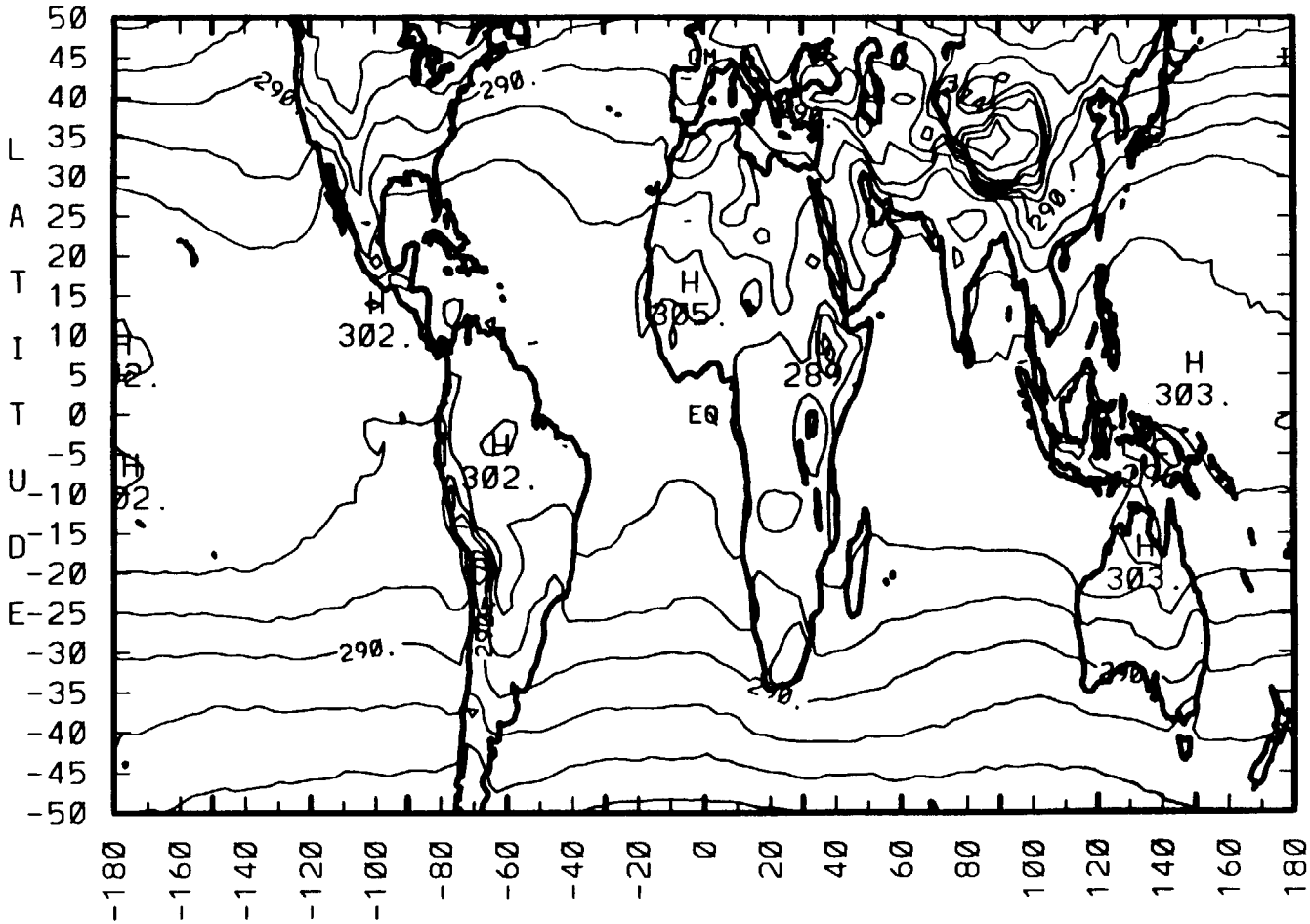

CONTOUR FROM 246.00 TO 310.00 CONTOUR INTERVAL OF 4.0000 PT(3,3)= 284.52

5-YR MONTHLY STANDARD DEVIATIONS
(1984 - 1989)
OCT SURFACE TEMP (DEG. K)

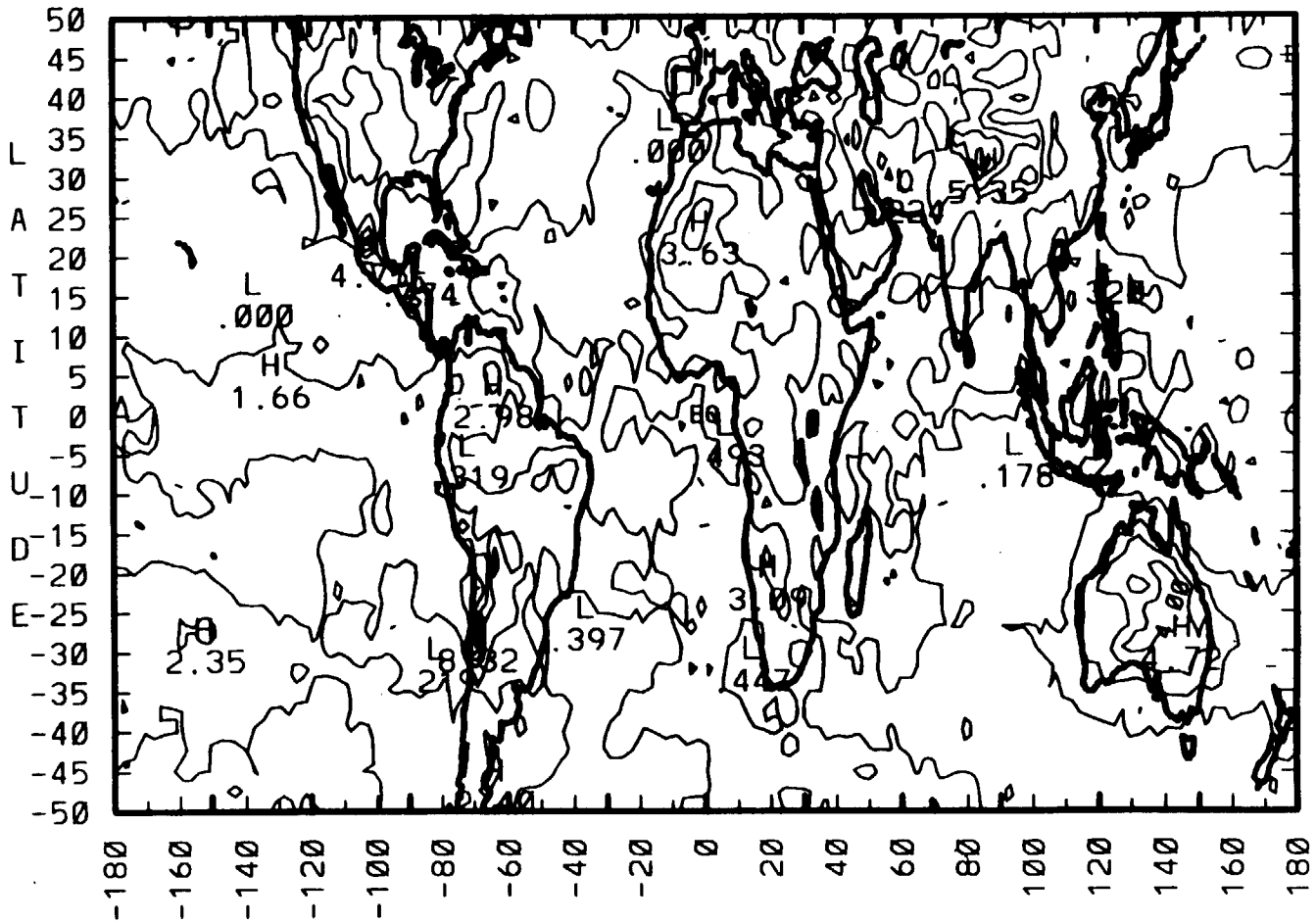

5-YEAR MONTHLY MEANS (12/84 - 11/89)
OCT CLOUD FRACTION (%)

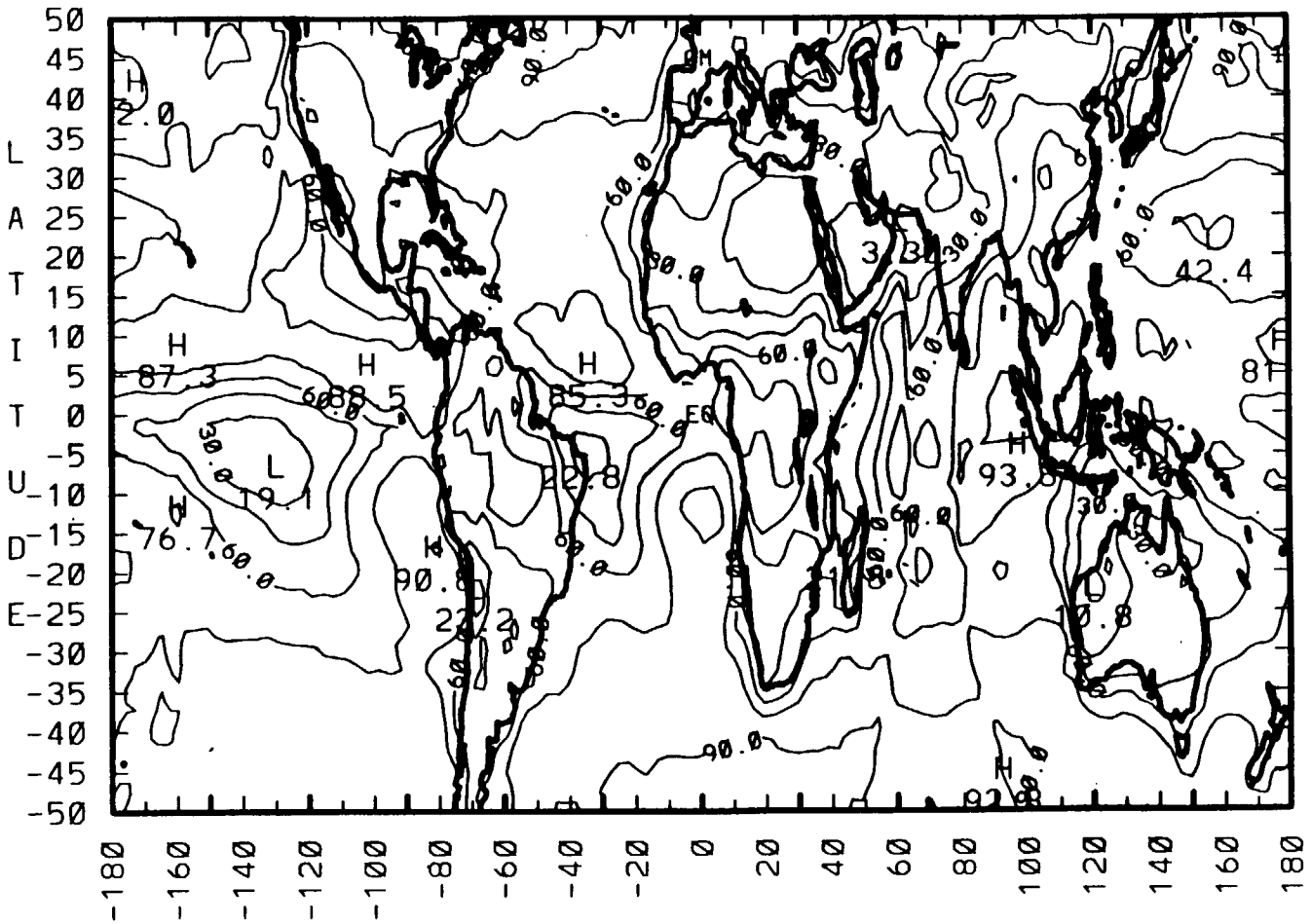

5-YR MONTHLY STANDARD DEVIATIONS

(1984 - 1989)

OCT CLOUD FRACTION (%)

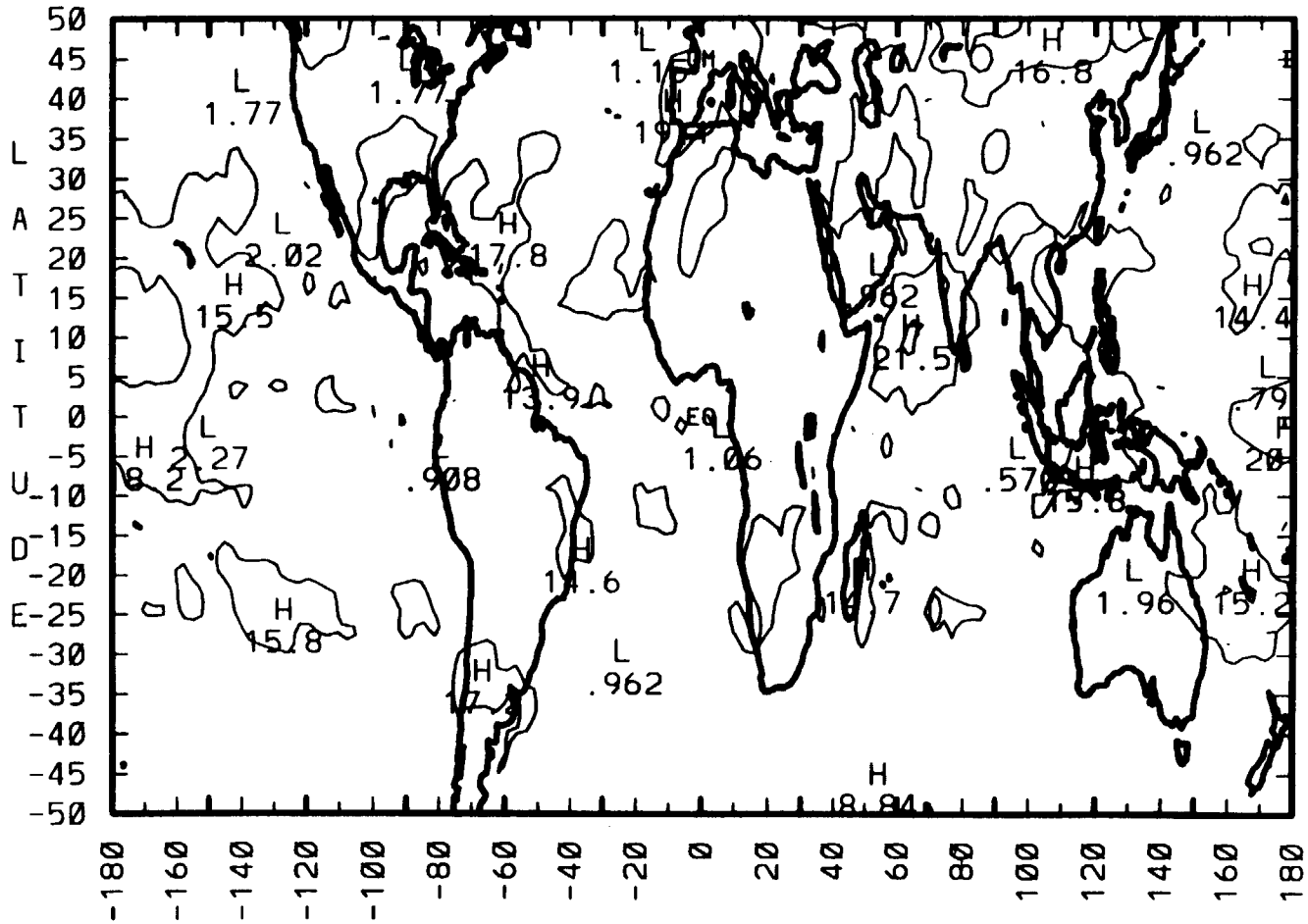

CONTOUR FROM 0.000000E+00 TO 50.000 CONTOUR INTERVAL OF 10.000 PT(3,3)= 6.3384

5-YEAR MONTHLY MEANS (12/84 - 11/89)
OCT CLD TOP TEMP (DEG. K)

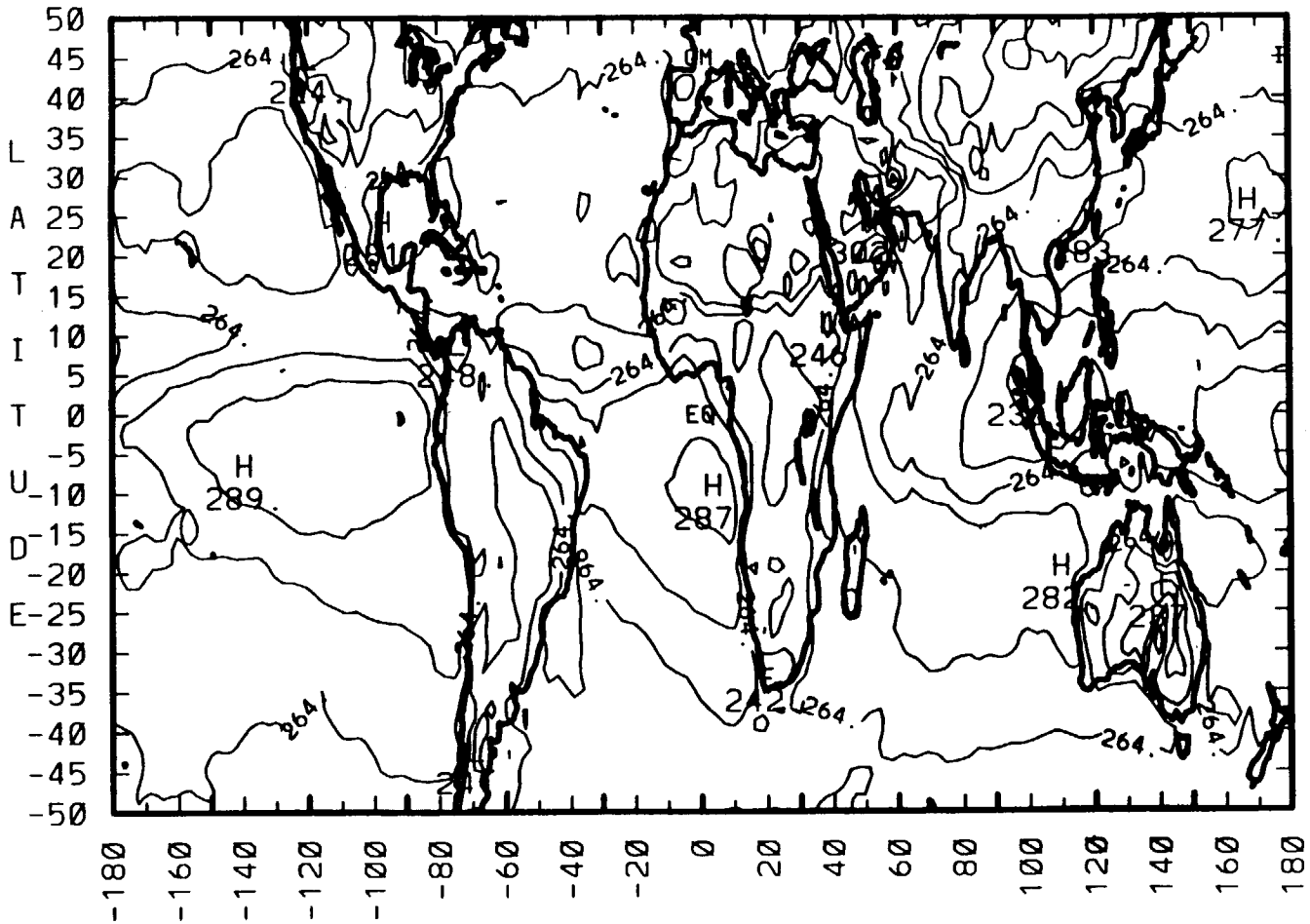

CONTOUR FROM 24.000 TO 284.00 CONTOUR INTERVAL OF 10.000 PT(3,3)= 262.50

5-YR MONTHLY STANDARD DEVIATIONS
(1984 - 1989)
OCT CLD TOP TEMP (DEG. K)

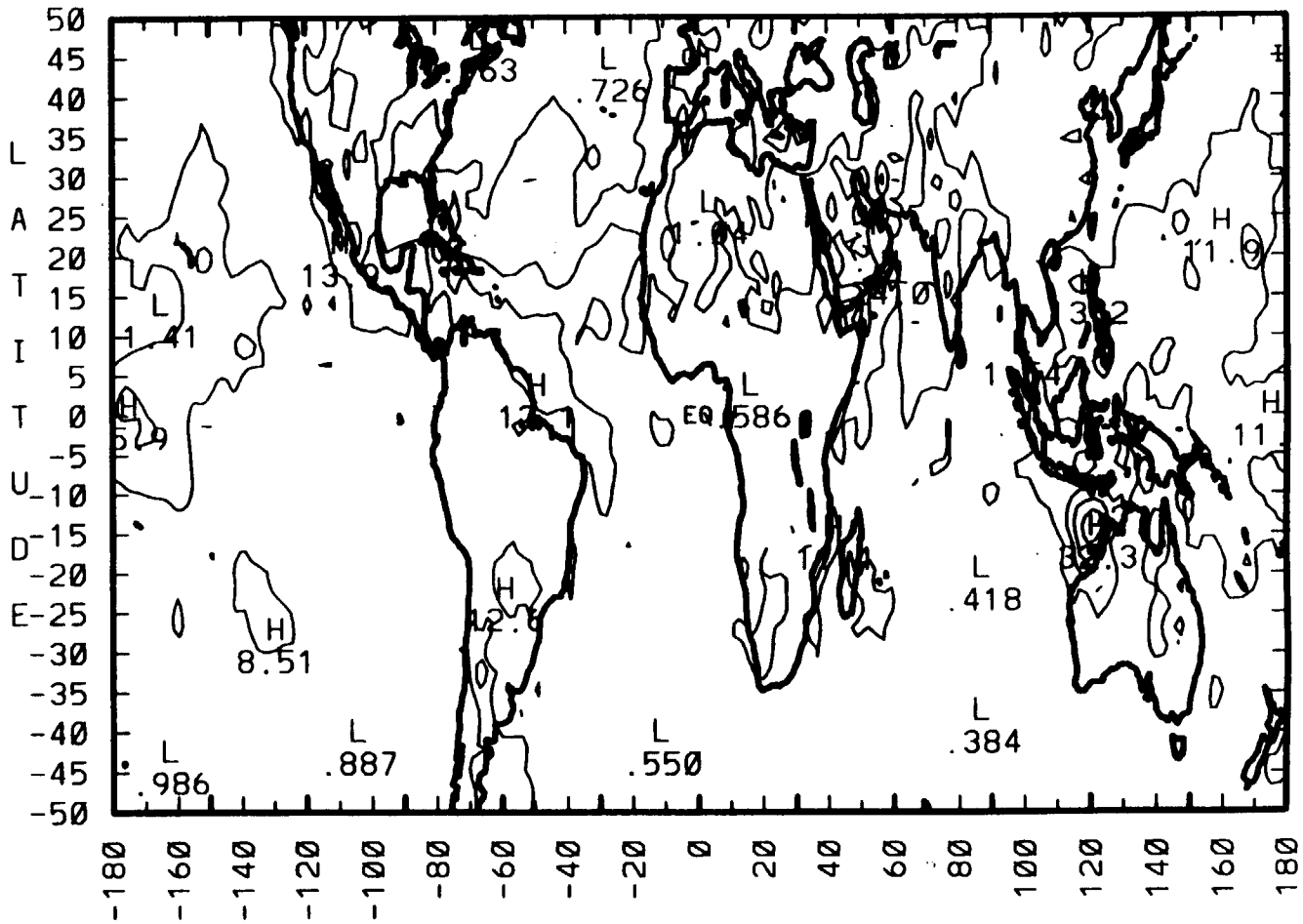

LONGITUDE

CONTOUR FROM 0.000000E+00 TO 48.000 CONTOUR INTERVAL OF 6.0000 PT(3,3)= 3.1642

M63

1986/1987 ENSO ANOMALIES

NET RADIATION (Wm**2)

4-YEAR ANNUAL MEAN - ENSO YEAR MEAN

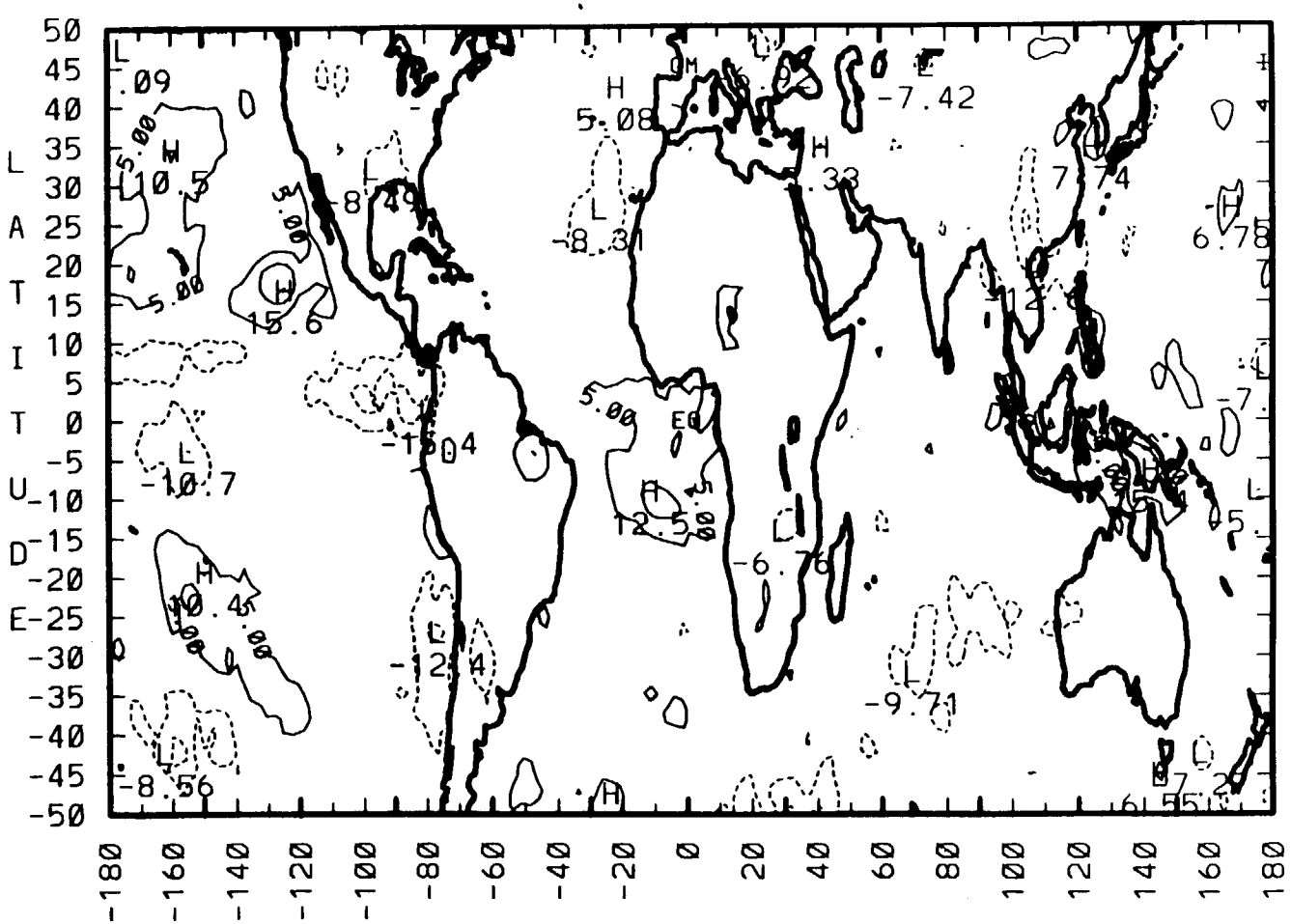

M61

CONTOUR FROM -888888 TO -888888 CONTOUR INTERVAL OF 5.8888 PT(3,3)= -2.8123

1986/1987 ENSO ANOMALIES

OLR (W/m**2)

4-YEAR ANNUAL MEAN - ENSO YEAR MEAN

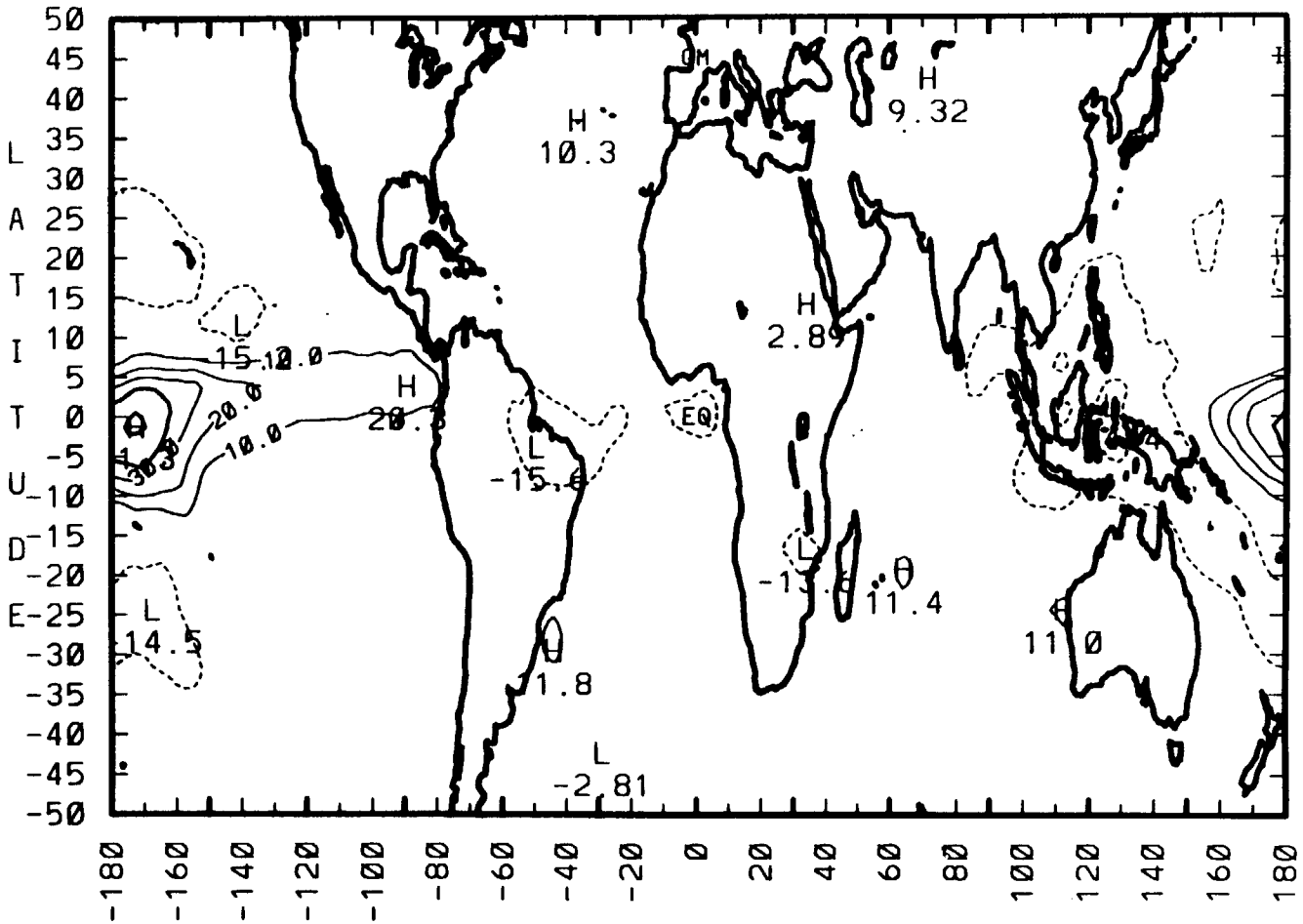

1986/1987 ENSO ANOMALIES

SW REFLECTED (WM**2)

4-YEAR ANNUAL MEAN - ENSO YEAR MEAN

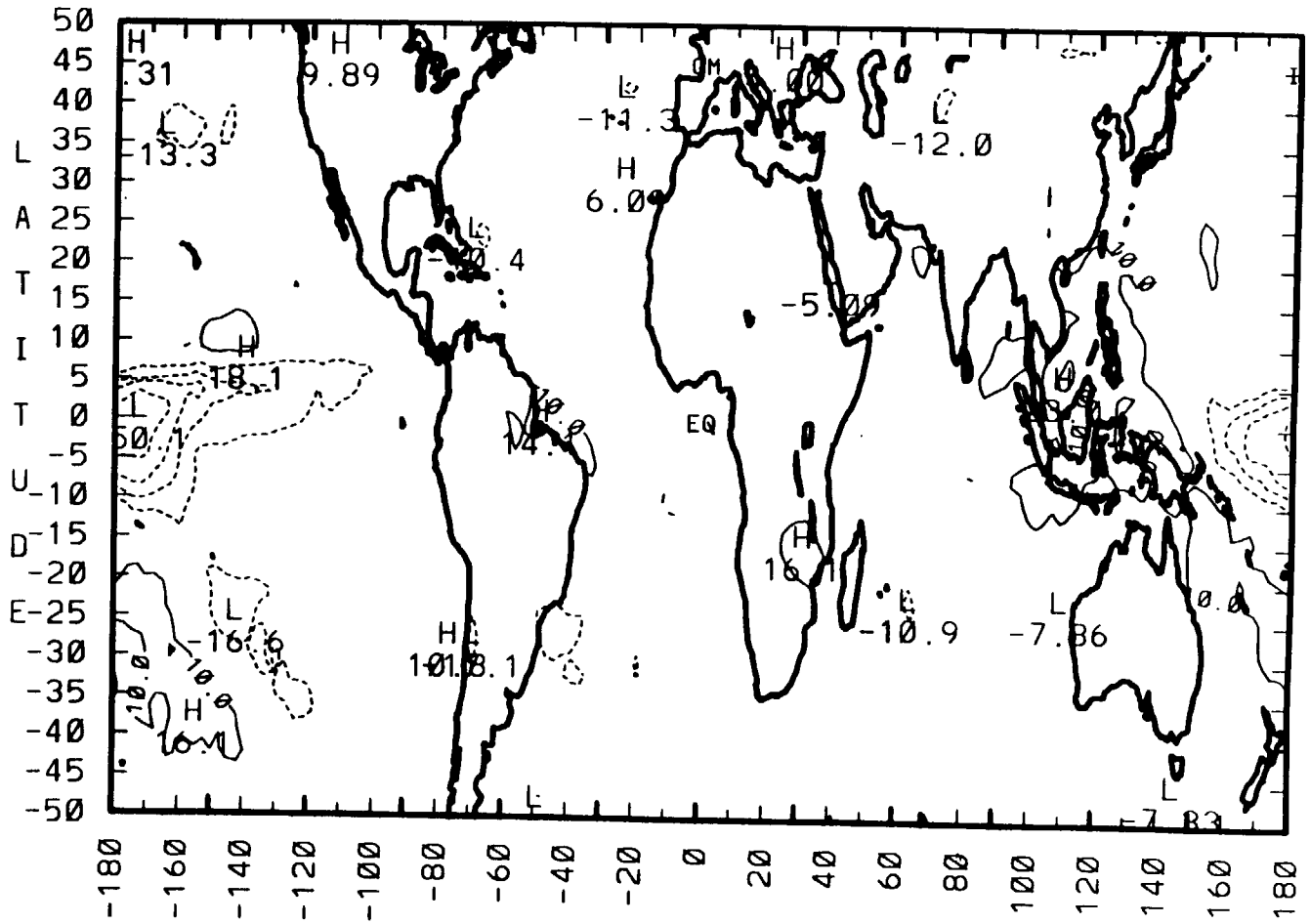

CONTOUR FROM -60.000 TO -60.000 CONTOUR INTERVAL OF 10.000 PT(3,3)= 2.6458

1986/1987 ENSO ANOMALIES

SURFACE TEMP (DEG. K)

4-YEAR ANNUAL MEAN - ENSO YEAR MEAN

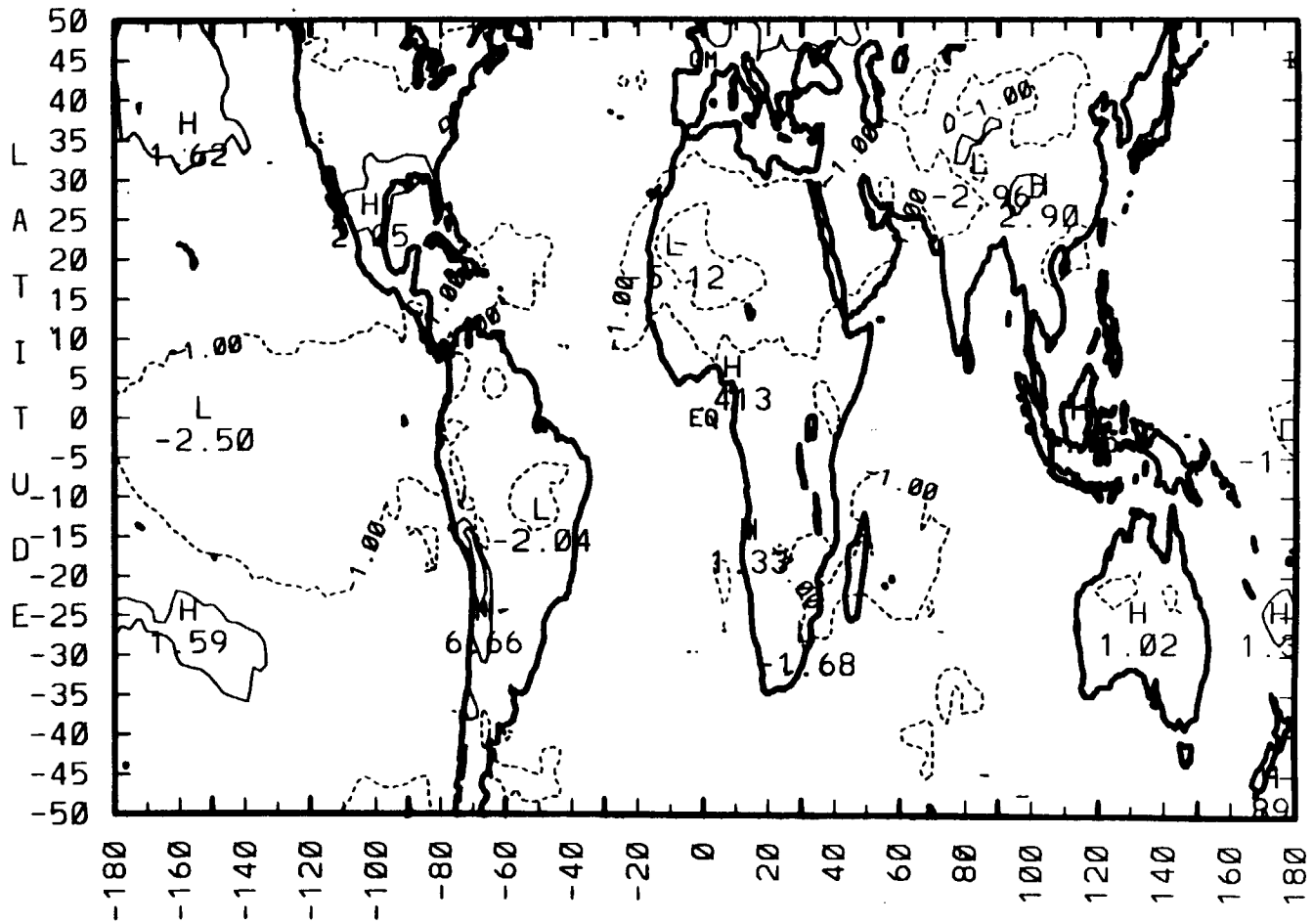

CONTOUR FROM -5.0000 TO 5.0000 CONTOUR INTERVAL OF 2.0000 PT(3,3)= 0.36854

1986/1987 ENSO ANOMALIES

CLOUD FRACTION (%)

4-YEAR ANNUAL MEAN - ENSO YEAR MEAN

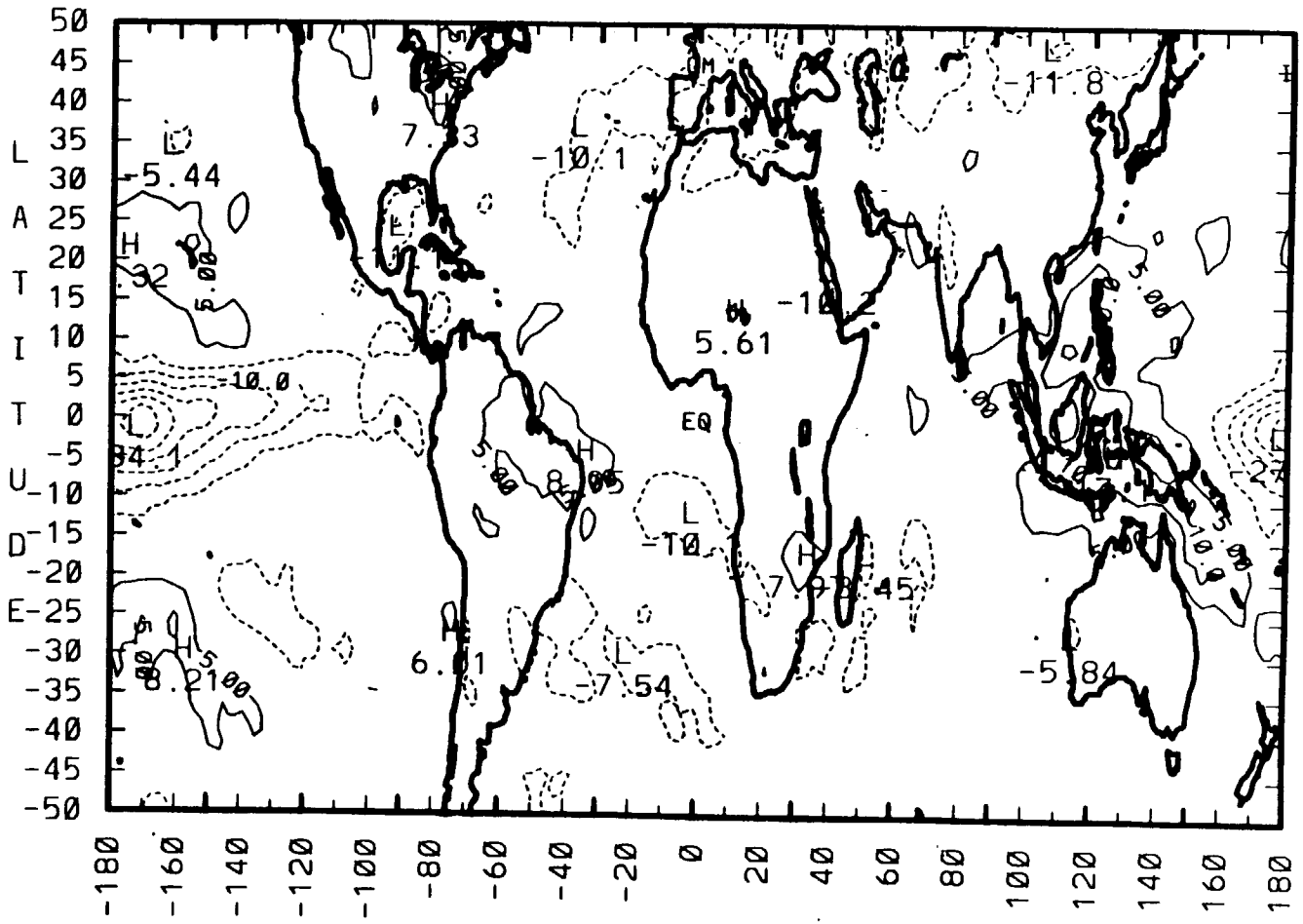

CONTOUR FROM -888888 TO -888888 CONTOUR INTERVAL OF 5.8888 PT(3,3)= 1.6354

1986/1987 ENSO ANOMALIES

CLD TOP TEMP (DEG. K)

4-YEAR ANNUAL MEAN - ENSO YEAR MEAN

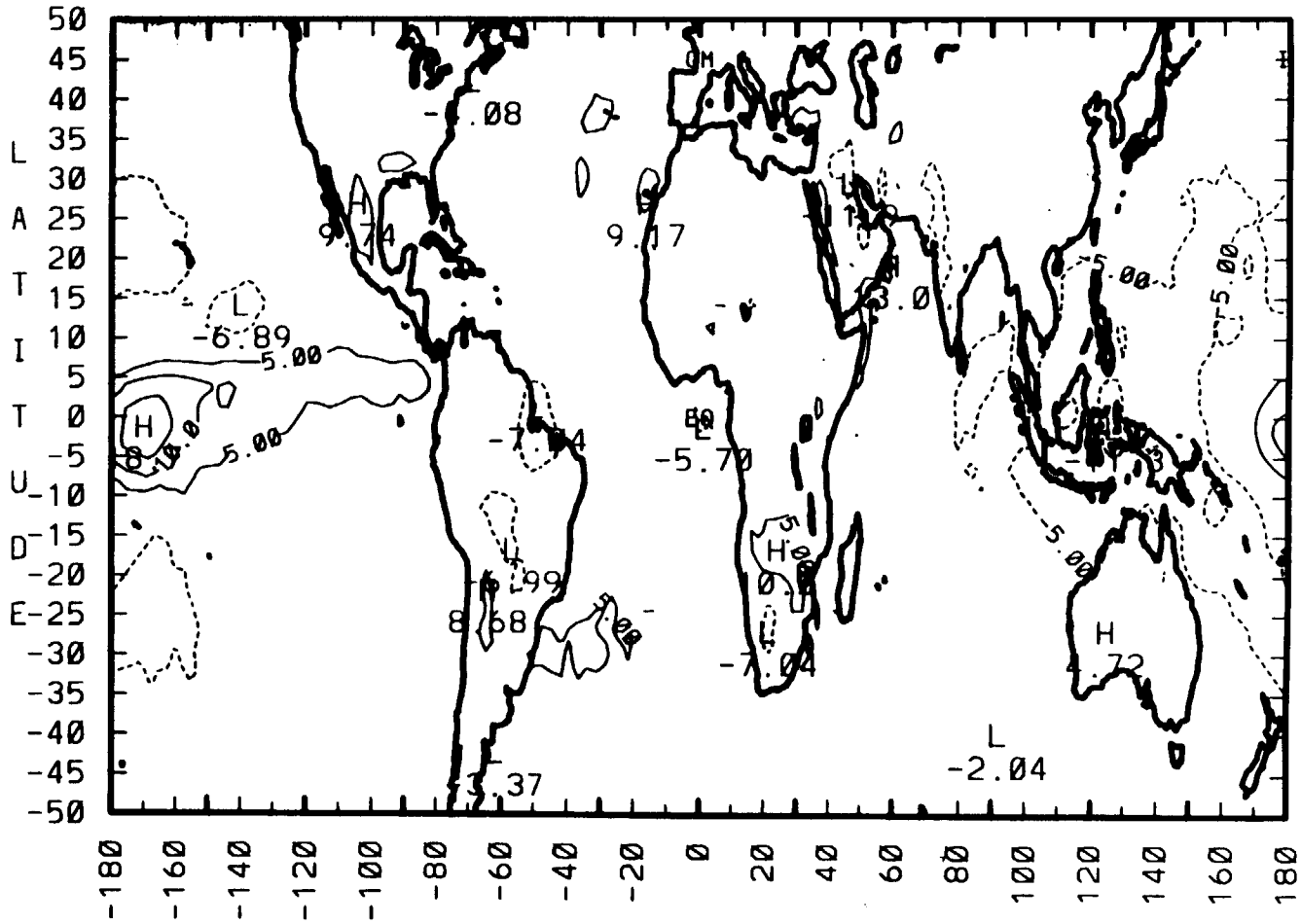

CONTOUR FROM -550000 TO -550000 CONTOUR INTERVAL OF 5.0000 PT(3,3)= -1.4582

M66

1986/1987 ENSO ANOMALIES

(4-YR MEAN - DEC'86) OLR (W/m**2)

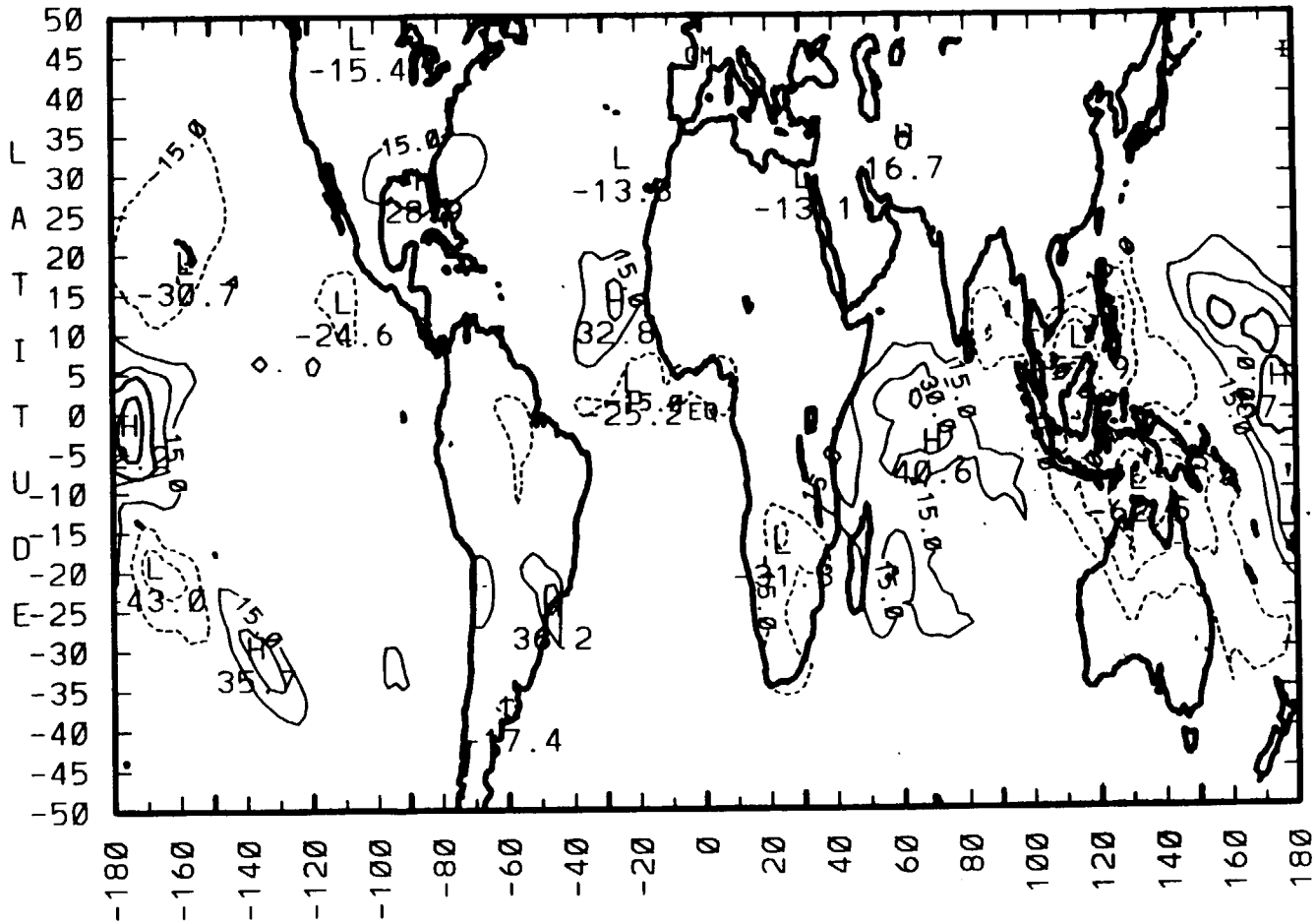

CONTOUR FROM -60.000 TO -60.000 CONTOUR INTERVAL OF 15.000 PT(3,3)= -1.8998

1967

1986/1987 ENSO ANOMALIES

(4-YR MEAN - JAN'87) NET RADIATION (Wm**2)

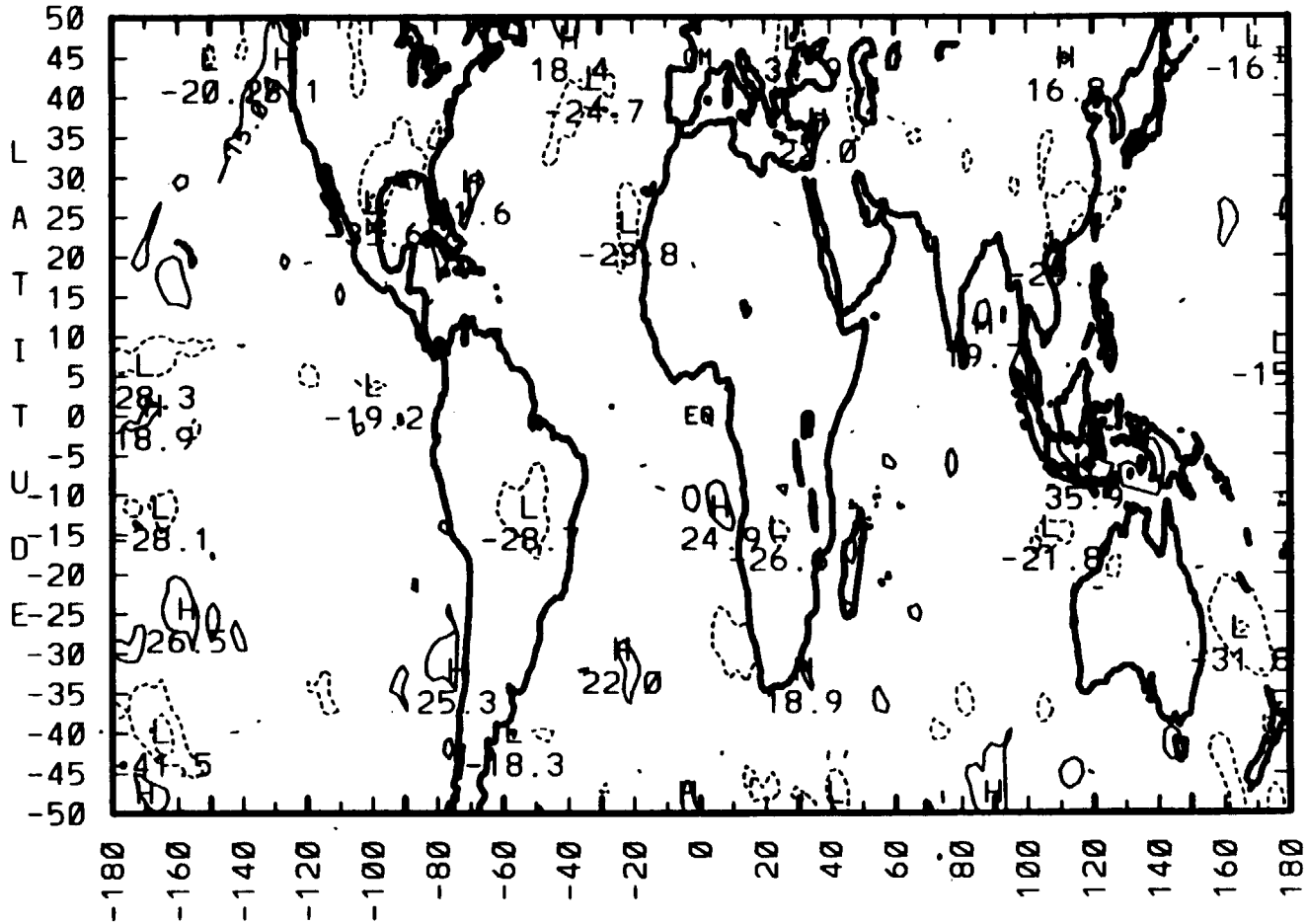

CONTOUR FROM -60.000 TO -90.000 CONTOUR INTERVAL OF 15.000 PT(3,3)= 9.4202

1986/1987 ENSO ANOMALIES

(4-YR MEAN - JAN'87) OLR (W/m**2)

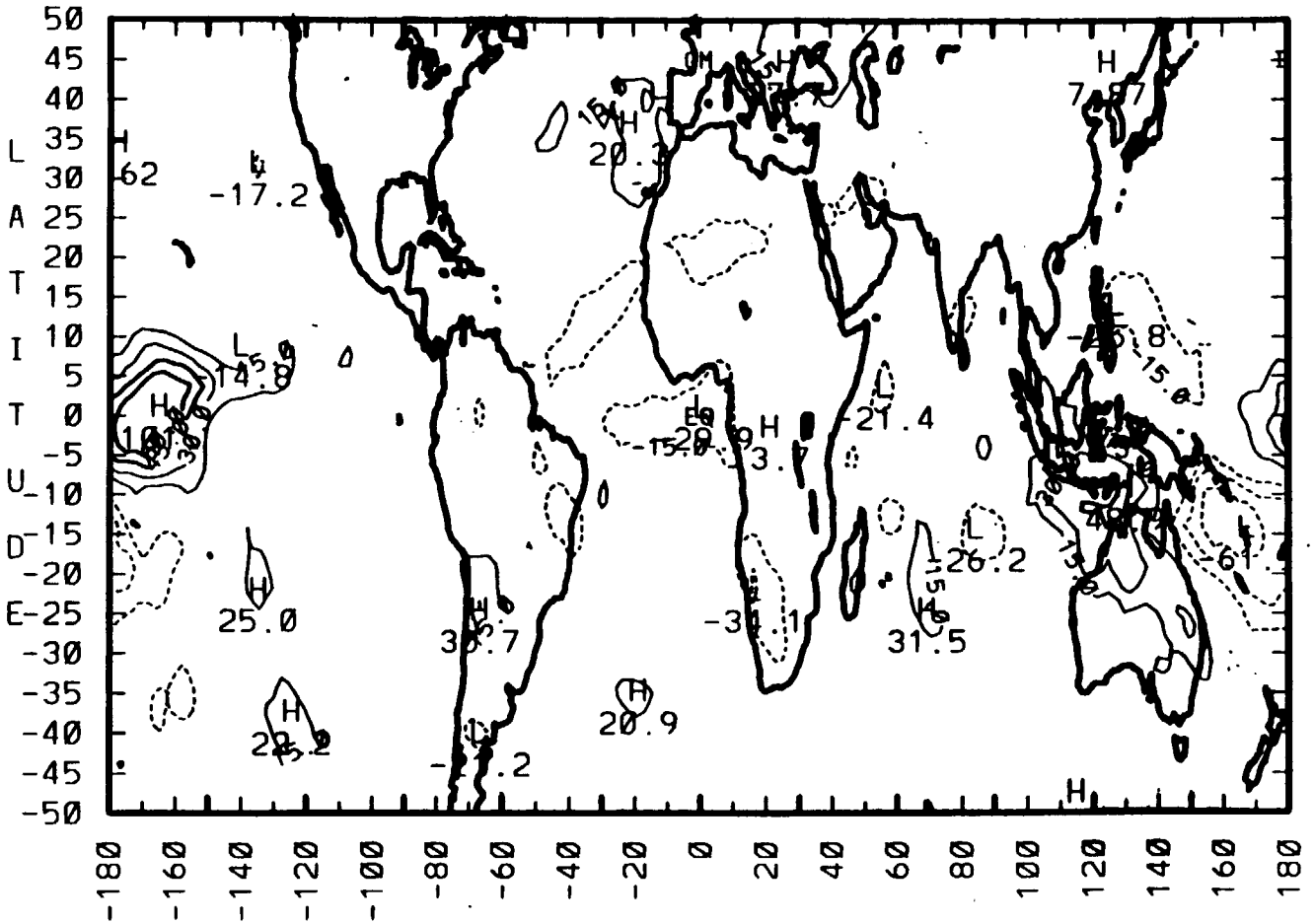

CONTOUR FROM -60.000 TO -90.000 CONTOUR INTERVAL OF 15.000 PT(3,3)= 6.4742

1986/1987 ENSO ANOMALIES

(4-YR MEAN - JAN'87) SW REFLECTED (WM**2)

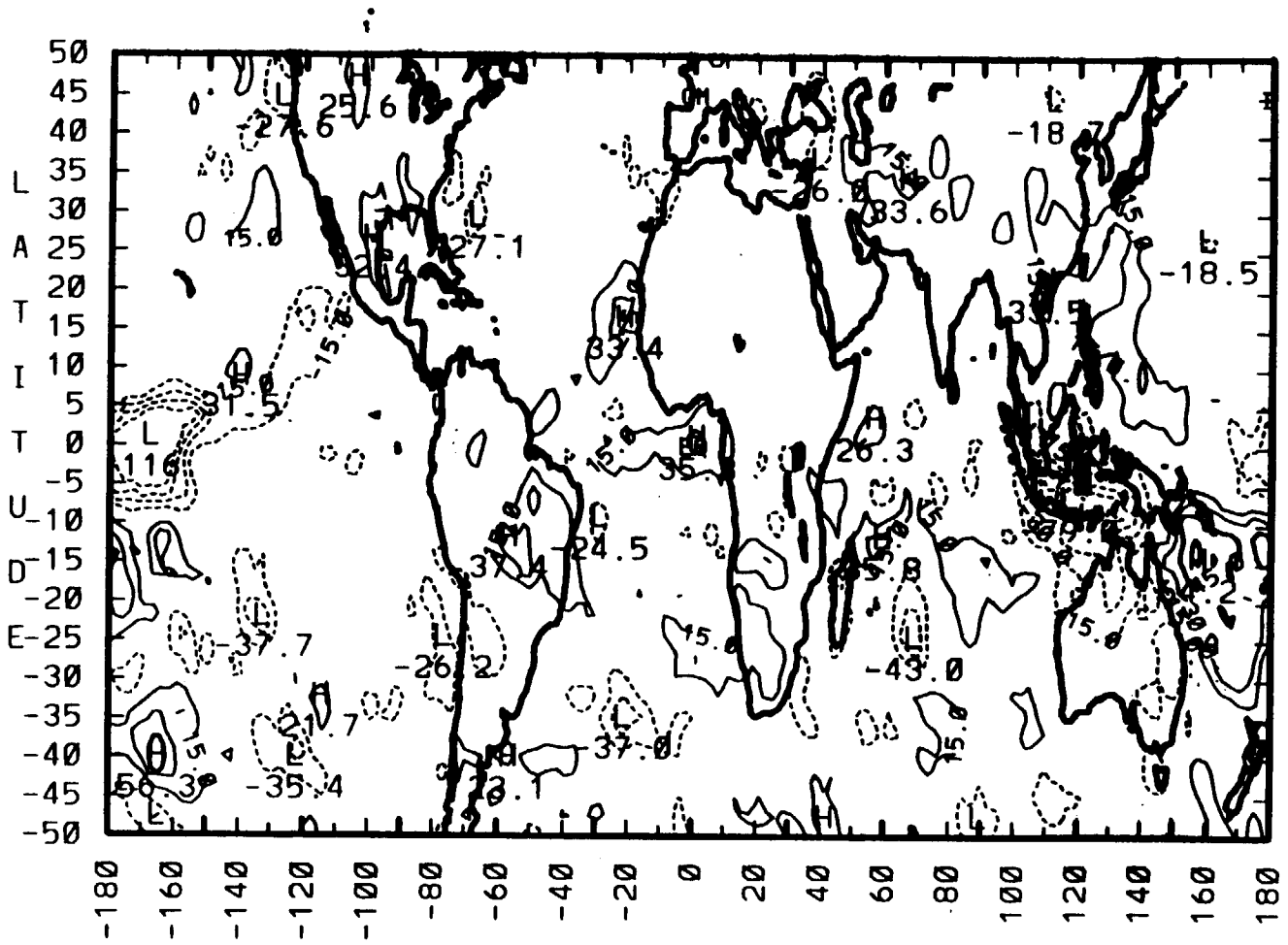

1986/1987 ENSO ANOMALIES

(4-YR MEAN - JAN'87) SURFACE TEMP (DEG. K)

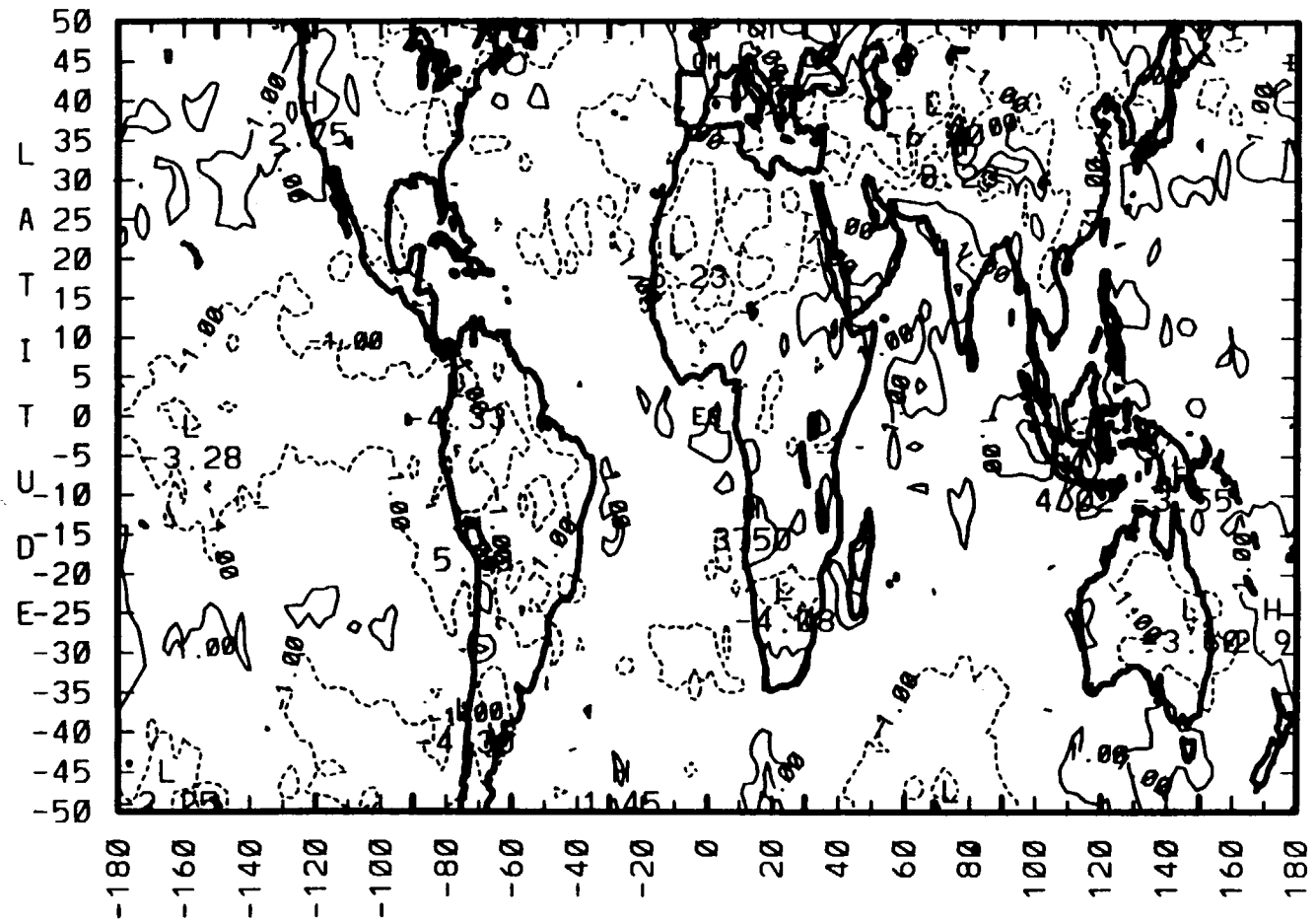

CONTOUR FROM -5.0000 TO -5.0000 CONTOUR INTERVAL OF 2.0000 PT(3,3)= -0.87500

1986/1987 ENSO ANOMALIES

(4-YR MEAN - JAN'87) CLOUD FRACTION (%)

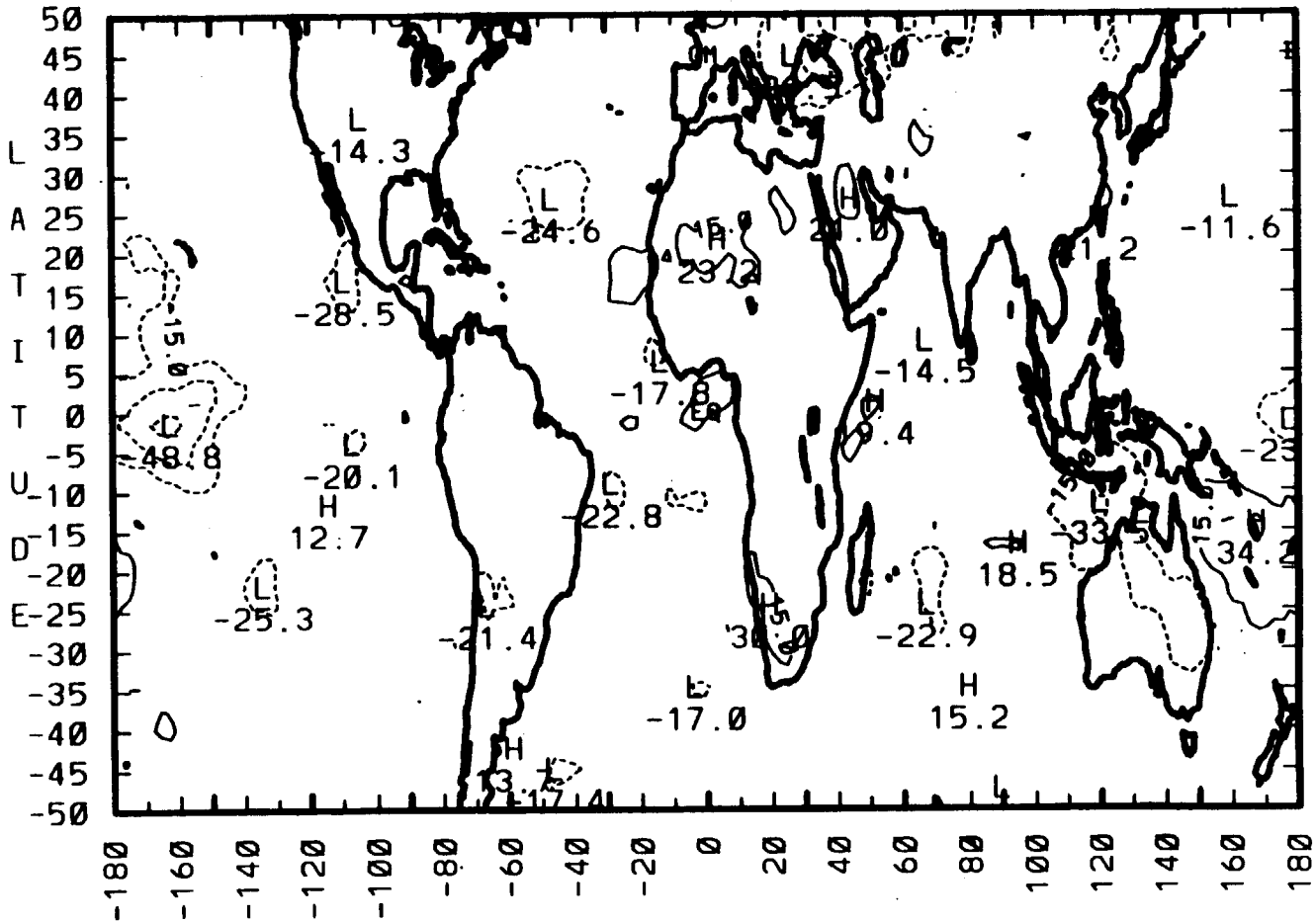

CONTOUR FROM -45.000 TO -45.000 CONTOUR INTERVAL OF 15.000 PT(3,3)= -1.5000

1986/1987 ENSO ANOMALIES

(4-YR MEAN - JAN'87) CLD TOP TEMP (DEG. K)

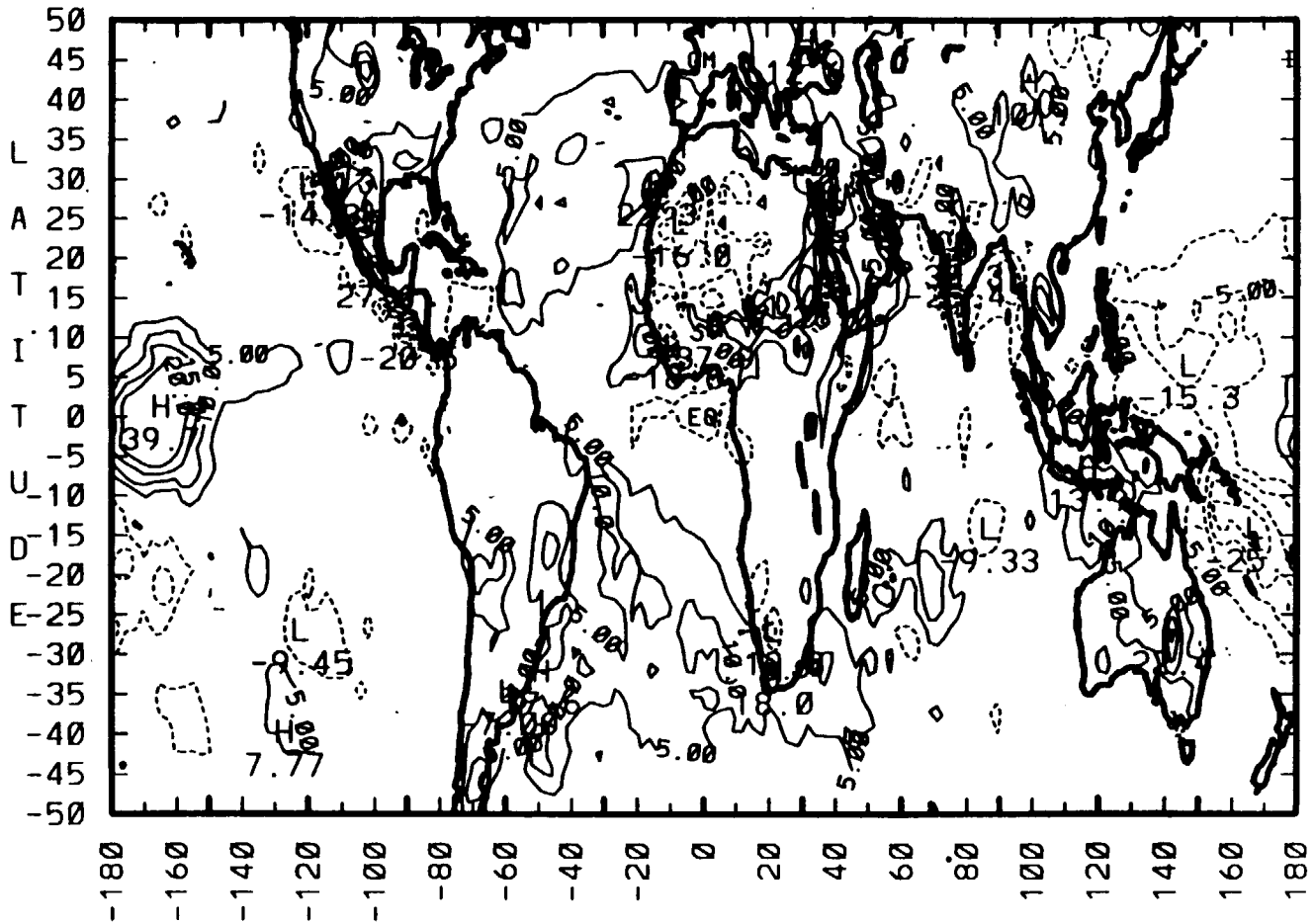

CONTOUR FROM -888888 TO -888888 CONTOUR INTERVAL OF 5.8888 PT(3,3)= 8.32575

M73

1986/1987 ENSO ANOMALIES

(4-YR MEAN - FEB'87) OLR (W/m**2)

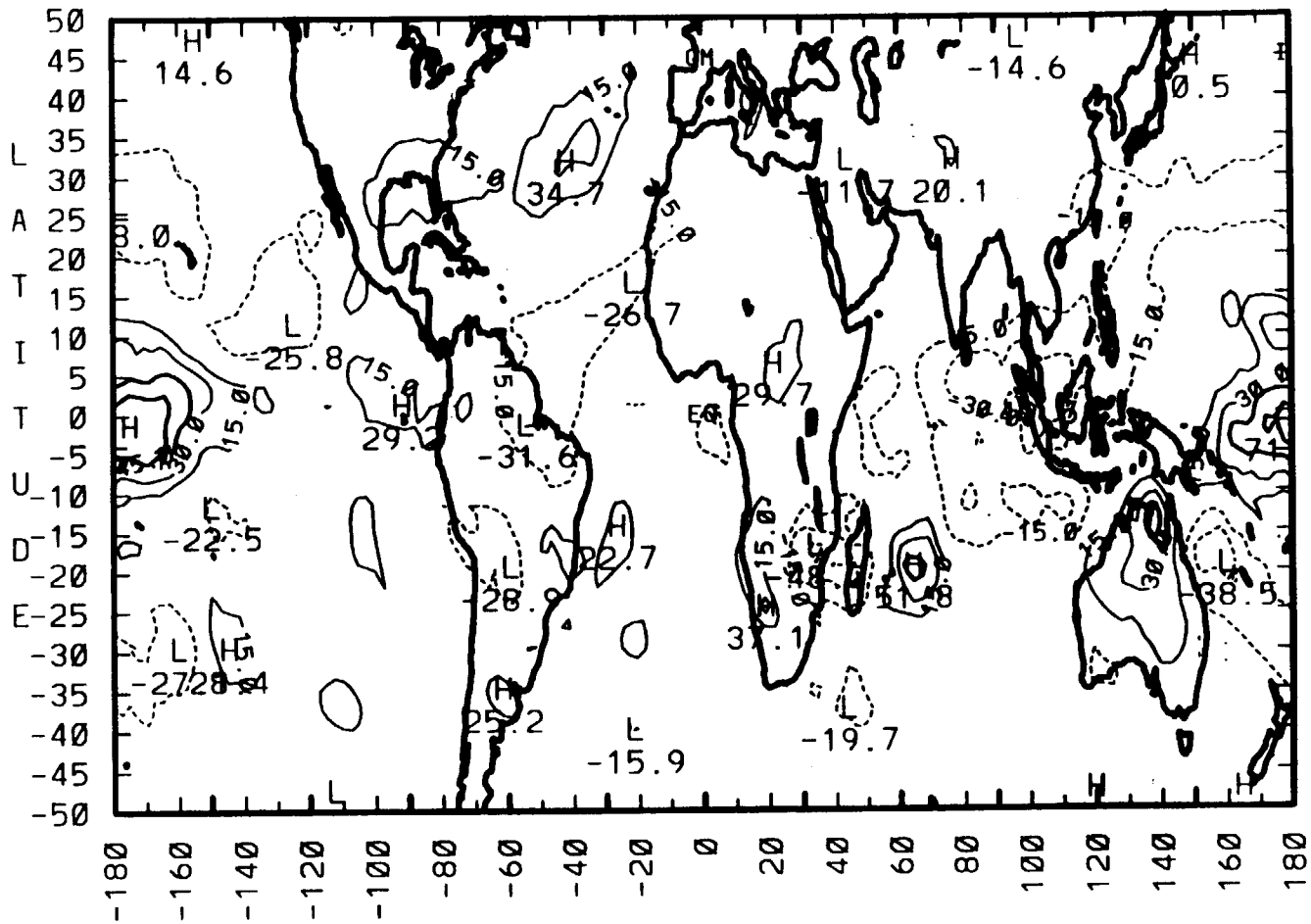

1986/1987 ENSO ANOMALIES

(4-YR MEAN - MAR'87) OLR (W/m**2)

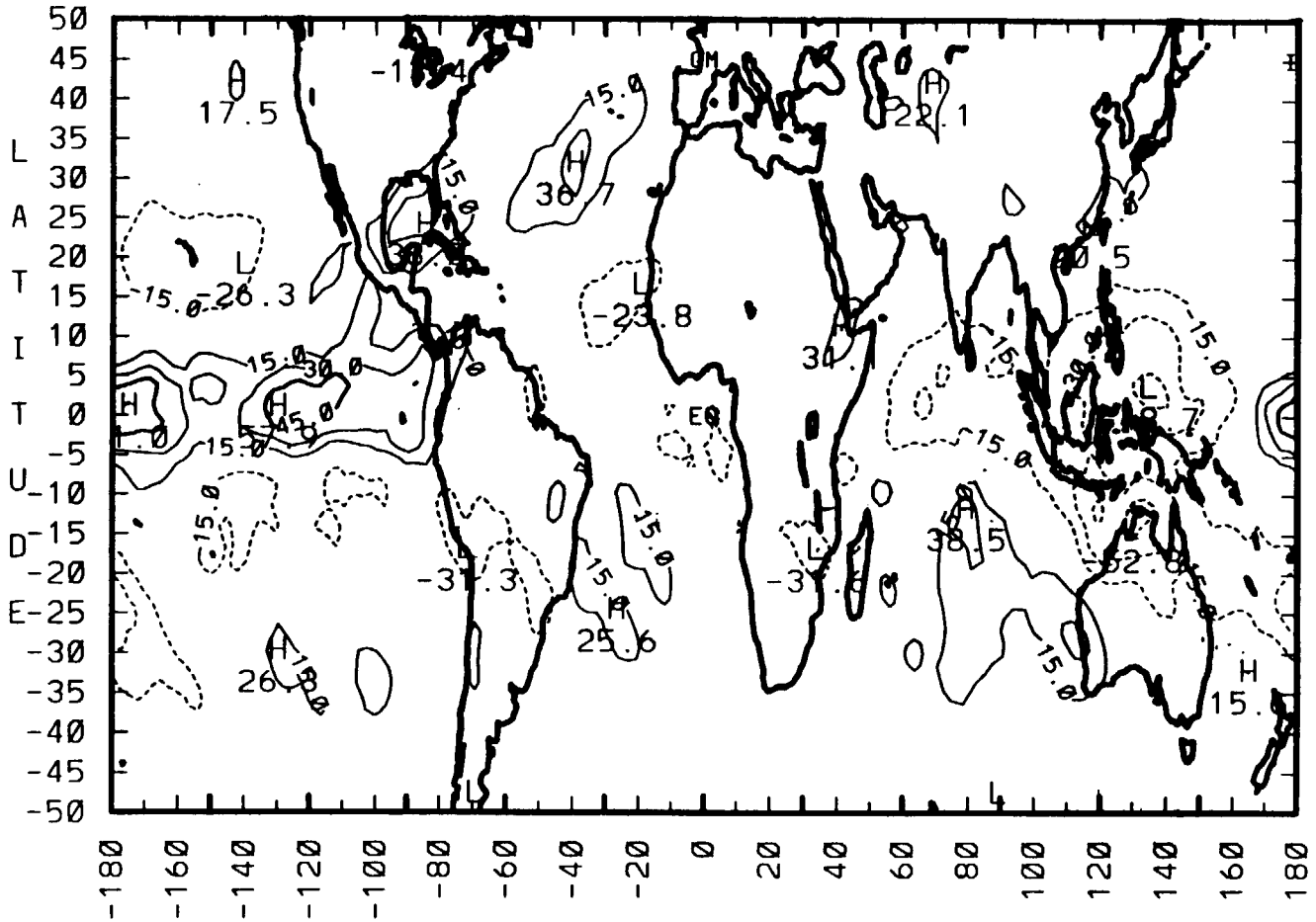

CONTOUR FROM -60.000 TO -60.000 CONTOUR INTERVAL OF 15.000 PT(3,3)= -0.17458

1986/1987 ENSO ANOMALIES

(4-YR MEAN - APR'87) NET RADIATION (Wm**2)

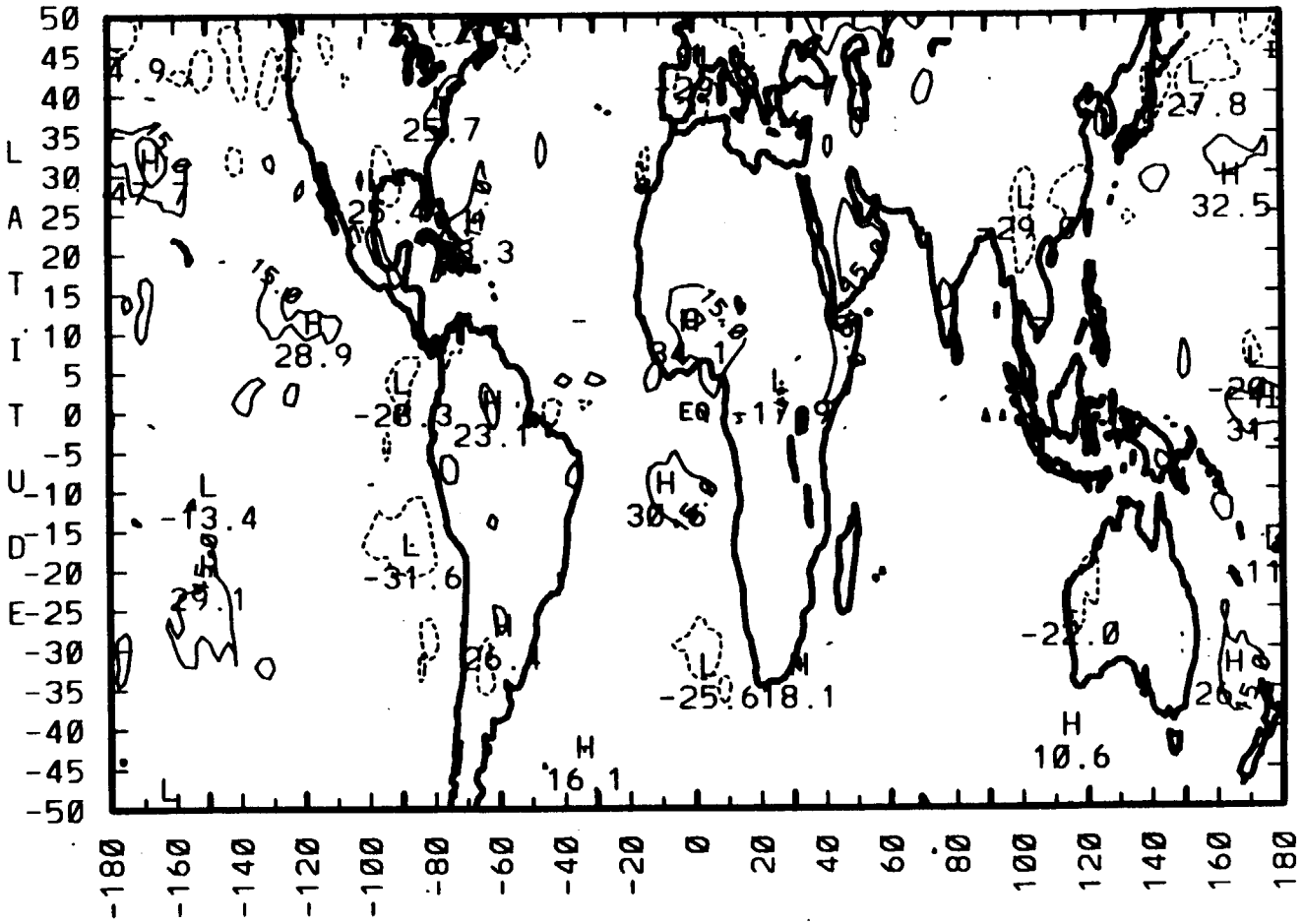

M76

1986/1987 ENSO ANOMALIES

(4-YR MEAN - APR'87) OLR (W/m**2)

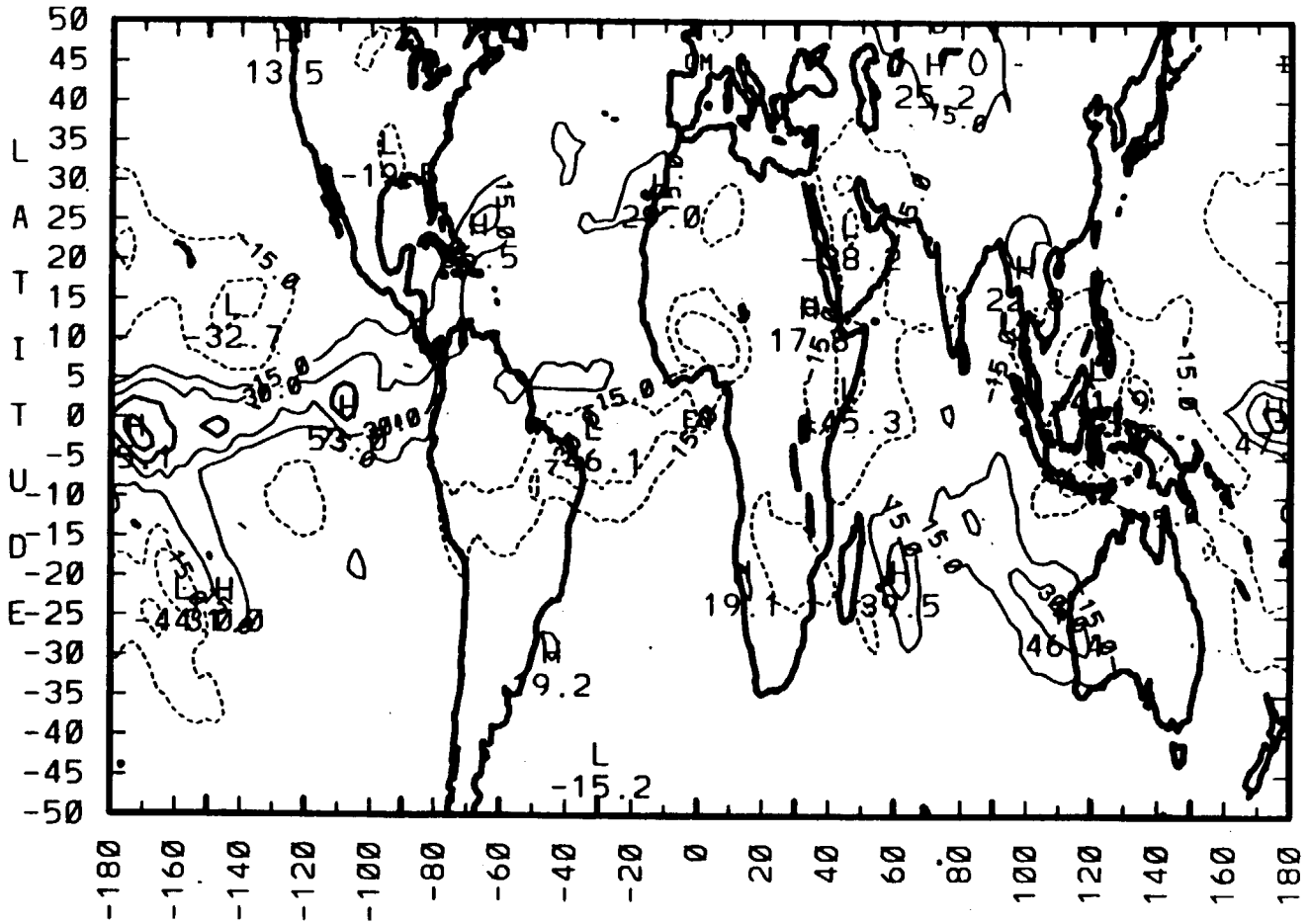

M77

1986/1987 ENSO ANOMALIES

(4-YR MEAN - APR'87) SW REFLECTED (WM**2)

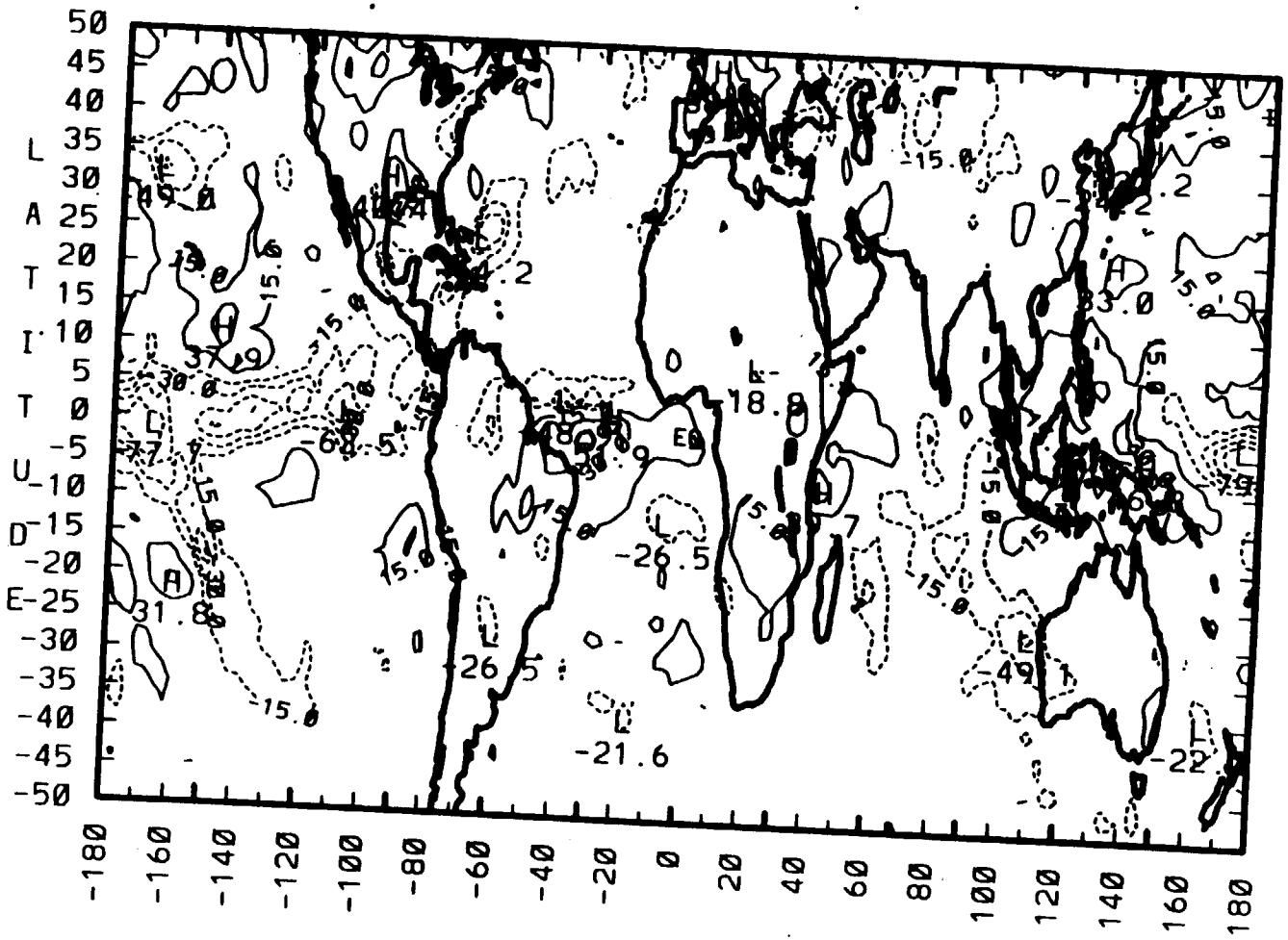

CONTOUR FROM -60.000 TO -60.000 CONTOUR INTERVAL OF 15.000 PT(3,3)= -6.3257

1986/1987 ENSO ANOMALIES

(4-YR MEAN - APR'87) SURFACE TEMP (DEG. K)

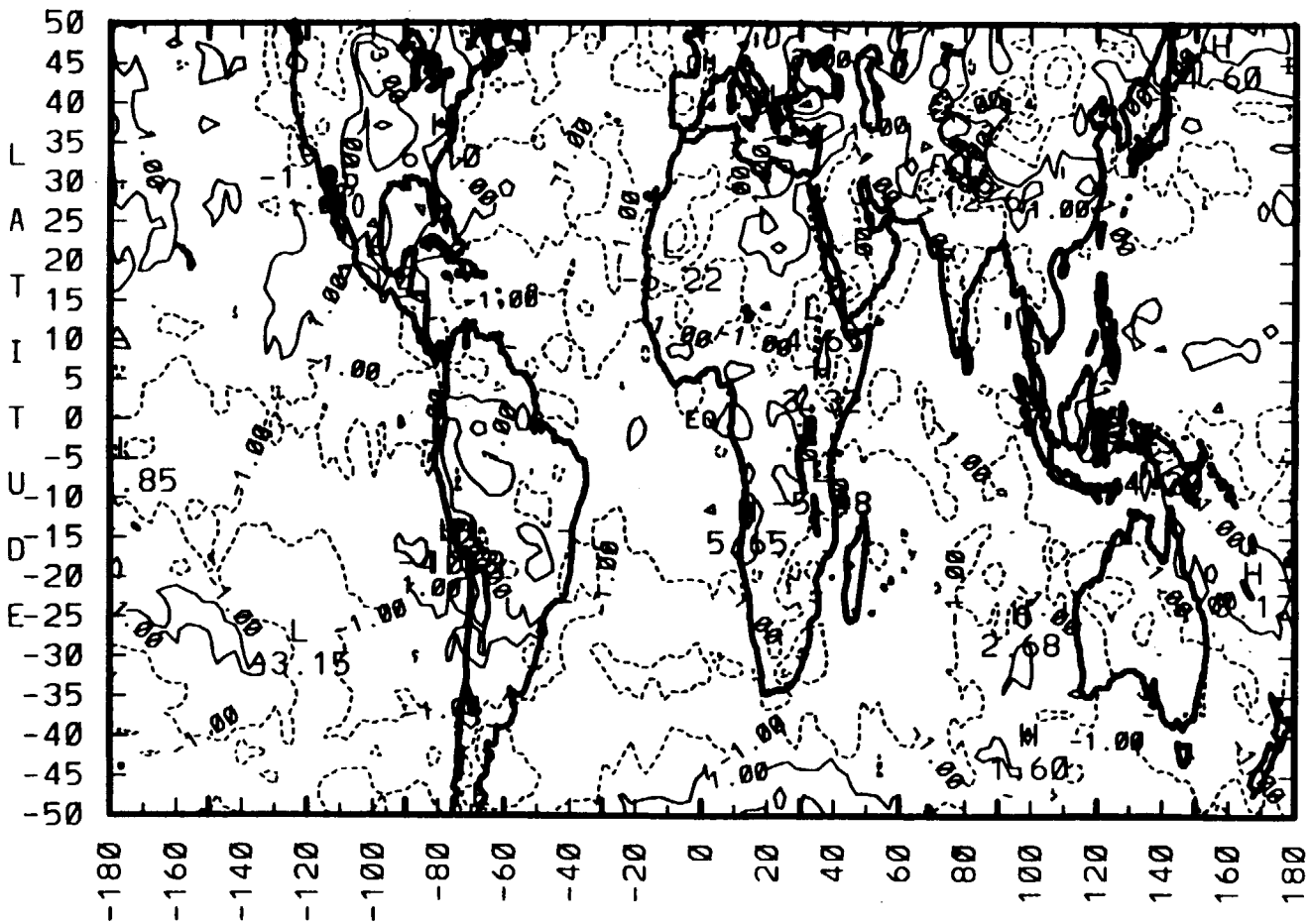

CONTOUR FROM -5.0000 TO -5.0000 CONTOUR INTERVAL OF 2.0000 PT(3,3)= -1.0758

1986/1987 ENSO ANOMALIES

(4-YR MEAN - APR'87) CLOUD FRACTION (%)

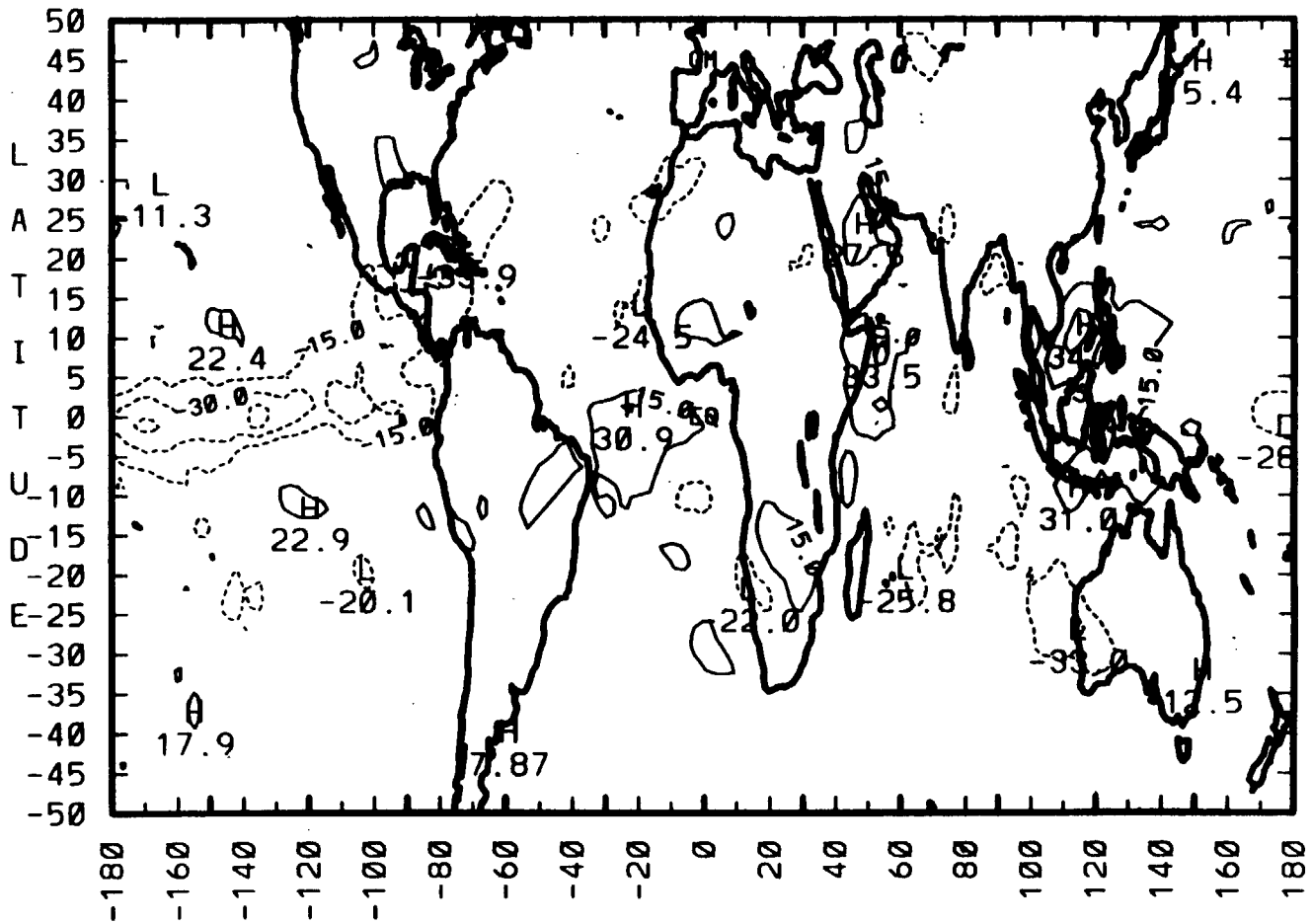

LONGITUDE

CONTOUR FROM -45.000 TO -45.000 CONTOUR INTERVAL OF 15.000 PT(3,3)= -4.3750

1986/1987 ENSO ANOMALIES

(4-YR MEAN - APR'87) CLD TOP TEMP (DEG. K)

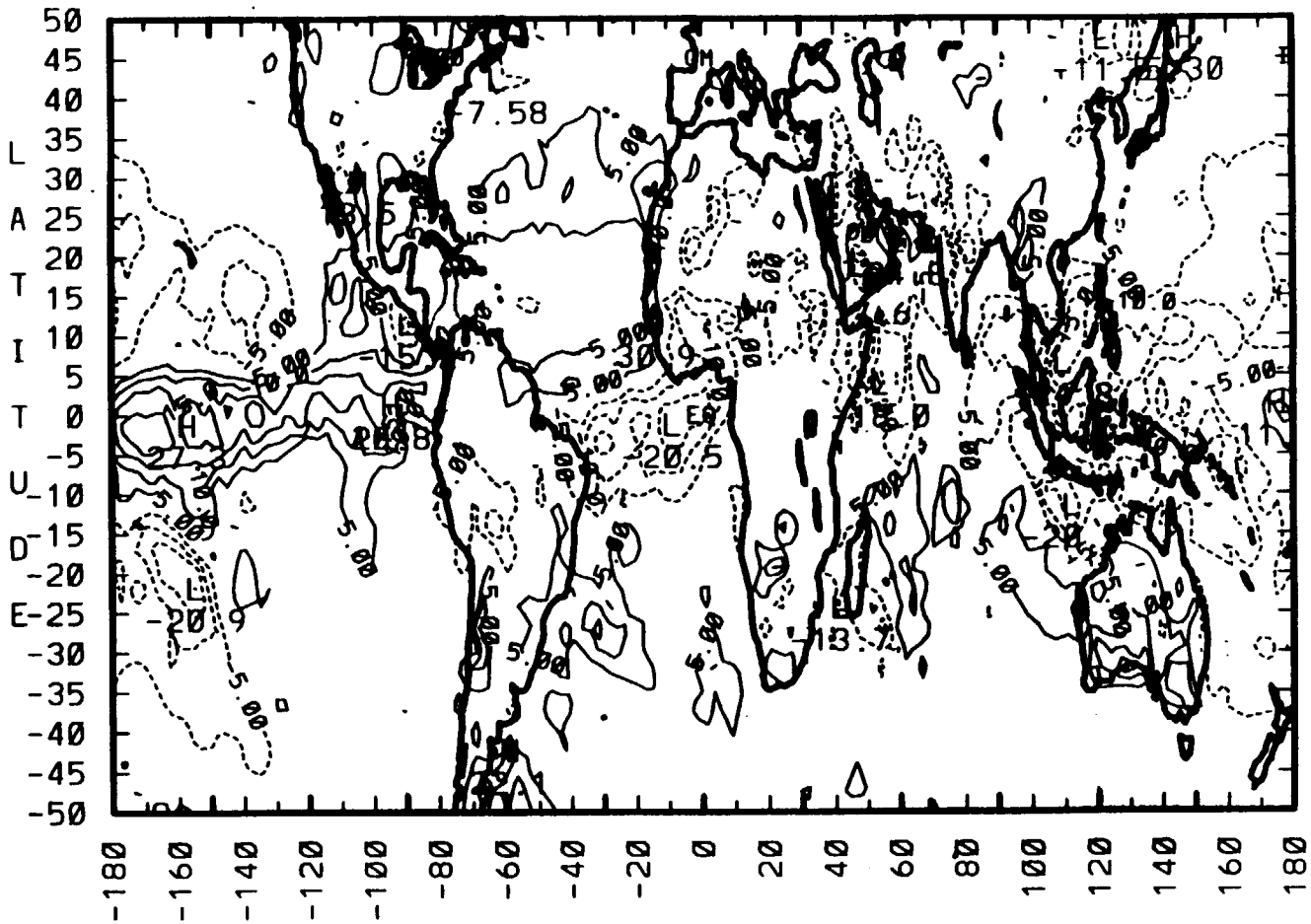

1986/1987 ENSO ANOMALIES

(4-YR MEAN - MAY'87) OLR (W/m**2)

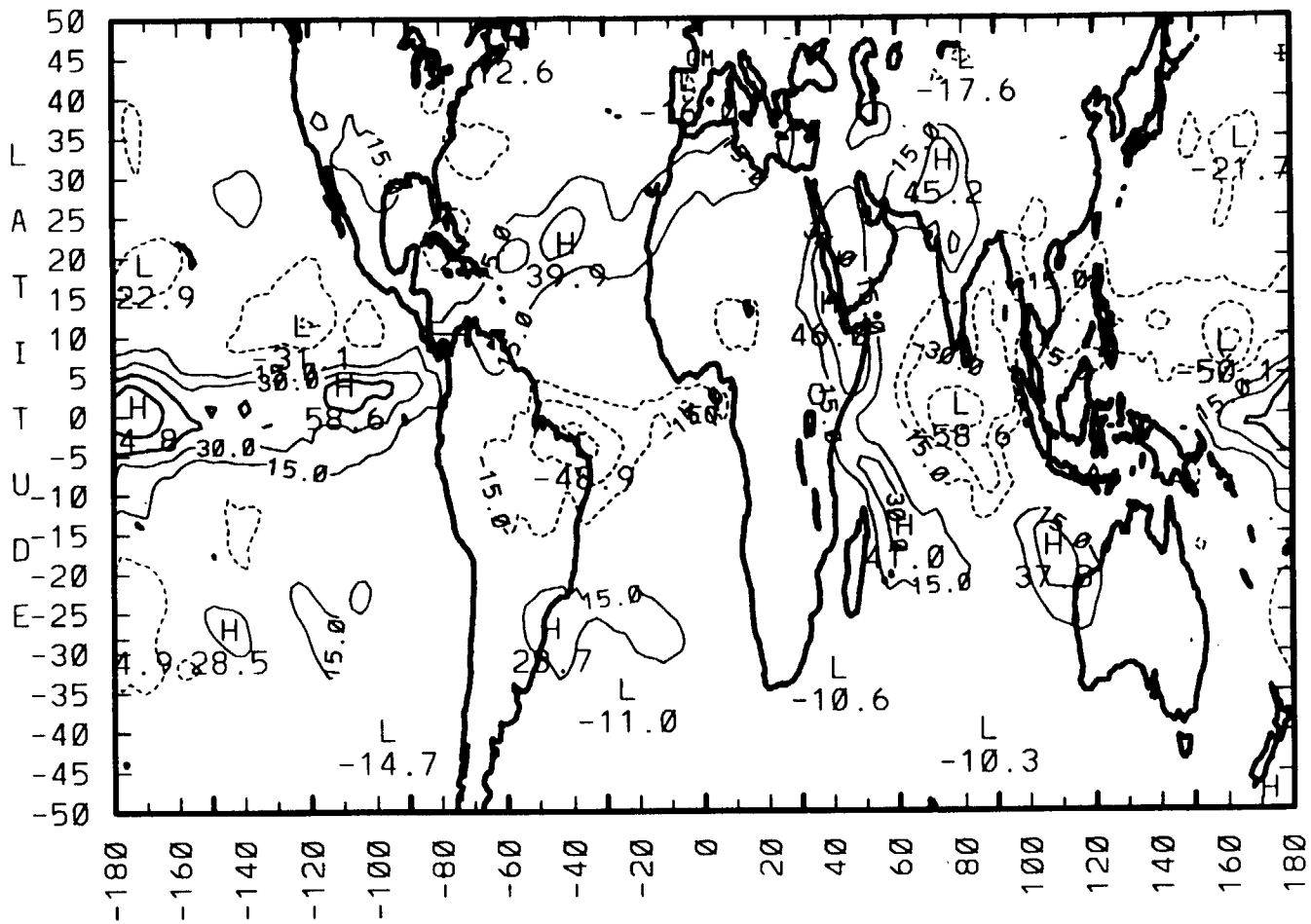

CONTOUR FROM -60.000 TO -60.000 CONTOUR INTERVAL OF 15.000 PT(3,3)= 6.0495

1986/1987 ENSO ANOMALIES

(4-YR MEAN - JUN'87) OLR (W/m**2)

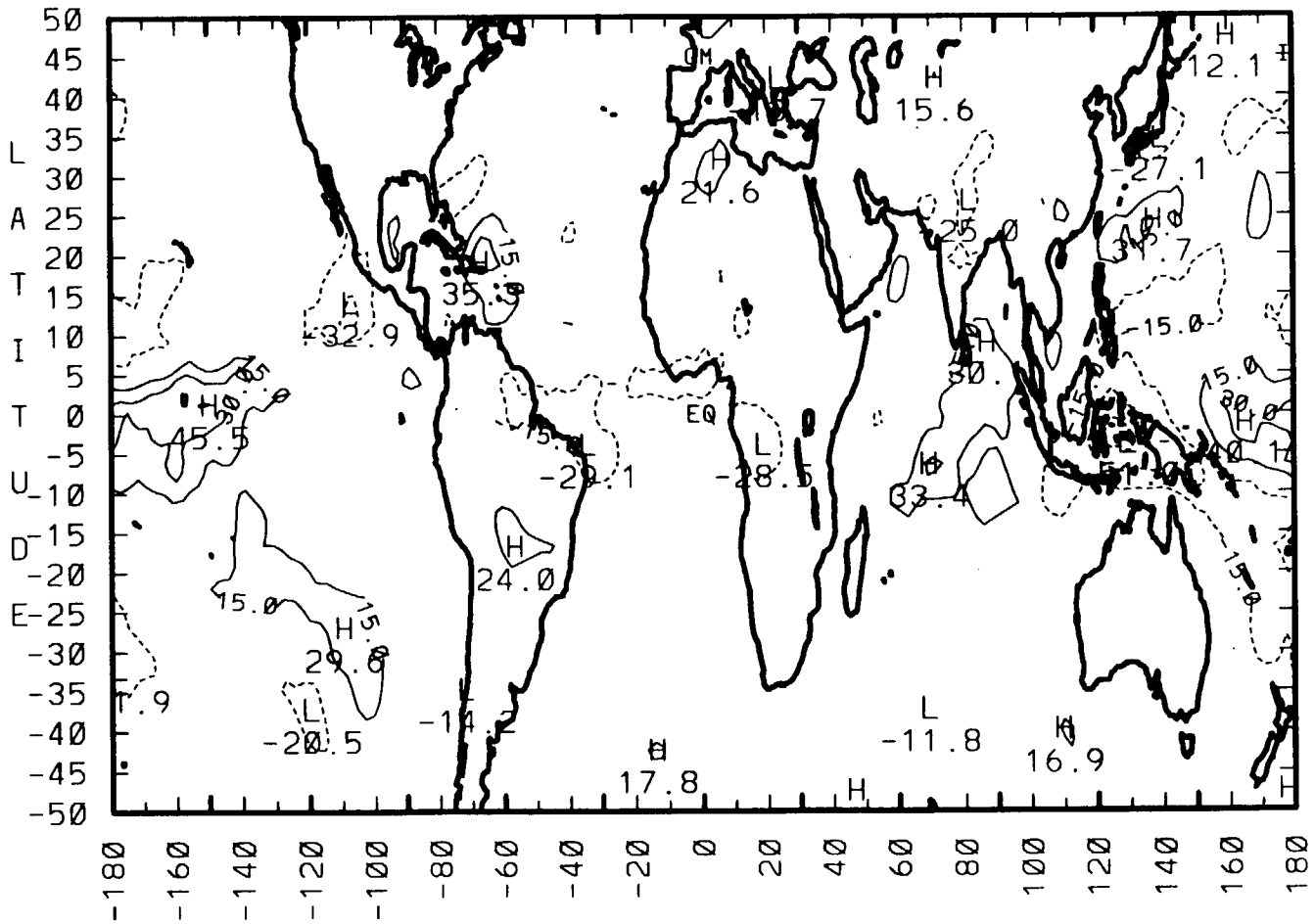

CONTOUR FROM -00.000 TO -00.000 CONTOUR INTERVAL OF 15.000 PT(3.3)= -1.5748

1986/1987 ENSO ANOMALIES

(4-YR MEAN - JULY'87) NET RADIATION (Wm**2)

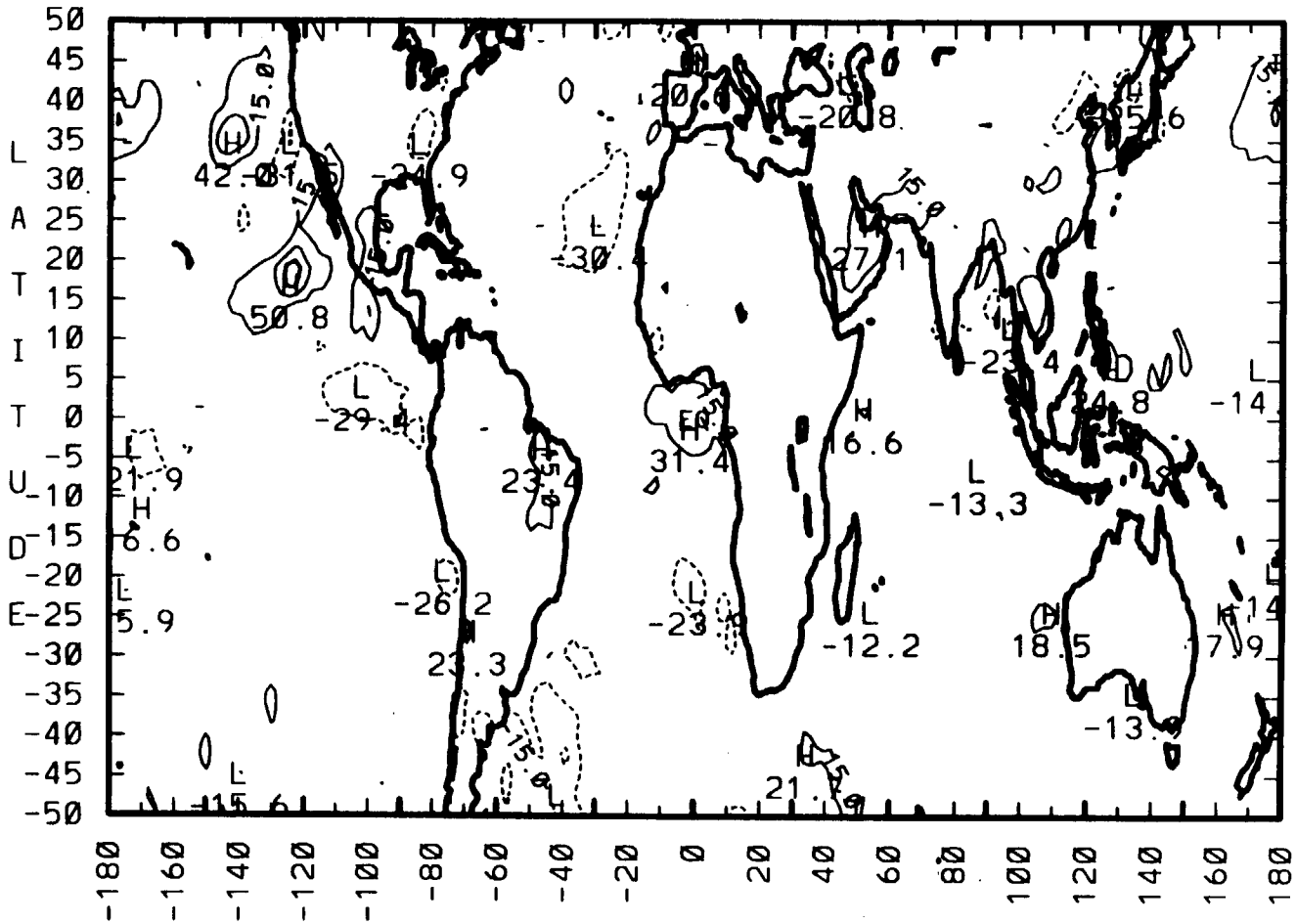

1986/1987 ENSO ANOMALIES

(4-YR MEAN - JULY'87) OLR (W/m**2)

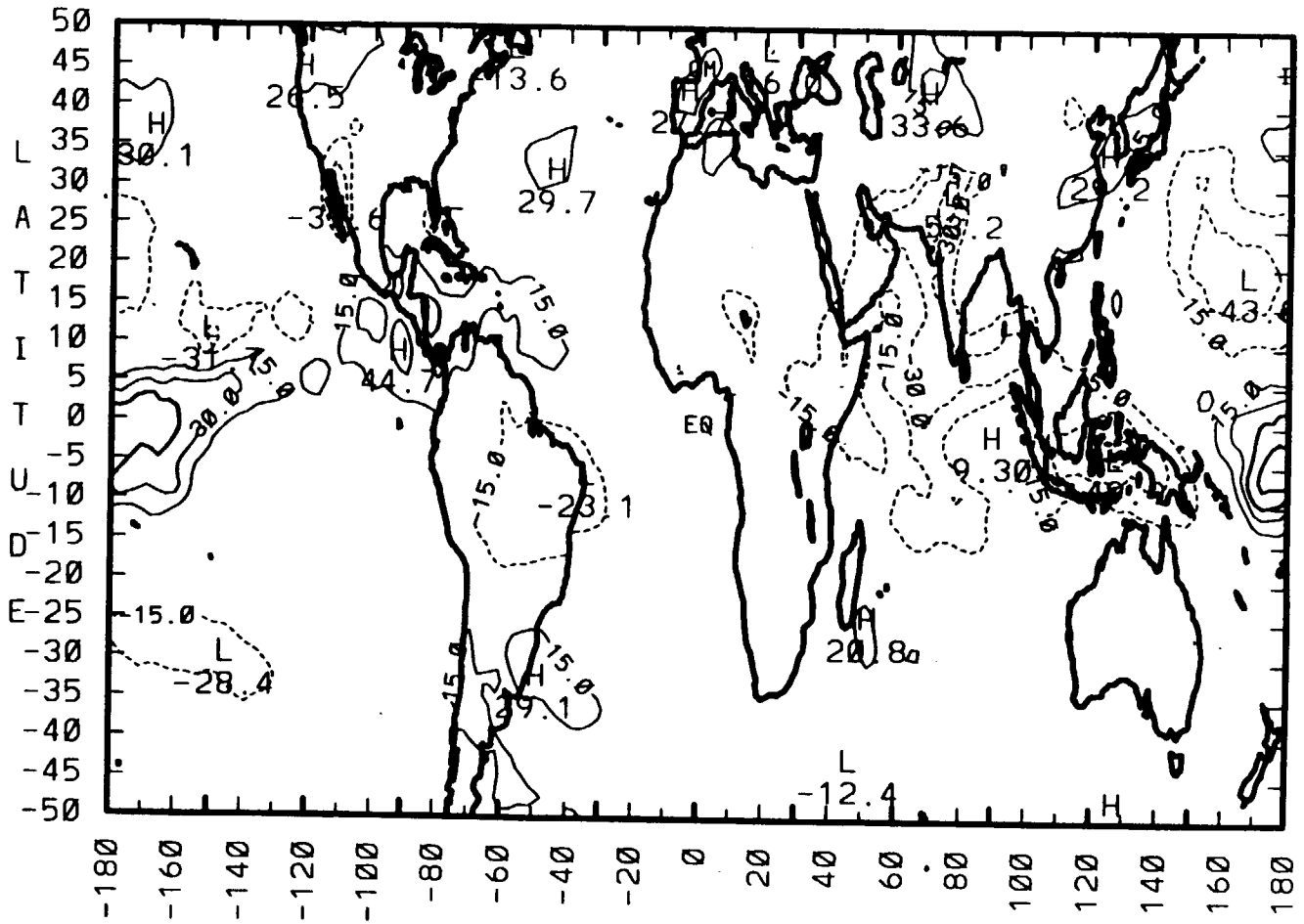

CONTOUR FROM -60.000 TO -30.000 CONTOUR INTERVAL OF 15.000 PT(3,3)= -6.1250

1986/1987 ENSO ANOMALIES

(4-YR MEAN - JULY'87) SW REFLECTED (WM**2)

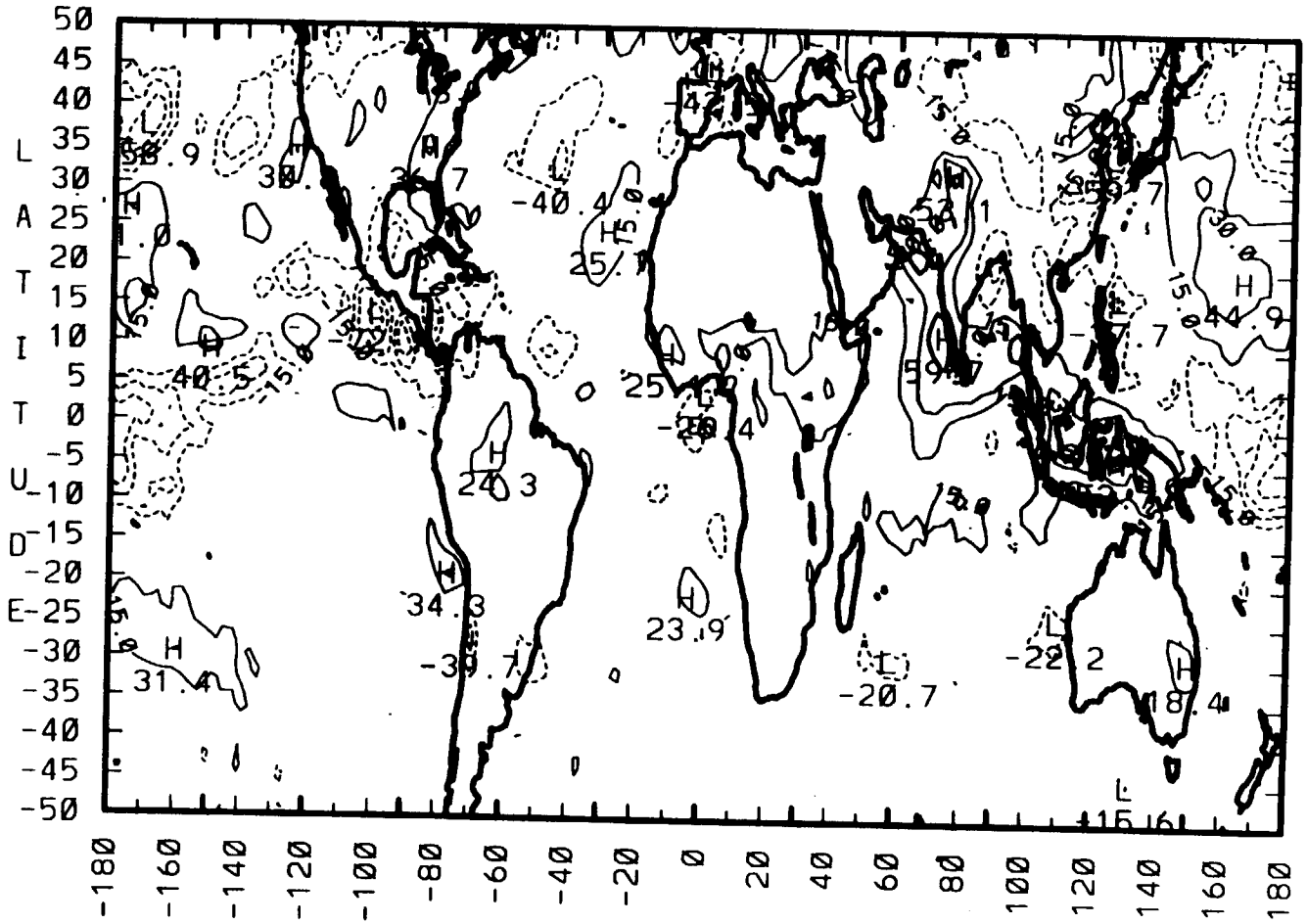

CONTOUR FROM -60.000 TO -60.000 CONTOUR INTERVAL OF 15.000 PT(3,3)= -4.0248

1986/1987 ENSO ANOMALIES

(4-YR MEAN - JULY'87) SURFACE TEMP (DEG. K)

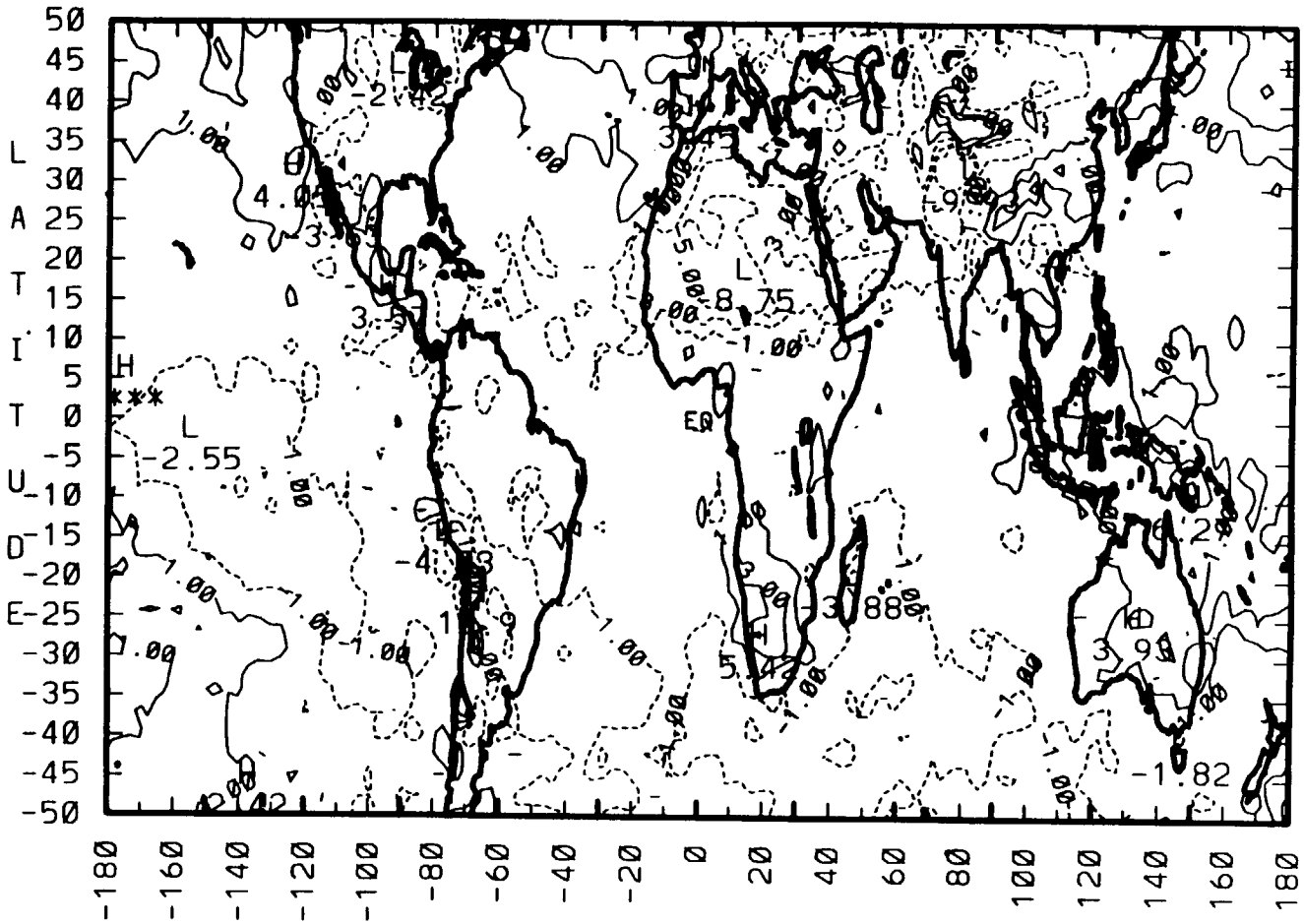

CONTOUR FROM -5.0000 TO -5.0000 CONTOUR INTERVAL OF 2.0000 PT(3,3)= 1.7993

1986/1987 ENSO ANOMALIES

(4-YR MEAN - JULY'87) CLOUD FRACTION (%)

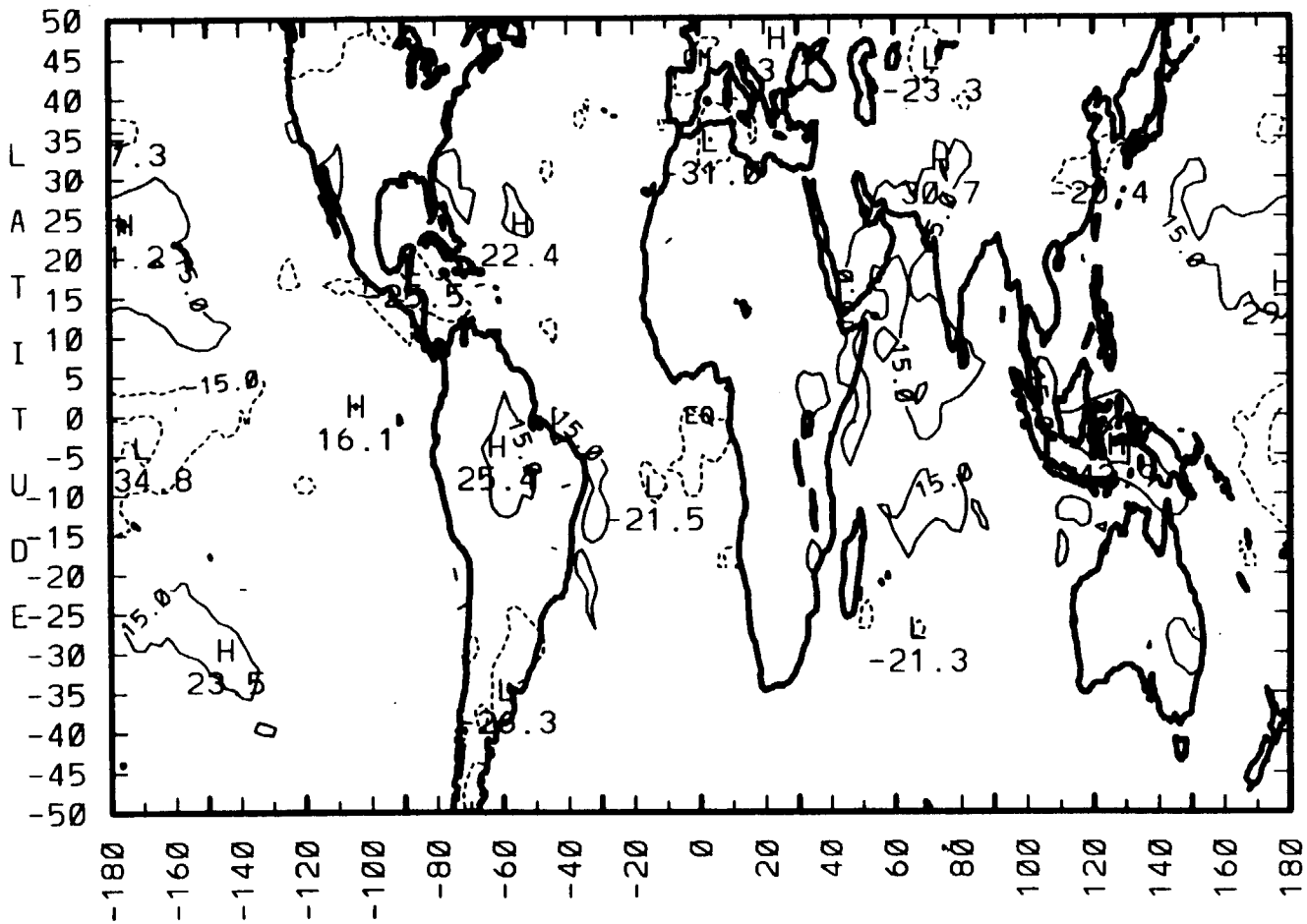

CONTOUR FROM -45.000 TO -45.000 CONTOUR INTERVAL OF 15.000 PT(3,3)= 0.25000

1986/1987 ENSO ANOMALIES

(4-YR MEAN - JULY'87) CLD TOP TEMP (DEG. K)

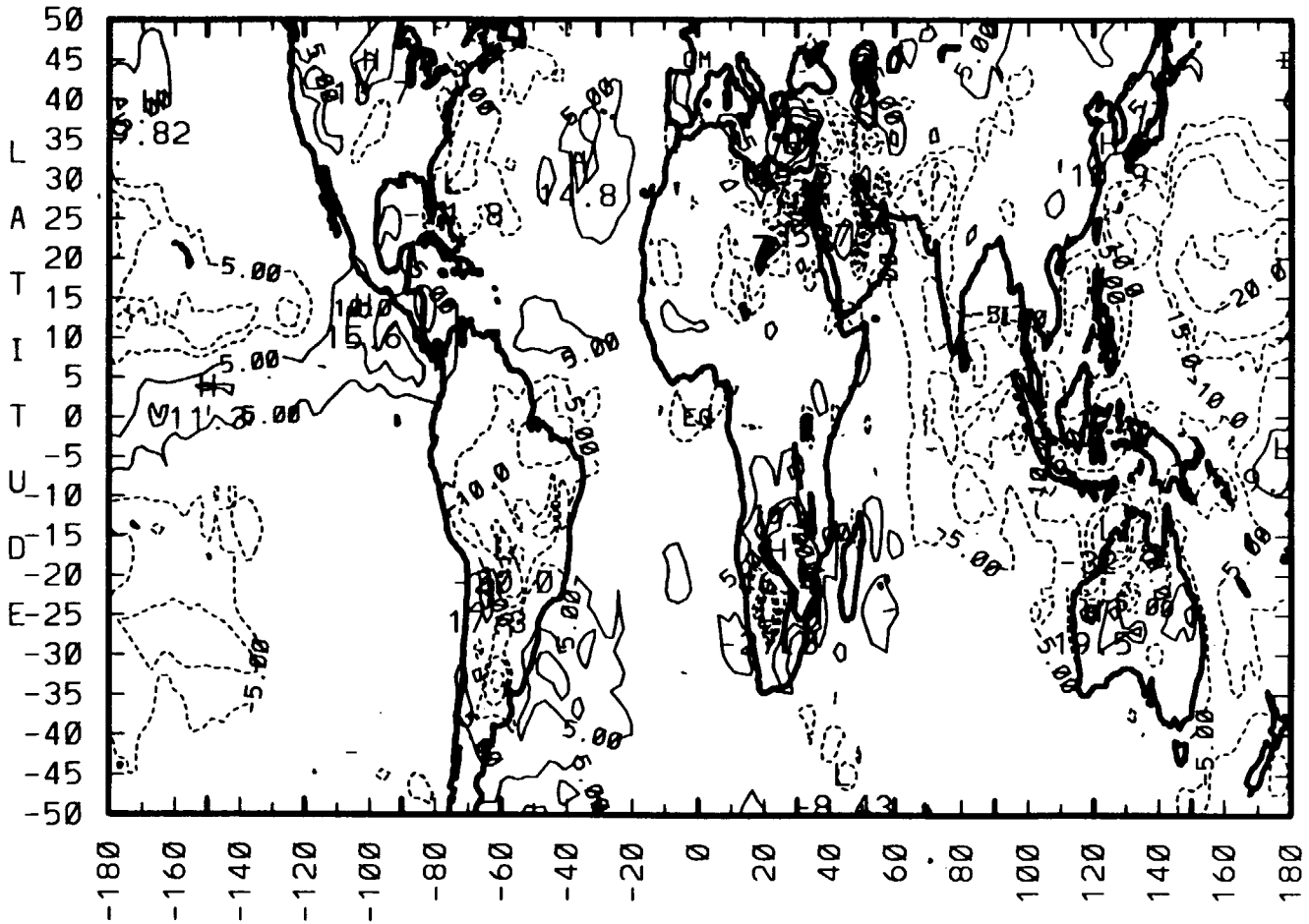

CONTOUR FROM -888888 TO -888888 CONTOUR INTERVAL OF 5.8888 PT(3,3)= -4.2748

1986/1987 ENSO ANOMALIES

(4-YR MEAN - AUG'87) OLR (W/m**2)

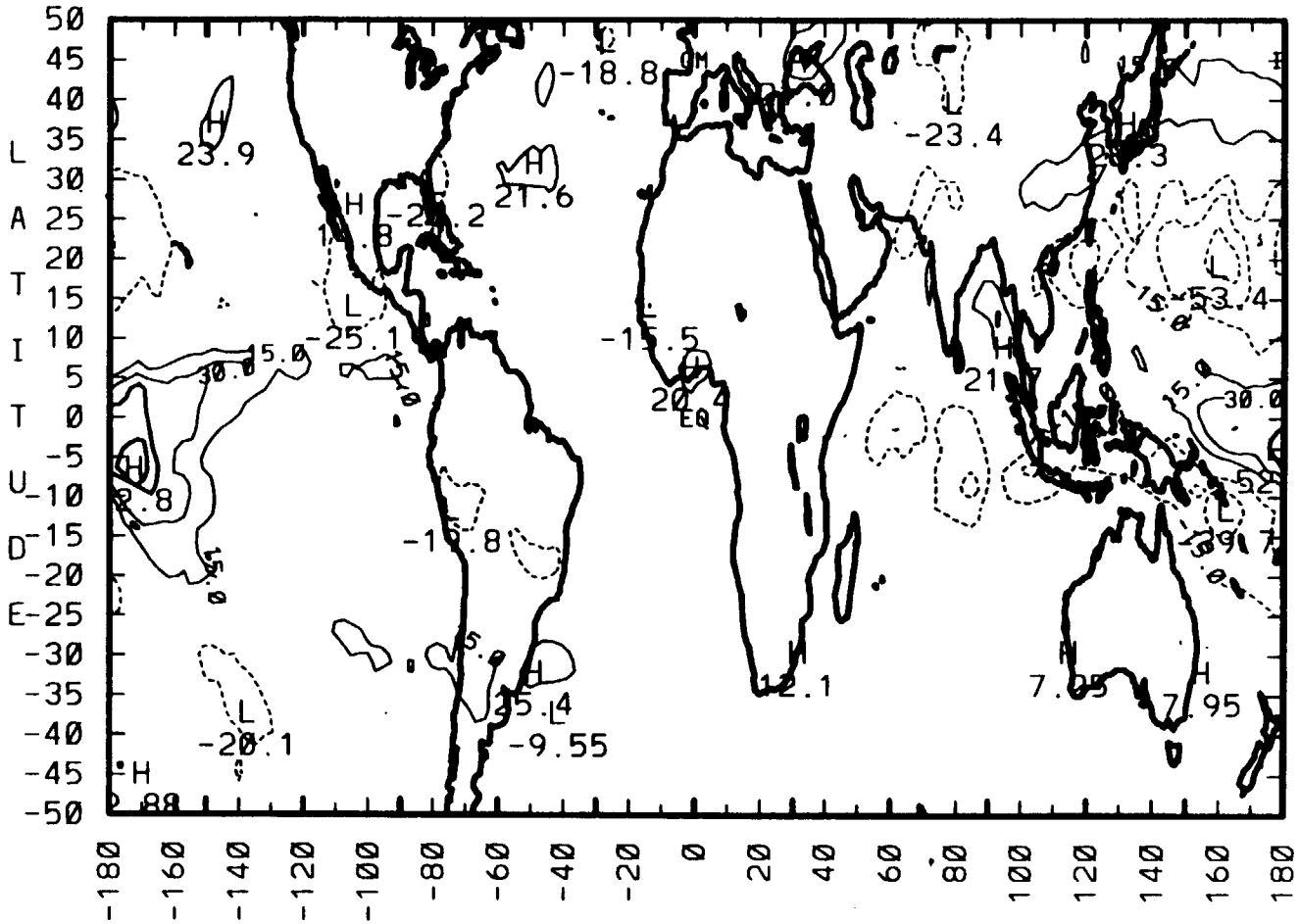

CONTOUR FROM -00.000 TO -00.000 CONTOUR INTERVAL OF 15.000 PT(3,3)= -7.2500

1986/1987 ENSO ANOMALIES

(4-YR MEAN - SEP'87) OLR (W/m**2)

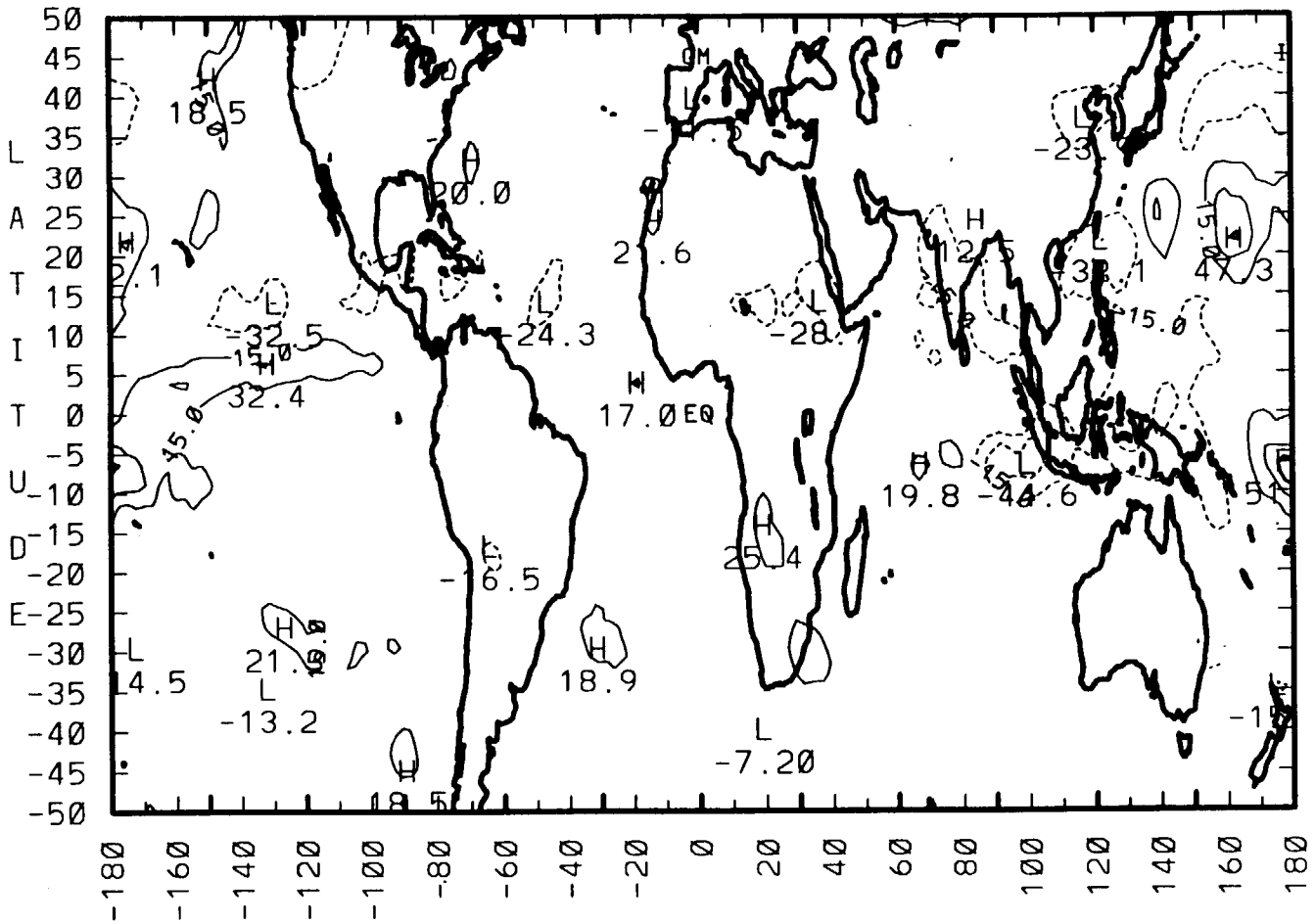

CONTOUR FROM -60.000 TO -60.000 CONTOUR INTERVAL OF 15.000 PT(3,3)= 1.2502

1986/1987 ENSO ANOMALIES

(4-YR MEAN - OCT'87) NET RADIATION (Wm**2)

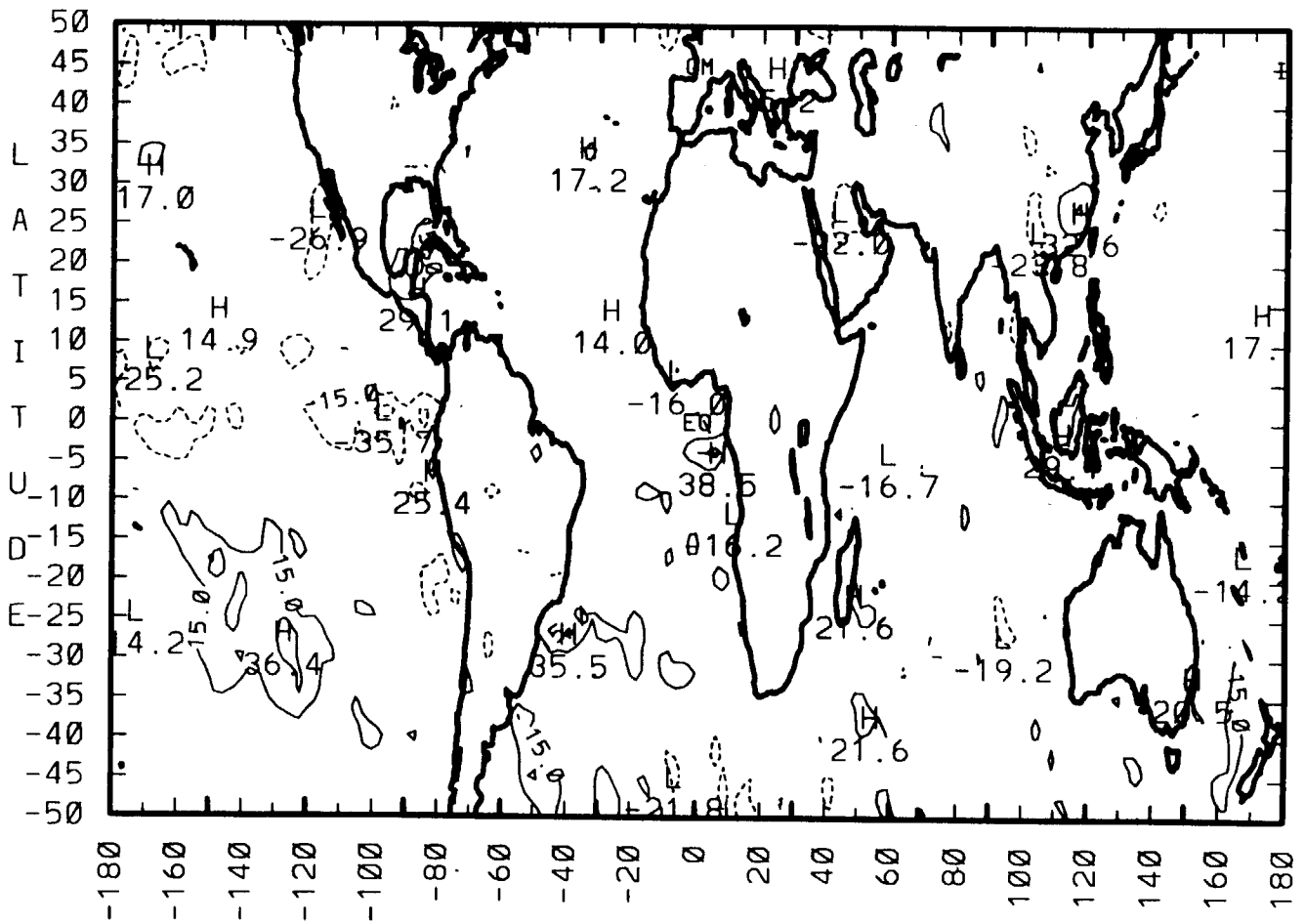

CONTOUR FROM -60.000 TO -60.000 CONTOUR INTERVAL OF 15.000 PT(3,3)= -6.1775

1986/1987 ENSO ANOMALIES

(4-YR MEAN - OCT'87) OLR (W/m**2)

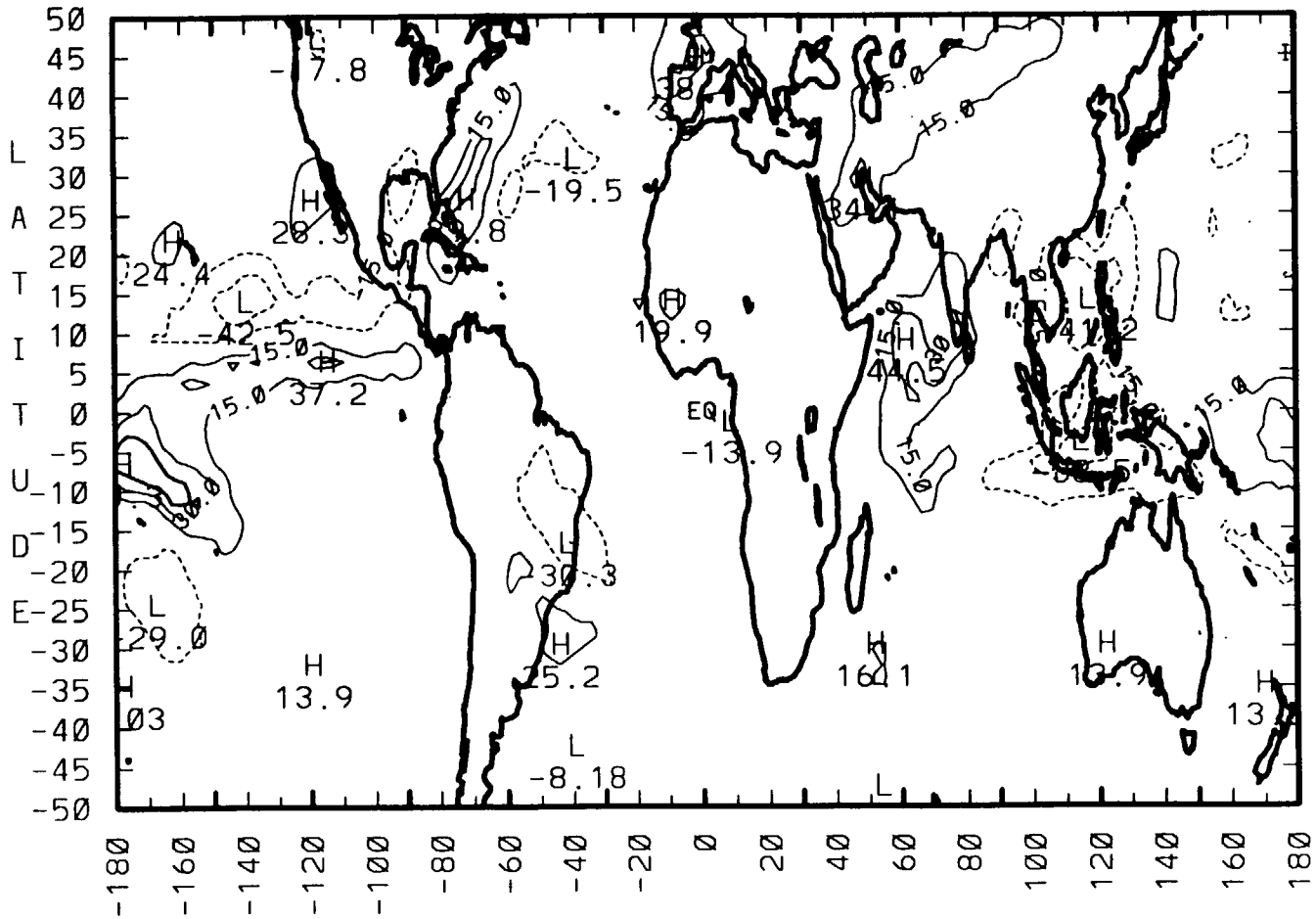

CONTOUR FROM -80.000 TO -80.000 CONTOUR INTERVAL OF 15.000 PT(3,3)= -6.3750

1986/1987 ENSO ANOMALIES

(4-YR MEAN - OCT'87) SW REFLECTED (WM**2)

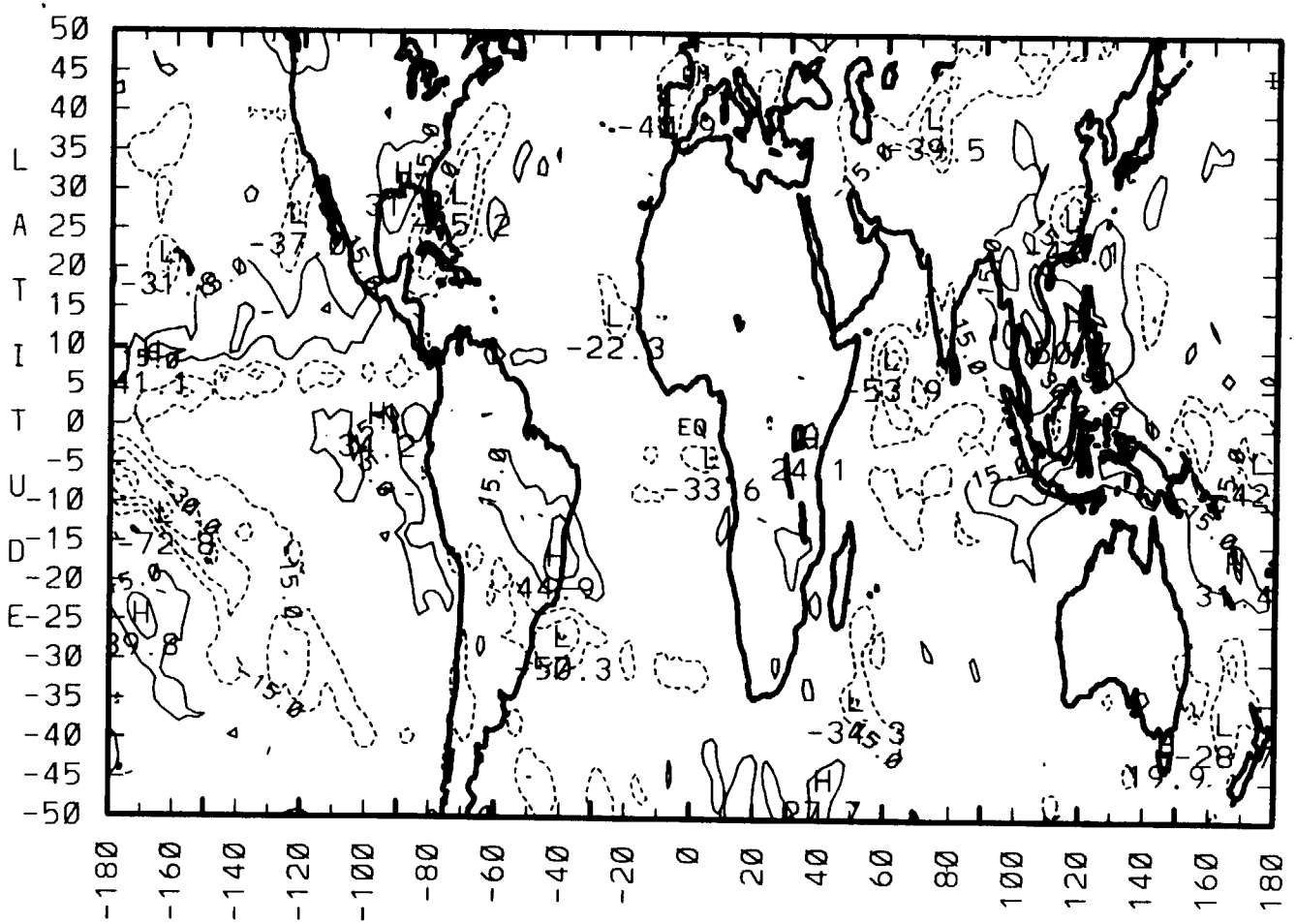

CONTOUR FROM -60.000 TO -90.000 CONTOUR INTERVAL OF 15.000 PT(3,3)= 14.200

1986/1987 ENSO ANOMALIES

(4-YR MEAN - OCT'87) SURFACE TEMP (DEG. K)

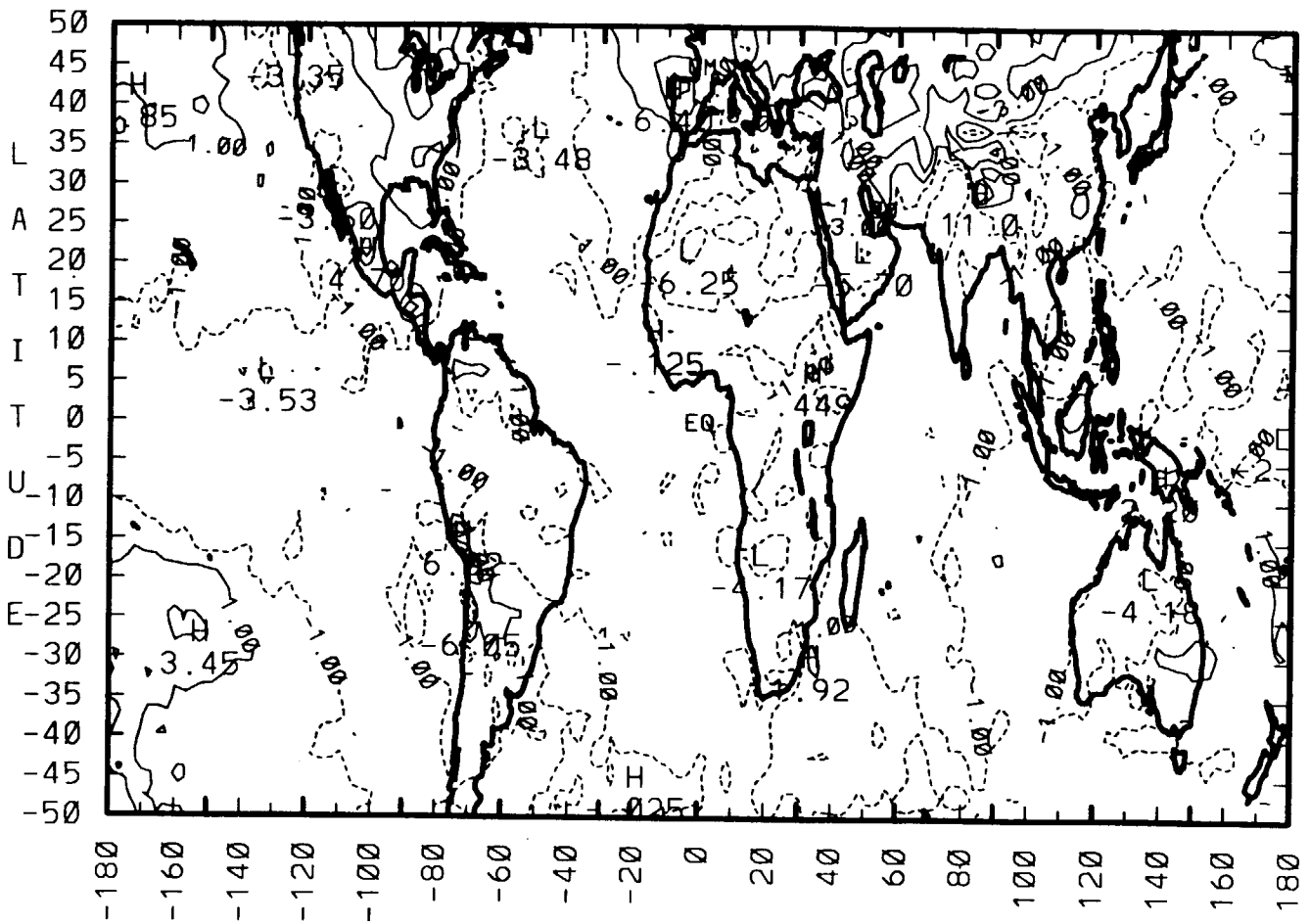

CONTOUR FROM -5.0000 TO -5.0000 CONTOUR INTERVAL OF 2.0000 PT(3,3)= 1.0252

1986/1987 ENSO ANOMALIES

(4-YR MEAN - OCT'87) CLOUD FRACTION (%)

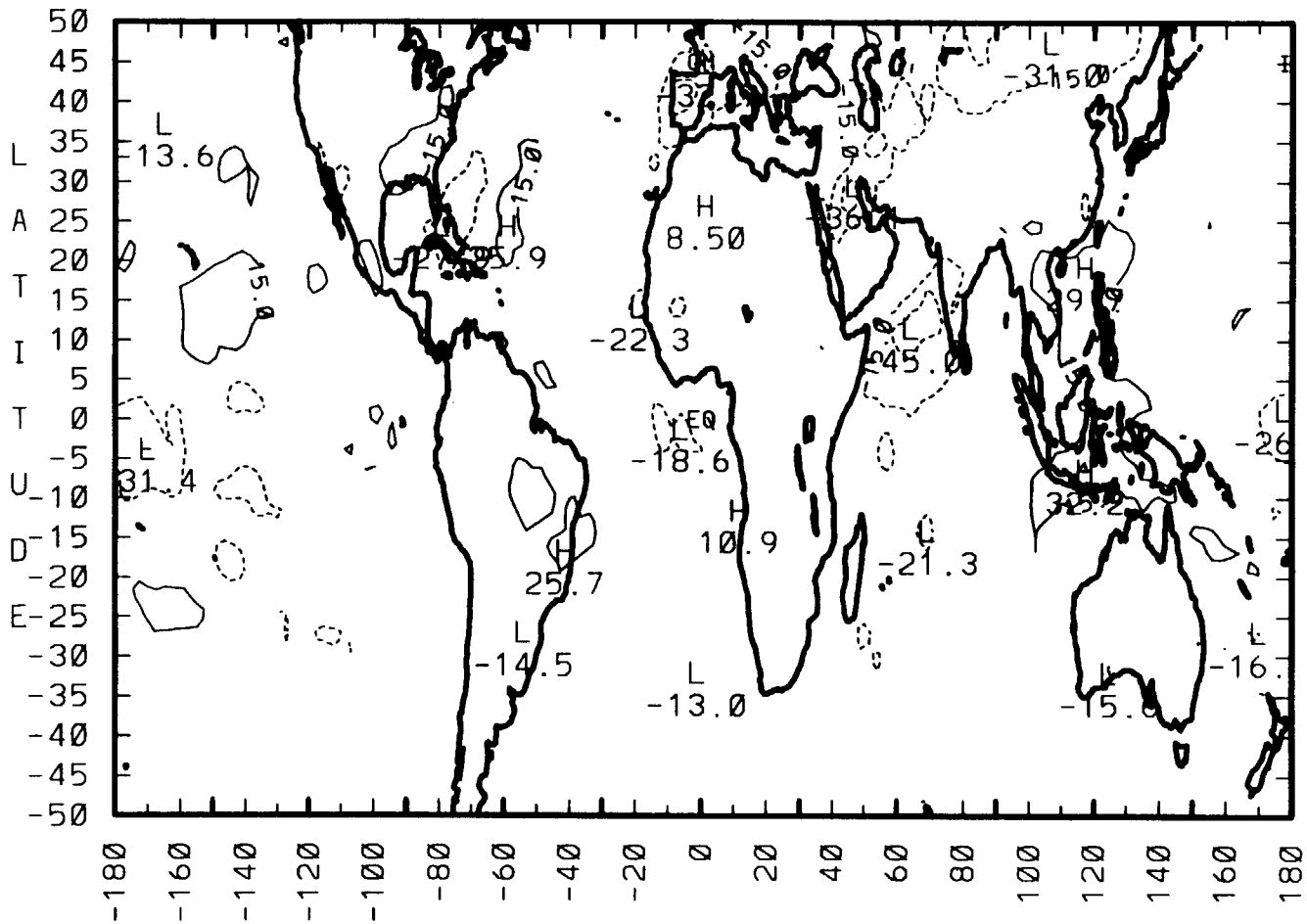

LONGITUDE

CONTOUR FROM -45.000 TO -45.000 CONTOUR INTERVAL OF 15.000 PT(3,3)= 0.50000

1986/1987 ENSO ANOMALIES

(4-YR MEAN - OCT'87) CLD TOP TEMP (DEG. K)

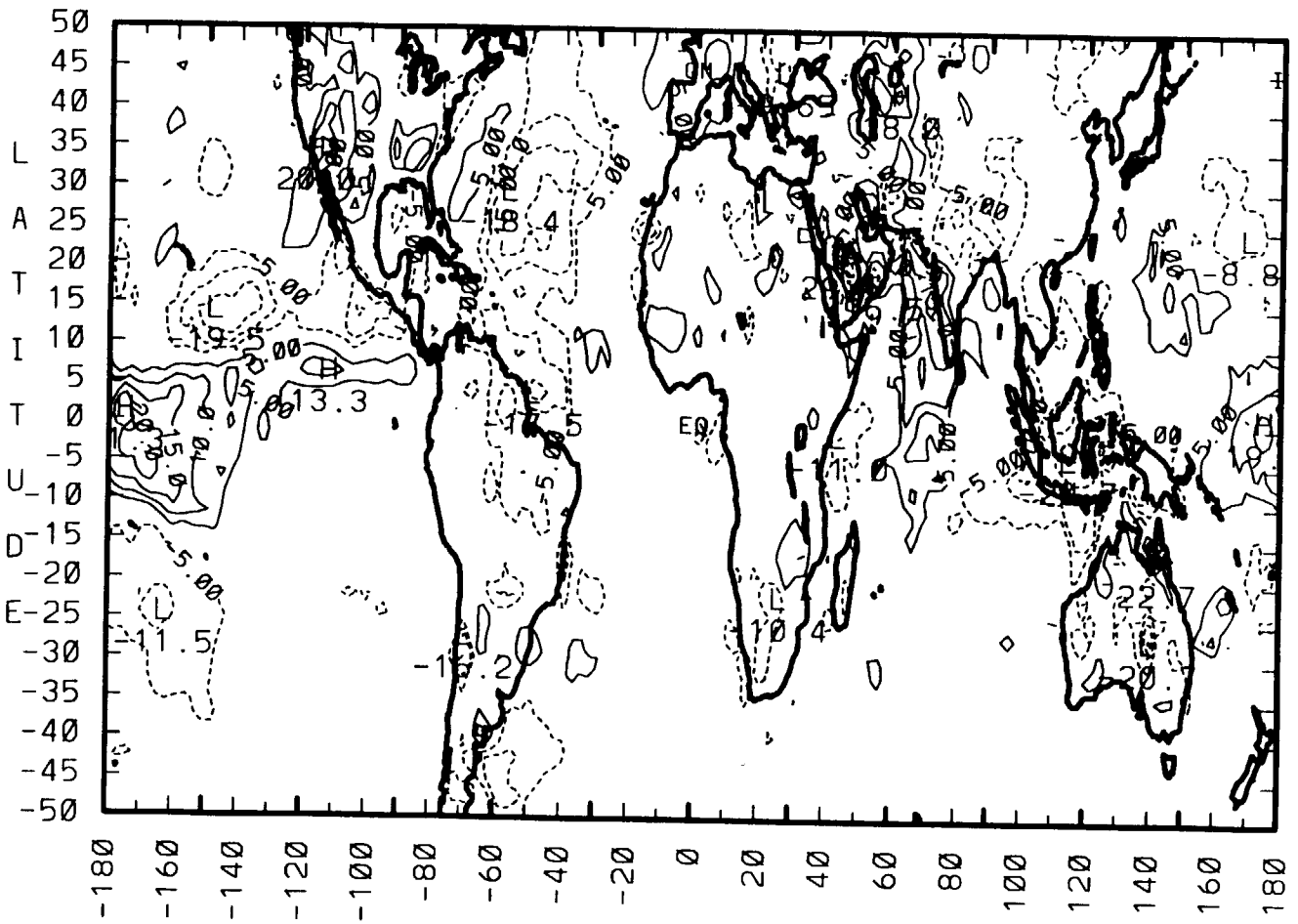

LONGITUDE

CONTOUR FROM -888888 TO -888888 CONTOUR INTERVAL OF 5.0000 PT(3,3)= -2.7495

1986/1987 ENSO ANOMALIES

(4-YR MEAN - NOV'87) OLR (W/m**2)

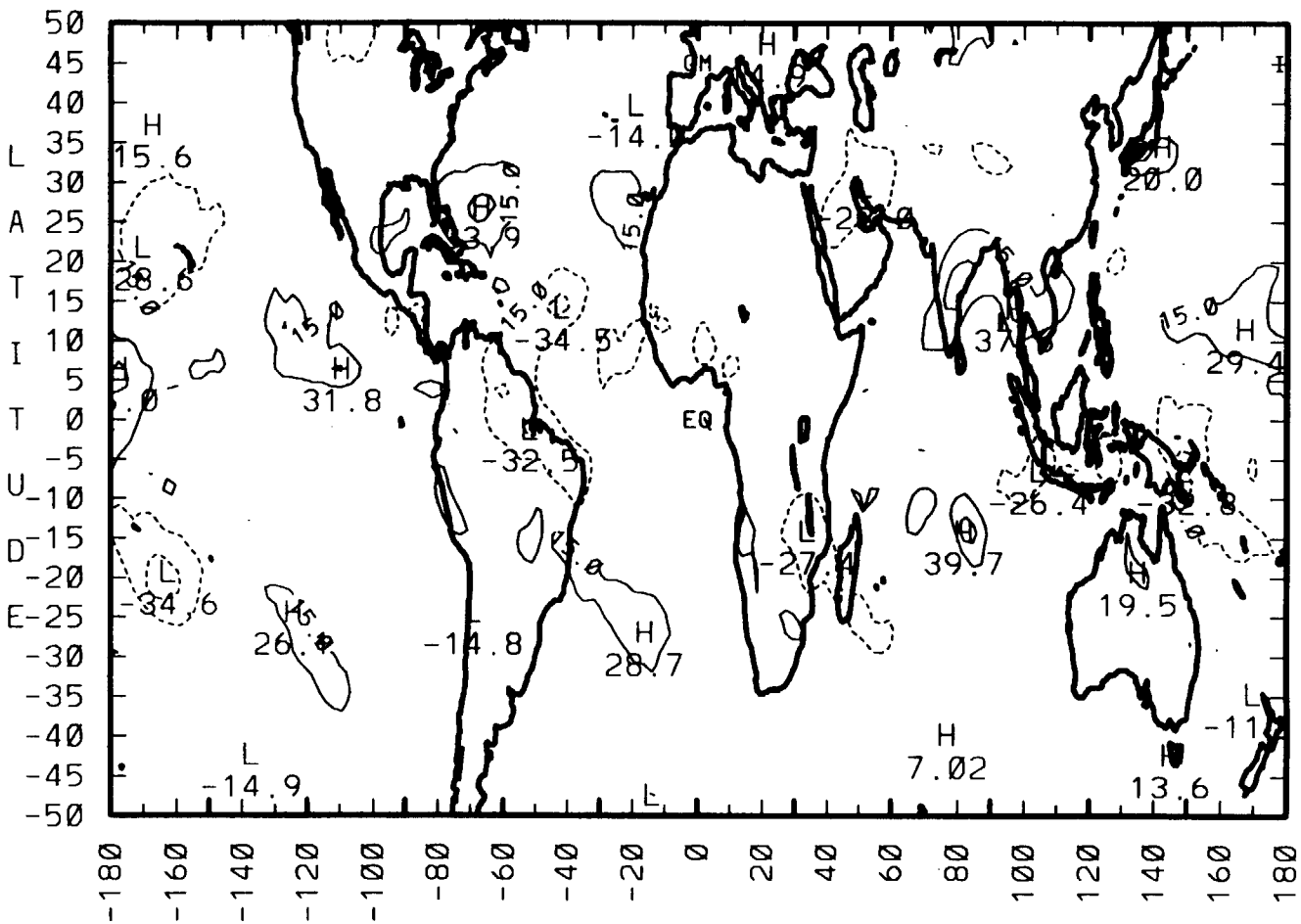

LONGITUDE

CONTOUR FROM -80.000 TO -80.000 CONTOUR INTERVAL OF 15.000 PT(3,3)= -4.5258

mgp

**Presentation A32C-1 at Spring AGU meeting
May 20-24,1996, Baltimore, Maryland,
1996 Spring Meeting supplement to EOS, p.S62.
Presented, revised abstract.**

Cloud and Radiation Budget Perturbations in the Indian Ocean During the 1986/87 ENSO

Harbans L Dhuria (University of the District of Columbia, Washington, DC 20008)
H Lee Kyle (NASA/Goddard Space Flight Center, Greenbelt, MD 20771: 301-286-9415; email lkyle@daac.gsfc.nasa.gov

Five years of cloud and Earth Radiation Budget Experiment (ERBE) data (Dec'84-Nov'89) are being examined to study the perturbations around the Indian ocean caused by the 1986/87 El Nino/Southern Oscillation (ENSO) event. The International Satellite Cloud Climatology Project (ISCCP) monthly mean C2 cloud products are also used. In December 1986 the cloud fraction is subnormal and the out-going longwave radiation is above normal over much of southern Africa in the west and in the east from central Australia north over Indonesia. The reverse occurs over the west central Indian Ocean. The situation oscillates for the next few months. The dry area over southern Africa moves about and then walks up the east coast following the Sun north. Cloud cover remains below normal over Indonesia but is normal to above normal over Australia. Over the Indian Ocean the above normal clouds move eastward. The Indian summer monsoon starts on schedule in June, but then in July fails badly over southern and western India. The monsoon recovers somewhat in August and over parts of southwest India extends an extra month into October. In the mean, the monsoon of 1987 was considered a failure over much of western India.

CLOUD and RADIATION BUDGET PERTURBATIONS in THE INDIAN OCEAN DURING the 1986/87 ENSO

- Harbans L. Dhuria (University of the District of Columbia, Washington, DC 20008
- H. Lee Kyle (NASA/Goddard Space Flight Center, Greenbelt, MD 20771

- AGU May 22, 1996

5-YRS (12/84-1189) OF ERBS (ERBE) & ISCCP DATA EXAMINED

- 5-YR MONTHLY MEANS AND STANDARD DEVIATIONS
- 1986/87 ENSO MONTHLY DIFFERENCES (4-YR MONTHLY MEAN - ENSO MONTH)
- CHIEF PARAMETERS USED HERE: (OLR, SURF. AIR TEMP., CLOUD TOP TEMP., NET RADIATION.
- DRAUGHT OCCURED IN BOTH AFRICA AND INDIA IN 1987

1986/1987 ENSO ANOMALIES
(4-YR MONTHLY MEAN (84,85,88,89) - DEC'86)

SURF AIR TEMP(K) OLR (W/m^2)

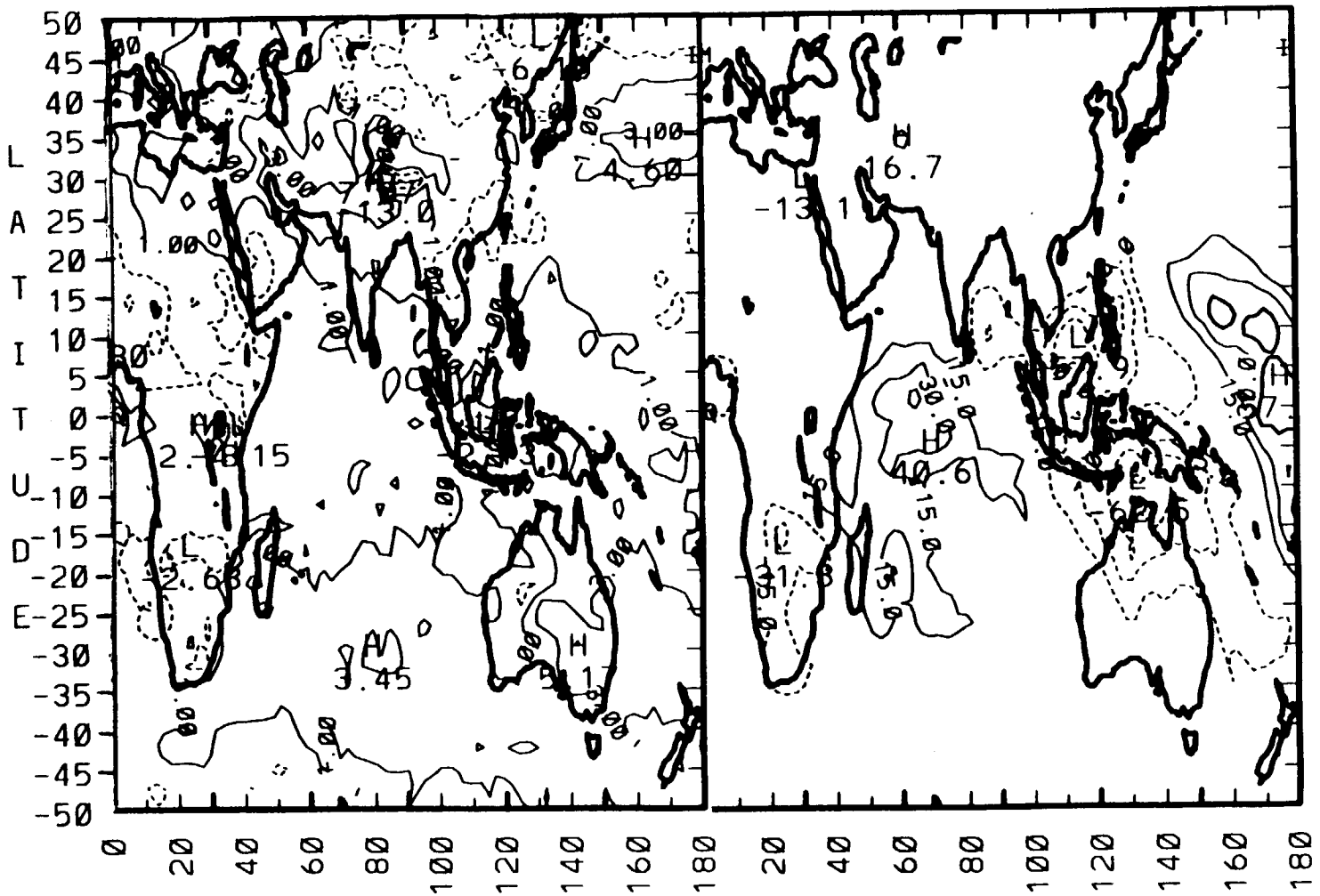

5-YEAR MONTHLY MEANS
(12/84 - 11/89)
SURF AIR TEMP (K) APR

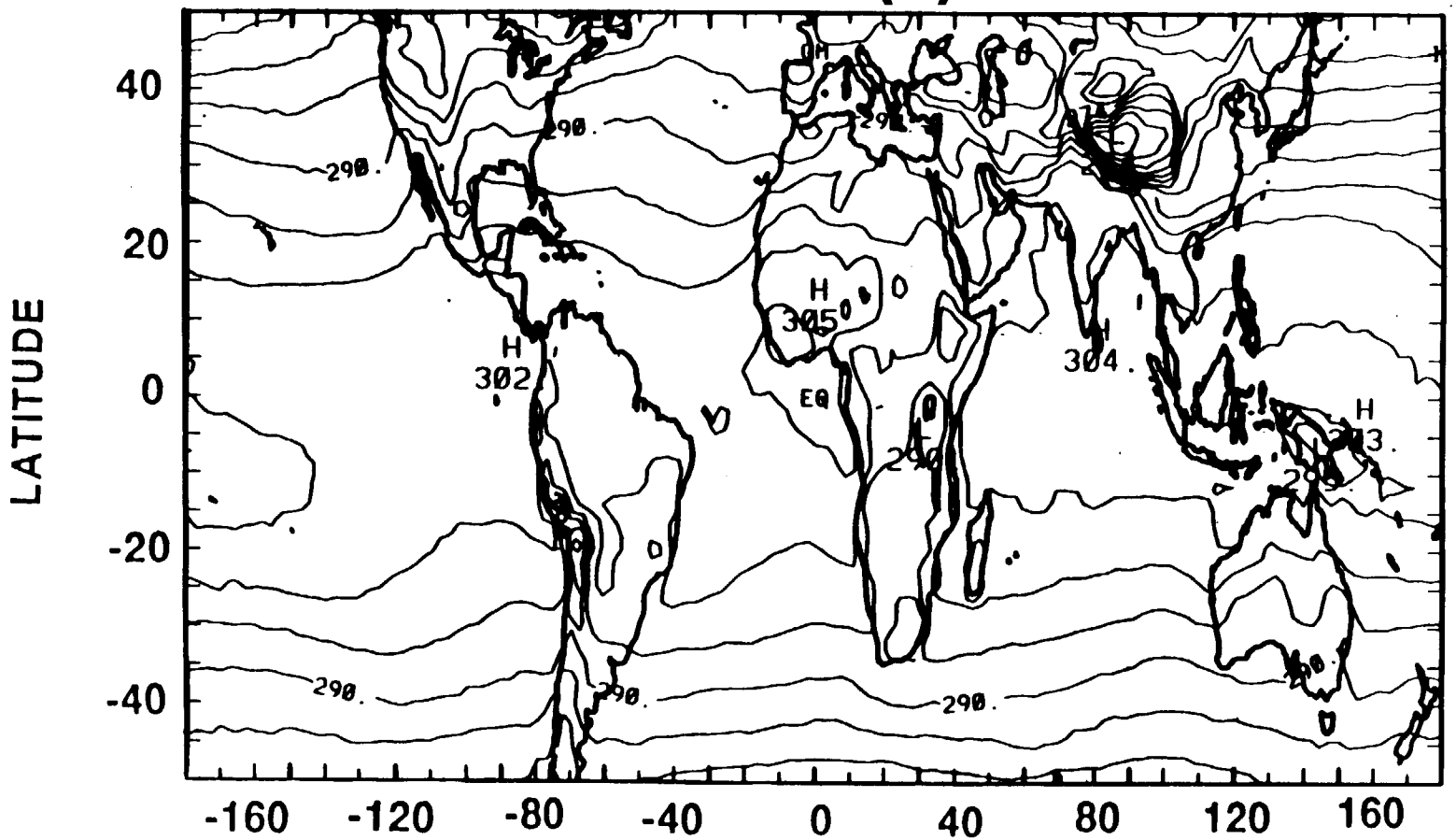

1986/1987 ENSO ANOMALIES
(4-YR MONTHLY MEAN (85,86,88,89) - APR'87)

OLR (W/M^2)

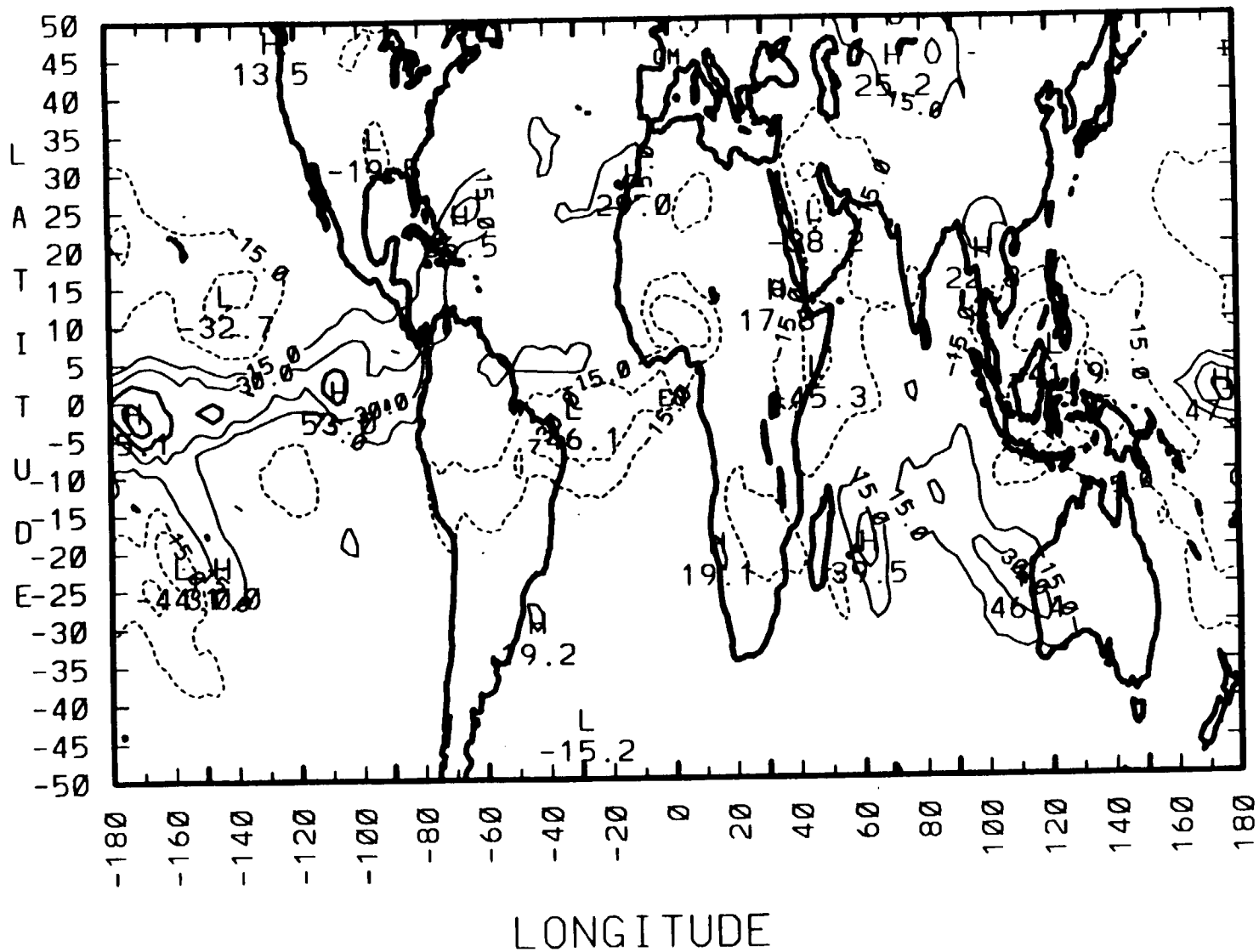

1986/1987 ENSO ANOMALIES
(4-YR MONTHLY MEAN (85,86,88,89) - APR'87)

CLD TOP TEMP(K) OLR(W/m^2)

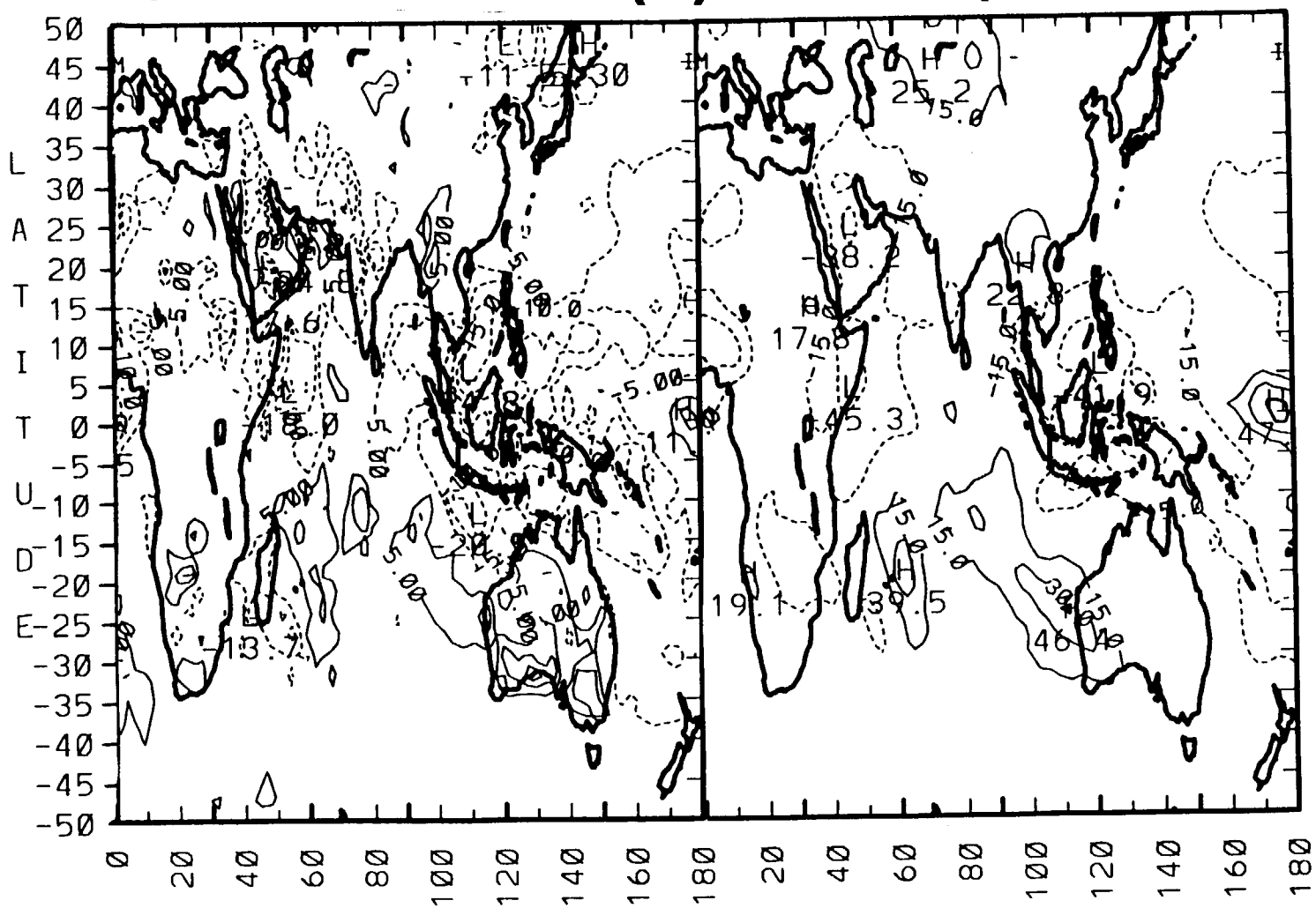

1986/1987 ENSO ANOMALIES
(4-YR MONTHLY MEAN (85,86,88,89)-MON'87)
OLR (W/M^2)

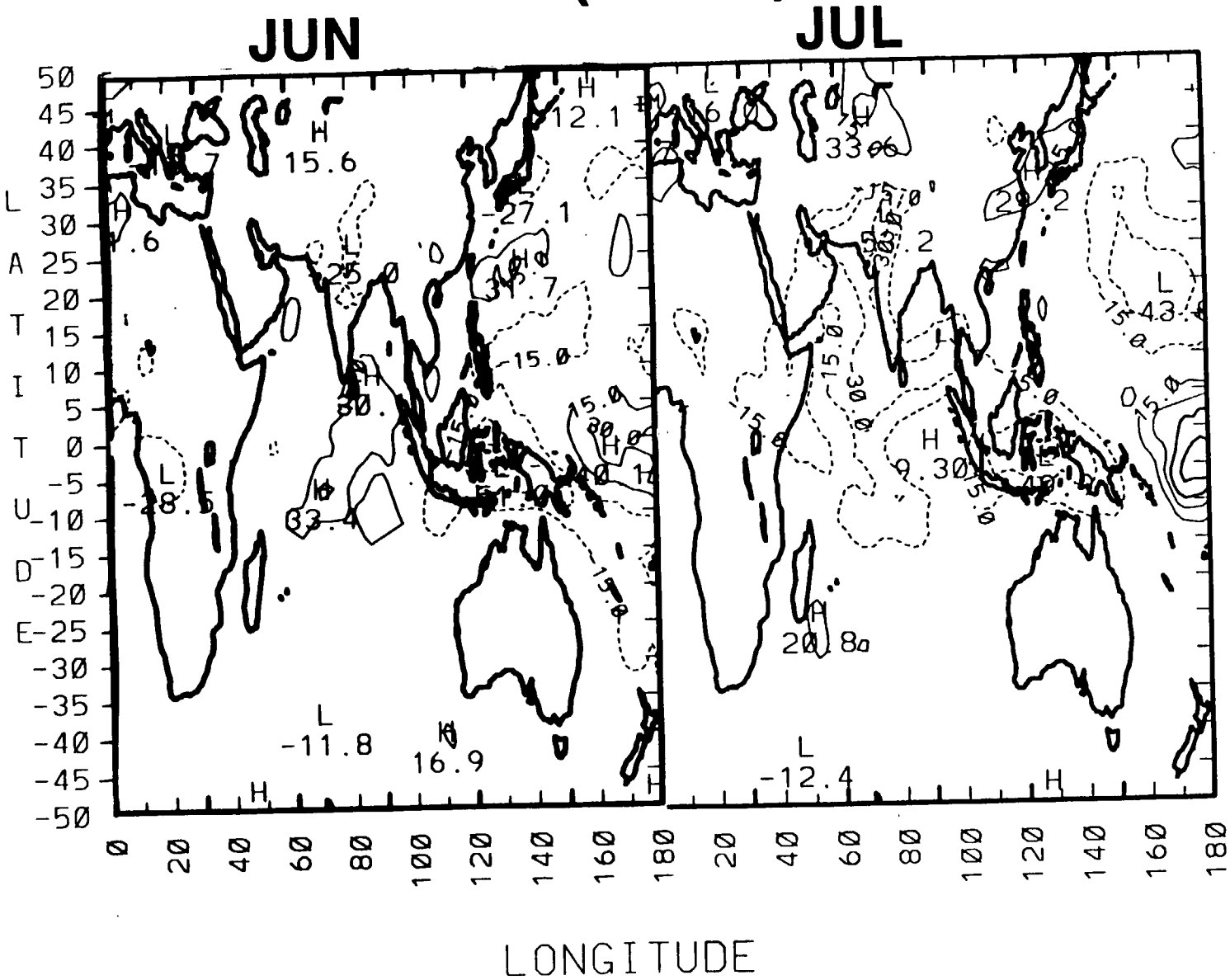

5-YEAR MONTHLY MEANS
(12/84 - 11/89)
JUL OLR (W/m^2)

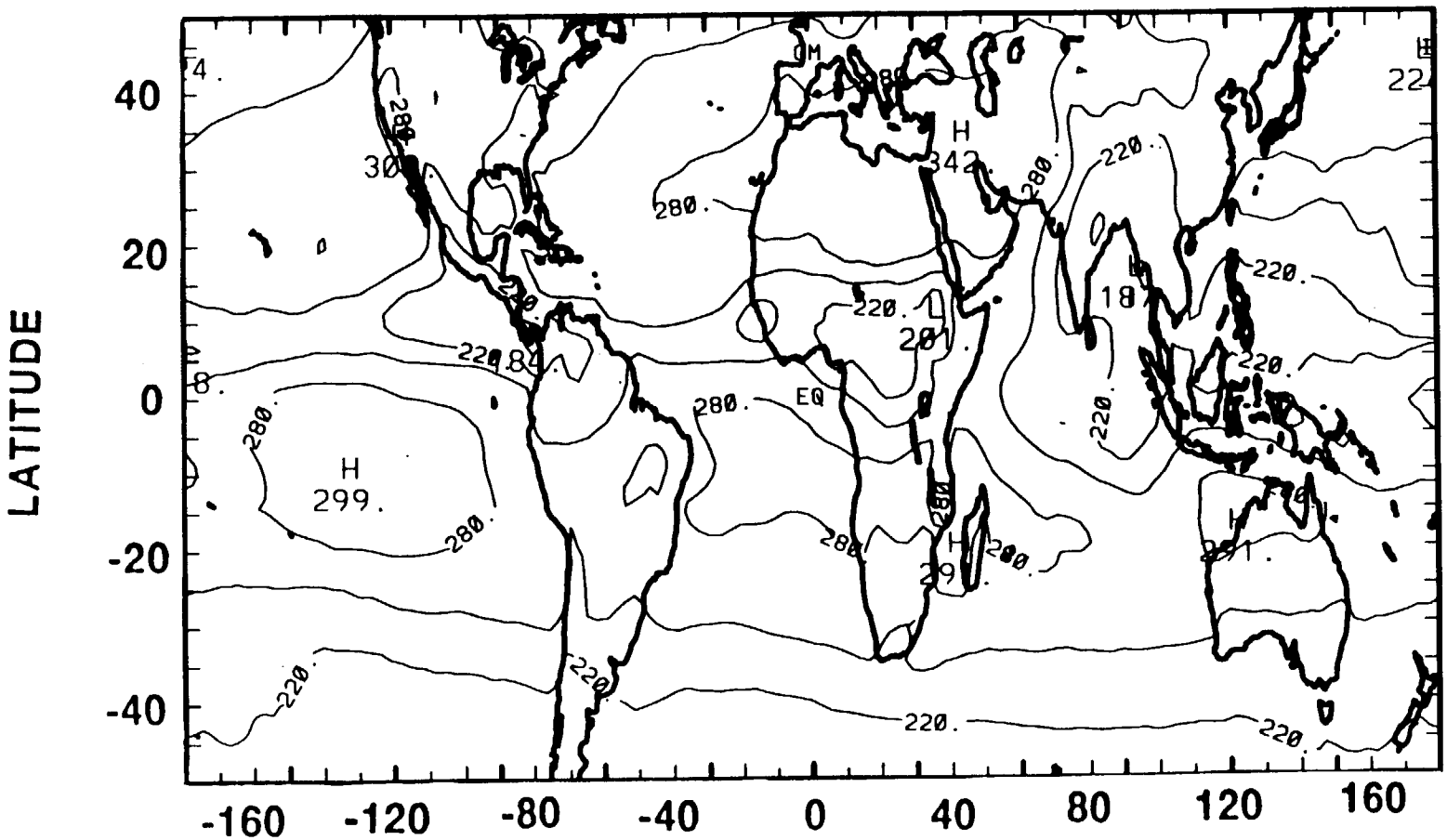

1986/1987 ENSO ANOMALIES

(4-YR MONTHLY MEAN (85,86,88,89)-MON'87)

OLR (W/M^2)

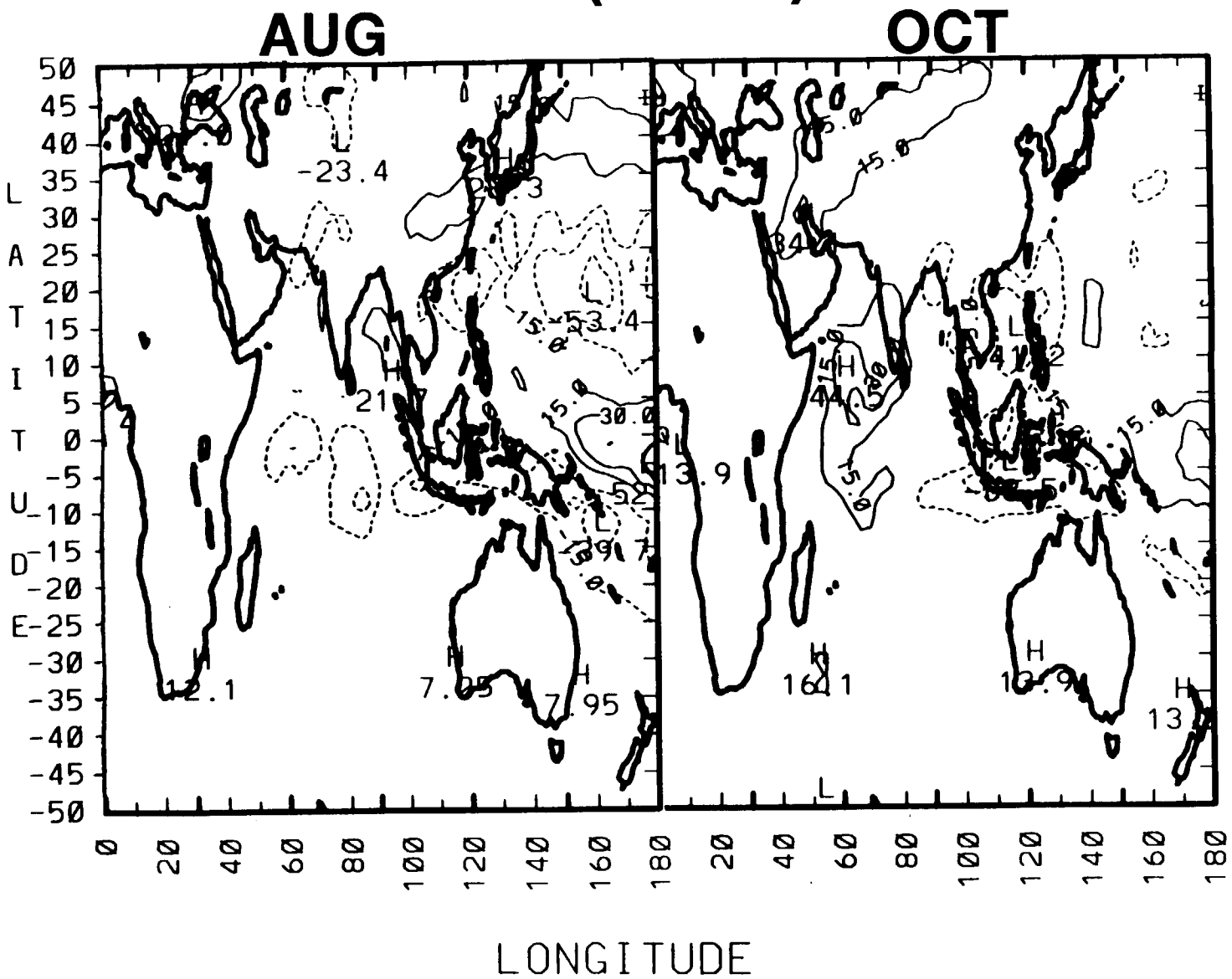

SUMMMARY

- FOR MOST OF DEC'86-OCT'87 CLOUDS WERE DEMINISHED AND OLR INCREASED OVER INDONESIA
- DECREASED CLOUD AND DROUGHT WORKED THEIR WAY INTERMITENTLY UP THE EAST COAST OF AFRICA FROM S. TO N. FROM DECEMBER TO JULY.
- THE MONSOON FAILED IN JULY IN MUCH OF WESTERN INDIA BUT THEN RETURNED TO MANY OF THE REGIONS IN AUG TO OCT.
- THIS IS NOT TO BE CONSIDERED NORMAL INDIAN OCEAN RESPONSE TO AN ENSO EVENT. THE RESPONSE IS VARIABLE.